Glycan-coated nanoparticles for the enhanced active targeting

TESI IN COTUTELA

Universidad del País Vasco   Euskal Herriko Unibertsitatea

Patricia Pérez Schmidt

Matr. No. 880967

Tutor: Dr. Paolo Bigini

Co-tutor: Dr. Sergio Moya

Supervisor: Dr. Laura Polito

Coordinator: Prof.ssa Paola Branduardi

Table of contents

Chapter 4: Protein corona studies of spherical and anisotropic gold nanoparticles

Chapter 5: PEGylated Glyco-Polyamine phosphate nanoparticles

Chapter 6: Conclusions

Abbreviations

Ac-	Acetyl
BBB	Blood brain barrier
BSA	Bovine serum albumin
ConA	Concanavalin A
COVID-19	Coronavirus disease 2019
CT	Computed tomography
DCM	Dichloromethane
DFM	Dark field microscopy
DIPEA	N,N-Diisopropylethylamine
DLS	Dynamic light scattering
DMF	N,N-Dimethylformamide
DNA	Deoxyribonucleic acid
EDC	1-Ethyl-3-(3-dimethylaminopropyl)carbodiimide
EMA	European medicines agency
EPR	Enhanced permeability and retention
ESI	Electrospray ionization
ESR	Early-stage researcher
ETN	European training network
FBS	Fetal bovine serum
FCS	Fluorescence correlation spectroscopy
FCCS	Fluorescence cross correlation spectroscopy
FDA	Food and drug administration
GAuNP	Glyco-gold nanoparticle
GUAuNP	Ultra-small Glyco-gold nanoparticle
HIV	Human immunodeficiency virus
IR	Infrared
LSPR	Localized surface plasmon resonance
MBL	Mannose binding lectin
MR	Mannose receptor
MRI	Magnetic resonance imaging
MS	Mass spectrometry
NMR	Nuclear magnetic resonance
NP	Nanoparticle
PC	Protein corona
PDT	Photodynamic therapy

PEG	Polyethylene glycol
PET	Positron emission tomography
PFP	Pentafluorophenol
PVP	Polyvinylpyrrolidone
RNA	Ribonucleic acid
ROS	Reactive Oxygen Species
RT	Room temperature
SARS-Cov-2	Severe acute respiratory syndrome coronavirus 2
SERS	Surface enhanced Raman spectroscopy
siRNA	Small interfering Ribonucleic acid
SPION	Superparamagnetic iron oxide nanoparticles
Sulfo-NHS	N-hydroxysulfosuccinimide
TEM	Transmission electron microscopy
THF	Tetrahydrofuran
TLC	Thin layer chromatography
TOAB	Tetraocthylammonium bromide
US	United States

Abstract

Gold nanoparticles (AuNPs) are nanomaterials with excellent physicochemical and optical properties for a broad range of applications. The surface functionalization of the AuNPs enables the formation of glyco-gold nanoparticles (GAuNPs). GAuNPs multivalency properties can trigger the cluster glycoside effect overcoming the low affinity between individual carbohydrate-protein interactions. Therefore, these nanoparticles (NPs) have been demonstrated to be excellent candidates for lectin targeting among other biological applications.

Moreover, AuNPs when in contact with biological media interact with the present proteins forming the protein corona (PC) which has an effect in the final fate and efficacy of the NPs. The study of the PC formation of the NPs is extremely important to assure the activity of the AuNPs. The PC formation can be modulated with the surface coating, size, and shape of the AuNPs. Ligand stabilizers as for example polyethylene glycol (PEG) can prevent the PC formation and the consequent recognition by the immune system and clearance of the body. Additionally, the glycan coating of the AuNPs can also modulate the PC composition and therefore the biodistribution of the GAuNPs can be modified.

The final aim of this project is the increase of the circulation time of glyco-nanomaterials in the body in order to enhance the active targeting. To accomplish this objective some features of the nanomaterials such as size, shape, surface coating, and composition were considered as they play a crucial role. The modulation of these features can highly impact the protein corona formation when in contact with biological media and consequently the half-life of the nanomaterials. The size was tuned by designing a new synthetic procedure for the synthesis of glyco ultra-small gold nanoparticles. The effect over the half-life of the nanoparticles of AuNPs with different surface coating was studied by performing biodistribution studies in healthy mice and novel Glyco-PEGylated polyamine phosphate nanoparticles were synthesized.

The results obtained throughout this thesis contribute to the advance of the research of glyco nanomaterials towards the production of new nanomedicines. As it provides a better understanding of crucial aspects regarding their future applications. Moreover, a novel synthetic procedure of ultra-small GAuNPs was developed overcoming some of the current challenges in nanoparticles production as it enables an easy scale-up, it is an automated system, and it offers a fine control over the surface coating of the nanoparticles

In order to fulfill the final aim, the thesis has been divided in 6 chapters which are summarized below.

The second chapter of this thesis consists in a biodistribution study in healthy mice of ultra-small gold nanoparticles (UAuNPs) coated with PEG chains of different length and/or with α-Galactose attached to a short aliphatic ligand. The UAuNPs were synthesized using a bench-top reactor and the NPs were injected to healthy mice. The liver kidneys and spleen were collected at 1,4 and 24 hours. The organs were then digested, and the gold content was analysed by Induced Couple Plasma Optical Emission Spectroscopy (ICP-OES). On the other hand, selected organs

were silver stained by autometallography (AMG) and analysed with bright-field microscopy. Moreover, organs were immune stained to detect the UAuNPs by confocal microscopy.

The UAuNPs coated solely by PEG$_{5000}$ presented the highest circulation time in the body, as expected. Additionally, the UAuNPs coated with a mix of PEG$_{500}$ and α-Gal-C$_2$ had a similar circulation time. These results prove that the length of the PEG chain is important but not the only path to follow to extend the half-life of the UAuNPs. Moreover, the UAuNPs coated with PEG were post-functionalized with α-Mannose and a variation in the biodistribution was observed as the UAuNPs accumulated less in the liver and kidneys. The mannosylated UAuNPs had also a different distribution inside the liver in the as proven by the AMG studies.

Microfluidic systems have brought the attention of numerous researchers in the last years for their advantages compares to batch synthetic procedures of AuNPs. These systems offer several advantages as a better control over the reaction parameters, a higher reproducibility between batches as well as a simple scale-up. The drawbacks presented when AuNPs are taken from research to clinical trials can be overcome by microfluidic synthetic procedures. Therefore, in our group we have focused on the development of microfluidic procedures to obtain AuNPs of different size and shape.

A novel microfluidic photo-induced procedure to obtain glyco 2 nm ultra-small gold nanoparticles (GUAuNPs) has been described ~~in Chapter 3~~. This system enables a one-pot synthesis of GUAuNPs avoiding the use of surfactants and reducing agents. The novel procedure exploits the photo-reduction of Au with a UV-lamp in the presence of ethanol, which can act as a photo initiator. A major advantage of the procedure is the possibility to recover the precious unreacted glycan derivatives in the purification step due to the absence of reducing agents in solution. The broad applicability of the system was proved by synthesizing a small library of UAuNPs coated with α-mannose, β-glucose and lactose bond to an amphiphilic ligand and a short aliphatic ligand. The system was further tested with a longer hydrophilic linker, in this case PEG$_{5000}$ and α-galactose-PEG$_{5000}$. Obtaining successfully in all cases 2 nm GUAuNPs.

Moreover, the calculation of the final loading of the NPs is crucial depending on the final bio application. Therefore, a quantitative analysis by ^{1}H-NMR of the small library was performed and a linear correlation was obtained between the ligands added in the initial solution and the ligands present in the UAuNPs independently of their glycan nature.

A similar microfluidic system developed by our group in the recent years was employed for the synthesis of a small library of 30 nm spherical and star shaped (70 nm tip-to-tip) glyco-gold nanoparticles (GAuNPs). The same glycan derivatives described before were used. The long-term stability of the GAuNPs in different media (water, PBS, FBS and RPMI) was analyzed by dynamic light scattering (DLS) and ζ-potential. Where the variation of the hydrodynamic diameter was observed to determine the formation of a soft corona and a hard corona layer.

The fifth chapter describes the wok performed during the secondments conducted at CIC BiomaGUNE (San Sebastian, Spain) under the supervision of Sergio Moya. Novel PEGylated glyco poly(allyl)amine phosphate NPs were synthesized in this project.

The PEGylation of polyamine phosphate nanoparticles (PANs) had been performed previously by Sergio Moya's group. The PEGylated PANs presented several advantages compared to PANs.

Some of them were lower toxicity, longer circulation time in the body, smaller size, and an absence of surface charge. These NPs also prevented the unspecific binding to proteins.

Therefore, to achieve specificity of binding towards some lectins as Con-A and Jacalin a small library of PEGylated glyco polyamine phosphate NPs was synthesized. The library was obtained using carbodiimide chemistry with heterobifunctional PEG compounds of two different length and α-mannose, β-glucose and lactose attached to an amphiphilic ligand. The NPs were characterized by DLS, ζ-potential and TEM and the effect of the self-assembly with different concentrations of PBS was studied. The formation by self-assembly of the nanoparticles and the interaction with the lectins was studied by Fluorescence correlation spectroscopy (FCS) and fluorescence cross-correlation spectroscopy (FCCS). In order to perform these studies, the poly(allyl)amine hydrochloride was fluorescently labelled, to then be reacted with the PEG and glycan derivatives.

Riassunto

Le nanoparticelle d'oro (AuNPs) sono caratterizzate da eccellenti proprietà fisico-chimiche e ottiche e per questo motivo impiegate in un'ampia gamma di applicazioni. Grazie alla robusta chimica superficiale, è possibile sintetizzare nanoparticelle glicosilate (GAuNPs) che, proprio come succede in natura, presentano i glicani in modo multivalente amplificando la debole affinità che esiste tra i carboidrati e i suoi recettori. Pertanto, è stato ampiamente dimostrato che le GAuNPs sono eccellenti candidati per le applicazioni biologiche mediate e promosse, per esempio, attraverso il targeting della lectine.

E' necessario considerare che, quando dispersi in mezzi o fluidi biologici, le AuNPs interagiscono con le proteine presenti formando nuove identità definite "proteina corona" (PC) che hanno un effetto fondamentale sul destino finale e sull'efficacia delle NPs. Lo studio della formazione delle PC è estremamente importante per preservare l'attività delle AuNPs. La formazione delle PC può essere modulata attraverso la corretta selezione del rivestimento superficiale, le dimensioni e la forma delle nanoparticelle. Ligandi in grado di stabilizzare le AuNPs come ad esempio il polietilenglicole (PEG) possono impedire la formazione della PC e il conseguente riconoscimento da parte del sistema immunitario e la clearance da parte dell'organismo. Tuttavia è noto che anche il rivestimento a base saccaridico può modulare la composizione della PC e, di conseguenza, la biodistribuzione delle GAuNPs.

Il secondo capitolo di questa tesi presenta i risultati di uno studio di biodistribuzione in topi sani di nanoparticelle d'oro ultra piccole (UAuNPs) rivestite con catene di PEG di diversa lunghezza e/o con α-galattosio, a sua volta decorato da un corto ligando alifatico in posizione anomerica. Le UAuNPs sono state sintetizzate utilizzando un reattore da banco e le NPs sono state iniettate in topi sani. Il fegato, i reni e la milza dei topi sacrificati sono stati campionati dopo 1,4 e 24 ore dall'iniezione. Gli organi sono stati quindi digeriti utilizzando una miscela di acqua regia a acqua ossigenata e il contenuto di oro è stato analizzato mediante spettrometria ad emissione atomica accoppiata induttivamente al plasma d'argon (Inductively Coupled Plasma) con rivelatore ottico (ICP-OES). Inoltre, gli organi selezionati sono stati marcati con argento mediante autometallografia (AMG) e analizzati con microscopia in campo chiaro e immunizzati per rilevare le UAuNPs mediante microscopia confocale.

Come atteso, le UAuNPs, rivestite esclusivamente da PEG_{5000}, hanno dimostrato di avere il tempo di circolazione più lungo, simile a quello osservato con le UAuNPs rivestite con una miscela di PEG_{500} e α-Gal-C2. Questi risultati supportano l'evidenza che la lunghezza della catena PEG è importante ma non è l'unico parametro da considerare per estendere il tempo di emivita delle UAuNPs. Le UAuNPs funzionalizzate con PEG-COOH sono state post-funzionalizzate con un derivato α-mannosidico: in questo caso è stato possibile apprezzare una diversa biodistribuzione poiché le UAuNPs si sono accumulate molto meno nel fegato e nei reni rispetto alle altre UAuNPs.

Recentemente, i sistemi microfluidici per la sintesi di AuNPs hanno attirato l'attenzione di numerosi ricercatori grazie ai numerosi vantaggi che li differenziano dalle procedure sintetiche in massa. Questi sistemi, infatti, offrono un controllo migliore sui parametri di reazione, una maggiore riproducibilità tra lotti e la possibilità di fare scale-up di produzione. Tutte queste osservazioni rappresentano fattori cruciali nell'ipotesi di un trasferimento in clinica delle AuNPs. Nel gruppo di ricerca in cui ho condotto questo dottorato ci siamo interessati proprio dello sviluppo di procedure microfluidiche per ottenere AuNP di diverse dimensioni e forma.

In particolare mi sono occupata della messa a punto di una nuova procedura microfluidica fotoindotta per ottenere nanoparticelle d'oro ultra-piccole (circa 2nm) funzionalizzate con glicani (GUAuNP): tale procedura è descritta nel Capitolo 3 della presente Tesi. Questo sistema consente una sintesi one-pot di GUAuNP evitando l'uso di tensioattivi e agenti riducenti. La procedura sfrutta la fotoriduzione dell'oro in seguito ad irraggiamento del precursore aurico con luce ultravioletta e mediata dalla presenza di etanolo, che funge da fotoiniziatore. Un grande vantaggio della procedura è rappresentato dalla possibilità di recuperare i preziosi derivati glicani non reagiti, durante la fase di purificazione. Abbiamo inoltre dimostrato che il sistema messo a punto è particolarmente versatile ed è stato possibile sintetizzare una piccola libreria di GUAuNPs ricoperte da α-mannosio, β-glucosio e lattosio decorati con due tipi di linker: uno di tipo anfifilico e uno alifatico, costituito da due o tre atomi di carbonio. Il sistema microfluidico è stato ulteriormente testato con successo utilizzando come derivato tiolato un linker idrofilico particolarmente lungo come il PEG_{5000} e un derivato saccaridico quale l' α-galattosio-PEG_{5000}.

Perché le AuNPs possano essere impiegate in ambito biomedico è cruciale conoscere in modo preciso la quantità di molecole bio-attive esposte sulla loro superficie. Pertanto, la nostra libreria è stata sottoposta ad un accurata analisi quantitativa mediante ^{1}H-NMR ed è stata ottenuta una correlazione lineare tra la quantità di ligandi aggiunti nella soluzione iniziale e i ligandi esposti sulla superficie delle UAuNP indipendentemente dalla loro natura saccaridica.

Negli ultimi anni nel gruppo in cui ho svolto il mio lavoro di dottorato è stato sviluppato un sistema microfluidico per la sintesi controllata di morfologie iso e anisotropiche. Sono state quindi sintetizzate due piccole librerie di nanoparticelle oro glicosilate (GAuNP) a forma sferiche (di circa 30 nm di diametro) e a forma di stella (70 nm da punta a punta). Per la funzionalizzazione sono stati utilizzati gli stessi derivati saccaridici descritti in precedenza. La libreria è stata analizzata per quanto riguarda la stabilità nel tempo ed il comportamento in diversi mezzi (acqua, PBS, FBS e RPMI) mediante Dynamic Light Scattering (DLS) e potenziale ζ.

L'ultimo capitolo descrive il lavoro svolto durante i periodi di *secondment* condotti presso il CIC BiomaGUNE (San Sebastian, Spagna) sotto la supervisione del dottor Sergio Moya. In questo progetto sono state sintetizzate nuove NP di glicopoli(allil)ammina fosfato PEGilato.

La funzionalizzazione con catene PEG di nanoparticelle di poli(allil)ammina fosfato (PAN) era già stata eseguita in precedenza dal gruppo del dr. Sergio Moya. I PAN così funzionalizzati presentavano numerosi vantaggi rispetto ai PAN di partenza: per esempio una minore tossicità, un tempo di circolazione più lungo nel corpo, dimensioni più ridotte e assenza di carica superficiale. Queste NP hanno dimostrato anche di impedire la formazione di legami non specifico con le proteine.

Pertanto, per ottenere la specificità del legame verso alcune lectine come Con-A e Jacalin è stata sintetizzata una piccola libreria di NP di glicopoli(allil)ammina fosfato PEGilati. La libreria è stata ottenuta utilizzando la chimica della carbodiimmide con composti PEG eterobifunzionali di due diverse lunghezze e α-mannosio, β-glucosio e lattosio attaccati a un ligando anfifilico. Le NP sono state caratterizzate tramite DLS, ζ-potenziale e TEM ed è stato studiato l'effetto dell'autoassemblaggio con diverse concentrazioni di PBS. La formazione per autoassemblaggio delle nanoparticelle e l'interazione con le lectine è stata studiata mediante spettroscopia di correlazione di fluorescenza (FCS) e spettroscopia di correlazione incrociata di fluorescenza (FCCS). Per eseguire questi studi, la poli(allil)ammina cloridrato è stata marcata in modo fluorescente, per poi essere fatta reagire con i derivati PEG e glicani.

Resumen

Las nanopartículas de oro (AuNP) son nanomateriales con excelentes propiedades fisicoquímicas y ópticas para una amplia gama de aplicaciones. La funcionalización de la superficie de las AuNP permite la formación de gliconanoparticulas de oro (GAuNP). Las propiedades de multivalencia características de las gliconanoparticulas que permite la presentación, en gran cantidad de carbohidratos. La multivalencia puede desencadenar el efecto cluster glicosídico (*cluster glycoside effect*). Este efecto permite mejorar la baja afinidad entre las interacciones individuales de carbohidratos y proteínas permitiendo la interacción de varios carbohidratos a la vez con las proteínas. Durante los últimos años se ha demostrado que estas nanopartículas son excelentes candidatas para el *targeting* de lectinas entre otras aplicaciones biológicas.

Además, las AuNP cuando están en contacto con medios biológicos interactúan con las proteínas presentes formando la proteína corona (PC) que tiene un efecto en el destino final y la eficacia de las NP. El estudio de la formación de la PC de las nanopartículas es de suma importancia para asegurar la actividad de las AuNPs. La formación de PC se puede modular con el recubrimiento de la superficie, el tamaño y la forma de las nanoparticulas. Ligandos como, por ejemplo, el polietilenglicol (PEG) pueden prevenir la formación de PC y el consiguiente reconocimiento por parte del sistema inmunitario y la eliminación del organismo. Además, el recubrimiento de con carbohidratos de las AuNP también puede modular la composición de la PC y, por lo tanto, se puede modificar la biodistribución de las GAuNP.

El segundo capítulo de esta tesis consiste en un estudio de biodistribución en ratones sanos de nanopartículas de oro ultra pequeñas (UAuNPs) recubiertas con cadenas de PEG de diferente longitud y/o con α-galactosa unida a un ligando alifático corto. Las UAuNPs se sintetizaron utilizando un reactor de sobremesa y fueron inyectadas en ratones sanos. El hígado, los riñones y el bazo se recogieron después de 1, 4 y 24 horas. A continuación, los órganos se digirieron y el contenido de oro se analizó mediante Induced Coupled Plasma Optical Emission Spectroscopy (ICP-OES). Por otro lado, los órganos seleccionados fueron teñidos con plata por auto metalografía (AMG) y analizados por microscopía. Además, los órganos se inmuno tiñeron para detectar las nanoparticulas mediante microscopía co-focal.

Las UAuNPs recubiertos únicamente por PEG_{5000} presentaron el mayor tiempo de circulación en el cuerpo, como se esperaba. Además, las UAuNPs recubiertos con una mezcla de PEG_{500} y α-$Gal-C_2$ tuvieron un tiempo de circulación similar. Estos resultados prueban que la longitud de la cadena PEG es importante pero no el único camino a seguir para extender la vida media de las UAuNPs. Además, las UAuNPs cubiertas con PEG se post-funcionalizaron con α-manosa y se observó una variación en la biodistribución, las UAuNPs se acumularon menos en el hígado y los riñones. Los estudios de AMG demostraron que las UAuNPs funcionalizadas con manosa mostraron una distribución distinta dentro del hígado.

Los sistemas de micro fluidos han llamado la atención de numerosos investigadores en los últimos años por sus grandes ventajas en comparación con los procedimientos de síntesis por tradicionales de AuNPs. Estos sistemas ofrecen varias ventajas como un mejor control sobre los parámetros de la reacción, una mayor reproducibilidad entre lotes y un escalado simple. Los

sistemas de micro fluidos permiten sobreponerse a los inconvenientes que se presentan cuando la síntesis de nanoparticulas es trasladada desde la investigación a ensayos clínicos. Por ello, nuestro grupo se ha centrado en el desarrollo de procedimientos micro fluídicos para la obtención de AuNPs de diferentes tamaño y forma.

En el Capítulo 3 se describió un nuevo procedimiento micro fluídico foto inducido para obtener gliconanopartículas de oro de 2 nm. Este sistema permite una síntesis de GUAuNPs *one-pot* evitando el uso de tensioactivos y agentes reductores. El nuevo procedimiento aprovecha la foto reducción de Au con una lámpara UV en presencia de etanol, que en este caso actúa como foto iniciador. Una gran ventaja del procedimiento es la posibilidad de recuperar los preciados derivados de carbohidratos que no han reaccionado en el paso de purificación debido a la ausencia de agentes reductores en la reaccion. La amplia aplicabilidad del sistema se demostró mediante la síntesis de una pequeña serie de UAuNPs recubiertas con α-manosa, β-glucosa y lactosa usando dos tipos de ligando uno anfifílico y uno corto alifático. El sistema se probó además con un ligando hidrofílico más largo, en este caso PEG_{5000} y α-galactosa-PEG_{5000}. Obteniendo con éxito en todos los casos GUAuNPs de 2 nm.

Además, el cálculo de la carga final de las NP es crucial según la bio aplicación final. Por tanto, se realizó un análisis cuantitativo por ^{1}H-NMR de las nanoparticulas y se obtuvo una correlación lineal entre los ligandos añadidos en la solución inicial y los ligandos presentes en la superficie de las UAuNPs independientemente del tipo de carbohidrato.

Se empleó un sistema de micro fluidos similar desarrollado por nuestro grupo en los últimos años para la síntesis de una pequeña serie de gliconanoparticulas (GAuNP) esféricas y en forma de estrella. Se utilizaron los mismos carbohidratos descritos anteriormente. La estabilidad a largo plazo de los GAuNP en diferentes medios (agua, PBS, FBS y RPMI) se analizó mediante *dynamic light scattering* (DLS) y *ζ-potential*. En estos análisis se observó la variación del diámetro hidrodinámico para determinar la formación de una capa de *soft corona* y *hard corona*.

El último capítulo describe el trabajo realizado durante la estancia realizada en CIC BiomaGUNE (San Sebastián, España) bajo la supervisión de Sergio Moya. En este proyecto se sintetizaron *PEGylated glyco poly(allyl)amine phosphate NPs.*

La PEGilación de nanopartículas de poly(allyl)amina fosfato (PANs) había sido realizada previamente por el grupo de Sergio Moya. Las PANs funcionalizadas con PEG presentaron varias ventajas en comparación con los PANs. Entre ellas la toxicidad nanoparticulas disminuyo, la circulación en el cuerpo se había extendido, tenían un tamaño más pequeño y la carga superficial se redujo a aproximadamente cero. Las características de estas nanoparticulas también impiden la unión inespecífica a las proteínas.

Por lo tanto, para lograr la especificidad hacia algunas lectinas como Con-A y Jacalin, se sintetizó una serie de PEGylated glyco-poly(allyl)amine nanoparticles. Las nanoparticulas se sintetizaron mediante química de carbodiimida con compuestos PEG hetero bifuncionales de dos longitudes diferentes y α-manosa, β-glucosa y lactosa unidos a un ligando anfifílico. Las nanoparticulas se analizaron por DLS, ζ-potencial y TEM y se estudió el efecto del auto ensamblaje con diferentes concentraciones de PBS. La formación por autoensamblaje de las nanopartículas y la interacción con las lectinas se estudió mediante *fluorescence correlation spectroscopy* (FCS) y *fluorescence cross-correlation spectroscopy* (FCCS). Para realizar estos estudios, el polímero de partide fue etiquetado con un fluorescente previo a la reacción con PEG y carbohidratos.

Chapter 1

Introduction

1.1 Nanotechnology and nanomedicine

Nanotechnology has been an emerging research field in the last two decades, it enables the production, measurement and manipulation of materials conducted at nanoscale (1 – 100 nm),[1] these materials are denominated nanomaterials. Nanomaterials are identified by three main aspects: size, particles size distribution, and surface area. In order to consider them nanomaterials, more than 50 % of the particles should be in the size range of 1 – 100 nm.[2]

Nanotechnology has been identified in the EU as a ''Key Enabling Technology capable of providing new and innovative medical solutions both for therapeutics and diagnostics for the benefit of patients'.[3] Nanomaterials have been proved to be optimum candidates for therapeutical and diagnostic purposes as they can be applied at biological processes which take place at nanostructure level.[2]

The use of nanotechnology in medicine is denominated nanomedicine. Nanomaterials can be exploited as nanomedicines for therapeutical purposes as for example drug delivery. Diseases such as cancer, where the main challenge of current treatments is the delivery of the drug in the tumour, can benefit from the robust properties of nanoparticles (NPs). NPs can enhance the solubility of the drugs, deliver the drug in the target site, and protect the drug from degradation, as well as decreasing the toxicity of the drug. Furthermore, nanomaterials can also be used for theragnostic purposes, bioimaging and biosensors because of their optical, and physicochemical properties which are not found in their bulk counterparts. Some of these properties are high-surface-to-volume ratio, unique magnetic and mechanical behaviours and high surface energy.[4,5] At the moment there are 70 nanomedicines approved by the Food and Drugs Administration (FDA) and the European Medicines Agency (EMA), including nanocrystals, lipid NPs, polymer NPs, dendrimer-based NPs, protein NPs and inorganic NPs[6] (Figure 1.1). The nanomedicines approved by FDA and EMA in the last 15 years are shown in table 1.1.
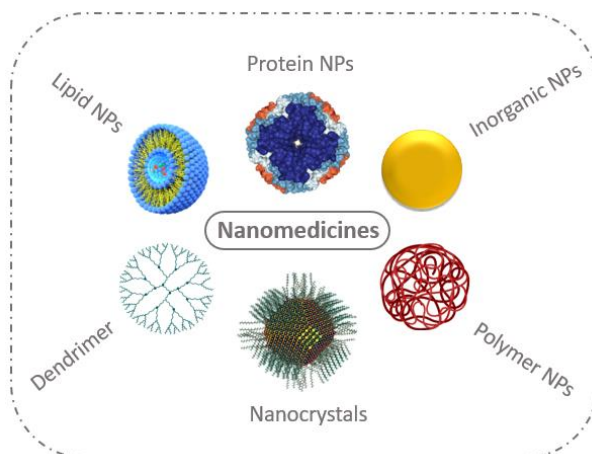

Figure 1.1. *FDA/EMA approved Nanomaterials*

Type	Trade name	Company	Date of approval	Indication
Nanocrystals	Ivemend®	Merk & Co. Inc.	FDA, EMA (2008)	Antiemetic drug
	Rapamune®	Wyeth Pharmaceuticals Inc.	FDA (2010)	Prevents rejection of kidney transplants
	Rapamune®	Wyeth Pharmaceuticals Inc.	FDA (2015)	A rare progressive lung disease (lymphangioleiomyomatosis)
	Focalin XR®	Novartis	FDA (2008)	ADHD in children
	Invega®	Janssen Pharmaceuticals	FDA (2009)	Schizophrenia
	Equivabone®	Zimmer Biomet	FDA (2009)	Bone substitute
	Ryanodex®	Eagle pharm	FDA (2014)	Malignant hyperthermia
Lipid NPs	Lipodox®	Sun Pharma Global FZE	FDA (2013)	Metastatic ovarian cancer, HIV-associated KS
	Onivyde®	Merrimack Pharmaceuticals	FDA (2015)	Metastatic pancreatic cancer
	Mepact®	Takeda France SAS	EMA (2009)	Osteogenic sarcoma
	Marquibo®	Talon therapeutics	FDA (2012)	Philadelphia chromosome-negative chronic myelogenous leukaemia in adult patients
	Onpattro®	Alnylam	FDA, EMA (2018)	Hereditary transthyretin mediated amyloidosis
	Lipusu®		FDA (2016)	Breast cancer, non-small-cell lung cancer
	Vyxeos®	Jazz Pharmaceutics	FDA (2017), EMA (2018)	Acute myeloid leukaemia
	Pfizer-BioNTech vaccine	Pfizer Pharmaceuticals	FDA (2020)	Prevents COVID-19 infection
	Moderna COVID-19 vaccine	Moderna TX Inc.	FDA (2020)	Prevents COVID-19 infection
Polymer NPs	Apealea®	Oasmia Pharmaceutical	EMA (2018)	Ovarian cancer, peritoneal cancer, fallopian tube cancer
	Oncaspar®	Enzon Pharmaceuticals Inc.	FDA (1994), EMA (2016)	Acute lymphoblastic leukemia, chronic myelogenous leukemia
	Genexol-PM®	Lupin Ltd.	FDA (2007)	Breast cancer
	Mircera®	Vifor	FDA (2018)	Anemia
	Rebinyn®	NovoNordisk	FDA (2017)	Hemophilia B
	Zilretta®	Flexion Therapeutics	FDA (2017)	Knee osteoarthritis
Protein NPs	Abraxane®	Celgene Pharmaceutical Co. Ltd.	FDA (2005, 2012, 2013),EMA (2008)	Metastatic breast cancer (2005), lung cancer (2012), and metastatic pancreatic adenocarcinoma (2013)
Inorganic NPs	Ferinject®	Vifor	FDA, EMA (2013)	Iron deficit anemia
	Ferrlecit®	Sanofi-Aventis	EMA (2013)	Iron deficiency

Table 1.1. FDA/EMA approved Nanomaterials since 2007

The latest nanomedicine approved by the FDA, is a lipid nanoparticle encapsulating a mRNA-based vaccine against SARS-CoV-2 virus. The COVID-19 vaccine, produced by Pfizer and Moderna, has proven the relevance of nanomedicines nowadays. The lipid NP vaccines have been demonstrated to be more effective than the conventional vaccines, in this case of the AstraZeneca vaccine. This has proven the technological advancement occurred in the recent years and the exceptional advantages of nanomedicines. Lipid NPs encapsulating mRNA require short development time due to the low-biosafety requirement and rapid scalability, therefore these NPs are excellent candidates for a more accessible vaccine.[7]

Among the other FDA approved nanomedicines, twenty-three polymer NPs nanomedicines have been approved in the past 20 years by FDA and EMA, these NPs allow the encapsulation of drugs or biological molecules. In the case of inorganic NPs, only nine nanomedicines have been approved as they present more challenges as slow dissolution and lack of biodegradation.

One of the main challenges encountered for the approval of nanomedicines is the lack of defined guidelines from the regulatory entities as EMA and FDA. Moreover, the nanomedicines are defined by FDA as a combination of products.[8] This means the approval of nanomedicines by FDA present a big number of challenges as each part of the NPs must be evaluated independently from the others.

Throughout this thesis glyco-gold nanoparticles as well as glyco-polyamine phosphate nanoparticles were developed.

1.2 Gold nanoparticles

Gold-based NPs (AuNPs) are nanomaterials which have been widely researched in the past 20 years, due to their unique features, that comprise optoelectronic properties, stability, biocompatibility and low toxicity.[9] Moreover, AuNPs morphology can be tuned to obtain different size, shape, while a robust surface chemistry allows to display on their shell several copies of molecules and ligands. All these factors contribute to the broad range of applications in which AuNPs can play relevant roles.

The most known property of AuNPs is the localised surface plasmon resonance (LSPR), which refers to the optical absorption and scattering of the electromagnetic radiation at a specific wavelength range. The surface plasmon resonance is strictly dependent to the AuNP morphology and can be modified with the different sizes and shape of AuNPs (figure 1.2).

The strong bond between gold and sulphur allows the surface functionalization of the NPs with a wide range of ligands depending on their final application. Furthermore, the surface can be coated with biomolecules as glycans,[10] peptides[11] and antibodies[12] among others.
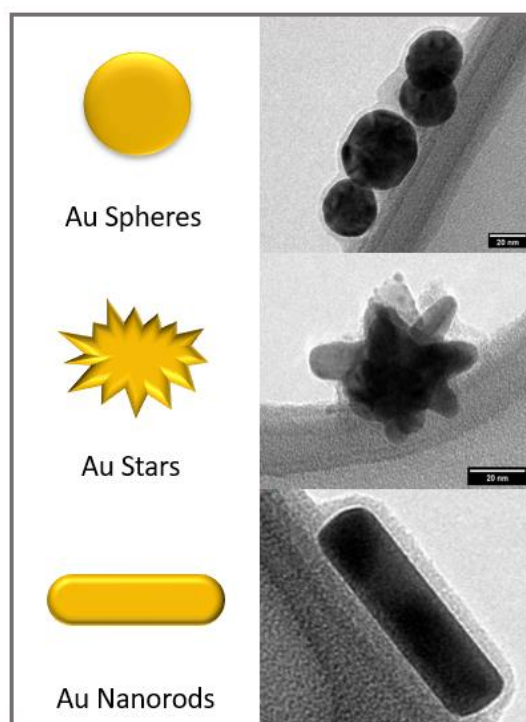
Figure 1.2. *Different shapes of AuNPs*

1.2.1 Gold nanoparticles biological applications

AuNPs can be used for a substantial number of biological applications due to their physicochemical and optical properties. These are some of the applications reported in the past years:

- **Bioimaging**

One of the applications in bioimaging of AuNPs is as contrast agents for computational tomography (CT). CT is an imaging technique based on X-rays, it enables the visualization of bones and mineralized tissue but, in order to distinguish among the soft issues, contrast agents are needed. The high electron density and atomic number characterize gold with a high X-ray absorption coefficient. Therefore, AuNPs are excellent candidates as contrast agents for CT. The first study of AuNPs as contrast agents was published by Smilowitz and co-workers,[13] they demonstrated the pharmacokinetic advantages of AuNPs compared to other contrast agents.

- **Biosensing**

AuNPs can be used as biosensors due to their optical properties. The SPR properties of the AuNPs are dependent on the size and shape, the change in the NPs size can result in a colour change which can be observed by naked eyes.[14] This property enables the production of biosensors. Functionalized AuNPs have been widely used to detect DNA pathogens due to its rapid and easy detection way.[15,16] Biosensors to detect cancer biomarkers have also been developed in the recent years.[12,17]

- **Drug Delivery**

AuNPs are well known for their advantages as drug delivery agents due to its properties as biocompatibility, low toxicity, and high surface to volume ratio. Recently AuNPs have been

4

employed for the treatment of neurodegenerative diseases for their high compatibility with the drugs. Several studies demonstrate that AuNPs are excellent candidate as drug carriers for neurodegenerative diseases as they avoid the drugs losing their.[18] Moreover AuNPs have been employed for the delivery of chemotherapeutics as methotrexate, doxorubicin and paclitaxel.[19–21]

1.2.2 Wet chemistry synthesis gold nanoparticles

The classical and most common synthetic method to produce AuNPs is the wet chemistry synthesis, which consists in the reduction of Au^{+3} salts to Au^0 using reducing agents, as for example sodium citrate (Na_3Ct), ascorbic acid (AA) or sodium borohydride ($NaBH_4$). Tetra chloroauric acid ($HAuCl_4$) is the common Au source used for these synthetic procedures. Depending on the reducing agents, different methods have been developed and tuned to obtain different sizes and shapes of AuNPs.

The two main synthetic methods, commonly used, are known as the Turkevich (1951)[22] and Brust-Schiffrin (1994).[23] Over the years these methods have been slightly improved with different modifications, in some cases the procedure has been modified in order to avoid the use organic solvents or harsh conditions.

- **Turkevich method**

The Turkevich synthetic method was developed in 1951 and consists in the reduction of the Au salts with trisodium citrate (Na_3Ct: this was the first method developed to obtain colloidal gold). This method was further improved by Frens in 1973[24].The empiric procedure is simple and has proven good results, it consists in the reduction of tetra chloroauric acid in a boiling water solution with trisodium citrated in a one-step synthesis, obtaining NPs with a size range of 10 - 50 nm, depending on the gold/citrate ratio. Sodium citrate was proven to act as a reducing agent and a stabilizer, capping the surface of the NPs and controlling in this way the growth of the NPs and the aggregation. The mechanism of the reduction of gold with citrate involves several steps as shown in figure 1.3.[25]
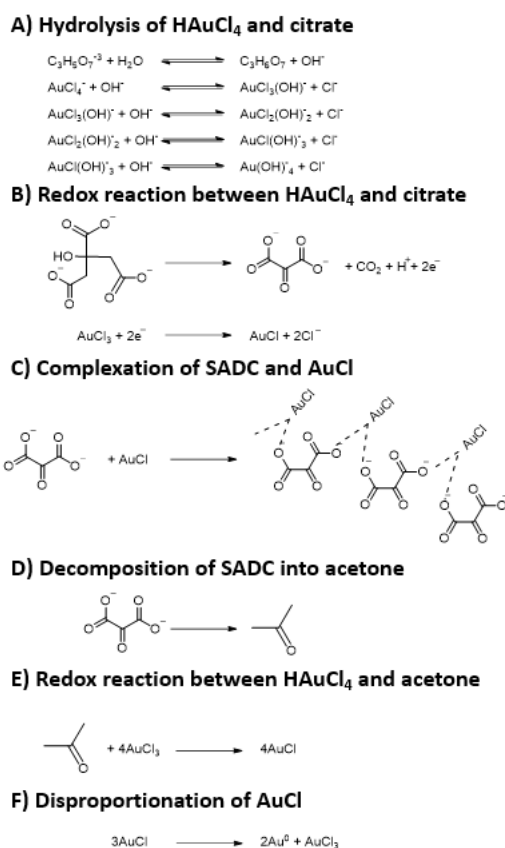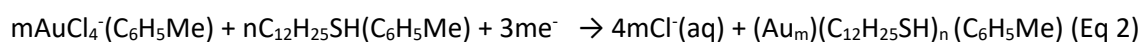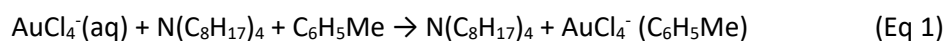
A) Hydrolysis of HAuCl₄ and citrate

$$C_3H_5O_7^{-3} + H_2O \rightleftharpoons C_3H_6O_7 + OH^-$$
$$AuCl_4^- + OH^- \rightleftharpoons AuCl_3(OH)^- + Cl^-$$
$$AuCl_3(OH)^- + OH^- \rightleftharpoons AuCl_2(OH)_2^- + Cl^-$$
$$AuCl_2(OH)_2^- + OH^- \rightleftharpoons AuCl(OH)_3^- + Cl^-$$
$$AuCl(OH)_3^- + OH^- \rightleftharpoons Au(OH)_4^- + Cl^-$$

B) Redox reaction between HAuCl₄ and citrate

$$AuCl_3 + 2e^- \rightarrow AuCl + 2Cl^-$$

C) Complexation of SADC and AuCl

D) Decomposition of SADC into acetone

E) Redox reaction between HAuCl₄ and acetone

F) Disproportionation of AuCl

$$3AuCl \rightarrow 2Au^0 + AuCl_3$$

Figure 1.3. Mechanism of formation of AuNPs in the Turkevich method.[25]

- **Brust-Schiffrin method**

In 1994 Brust and Schiffrin established a new synthetic protocol for the synthesis of smaller NPs. In this case NaBH₄, a stronger reducing agent, was used to obtain NPs with the size range of 3-8 nm. The method consists in reducing the gold salt to obtain metallic clusters and simultaneously functionalize the NPs with thiol monolayers, this procedure was possible as it was performed in a two-phase system, of water and toluene. Tetraoctylammonium bromide (TOAB) was used as a phase transfer reagent, in this way $AuCl^{-4}$ passed from the aqueous solution to toluene and was reduced by sodium borohydride in the presence of an aliphatic thiol chain. The reaction is described in the following equations:

$$AuCl_4^-(aq) + N(C_8H_{17})_4 + C_6H_5Me \rightarrow N(C_8H_{17})_4 + AuCl_4^- (C_6H_5Me) \qquad \text{(Eq 1)}$$

$$mAuCl_4^-(C_6H_5Me) + nC_{12}H_{25}SH(C_6H_5Me) + 3me^- \rightarrow 4mCl^-(aq) + (Au_m)(C_{12}H_{25}SH)_n (C_6H_5Me) \text{ (Eq 2)}$$

Even though these are very well stablished methods, batch synthetic procedures present several disadvantages as low reproducibility and they are dependent on the operator, therefore in order to synthesize AuNPs in bigger scale flow chemistry systems have shown numerous advantages.

1.2.3 Microfluidic synthesis

Since 1990s a significant number of researchers have focused on the development of microfluidic synthetic procedures of NPs.[26] Microfluidic systems are a promising technology to synthesize AuNPs as they present several advantages as a better control in the reagent mixing

and reaction parameters, this enhances a higher reproducibility between batches. Moreover flow reactors allow an improved mass to heat transfer and a simple scale-up without causing aggregation or polydispersity.[27,28]

Microfluidic systems are expected to accelerate the transition of AuNPs used for biological applications to clinical trials, as they offer a higher control over the reaction parameters, an easy scale-up; moreover the protocols afford reproducible NPs and are also economical.[29]

The synthesis of AuNPs consists in two main steps, nucleation and particle growth, these steps in batch synthesis are simultaneous and lead to variations between batch to batch as they cannot be controlled. Microfluidic systems enable the separation of the two steps and therefore they provide a better control in the morphology, size distribution and size. [29]

Microfluidic synthesis of AuNPs can be performed by different techniques. The droplet mixing technique has been widely used as the reactions can be performed in picolitre sized droplets this prevents the interactions between the reagents and the walls. Lazarus et al. developed a two-phase microfluidic system to synthesize Au and Ag NPs using a T-junction device, the NPs were synthesized in an ionic liquid which enhanced the stability of the NPs.[30]

Our group developed in the past years a microfluidic system based on a syringe pump and a T junction to obtain isotropic and anisotropic AuNPs,[31] by modulating the formulation of the initial solutions inserted in the syringe pump and the ratio between the gold precursor and the reducing agents. Moreover modifying the formulation hybrid nanomaterials[32] could also be obtained.

One of the major advantages of microfluidic systems is the implementation of analytical techniques directly in the systems,[33,34] this offers a better control of the synthesis and a rapid response to modify the parameters if needed which could mean reduction of the time and cost of the development of NPs.

Overall, microfluidic systems present numerous advantages compared to conventional batch synthetic procedures.

1.2.3.1 Photo-induced microfluidic synthesis

All the above-mentioned synthetic procedures involve the use of reducing agents in order to obtain colloidal gold, reducing agents can be toxic therefore in the past years other reducing procedures have been developed to obtain a green synthetic procedure. Photo chemical reduction of HAuCl$_4$ under UV irradiation enables the formation of AuNPs, this method has been used in the recent years by different researchers.[35,36] Photoreduction methods avoid the use of toxic reducing agents, these methods are mostly performed at room temperature and offer a spatial and temporal control[37] of the reaction therefore these procedures are considered very advantageous. Harada et al in 2009 studied the reduction mechanism of Au and the particles formation by Uv-vis and the laser-induced transient grating (TG)[36] and by X-ray absorption fine structure (XAFS)[38] measurements. All studies were performed in a water ethanol Au solution containing poly(N-vinyl-2-pyrrolidone) (PVP), they demonstrated that AuCl$_4^-$ (Au^{3+}) is reduced to AuCl$_2^-$(Au$^+$) in few minutes when exposed to a UV lamp of 500 W, while the reduction from AuCl$_2^-$ (Au$^+$) to Au^0 is a slower process. Following the reaction by UV-vis, AuCl$_4^-$ displays an absorption band around 320 nm, which is attributed to the ligand to-metal charge transfer (LMCT), after

few minutes of irradiation the absorption band disappears and after 30 min the plasmon absorption peak at 545 nm appeared, and its intensity gradually became higher until the irradiation time of 60 min. The maximum peak is shifted to 530 nm when the irradiation time is over 240 min.[38] The photoreduction of Au can also be followed by the changes in colour, $AuCl_4^-$ shows a light yellow colour before irradiation, the solution turns transparent and when the AuNPs are formed it becomes purple.

In this thesis a new synthetic procedure is proposed exploiting the advantages of photo-induced reduction of gold and microfluidic systems to obtain glyco-gold NPs (GAuNPs).

1.3 Biomolecular Corona

Nanomaterials in contact with biological fluids, as for example human plasma, undergo a phenomenon where the NP surface is covered by biomolecules. This coating shell formed is denominated protein corona.[39] The protein corona is formed by two layers: the hard corona (HC) and the soft corona (SC) (figure 1.4). The hard corona consists in a layer of proteins located near to the NPs. The HC is formed by proteins tightly absorbed on the NPs, even though this bond is not irreversible. A second layer of proteins is formed covering the hard corona, the so-called soft corona. The SC is a dynamic layer with a lower affinity towards the NPs, which present a faster protein exchange rate.[40]
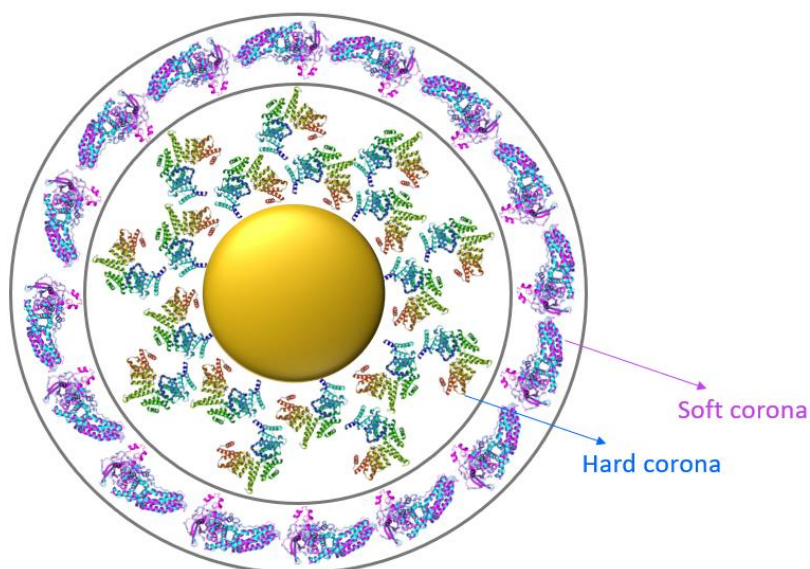

Figure 1.4. Protein corona layers: hard corona (HC) and soft corona (SC)

The protein corona formation varies in every case depending on the size,[41] the shape,[42] and the surface coating[43] of the NPs. Regarding the size the tendency observed is that the higher the total surface area more proteins are adsorbed, therefore smaller NPs present a higher number

of proteins. Nevertheless, ultra-small NPs with a diameter of 2 nm, do not present a HC and only present a pseudo-protein corona layer.[44]

The morphology of the NPs has a significant impact on the protein adsorption. Spherical NPs present a lower affinity towards proteins compared to nanorods[42] and nanostars.[45] Moreover the NPs surface charge can modulate the protein corona formation as neutral NPs have shown a lower interaction with proteins compared to charged NPs.[46] Hydrophobicity is another important feature to take into account, as the less hydrophobic NPs the lees amount of proteins are bound. The hydrophobicity can be regulated with the coating of the NPs with linkers as for example poly(ethylene glycol) (PEG).[46]

Apart from the NP characteristics, the effect of the protein corona depends on the proteins that are adsorbed. The protein corona composition can affect the final fate of the NPs in biodistribution studies as it can vary the half-life of the NPs, the immune response as well as the clearance pathway. Some proteins as albumin can increase the circulation time of the NPs.[47] On the other hand opsonins can enhance the clearance of the NPs by triggering phagocytosis.[48]

In the last years the protein corona formation has been studied after modification of the surface coating with polymers. For example PEG and polyphosphoester (PEEP) have been proven to reduce the amount of proteins adsorbed as well as modifying the corona composition to prevent the non-specific cellular uptake.[49]

Overall, the study of the protein corona formation in NPs is very important as the interaction with the physiological environment can modify the biodistribution of the NPs as they gain a new biological identity.

1.4 Glyco-gold nanoparticles

Carbohydrates are one of the main class of biomolecules alongside with nucleic acids, proteins and lipids. Carbohydrates are of great interest as they play key roles in physiological processes, they are present in all human cells forming the so called glycocalyx and therefore are involved in cell-environment interactions as well as in cell-cell interactions.[50–52] The multivalent presentation of glycans overcomes the weak protein-carbohydrate and carbohydrate-carbohydrate interactions and can trigger the cluster glycose effect.[53]

Carbohydrates present several advantageous to be used in nanomaterials as for example: chemically well-defined structures, hydrophilicity, biocompatibility, they are biodegradable and prevent the aggregation of the NPs.[54] Gold NPs surface can easily be modified by exploiting the strong interactions between gold and sulphur, therefore they are perfect candidates for multivalent glyco-systems, in this way the carbohydrates can be bound to the gold through a thiol linker and be exposed in the surface, moreover a wide range of thiol linkers can be used depending on the application of the glyco-AuNPs (GAuNPs).

GAuNPs are able to mimic the natural design of cells, allowing a multivalent presentation of carbohydrates on the surface of the gold NPs. GAuNPs were first introduced by Penadès group

in 2001[55], they described a one-pot method to synthesize GAuNPs, which consists in a modification of the Brust-Schiffrin method adding thiol-ending glycol conjugates in the presence of Au salts and $NaBH_4$. Moreover this method allows the functionalization of the surface with other ligands or molecules as fluorescent molecules, DNA, RNA or peptides for example.[10,55,56] This is the more direct synthetic method developed until now, even though GAuNPs can also be obtained in two steps: the first step consisting in the synthesis of AuNPs by any of the above mentioned methods containing stabilizers as citrate or phosphine and a second step of liquid phase ligand exchange (LPE) with thiol-ending carbohydrate molecules.[57–59] Furthermore, there is a third synthetic strategy to obtain GAuNPs which consists in the chemical conjugation of carbohydrates to the linkers displayed on the surface of the previously synthesized AuNPs, this is the so-called post-functionalization of AuNPs. The post-functionalization can be performed by exploiting different orthogonal chemical reactions as click reaction[60], amidation[61], conjugation via carbodiimide[62] or pentafluorophenol (PFP) among others. Even though this procedure is longer than the one developed by Penadés and co-workers this procedure allows the conjugation of glycans to the NPs using lower amount of precious glycan residues, all three methods are represented in Table 1.2.
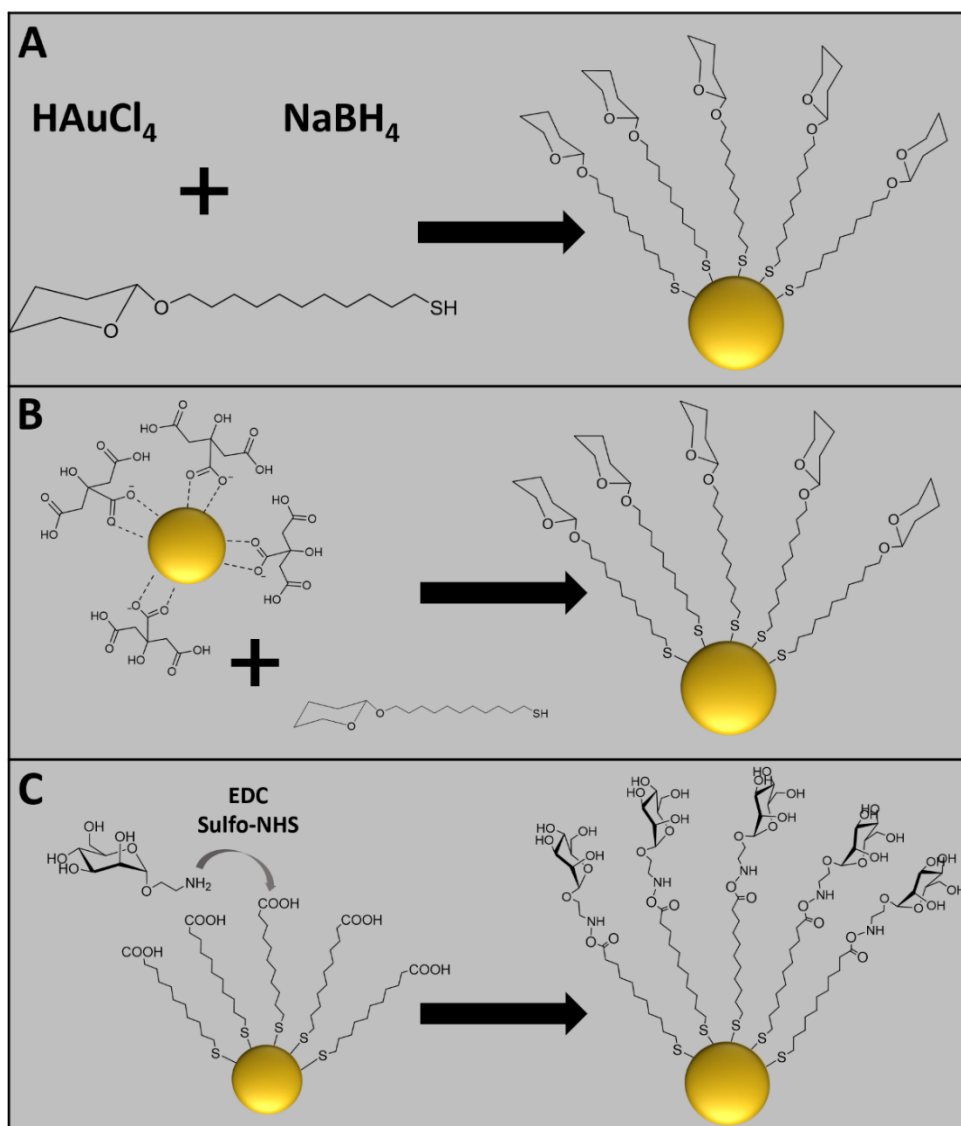
Table 1.2. *Synthetic procedures of GAuNPs. A) Penadés synthetic procedure B) Citrate AuNPs + LPE C) Post-functionalization of AuNPs*

1.4.1 Biological applications of glyco-gold nanoparticles

GAuNPs have a wide range of applications due to their high surface to volume ratio which enables the multivalent presentation of glycans which overcomes the low affinity of individual protein-carbohydrate interactions.[53] The final bio-application of the GAuNPs is determined by the structural properties as size, morphology, and surface.

The metallic core size can modulate the optical properties, AuNPs with a core diameter smaller than 2 nm are luminescent in the near infrared region (NIR),[63] the photoluminescence enabled the study of the internalization pathway of the NPs in dendritic cells,[64] as the light emitted is much stronger than the one obtained by a fluorescent dye the AuNPs can be followed employing confocal laser microscopy, flow cytometry or even dark field microscopy.[65,66]

However, AuNPs with a diameter >2 nm do not present photoluminescence, but they show a localized surface plasmon resonance (LSPR) ~ 520 nm which can be modulated through the

visible and near IR spectra. In the case of spherical NPs, the LSPR is located around 520 nm however anisotropic NPs show and intense absorption in the IR optical window, which enhances the intensity of Raman signals near the AuNPs and therefore can be used for diagnostics using techniques as surface enhanced Raman spectroscopy (SERS).

In the past years the effect of the shape of GAuNPs has been studied by different groups, Li et al. studied the effect of the immunological response depending on the shape of the NPs, they concluded that spherical and cylindrical GAuNPs are internalized through different endocytosis pathways and therefore spherical NPs are internalized in a bigger extent. The shape of the NPs has also an effect on the immunological response: spherical and short cylindrical GAuNPs have a similar immunological response while long cylindrical GAuNPs can induce a more efficient inflammatory response.[67] The shape of GAuNPs has a significant effect on the carbohydrate-protein interaction as it was examined by Chaudhary et al. in the first studied they demonstrated that nanorods functionalized with mannose had better affinity towards bacteria compared to star shaped and spherical AuNPs functionalized with mannose,[68] in a second study the different shape GAuNPs were injected to zebrafish and it was proven that rod shaped NPs had a faster clearance and uptake while star shaped NPs had a longer half-life.[69,70]

Furthermore, the carbohydrate density and linker nature are also very important features which can affect the binding affinity towards lectins, the most common carbohydrate binding proteins. Several research groups have studied the influence of the density of carbohydrates exposed on the NPs in the interactions with bacteria and lectins [50,56,71,72] proving that high density of carbohydrates doesn't translate into a higher binding affinity as lectins present different subunits which are separated by a determined distance. Therefore, it is suggested to synthesize the GAuNPs with a lower density of precious carbohydrates combined with linker without any active targeting molecule or other biomolecules as for example peptides or fluorescent probes.[50]

Longer linkers have been demonstrated to be the best spacers as they give a better access to the protein pockets and provide a higher stability to the NPs.[73] However not only the length of the linker is crucial but also the nature of the linker, Geourgiou et al investigated the effect of using poly(N-(2-hydroxypropyl)-methacrylamide (PHMA) and poly(N-hydroxyethyl acrylamide) (PHEA) with a terminal galactosamine by studying the binding affinity and the aggregation of the NPs using biolayer interferometry and UV-vis analysis, they concluded that PHMA showed a similar binding affinity than PHEA but avoided the aggregation.[74]

In summary its crucial to deeply study the design of the GAuNPs as this can have a great impact in their behaviour and consequently in their bio applications.

1.4.1.1 Glyco-gold nanoparticles in diagnosis

Several studies have proven that GAuNPs are pivotal candidates for diagnosis of numerous diseases as for example cancer. Heparin-dye mobilized gold NPs were developed by Lee et al for the theragnostic of metastatic cancer, the NPs enhanced fluorescent signals by specific cleavage of heparin by heparinase which is secreted by metastatic cancer cells. In a second step the NPs were functionalized additionally by a PEG-RGD ligand which proved highly specific apoptotic activities for cancer cells presenting over-expressed RGD receptors.[75] Gwan Park's group also studied the diagnosis application of near-infrared fluorescence (NIRF) dye labelled hyaluronic acid functionalized AuNPs for the detection of reactive oxygen species (ROS). ROS and

hyaluronidase are rheumatoid arthritis and metastatic cancer biomarkers, during the study it was proven that the NPs could detect arthritis within 6 hours after the intravenous injection and human ovarian cancer in 4 hours.[76] In 2020 after the pandemic of COVID-19 started there was a huge need for a diagnostic tool accessible to everybody without the need of dedicated laboratory facilities and trained personnel as it's the case for RT-PCR (reverse transcription polymerase chain reaction). Therefore, Gibson's group developed a novel COVID-19 detection platform which consists in a lateral flow device (LFD). AuNPs were functionalized with sialic acid polymer ligands and were the mobile phase of the LFD for their high binding affinity towards SARS-COV-2 virus.[77] This group also developed a lateral flow glyco-assay in order to detect lectins which could be further used for diagnostics.[78]

GAuNPs have also been proven to be excellent contrast agents, Polito and co-workers exploited the gold high X-ray absorption to create computed tomography (CT) contrast agents by synthesizing glucosamine AuNPs which can target glucose receptors present in damaged lung from pneumonia.[57] Gadolinium complexes are extensively used as contrast agents for magnetic resonance imaging (MRI), therefore Candiota et al. synthesized GAuNPs decorated with Gd^{+3}, the glycan surface of the NPs enabled the targeting properties and the Gd^{+3} acted as the MRI contrast agent.[79]

Penades and co-workers designed ^{68}Ga labelled glyco-gold NPs combining the radioactivity of the chelator gallium-68 and enabling the cross of the blood brain barrier (BBB) through the surface modification of the NPs with glucose and BBB-permeable neuropeptides. This study proved that positron emission tomography (PET) is highly sensitive technique that allows the evaluation of the BBB permeability of the GAuNPs.[80]

1.4.1.2 Glyco-gold nanoparticles as therapeutics

During the last years researchers have shown a great interest in the bio applications of GAuNPs as therapeutics, being the majority focused on treatments for cancer as it's one of the main causes of death in the world.[81] Cancer cells present specific lectins differing from the ones in healthy cells,[82] these lectins have high affinity towards carbohydrates.[83] Therefore, researchers have focused their effort in the past years in the synthesis of GAuNPs to enable the targeting of cancer cells and consequently investigating new treatments for cancer. Yi et al. exploited the affinity of glucose towards glucose transporter 1 (GLUT1) overexpressed in breast cancer cells and achieved in this way the delivery of siRNA to the cancer cells.[84] Glucose was conjugated to the gold NPs by a PEG chain, which enables the water solubility of the NPs, this chain was linked to a poly-lysine of 40 units and a final lipoic acid providing the thiols binding the gold. The lysine is used to introduce siRNA in the GAuNPs.[84] In this study they proved the specifically targeting of GLUT1 with glucose AuNPs. Garcia Calavia et al. performed a study with AuNPs functionalized with lactose to target galectin-1, a lectin expressed in breast cancer cells. The NPs carried the disaccharide lactose, bond to a short PEG linker and phthalocyanine, a photosensitizer for photodynamic therapy.[85]

The application of GAuNPs for immunotherapy treatments has also been deeply studied as it has become a powerful strategy to treat cancer and infectious diseases. Recently Hiroyuki-Shinchi et al. have published a study in which GAuNPs functionalized with α-Mannose and toll-like receptor 7 (TLR7) ligand showed a higher immunostimulatory effect than the unconjugated

ligand. TLR7 is located in the endosomal compartment of the immune cells therefore a carrier as GAuNPs is needed to improve the efficiency of the TLR7 ligand.[86] In the first article they demonstrated these NPs were safe and effective adjuvants for vaccines for cancer and infectious diseases, in a second study they demonstrated the impact of the linker length bond to the TLR7 ligand attached to the nanoparticle in the immunostimulatory effects.[87] The innate immunity of GAuNPs has been investigated by Peter H. Seeberger's group, it was demonstrated that ultra-small gold nanoparticles (UAuNPs) decorated with α-(1-6)-oligomannans can trigger an innate immune response without activating the complement system, this system when activated can trigger an allergic response and result in clearance of the NPs.[62] In this study it was demonstrated that these UAuNPs could be used as an alternative for current cancer treatments and as vaccine adjuvants. Furthermore GAuNPs combining high mannose ligands and HIV peptides antigen were proven to enhance an adjuvant effect resulting in an increased T-cell mediated immune response, which could result in a successful vaccination strategy for HIV.[88]

In conclusion GAuNPs biological applications can vary depending on the different glycans exposed on the NPs surface as they can target various receptors, several studies also proved the advantages of combining glycans with other biomolecules as peptides improving in this way the properties of the GAuNPs and therefore expanding the possible bio application of the NPs.

1.5 Polyamine phosphate nanoparticles

Colloidal complexes formed by crosslinking of polyelectrolytes have brought the attention of numerous researchers in the last 20 years for their possible application as nanocarriers. These complexes can be formed under mild conditions as its only needed to mix the polyelectrolytes with the desired salt.[89] Additionally, they are pH sensitive and therefore are excellent carriers as they can be for example loaded with a drug and when internalized in the cells the drug can be released.[90]

The two main polyelectrolytes used to form the ionically crosslinked colloids are: polysaccharide-based polyelectrolytes as chitosan or pectate and synthetic polyelectrolytes as poly(allylamine hydrochloride) (PAH) or poly(acrylic acid) (PAA).[91]

Polyamine phosphate NPs (PANs) are formed by crosslinking of poly (allylamine hydrochloride) with phosphate ions.

The formation of the PANs with different phosphate salts (Na_3PO_4, $Na_4P_2O_7$, $Na_5P_3O_{10}$, $Na_6P_6O_{18}$ and $(NaPO_3)_{26}$) was studied deeply by Cuenca et al. This study demonstrated that the PANs formed in all cases, but the pH stability of the PANs depends on the type of phosphate salt used during the self-assembly step, long phosphate enable the formation of PANs stable at acidic pHs. Another interesting aspect of PANs formation is that by using polyphosphates with a higher number of phosphate units a lower concentration is needed to form the NPs. Overall, the data obtained showed that a fine tuning of the pH sensitivity of PANs is possible by varying the phosphate salts used for the self-assembly, this feature could be crucial for future application in drug delivery.[92]

Supramolecular colloids as PANs have in the past years taken the attention of the scientific community as they are capable of encapsulating small molecules as for example siRNA [93] and can therefore be used as nanocarriers.[94] These nanocarriers are capable of releasing small molecules in specific sites due to their pH sensitivity. Some diseases as cancer present a dysregulated pH in their cells,[95] pH responsive nanocarriers are excellent candidates for future cancer treatments.[91]

Di Silvio et al. studied the complexation of siRNAs and PAH by fluorescent correlation spectroscopy (FCS) which is a spectroscopic technique that measures the diffusion time of fluorescent molecules this technique and provides information about the organization of the NPs at molecular level. Fluorescent cross-correlation spectroscopy (FCCS) is a more advanced technique that can study the dynamic interactions of two molecules labelled with different dyes. The stability, formation and complexation of the NPs was determined by FCCS, and this proved that they were dependent on the ratio of siRNA and PAH. In this study they also proved that the NPs were stable at a pH from 6 to 9, and disassembled releasing the siRNa at low endosomal pH as shown in figure 1.5.[93]
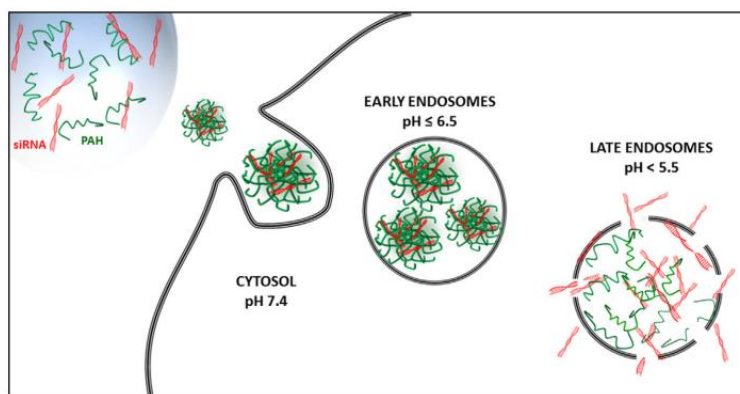
***Figure 1.5**. Uptake and intracellular fate of PAH/siRNA NPs. The scheme describes the uptake and degradation of the NPs into endosomes. The degradation of the NPs is shown by the presence of free PAH (red) and siRNA (green) at low endosomal pH. The translocation of the siRNAs from the endosomes to the cytoplasm is indicated by the presence of free siRNA outside endosomal compartments.[93]*

Andreozzi et al. studied the reduction of toxicity of PANs through different levels of PEGylation, they demonstrated the introduction of PEG chains did not prevent the NPs formation but it significantly modifies the size and charge of the PANs.[96] A PEG core-shell structure was hypothesized as the charge of the NPs was lowered and the size of the PANs was decreased when the PEGylation degree was increased (figure 1.6). The core-shell structure was confirmed by the SAXS measurements. 10 PEG chains per nanoparticle lowered the charge of the PANs to 0, this is due to the shielding of the PAH amino groups, it resulted that those were the less toxic NPs.[96] Moreover the in vivo biodistribution studies demonstrated the PEGylated PANs had a longer circulation time in the body and they were eliminated through the urine.

Overall, this study demonstrated the advantages achieved with the PEGylation of PANs in terms of size and charge but specially in terms of toxicity.
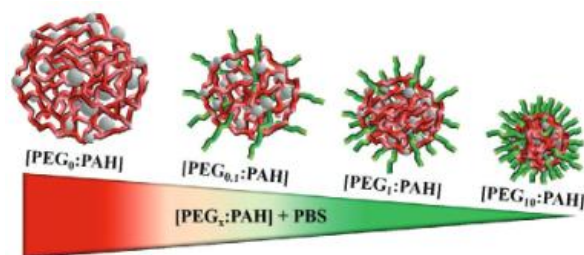
Figure 1.6. Scheme of PANs with different grade of PEGylation[96]

During this thesis a modification of PEGylated PANs with amphiphilic chains bond to a terminal carbohydrate will be studied. This project was performed during my secondments in Dr. Sergio Moya's group at CIC BiomaGUNE (Spain). The interaction of the NPs with different lectins was studied by FCS/FCCS.

1.6 Aim and objectives

The work described in this thesis is part of NanoCarb (Glyco-NPs for Applications in Advanced Nanomedicine), an ETN (European training network) project with the aim to develop glycosylated NPs with enhanced therapeutic actions for healthcare applications.

As described in section 2.3, GAuNPs are a platform of interest for a broad range of applications as the system allows a multivalent presentation of glycans. These NPs present excellent characteristics for biotechnological and clinical use. Even though these NPs have been extensively researched in the past 20 years there is still some safety concerns which have to be addressed, as well as there is a need of developing new synthetic procedures to be able to produce GAuNPs in a more efficient system.

The contribution to this ETN has focused on the development of a new photo-induced microfluidic synthetic procedure of UAuNPs, the study of biodistribution of UAuNPs, the effect of different shape GAuNPs in the interaction with diverse media and the synthesis of novel polymeric glyco NPs.

Three glycans were selected for this thesis α-mannose, β-glucose and lactose. These glycans were selected as model compounds of monosaccharides and disaccharides. Their involvement in biological processes and their high affinity towards lectins involved in diverse diseases make them particularly interesting for active targeting. For example, mannose binding lectin (MBL) is present in the damaged tissue caused by ischemic events, lactose binding lectin is present in colon carcinomas.

The final aim of this thesis is the development of novel glyco-nanomaterials to enhance the active targeting. One of the major challenges related to the active targeting of biomolecules is the half-life of the nanoparticles. In order to fulfil this objective several physical and chemical properties of the nanoparticles must be contemplated as the size, shape, surface coating and composition. Therefore, during this thesis several experiments have been developed to tune the nanoparticles features in order to maximize their characteristics for the final aim as shown in figure 1.7.
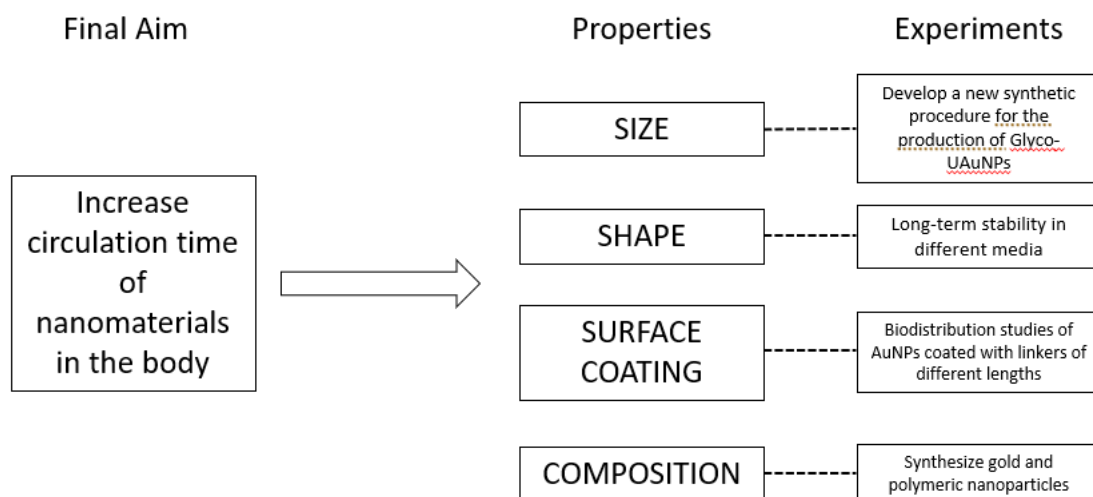
Figure 1.7 *Design of experiments to accomplish the final aim of the thesis*

In order to develop the previously explained experiments the thesis has been divided into six chapters which are summarized below.

Chapter 2 focuses on the study of the biodistribution in healthy mice of UAuNPs and GAuNPs with different ligand lengths, demonstrating the influence of the NP surface coating. PEG derivatives

A short PEG chain (PEG$_{500}$) and a long PEG chain (PEG$_{5000}$) were used in order to compare the effect of the linker length on the biodistribution of the NPs. For this purpose, AuNPs with the 2 PEG ligands were synthesized in a bench-top reactor following a batch synthetic procedure.

GAuNPs were obtained by exploiting the post-functionalization method. This work was performed in collaboration with Paolo Bigini's group at Istituto Mario Negri, where the *in-vivo* studies were performed. The final aim of this chapter is to provide a better understanding of the influence of the ligand length on the final fate of the NPs and the effect of the presence of α-mannose in the surface coating of the AuNPs.

In Chapter 3 a new methodology for the synthesis of GAuNPs is described. The presented method is a microfluidic synthetic procedure in which the advantages of photo-induced reduction of Au are exploited, obtaining highly stable and functionalized AuNPs in one-pot procedure. The present work also describes the study of the loading of the NPs and the modulation of it by modifying the ratio carbohydrate/Au. The loading of the NPs was performed by quantitative ^{1}H-NMR in collaboration with Laura Ragona's group at SCITEC-CNR.

In Chapter 4 the interaction of different shaped GAuNPs with biological matter is described. The hydrodynamic size of the NPs is modified when in contact with biological media due to the formation of the protein corona. For this purpose, 6 different GAuNPs with spherical and star shape were analysed overtime by dynamic light scattering (DLS), this study also investigated the effect of the diverse linker lengths for 3 glycans (lactose, β-glucose, and α-mannose).

Chapter 5 is focused on the synthesis and characterization of pegylated polyamine NPs (PANs) modified with an aliphatic linker with a terminal carbohydrate. This work also presents the

interactions of the PANs with specific lectins studied by Fluorescent Correlation Spectroscopy (FCS) and Fluorescent Cross-correlation Spectroscopy (FCCS) in collaboration with Sergio Moya's group at CIC BiomaGUNE.

1.7 References

(1) Bayda, S.; Adeel, M.; Tuccinardi, T.; Cordani, M.; Rizzolio, F. The History of Nanoscience and Nanotechnology: From Chemical–Physical Applications to Nanomedicine. *Molecules* **2019**, *25* (1), 112. https://doi.org/10.3390/molecules25010112.

(2) Soares, S.; Sousa, J.; Pais, A.; Vitorino, C. Nanomedicine: Principles, Properties, and Regulatory Issues. *Front. Chem.* **2018**, *6*, 360. https://doi.org/10.3389/fchem.2018.00360.

(3) Pita, R.; Ehmann, F.; Papaluca, M. Nanomedicines in the EU—Regulatory Overview. *AAPS J* **2016**, *18* (6), 1576–1582. https://doi.org/10.1208/s12248-016-9967-1.

(4) He, Z.; Ranganathan, N.; Li, P. Evaluating Nanomedicine with Microfluidics. *Nanotechnology* **2018**, *29* (49), 492001. https://doi.org/10.1088/1361-6528/aae18a.

(5) Chen, G.; Roy, I.; Yang, C.; Prasad, P. N. Nanochemistry and Nanomedicine for Nanoparticle-Based Diagnostics and Therapy. *Chem. Rev.* **2016**, *116* (5), 2826–2885. https://doi.org/10.1021/acs.chemrev.5b00148.

(6) Halwani, A. A. Development of Pharmaceutical Nanomedicines: From the Bench to the Market. *Pharmaceutics* **2022**, *14* (1), 106. https://doi.org/10.3390/pharmaceutics14010106.

(7) Piccaluga, P. P.; Di Guardo, A.; Lagni, A.; Lotti, V.; Diani, E.; Navari, M.; Gibellini, D. COVID-19 Vaccine: Between Myth and Truth. *Vaccines* **2022**, *10* (3), 349. https://doi.org/10.3390/vaccines10030349.

(8) D'Mello, S. R.; Cruz, C. N.; Chen, M.-L.; Kapoor, M.; Lee, S. L.; Tyner, K. M. The Evolving Landscape of Drug Products Containing Nanomaterials in the United States. *Nature Nanotech* **2017**, *12* (6), 523–529. https://doi.org/10.1038/nnano.2017.67.

(9) Murali, K.; Thomas, S. Biomedical Applications of Gold Nanoparticles. **2018**, 6.

(10) Barrientos, Á. G.; de la Fuente, J. M.; Rojas, T. C.; Fernández, A.; Penadés, S. Gold Glyconanoparticles: Synthetic Polyvalent Ligands Mimicking Glycocalyx-Like Surfaces as Tools for Glycobiological Studies. *Chem. Eur. J.* **2003**, *9* (9), 1909–1921. https://doi.org/10.1002/chem.200204544.

(11) Gao, W.; Wang, L.; Wang, K.; Sun, L.; Rao, Y.; Ma, A.; Zhang, M.; Li, Q.; Yang, H. Enhanced Anti-Inflammatory Activity of Peptide–Gold Nanoparticle Hybrids upon Cigarette Smoke Extract Modification through TLR Inhibition and Autophagy Induction. *ACS Appl. Mater. Interfaces* **2019**, *11* (36), 32706–32719. https://doi.org/10.1021/acsami.9b10536.

(12) Li, R.; Feng, F.; Chen, Z.-Z.; Bai, Y.-F.; Guo, F.-F.; Wu, F.-Y.; Zhou, G. Sensitive Detection of Carcinoembryonic Antigen Using Surface Plasmon Resonance Biosensor with Gold Nanoparticles Signal Amplification. *Talanta* **2015**, *140*, 143–149. https://doi.org/10.1016/j.talanta.2015.03.041.

(13) Hainfeld, J. F.; Slatkin, D. N.; Focella, T. M.; Smilowitz, H. M. Gold Nanoparticles: A New X-Ray Contrast Agent. *BJR* **2006**, *79* (939), 248–253. https://doi.org/10.1259/bjr/13169882.

(14) Patil, T.; Gambhir, R.; Vibhute, A.; Tiwari, A. P. Gold Nanoparticles: Synthesis Methods, Functionalization and Biological Applications. *J Clust Sci* **2022**. https://doi.org/10.1007/s10876-022-02287-6.

(15) Ganguly, K.; Patel, D. K.; Dutta, S. D.; Lim, K.-T. TEMPO-Cellulose Nanocrystal-Capped Gold Nanoparticles for Colorimetric Detection of Pathogenic DNA. *ACS Omega* **2021**, *6* (19), 12424–12431. https://doi.org/10.1021/acsomega.1c00359.

(16) Verma, M. S.; Rogowski, J. L.; Jones, L.; Gu, F. X. Colorimetric Biosensing of Pathogens Using Gold Nanoparticles. *Biotechnology Advances* **2015**, *33* (6), 666–680. https://doi.org/10.1016/j.biotechadv.2015.03.003.

(17) Tang, L.; Casas, J. Quantification of Cardiac Biomarkers Using Label-Free and Multiplexed Gold Nanorod Bioprobes for Myocardial Infarction Diagnosis. *Biosensors and Bioelectronics* **2014**, *61*, 70–75. https://doi.org/10.1016/j.bios.2014.04.043.

(18) Silveira, G. deBem; Muller, A.; Machado-de-Ávila, R.; Silveira, P. L. Advance in the Use of Gold Nanoparticles in the Treatment of Neurodegenerative Diseases: New Perspectives. *Neural Regen Res* **2021**, *16* (12), 2425. https://doi.org/10.4103/1673-5374.313040.

(19) Ramalingam, V.; Varunkumar, K.; Ravikumar, V.; Rajaram, R. Target Delivery of Doxorubicin Tethered with PVP Stabilized Gold Nanoparticles for Effective Treatment of Lung Cancer. *Sci Rep* **2018**, *8* (1), 3815. https://doi.org/10.1038/s41598-018-22172-5.

(20) Paciotti, G. F.; Zhao, J.; Cao, S.; Brodie, P. J.; Tamarkin, L.; Huhta, M.; Myer, L. D.; Friedman, J.; Kingston, D. G. I. Synthesis and Evaluation of Paclitaxel-Loaded Gold Nanoparticles for Tumor-Targeted Drug Delivery. *Bioconjugate Chem.* **2016**, *27* (11), 2646–2657. https://doi.org/10.1021/acs.bioconjchem.6b00405.

(21) Yafout, M.; Ousaid, A.; Khayati, Y.; El Otmani, I. S. Gold Nanoparticles as a Drug Delivery System for Standard Chemotherapeutics: A New Lead for Targeted Pharmacological Cancer Treatments. *Scientific African* **2021**, *11*, e00685. https://doi.org/10.1016/j.sciaf.2020.e00685.

(22) Turkevich, J.; Stevenson, P. C.; Hillier, J. A Study of the Nucleation and Growth Processes in the Synthesis of Colloidal Gold. *Discuss. Faraday Soc.* **1951**, *11*, 55. https://doi.org/10.1039/df9511100055.

(23) Brust, M.; Walker, M.; Bethell, D.; Schiffrin, D. J.; Whyman, R. Synthesis of Thiol-Derivatised Gold Nanoparticles in a Two-Phase Liquid–Liquid System. *J. Chem. Soc., Chem. Commun.* **1994**, *0* (7), 801–802. https://doi.org/10.1039/C39940000801.

(24) Frens G. Controlled Nucleation for the Regulation of the Particle Size in Monodisperse Gold Suspensions. *Natural Physical Science*. https://doi.org/10.1038/physci241020a0.

(25) Xia, H.; Bai, S.; Hartmann, J.; Wang, D. Synthesis of Monodisperse Quasi-Spherical Gold Nanoparticles in Water via Silver(I)-Assisted Citrate Reduction. *Langmuir* **2010**, *26* (5), 3585–3589. https://doi.org/10.1021/la902987w.

(26) Ma, J.; Lee, S. M.-Y.; Yi, C.; Li, C.-W. Controllable Synthesis of Functional Nanoparticles by Microfluidic Platforms for Biomedical Applications – a Review. *Lab Chip* **2017**, *17* (2), 209–226. https://doi.org/10.1039/C6LC01049K.

(27) Panariello, L. Highly Reproducible, High-Yield Flow Synthesis of Gold Nanoparticles Based on a Rational Reactor Design Exploiting the Reduction of Passivated Au(Iii). **2020**, 15.

(28) Huang, H.; du Toit, H.; Ben-Jaber, S.; Wu, G.; Panariello, L.; Thanh, N. T. K.; Parkin, I. P.; Gavriilidis, A. Rapid Synthesis of Gold Nanoparticles with Carbon Monoxide in a Microfluidic Segmented Flow System. *React. Chem. Eng.* **2019**, *4* (5), 884–890. https://doi.org/10.1039/C8RE00351C.

(29) Valencia, P. M.; Farokhzad, O. C.; Karnik, R.; Langer, R. Microfluidic Technologies for Accelerating the Clinical Translation of Nanoparticles. *Nature Nanotech* **2012**, *7* (10), 623–629. https://doi.org/10.1038/nnano.2012.168.

(30) Lazarus, L. L.; Riche, C. T.; Marin, B. C.; Gupta, M.; Malmstadt, N.; Brutchey, R. L. Two-Phase Microfluidic Droplet Flows of Ionic Liquids for the Synthesis of Gold and Silver Nanoparticles. *ACS Appl. Mater. Interfaces* **2012**, *4* (6), 3077–3083. https://doi.org/10.1021/am3004413.

(31) Silvestri, A.; Lay, L.; Psaro, R.; Polito, L.; Evangelisti, C. Fluidic Manufacture of Star-Shaped Gold Nanoparticles. *Chem. Eur. J.* **2017**, *23* (41), 9732–9735. https://doi.org/10.1002/chem.201701617.

(32) Marelli, M.; Bossola, F.; Spinetti, G.; Sangalli, E.; Santo, V. D.; Psaro, R.; Polito, L. Microfluidic Synthesis of Hybrid TiO $_2$ -Anisotropic Gold Nanoparticles with Visible and Near-Infrared Activity. *ACS Appl. Mater. Interfaces* **2020**, *12* (34), 38522–38529. https://doi.org/10.1021/acsami.0c08241.

(33) Li, D.-E.; Lin, C.-H. Microfluidic Chip for Droplet-Based AuNP Synthesis with Dielectric Barrier Discharge Plasma and on-Chip Mercury Ion Detection. *RSC Adv.* **2018**, *8* (29), 16139–16145. https://doi.org/10.1039/C8RA02468E.

(34) Yaghmur, A.; Hamad, I. Microfluidic Nanomaterial Synthesis and In Situ SAXS, WAXS, or SANS Characterization: Manipulation of Size Characteristics and Online Elucidation of Dynamic Structural Transitions. *Molecules* **2022**, *27* (14), 4602. https://doi.org/10.3390/molecules27144602.

(35) du Toit, H.; Macdonald, T. J.; Huang, H.; Parkin, I. P.; Gavriilidis, A. Continuous Flow Synthesis of Citrate Capped Gold Nanoparticles Using UV Induced Nucleation. *RSC Adv.* **2017**, *7* (16), 9632–9638. https://doi.org/10.1039/C6RA27173A.

(36) Harada, M.; Okamoto, K.; Terazima, M. Diffusion of Gold Ions and Gold Particles during Photoreduction Processes Probed by the Transient Grating Method. *Journal of Colloid and Interface Science* **2009**, *332* (2), 373–381. https://doi.org/10.1016/j.jcis.2008.12.041.

(37) Harada, M.; Kizaki, S. Formation Mechanism of Gold Nanoparticles Synthesized by Photoreduction in Aqueous Ethanol Solutions of Polymers Using In Situ Quick Scanning X-Ray Absorption Fine Structure and Small-Angle X-Ray Scattering. *Crystal Growth & Design* **2016**, *16* (3), 1200–1212. https://doi.org/10.1021/acs.cgd.5b01168.

(38) Harada, M.; Einaga, H. In Situ XAFS Studies of Au Particle Formation by Photoreduction in Polymer Solutions. *Langmuir* **2007**, *23* (12), 6536–6543. https://doi.org/10.1021/la0701071.

(39) Clemente, E.; Martinez-Moro, M.; Trinh, D. N.; Soliman, M. G.; Spencer, D. I. R.; Gardner, R. A.; Kotsias, M.; Sánchez Iglesias, A.; Moya, S.; Monopoli, M. P. Probing the Glycans Accessibility in the Nanoparticle Biomolecular Corona. *Journal of Colloid and Interface Science* **2022**, *613*, 563–574. https://doi.org/10.1016/j.jcis.2021.11.140.

(40) Monopoli, M. P.; Åberg, C.; Salvati, A.; Dawson, K. A. Biomolecular Coronas Provide the Biological Identity of Nanosized Materials. *Nature Nanotech* **2012**, *7* (12), 779–786. https://doi.org/10.1038/nnano.2012.207.

(41) Piella, J.; Bastús, N. G.; Puntes, V. Size-Dependent Protein–Nanoparticle Interactions in Citrate-Stabilized Gold Nanoparticles: The Emergence of the Protein Corona. *Bioconjugate Chem.* **2017**, *28* (1), 88–97. https://doi.org/10.1021/acs.bioconjchem.6b00575.

(42) Gagner, J. E.; Lopez, M. D.; Dordick, J. S.; Siegel, R. W. Effect of Gold Nanoparticle Morphology on Adsorbed Protein Structure and Function. *Biomaterials* **2011**, *32* (29), 7241–7252. https://doi.org/10.1016/j.biomaterials.2011.05.091.

(43) Casals, E.; Pfaller, T.; Duschl, A.; Oostingh, G. J.; Puntes, V. Time Evolution of the Nanoparticle Protein Corona. *ACS Nano* **2010**, *4* (7), 3623–3632. https://doi.org/10.1021/nn901372t.

(44) Boselli, L.; Polo, E.; Castagnola, V.; Dawson, K. A. Regimes of Biomolecular Ultrasmall Nanoparticle Interactions. *Angew. Chem. Int. Ed.* **2017**, *56* (15), 4215–4218. https://doi.org/10.1002/anie.201700343.

(45) García-Álvarez, R.; Hadjidemetriou, M.; Sánchez-Iglesias, A.; Liz-Marzán, L. M.; Kostarelos, K. *In Vivo* Formation of Protein Corona on Gold Nanoparticles. The Effect of Their Size and Shape. *Nanoscale* **2018**, *10* (3), 1256–1264. https://doi.org/10.1039/C7NR08322J.

(46) Chen, D.; Ganesh, S.; Wang, W.; Amiji, M. Plasma Protein Adsorption and Biological Identity of Systemically Administered Nanoparticles. *Nanomedicine* **2017**, *12* (17), 2113–2135. https://doi.org/10.2217/nnm-2017-0178.

(47) Lesniak, A.; Fenaroli, F.; Monopoli, M. P.; Åberg, C.; Dawson, K. A.; Salvati, A. Effects of the Presence or Absence of a Protein Corona on Silica Nanoparticle Uptake and Impact on Cells. *ACS Nano* **2012**, *6* (7), 5845–5857. https://doi.org/10.1021/nn300223w.

(48) Owensiii, D.; Peppas, N. Opsonization, Biodistribution, and Pharmacokinetics of Polymeric Nanoparticles. *International Journal of Pharmaceutics* **2006**, *307* (1), 93–102. https://doi.org/10.1016/j.ijpharm.2005.10.010.

(49) Schöttler, S.; Becker, G.; Winzen, S.; Steinbach, T.; Mohr, K.; Landfester, K.; Mailänder, V.; Wurm, F. R. Protein Adsorption Is Required for Stealth Effect of Poly(Ethylene Glycol)- and Poly(Phosphoester)-Coated Nanocarriers. *Nature Nanotech* **2016**, *11* (4), 372–377. https://doi.org/10.1038/nnano.2015.330.

(50) Marradi, M.; Chiodo, F.; García, I.; Penadés, S. Glyconanoparticles as Multifunctional and Multimodal Carbohydrate Systems. *Chem. Soc. Rev.* **2013**, *42* (11), 4728. https://doi.org/10.1039/c2cs35420a.

(51) Compostella, F.; Pitirollo, O.; Silvestri, A.; Polito, L. Glyco-Gold Nanoparticles: Synthesis and Applications. *Beilstein J. Org. Chem.* **2017**, *13*, 1008–1021. https://doi.org/10.3762/bjoc.13.100.

(52) Dwek, R. A. Glycobiology: Toward Understanding the Function of Sugars. *Chem. Rev.* **1996**, *96* (2), 683–720. https://doi.org/10.1021/cr940283b.

(53) Lundquist, J. J.; Toone, E. J. The Cluster Glycoside Effect. *Chem. Rev.* **2002**, *102* (2), 555–578. https://doi.org/10.1021/cr000418f.

(54) Kang, B.; Opatz, T.; Landfester, K.; Wurm, F. R. Carbohydrate Nanocarriers in Biomedical Applications: Functionalization and Construction. *Chem. Soc. Rev.* **2015**, *44* (22), 8301–8325. https://doi.org/10.1039/C5CS00092K.

(55) de la Fuente, J. M.; Barrientos, A. G.; Rojas, T. C.; Rojo, J.; Cañada, J.; Fernández, A.; Penadés, S. Gold Glyconanoparticles as Water-Soluble Polyvalent Models To Study Carbohydrate Interactions. *Angew. Chem. Int. Ed.* **2001**, *40* (12), 2257–2261. https://doi.org/10.1002/1521-3773(20010618)40:12<2257::AID-ANIE2257>3.0.CO;2-S.

(56) Martínez-Ávila, O.; Hijazi, K.; Marradi, M.; Clavel, C.; Campion, C.; Kelly, C.; Penadés, S. Gold *Manno* -Glyconanoparticles: Multivalent Systems to Block HIV-1 Gp120 Binding to the Lectin DC-SIGN. *Chem. Eur. J.* **2009**, *15* (38), 9874–9888. https://doi.org/10.1002/chem.200900923.

(57) Silvestri, A.; Zambelli, V.; Ferretti, A. M.; Salerno, D.; Bellani, G.; Polito, L. Design of Functionalized Gold Nanoparticle Probes for Computed Tomography Imaging: Design of Tailored Engineered AuNPs as CT Contrast Agents. *Contrast Media Mol. Imaging* **2016**, *11* (5), 405–414. https://doi.org/10.1002/cmmi.1704.

(58) Fyrner, T.; Ederth, T.; Aili, D.; Liedberg, B.; Konradsson, P. Synthesis of Oligo(Lactose)-Based Thiols and Their Self-Assembly onto Gold Surfaces. *Colloids and Surfaces B: Biointerfaces* **2013**, *105*, 187–193. https://doi.org/10.1016/j.colsurfb.2013.01.002.

(59) Combemale, S.; Assam-Evoung, J.-N.; Houaidji, S.; Bibi, R.; Barragan-Montero, V. Gold Nanoparticles Decorated with Mannose-6-Phosphate Analogues. *Molecules* **2014**, *19* (1), 1120–1149. https://doi.org/10.3390/molecules19011120.

(60) Hu, X.-L.; Jin, H.-Y.; He, X.-P.; James, T. D.; Chen, G.-R.; Long, Y.-T. Colorimetric and Plasmonic Detection of Lectins Using Core–Shell Gold Glyconanoparticles Prepared by Copper-Free Click Chemistry. *ACS Appl. Mater. Interfaces* **2015**, *7* (3), 1874–1878. https://doi.org/10.1021/am5076293.

(61) Telli, F. C.; Demir, B.; Barlas, F. B.; Guler, E.; Timur, S.; Salman, Y. Novel Glyconanoconjugates: Synthesis, Characterization and Bioapplications. *RSC Adv.* **2016**, *6* (107), 105806–105813. https://doi.org/10.1039/C6RA21976D.

(62) Ghosh, C.; Priegue, P.; Leelayuwapan, H.; Fuchsberger, F. F.; Rademacher, C.; Seeberger, P. H. Synthetic Glyconanoparticles Modulate Innate Immunity but Not the Complement System. *ACS Appl. Bio Mater.* **2022**, *5* (5), 2185–2192. https://doi.org/10.1021/acsabm.2c00026.

(63) Gong, L.; He, K.; Liu, J. Concentration-Dependent Subcellular Distribution of Ultrasmall Near-Infrared-Emitting Gold Nanoparticles. *Angew. Chem. Int. Ed.* **2021**, *60* (11), 5739–5743. https://doi.org/10.1002/anie.202014833.

(64) Le Guével, X.; Perez Perrino, M.; Fernández, T. D.; Palomares, F.; Torres, M.-J.; Blanca, M.; Rojo, J.; Mayorga, C. Multivalent Glycosylation of Fluorescent Gold Nanoclusters Promotes Increased Human Dendritic Cell Targeting via Multiple Endocytic Pathways. *ACS Appl. Mater. Interfaces* **2015**, *7* (37), 20945–20956. https://doi.org/10.1021/acsami.5b06541.

(65) Jin, H.-Y.; Li, D.-W.; Zhang, N.; Gu, Z.; Long, Y.-T. Analyzing Carbohydrate–Protein Interaction Based on Single Plasmonic Nanoparticle by Conventional Dark Field Microscopy. *ACS Appl. Mater. Interfaces* **2015**, *7* (22), 12249–12253. https://doi.org/10.1021/acsami.5b02744.

(66) Jain, P. K.; Lee, K. S.; El-Sayed, I. H.; El-Sayed, M. A. Calculated Absorption and Scattering Properties of Gold Nanoparticles of Different Size, Shape, and Composition: Applications in Biological Imaging and Biomedicine. *J. Phys. Chem. B* **2006**, *110* (14), 7238–7248. https://doi.org/10.1021/jp057170o.

(67) Li, Z.; Sun, L.; Zhang, Y.; Dove, A. P.; O'Reilly, R. K.; Chen, G. Shape Effect of Glyco-Nanoparticles on Macrophage Cellular Uptake and Immune Response. *ACS Macro Lett.* **2016**, *5* (9), 1059–1064. https://doi.org/10.1021/acsmacrolett.6b00419.

(68) Chaudhary, P. M.; Sangabathuni, S.; Murthy, R. V.; Paul, A.; Thulasiram, H. V.; Kikkeri, R. Assessing the Effect of Different Shapes of Glyco-Gold Nanoparticles on Bacterial Adhesion and Infections. *Chem. Commun.* **2015**, *51* (86), 15669–15672. https://doi.org/10.1039/C5CC05238F.

(69) Sangabathuni, S.; Vasudeva Murthy, R.; Chaudhary, P. M.; Surve, M.; Banerjee, A.; Kikkeri, R. Glyco-Gold Nanoparticle Shapes Enhance Carbohydrate–Protein Interactions in Mammalian Cells. *Nanoscale* **2016**, *8* (25), 12729–12735. https://doi.org/10.1039/C6NR03008D.

(70) Guarino, G.; Rastrelli, F.; Mancin, F. Mapping the Nanoparticle-Coating Monolayer with NMR Pseudocontact Shiftswz. **2012**, 3.

(71) Marradi, M.; Di Gianvincenzo, P.; Enríquez-Navas, P. M.; Martínez-Ávila, O. M.; Chiodo, F.; Yuste, E.; Angulo, J.; Penadés, S. Gold Nanoparticles Coated with Oligomannosides of HIV-1 Glycoprotein Gp120 Mimic the Carbohydrate Epitope of Antibody 2G12. *Journal of Molecular Biology* **2011**, *410* (5), 798–810. https://doi.org/10.1016/j.jmb.2011.03.042.

(72) Manea, F.; Bindoli, C.; Fallarini, S.; Lombardi, G.; Polito, L.; Lay, L.; Bonomi, R.; Mancin, F.; Scrimin, P. Multivalent, Saccharide-Functionalized Gold Nanoparticles as Fully Synthetic Analogs of Type A *Neisseria Meningitidis* Antigens. *Adv. Mater.* **2008**, *20* (22), 4348–4352. https://doi.org/10.1002/adma.200800737.

(73) Grant, O. C.; Smith, H. M.; Firsova, D.; Fadda, E.; Woods, R. J. Presentation, Presentation, Presentation! Molecular-Level Insight into Linker Effects on Glycan Array Screening Data. *Glycobiology* **2014**, *24* (1), 17–25. https://doi.org/10.1093/glycob/cwt083.

(74) Georgiou, P. G.; Baker, A. N.; Richards, S.-J.; Laezza, A.; Walker, M.; Gibson, M. I. "Tuning Aggregative *versus* Non-Aggregative Lectin Binding with Glycosylated Nanoparticles by the Nature of the Polymer Ligand." *J. Mater. Chem. B* **2020**, *8* (1), 136–145. https://doi.org/10.1039/C9TB02004G.

(75) Lee, K.; Lee, H.; Bae, K. H.; Park, T. G. Heparin Immobilized Gold Nanoparticles for Targeted Detection and Apoptotic Death of Metastatic Cancer Cells. *Biomaterials* **2010**, *31* (25), 6530–6536. https://doi.org/10.1016/j.biomaterials.2010.04.046.

(76) Lee, H.; Lee, K.; Kim, I. K.; Park, T. G. Synthesis, Characterization, and in Vivo Diagnostic Applications of Hyaluronic Acid Immobilized Gold Nanoprobes. *Biomaterials* **2008**, *29* (35), 4709–4718. https://doi.org/10.1016/j.biomaterials.2008.08.038.

(77) Baker, A. N.; Richards, S.-J.; Guy, C. S.; Congdon, T. R.; Hasan, M.; Zwetsloot, A. J.; Gallo, A.; Lewandowski, J. R.; Stansfeld, P. J.; Straube, A.; Walker, M.; Chessa, S.; Pergolizzi, G.; Dedola, S.; Field, R. A.; Gibson, M. I. The SARS-COV-2 Spike Protein Binds Sialic Acids and Enables Rapid Detection in a Lateral Flow Point of Care Diagnostic Device. *ACS Cent. Sci.* **2020**, *6* (11), 2046–2052. https://doi.org/10.1021/acscentsci.0c00855.

(78) Baker, A. N.; Muguruza, A. R.; Richards, S.; Georgiou, P. G.; Goetz, S.; Walker, M.; Dedola, S.; Field, R. A.; Gibson, M. I. Lateral Flow Glyco-Assays for the Rapid and Low-Cost Detection of Lectins–Polymeric Linkers and Particle Engineering Are Essential for Selectivity and Performance. *Adv. Healthcare Mater.* **2021**, 2101784. https://doi.org/10.1002/adhm.202101784.

(79) Candiota, A. P.; Acosta, M.; Simões, R. V.; Delgado-Goñi, T.; Lope-Piedrafita, S.; Irure, A.; Marradi, M.; Bomati-Miguel, O.; Miguel-Sancho, N.; Abasolo, I.; Schwartz, S.; Santamaria, J.; Penadés, S.; Arús, C. A New Ex Vivo Method to Evaluate the Performance of Candidate MRI Contrast Agents: A Proof-of-Concept Study. *J Nanobiotechnol* **2014**, *12* (1), 12. https://doi.org/10.1186/1477-3155-12-12.

(80) Frigell, J.; García, I.; Gómez-Vallejo, V.; Llop, J.; Penadés, S. [68] Ga-Labeled Gold Glyconanoparticles for Exploring Blood–Brain Barrier Permeability: Preparation, Biodistribution Studies, and Improved Brain Uptake via Neuropeptide Conjugation. *J. Am. Chem. Soc.* **2014**, *136* (1), 449–457. https://doi.org/10.1021/ja411096m.

(81) Wang, H.; Naghavi, M. et al. Global, Regional, and National Life Expectancy, All-Cause Mortality, and Cause-Specific Mortality for 249 Causes of Death, 1980–2015: A Systematic Analysis for the Global Burden of Disease Study 2015. *The Lancet* **2016**, *388* (10053), 1459–1544. https://doi.org/10.1016/S0140-6736(16)31012-1.

(82) Lotan, R.; Raz, A. Lectins in Cancer Cells. *Ann NY Acad Sci* **1988**, *551* (1 Membrane in C), 385–398. https://doi.org/10.1111/j.1749-6632.1988.tb22372.x.

(83) Yamazaki, N.; Kojima, S.; Bovin, N. V.; André, S.; Gabius, S.; Gabius, H.-J. Endogenous Lectins as Targets for Drug Delivery. *Advanced Drug Delivery Reviews* **2000**, *43* (2–3), 225–244. https://doi.org/10.1016/S0169-409X(00)00071-5.

(84) Yi, Y.; Kim, H. J.; Zheng, M.; Mi, P.; Naito, M.; Kim, B. S.; Min, H. S.; Hayashi, K.; Perche, F.; Toh, K.; Liu, X.; Mochida, Y.; Kinoh, H.; Cabral, H.; Miyata, K.; Kataoka, K. Glucose-Linked Sub-50-Nm Unimer Polyion Complex-Assembled Gold Nanoparticles for Targeted SiRNA Delivery to Glucose Transporter 1-Overexpressing Breast Cancer Stem-like Cells. *Journal of Controlled Release* **2019**, *295*, 268–277. https://doi.org/10.1016/j.jconrel.2019.01.006.

(85) García Calavia, P.; Chambrier, I.; Cook, M. J.; Haines, A. H.; Field, R. A.; Russell, D. A. Targeted Photodynamic Therapy of Breast Cancer Cells Using Lactose-Phthalocyanine Functionalized Gold Nanoparticles. *Journal of Colloid and Interface Science* **2018**, *512*, 249–259. https://doi.org/10.1016/j.jcis.2017.10.030.

(86) Shinchi, H.; Yamaguchi, T.; Moroishi, T.; Yuki, M.; Wakao, M.; Cottam, H. B.; Hayashi, T.; Carson, D. A.; Suda, Y. Gold Nanoparticles Coimmobilized with Small Molecule Toll-Like Receptor 7 Ligand and α-Mannose as Adjuvants. *Bioconjugate Chem.* **2019**, 11.

(87) Shinchi, H.; Komaki, F.; Yuki, M.; Ohara, H.; Hayakawa, N.; Wakao, M.; Cottam, H. B.; Hayashi, T.; Carson, D. A.; Moroishi, T.; Suda, Y. Glyco-Nanoadjuvants: Impact of Linker Length for Conjugating a Synthetic Small-Molecule TLR7 Ligand to Glyco-Nanoparticles on Immunostimulatory Effects. *ACS Chem. Biol.* **2022**, *17* (4), 957–968. https://doi.org/10.1021/acschembio.2c00108.

(88) Climent, N.; García, I.; Marradi, M.; Chiodo, F.; Miralles, L.; Maleno, M. J.; Gatell, J. M.; García, F.; Penadés, S.; Plana, M. Loading Dendritic Cells with Gold Nanoparticles (GNPs) Bearing HIV-Peptides and Mannosides Enhance HIV-Specific T Cell Responses.

Nanomedicine: Nanotechnology, Biology and Medicine **2018**, *14* (2), 339–351. https://doi.org/10.1016/j.nano.2017.11.009.

(89) Bagaria, H. G.; Wong, M. S. Polyamine–Salt Aggregate Assembly of Capsules as Responsive Drug Delivery Vehicles. **2011**, 13.

(90) Lin, Y.-H.; Sonaje, K.; Lin, K. M.; Juang, J.-H.; Mi, F.-L.; Yang, H.-W.; Sung, H.-W. Multi-Ion-Crosslinked Nanoparticles with PH-Responsive Characteristics for Oral Delivery of Protein Drugs. *Journal of Controlled Release* **2008**, 9.

(91) Lapitsky, Y. Ionically Crosslinked Polyelectrolyte Nanocarriers: Recent Advances and Open Problems. *Current Opinion in Colloid & Interface Science* **2014**, *19* (2), 122–130. https://doi.org/10.1016/j.cocis.2014.03.014.

(92) Cuenca, V. E.; Martinelli, H.; Ramirez, M. de los A.; Ritacco, H. A.; Andreozzi, P.; Moya, S. E. Polyphosphate Poly(Amine) Nanoparticles: Self-Assembly, Thermodynamics, and Stability Studies. *Langmuir* **2019**, *35* (44), 14300–14309. https://doi.org/10.1021/acs.langmuir.9b02636.

(93) Di Silvio, D.; Martínez-Moro, M.; Salvador, C.; de los Angeles Ramirez, M.; Caceres-Velez, P. R.; Ortore, M. G.; Dupin, D.; Andreozzi, P.; Moya, S. E. Self-Assembly of Poly(Allylamine)/SiRNA Nanoparticles, Their Intracellular Fate and SiRNA Delivery. *Journal of Colloid and Interface Science* **2019**, *557*, 757–766. https://doi.org/10.1016/j.jcis.2019.09.082.

(94) Davoodi, P. Drug Delivery Systems for Programmed and On-Demand Release. **2018**, 35.

(95) Webb, B. A. Dysregulated PH: A Perfect Storm for Cancer Progression. *c a n ce r* **2011**, 7.

(96) Andreozzi, P.; Simó, C.; Moretti, P.; Porcel, J. M.; Lüdtke, T. U.; Ramirez, M. de los A.; Tamberi, L.; Marradi, M.; Amenitsch, H.; Llop, J.; Ortore, M. G.; Moya, S. E. Novel Core–Shell Polyamine Phosphate Nanoparticles Self-Assembled from PEGylated Poly(Allylamine Hydrochloride) with Low Toxicity and Increased In Vivo Circulation Time. *Small* **2021**, *17* (35), 2102211. https://doi.org/10.1002/smll.202102211.

Chapter 2

Ultra-small gold nanoparticles biodistribution

2.1 Introduction

Gold NPs have brought the attention in the past years of numerous researchers for their wide range of bio applications, although one of the main challenges is understanding better the biodistribution of the AuNPs and examining the biological obstacles in detail. Some of these obstacles are related to opsonization process, cellular internalization and clearance of the body: issues that can be faced and overcome by modulating the size, shape and surface functionalization of the nanoparticles (NPs).[1]

The final fate of the NPs is dependent on the size, shape and surface coating of the NPs. Spherical AuNPs with a diameter bigger than 5 nm mostly accumulate in the liver and spleen and are metabolized for a longer period of time.[1,2] In the other hand, AuNPs < 5 nm, so called ultra-small gold NPs (UAuNPs) are eliminated by renal clearance, as due to their smaller size,[3–5] they can pass the renal glomerulus. Moreover, UAuNPs are also characterized by a negligible protein corona,[6] therefore their final fate differs from bigger NPs.

The biodistribution and organ accumulation of AuNPs depends not only on the size of the core diameter but it can also be varied by modifying the surface coating of the NPs. Polyethylene glycol (PEG) is a common ligand stabilizer used to avoid aggregation and, in this way, reduce the toxicity of the NPs.[7] PEG surface coating is also employed in order to avoid the NPs sequestration by cells of the mononuclear phagocyte system (MPS) and reticulon endothelial system (RES) after the intravenous injection.[8] Both systems are responsible for the clearance of the NPs, thus modifying the NPs surface with PEG can prevent the rapid clearance of the AuNPs.

Glycan surface coating of the NPs can impact the final fate of the AuNPs as glycans have been demonstrated to modulate the biodistribution of the NPs. α − Mannose coated AuNPs were shown to have a different biodistribution in zebra fish compared to PEGylated AuNPs in Zebrafish.[9] Kikkeri and co-workers studied the biodistribution of α − mannose-AuNPs and PEGylated AuNPs in zebrafish. Mannose-AuNPs were found in the digestive system, bladder, and heart. On the other hand, the PEGylated AuNPs had a much lower accumulation in those organs and presented a higher accumulation in the brain and the eyes for rod and star shaped AuNPs. In the case of the PEGylated spherical NPs accumulated more in the muscles. Moreover, the PEGylated AuNPs had a rapid clearance compared to the mannose-AuNPs. The shape of the NPs also modified the distribution and circulation time in the zebrafish, the rod shaped AuNPs were the first to be eliminated, on the contrary the star shaped AuNPs showed a slower uptake and clearance.

Surface coating of AuNPs with glycans can be performed with several procedures as described previously. (Chapter 1 section 1.4) Post-functionalization of AuNPs can be executed through several pathways:

- Isothiourea condensation: consists in the reaction between isothiocyanate and an amine and its normally performed at alkaline pH. This reaction can be performed in few hours in an aqueous solution.[10]
- Amide condensation: coupling between a carboxylic acid and an amine. The reaction takes few hours and can be performed in organic solvents as DMSO or in water. The reaction requires the use of activating agents as for example 1-ethyl-3-(3-dimethylaminopropyl)carbodiimide (EDC) and N-hydroxysuccinimide (NHS) or N-hydroxysulfosuccinimide (sulfo-NHS).[11]
- Anhydride and amine condensation: coupling between an amine and an anhydride adding to an amide formation. The reaction can be performed in water or organic solvents without the need of activating reagents.[6]
- Click chemistry: is the cupper promoted azide alkyne cycloaddition. The reaction can be performed in few hours in water from pH 4-12.[12,13]

Midatech Pharma used the amide condensation with success to couple 2 nm UAuNPs to SIKVAV peptide,[14] therefore during this chapter the same procedure will be presented.

2.2 Aim of the work

The intended goal is to better understand the *in vivo* biodistribution and the clearance pathways of PEGylated ultra-small gold NPs in healthy mice. To achieve that UAuNPs with a surface coating of PEG were synthesized, and in a second step the UAuNPs were post-functionalized with α-mannose.

In the first part of this chapter is reported the synthesis of three hetero bifunctional UAuNPs functionalized with HS-PEG$_{0.5}$-COOH, HS-PEG$_{0.5}$-COOH + α-galactose-C$_2$-SH and HS-PEG$_{5000}$-COOH. The 4 nm UAuNPs were synthesized following a modified Brust-Schiffrin procedure[15] using an automated bench-top reactor in order to overcome the variations from batch to batch and obtain reproducible stable UAuNPs.[14,16] In particular we were interested in evaluating the *in vivo* behaviour of PEGylated UAuNPs by studying the biodistribution and the clearance pathways. The synthesis of α-mannose-C$_2$-NH$_2$ is described and the further post-functionalization via carbodiimide reactions[17] of the PEGylated UAuNPs.

In the second part of this chapter all NPs were injected to healthy mice and the gold content in the organs was further evaluated by ICP-OES at 3 time points, silver staining by auto metallography (AMG) studies were also performed to observe the particles with bright-field microscopy, moreover organs were immune stained to observe the NPs with reflective confocal microscopy.

This project was performed in collaboration with Paolo Bigini's group at Istituto Mario Negri who oversaw the biodistribution study and performed the auto metallography and immunostaining

studies. The synthesis and characterization of UAuNPs was performed at Midatech Pharma and the evaluation of the gold content in organs by ICP-OES was performed at SCITEC-CNR.

The final goal is to determine the effect of the PEG chain length and further addition of a monosaccharide in the clearance pathways and biodistribution of the NPs.

2.3   Results and discussion

2.3.1   Synthesis and characterization of ultra-small gold nanoparticles

4 nm ultra-small gold NPs were synthesized modifying a reported procedure for 2 nm UAuNPs. [14,16] The NPs were prepared by a Brust-Schiffrin method and passivated with covalent surface coating PEG thiol ligands with a terminal carboxylic group and 1-(2-mercaotoethoxy-)-α-galactose (α-GalC$_2$). The NPs were then purified using an automated Tangential Flow Filtration (TFF) system which performs diafiltration[18] as shown in figure 2.1. The TFF system consists in a feed tank with the crude solution which is pumped passing by a membrane column with a MWCO cut off, the contaminants with a lower MWCO pass through the TFF column to the permeate. The AuNPs solution goes back to the feed tank and the solution is each time more concentrated and the contaminants are removed. The system is automated. The most common purification of AuNPs in research is performed using centrifugal ultrafiltration, however when advancing towards clinical stages purification systems as TFF are required.

The synthesis was performed in an automated bench-top reactor which is a very robust system, operator friendly and allows highly reproducible synthesis, the synthesis was performed following a reported procedure[14,16]. The reactor enables the production of a monodisperse population of NPs and a virtually non-existent variation batch to batch therefore this system enables the scale-up of the synthetic procedure overcoming the current issue in nanotechnology[19].
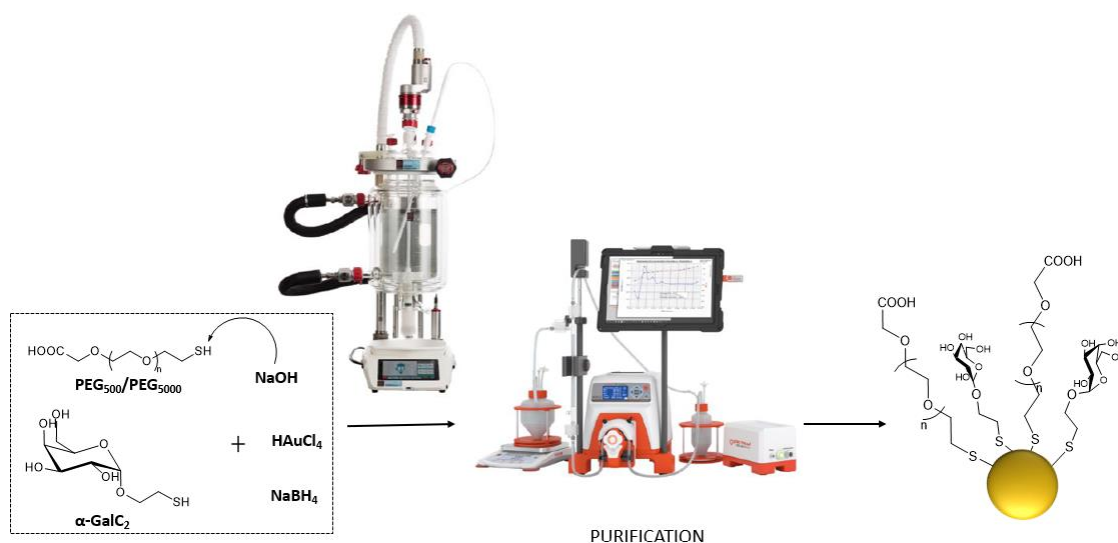
Figure 2.1*. Synthesis of UAuNPs with bench-top reactor*

UAuNPs 1-3 were synthetized as shown in table 2.1 with PEG_{500} and PEG_{5000}, while UAuNP-2 were synthesized employing a ratio 50:50 of α-galactose and PEG_{500}.

	Ligand I	Ligand II	Ligand ratio
UAuNPs – 1	HS-PEG_{500}-COOH	-	-
UAuNPs – 2	HS-PEG_{500}-COOH	α-$GalC_2$	50:50
UAuNPs – 3	HS-PEG_{5000}-COOH	-	-
UAuNPs – 7	-	α-$GalC_2$	-

Table 2.1. *UAuNPs 1-3, -7*

Optimal characterization of physicochemical properties is of extreme importance to predict the behaviour of the NPs in biological media; therefore, all NPs were characterized by UV-vis, dynamic light scattering (DLS), ζ-potential, transmission electron microscopy (TEM) as shown in table 2.2 and figure 2.2.

	Hydrodynamic diameter (nm)	Core diameter (nm)	ζ-potential (mV)
UAuNPs – 1	10.3	3.42 ± 1.29	- 43.8
UAuNPs – 2	9	3.98 ± 1.23	- 17.2
UAuNPs – 3	11	4.56 ± 1.79	- 33.8
UAuNPs – 7	5	3.15 ± 1.07	- 35.8

Table 2.2. *UAuNPs 1-3, -7*
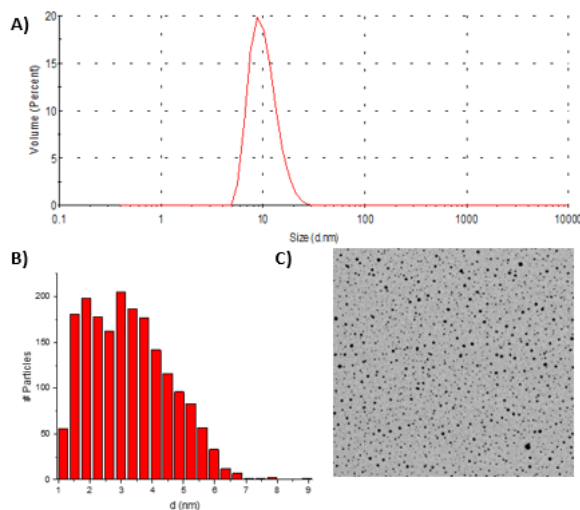
Figure 2.2. *Characterization of UAuNPs – 1 A) Hydrodynamic diameter measured by DLS B) Size distribution obtained by TEM analysis C) TEM micrograph*

2.3.2 Synthesis of 2-aminoethyl-α-D-mannopyranoside

Mannose was selected for the post-functionalization of the NPs and the consequent study of the biodistribution as it has been extensively used in NPs functionalization[20,21] and it is involved in biological functions (i.e. pathogenic infections, cancer, inflammation).[22]
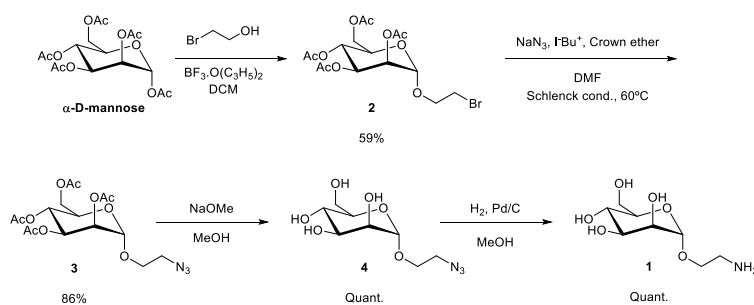
Scheme 2.1. Synthesis of 2-aminoethyl-α-D-mannopyranoside

The synthesis of compound **1** (scheme 2.1) started with the introduction of the linker 2-bromoethanol on the anomeric position of the peracetylated alpha-mannose, affording compound **2** as alpha- derivative. After the glycosylation reaction, compound **3** was obtained by replacing the bromine atom with an azido group via nucleophilic substitution. Deacetylation under Zemplen conditions provided 2-Azidoethyl-α-D-mannopyranoside (compound **4**) with a quantitative yield. The final step was the reduction of the azido group to amino group by hydrogenation in the presence of catalytic amount of Pd/C: compound **1** was obtained successfully and the structure was confirmed by ^{1}H-NMR and ^{13}C-NMR.

2.3.2.1 Post-functionalization of ultra-small gold nanoparticles

The post-functionalization of UAuNPs was performed through an amide condensation pathway, which consists in the coupling of a carboxylic acid to an amine: the reaction can be performed at room temperature as it forms an amide bond which is very stable. This procedure requires the activation of the carboxylic group present in PEG linkers, in situ using N-hydroxysulfosuccinimide (Sulfo-NHS) and 1-ethyl-3-(3-dimethylaminopropyl) carbodiimide (EDC) followed by the addition of compound **1.** The mechanism of the post-functionalization with EDC and Sulfo-NHS is shown in scheme 2.2.
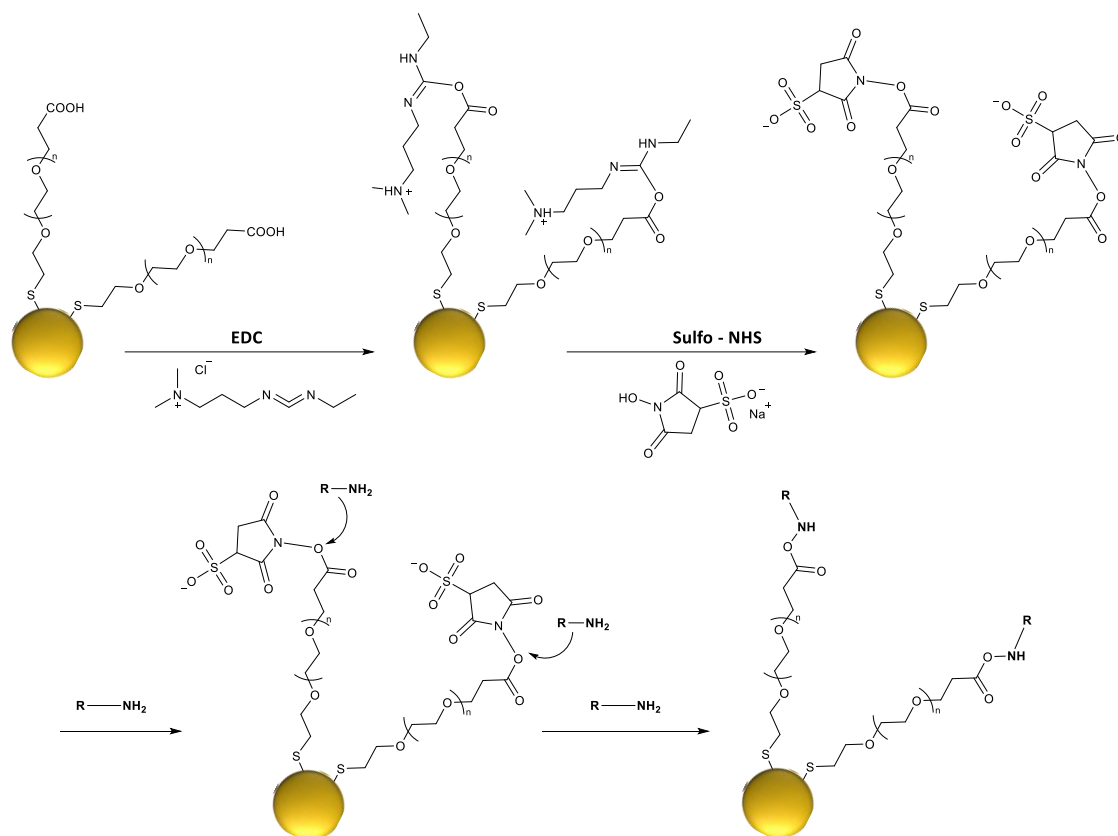
Scheme 2.2. Post-functionalization of UAuNPs with EDC and sulfo-NHS

After the post-functionalization the NPs were purified successfully by ultracentrifugation, obtaining the set of UAuNPs in table 2.3.

	Ligand I	Ligand II	Ligand ratio	Carbohydrate moiety
UAuNPs – 4	HS-PEG$_{500}$-COOH	-	-	α-ManC$_2$
UAuNPs – 5	HS-PEG$_{500}$-COOH	α-GalC$_2$	50:50	α-ManC$_2$
UAuNPs – 6	HS-PEG$_{5000}$-COOH	-	-	α-ManC$_2$

Table 2.3. UAuNPs 4-6

2.3.3 Biodistribution study

UAuNPs 1-6 were injected intravenously to each mouse with a dose of 300 µg of UAuNPs per kilogram (µg/kg) and after 1, 4 and 24 hours the mice were sacrificed and kidneys, liver spleen and blood were collected. A total of 105 mice were used during this experiment. The administrated dose was selected because it could be compared to previous biodistribution studies performed at Midatech Pharma[16]. Moreover, this dose had not presented any toxicity. The amount of gold present in the organs was quantified by ICP-OES and the biodistribution was analysed by immunofluorescence and auto metallography studies. The organs extracted were digested with acid solutions and heat in order to perform the ICP-OES studies.

2.3.3.1 Renal clearance of nanoparticles

UAuNPs are mostly eliminated by renal clearance as they can pass the renal pores, therefore the accumulation of gold in the kidneys was analysed. In figure 2.3A is shown the concentration of gold in kidneys which was quantified by ICP-OES at 1,4 and 24 hours after the treatment. The digestion and analysis by ICP-OES was performed at SCITEC-CNR. The quantity of gold present in kidneys for the UAuNPs coated solely with PEG were significantly higher compared to the UAuNPs with a carbohydrate moiety, being the highest for PEG_{500} at early time points. As expected, we observed an accumulation of gold in the kidney when the mice were treated with UAuNPs functionalized with shorter PEG (UAuNPs – 1, about 5500 ng/g, red) respect the mice treated with UAuNPs functionalized with long chain PEG (UAuNPs – 3, about 3500 ng/g, light green). The next time point, 4 hours, shows a decrease for UAuNPs – 1 to 5000 ng/g, this value is then increased at 24 hours to 6000 ng/g(red).
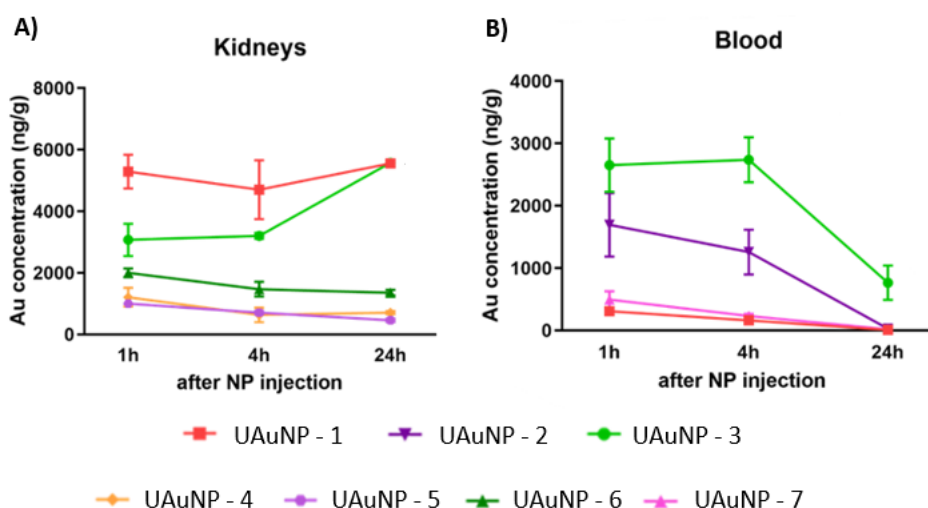
Figure 2.3*. Quantification of gold content in kidneys and blood after intravascular injection. A) Concentration of gold (ng/g) in kidneys measured by ICP-OES from mice treated with 5 different AuNPs at 1,4 and 24 hours after treatment. B) Concentration of gold (ng/g) in blood measured by ICP-OES from mice treated with 4 different AuNPs at 1,4 and 24 hours after treatment.*

It is important to underline that the organs of this study were not perfused and therefore the values of gold concentration after 1 hour are high as the NPs were still circulating at that time point; the values then decreased at 4 hours. The level of gold in kidneys of UAuNPs – 3 at the initial time points remain very similar as the NPs are still in circulation, once the NPs decrease in the bloodstream (figure 2.3B), the concentration of gold in the kidneys increases drastically arriving to 6000 ng/g.

UAuNPs – 4, UAuNPs – 5, UAuNPs – 6 which are coated with PEG_{500}-α-ManC$_2$, PEG_{500}-α-ManC$_2$+ α-GalC$_2$ and PEG_{5000}-α-ManC$_2$ present a different behaviour than the ones coated with only PEG, this demonstrates that attaching a terminal α-mannose can significantly change the final fate of the NPs. In all cases the maximum gold content levels were found at 1 hour after the administration, for UAuNPs – 4 and UAuNPs – 5 the concentration was 1000 ng/g and for UAuNPs – 6 2000 ng/g. These gold levels in the kidneys were lowered overtime this

demonstrates the effect of the presence of a terminal carbohydrate in the biodistribution of the NPs.

In figure 2.3B the amount of gold in blood is shown, this represents the half-life circulation time of the NPs. As expected, NPs with longer PEG linkers have a longer circulation life as less opsonization occurs, therefore UAuNPs – 3 have the higher concentration of gold in blood in the initial time points but it gets lower after 24 hours when the NPs start to be cleared of the body. On the other hand, UAuNPs – 1 have a shorter half-life, this could be caused by several reasons, they could be forming a protein corona and therefore they are recognised by RES organs and eliminated faster of the body. During this study UAuNPs coated solely with α-GalC$_2$ (UAuNP – 7) were included in order to have a control and compare them with PEG coated NPs. UAuNPs – 7 had a very short half-life as UAuNPs – 1. However, the combination of the PEG$_{500}$ with α-GalC$_2$ (UAuNP – 2) showed a longer half-life as the gold content was increased three times, this proved that a shorter PEG linker in combination with an aliphatic ligand bond to a monosaccharide can be also employed for coating NPs for example for nanocarrier purposes.

The kidneys collected from mice after 1 and 24 hours of the treatment with UAuNPs – 4, and UAuNPs – 6 were immune stained in order to analyse the samples with confocal microscopy as shown in figure 2.4.
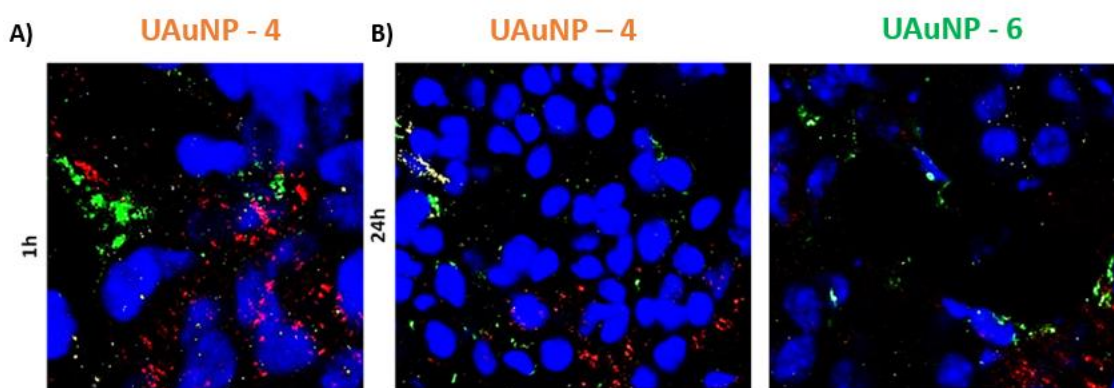
Figure 2.4. A) *Co-localization of UAuNPs in kidney tissue. Reflective SIM in kidney sections 1 hour after treatment. B) Co-localization of 4 nm UAuNPs in kidney tissue. Reflective SIM in kidney sections 24 hours after treatment. In blue, it is shown the nuclei (Hoescht), in green the macrophages (CD68), in yellow the lymphatic endothelial cells (Lyve-1) and in red UAuNPs (gold-reflective signal).*

In figure 2.4B the image of the confocal microscope shows the gold reflected of the UAuNPs in the kidney parenchyma, this proves that there is a high number of NPs in the tissue. After 24 hours the amount of UAuNPs functionalized with α-ManC$_2$ was lower as shown in figure 4B moreover this was also demonstrated by ICP-OES.

To better understand the renal interactions and their position in the kidney the NPs were observed by bright-field microscopy after silver staining by autometallography (AMG) as shown in figure 2.5. Only the UAuNPs coated by PEG and α-GalC$_2$ were observed by silver staining as the NPs must be aggregated in order to the silver to deposit on them. Therefore, the UAuNPs with terminal α-ManC$_2$ could not be observed as the levels of UAuNPs were lower than in the case of PEGylated NPs. UAuNPs coated with long PEG$_{5000}$ and short PEG$_{500}$ were mostly found in

the renal tubules as indicated in figure 2.5A. The long tubules in the nephrons which are responsible for the excretion filtration and reabsorption also filter the small molecules from the plasma[23], and therefore the UAuNPs are located in the renal tubules. The UAuNPs were eliminated by the urine as a change of colour from yellow to green was observed. The small size, PEGylation and the gold content allowed the NPs to bypass the glomerular filtration barrier of the kidneys even though typically the negative charged NPs are blocked by the filtration barrier.[24] The silver stained areas in the renal tubules were quantified, demonstrating there is a decrease after 24 hours, this proves the elimination of the NPs through the urine as they have already crossed a glomerular barrier as shown in figure 2.5B. The accumulation of the UAuNPs in other organs as liver and spleen is also a possibility.
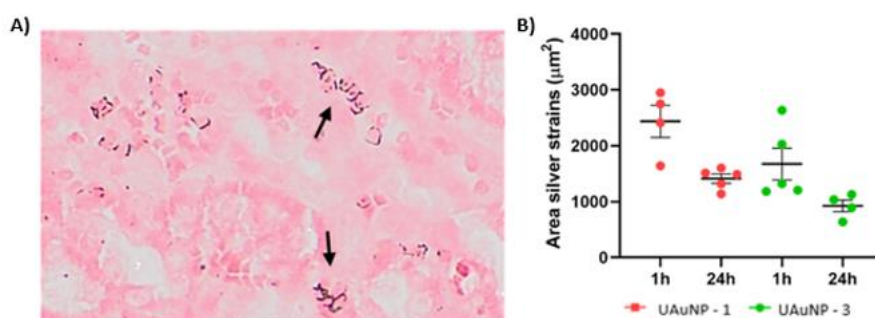
Figure 2.5*. A) AMG of UAuNPs in kidneys, localized mostly in the tubule system of the kidneys (black arrowheads) 1 hour after injection. Scale bars = 20 μm. B) Scatter plot of silver-stained area in renal tubules, comparing the two different PEG chain length.*

2.3.3.2 Liver clearance of nanoparticles

In order to fully evaluate the clearance pathways of the UAuNPs the liver was also analysed. The same tendency as in the kidneys was observed, UAuNPs – 1 and UAuNPs – 3, which are only coated with PEG accumulated more in the liver than the NPs with a terminal α-ManC$_2$ as shown in figure 2.6.

The opsonization and capture by MPS organs of UAuNPs was reduced with longer PEG chains as expected[25].In the other hand the UAuNPs coated with shorter PEG chains had a higher uptake, after the first hour the gold amount of UAuNPs – 1 was 8000 ng/g this value decreased after 4 hours to 5000 ng/g , this could be due to the NPs being still in the bloodstream. The mice treated with UAuNPs containing longer PEG chains (UAuNPs – 3) presented at 4 hours 3000 ng/g of gold and arrived at 3800 ng/g after 24 hours.
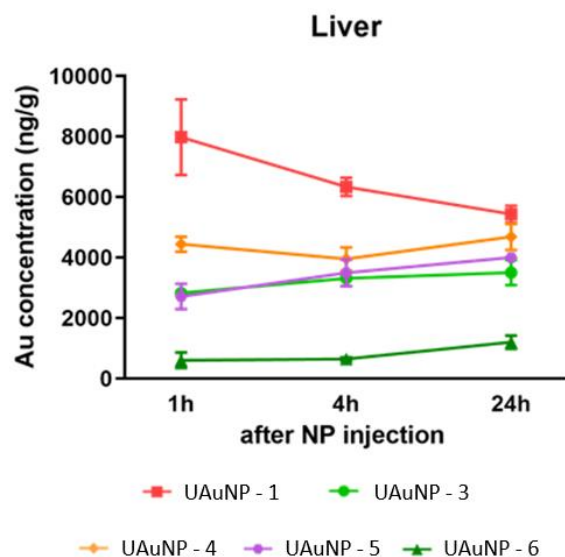
Figure 2.6. *Distribution of UAuNPs in liver after injection. A) Quantification of gold content in liver. Concentration of gold (ng/g) measured by ICP-OES from mice treated with 5 different UAuNPs at 1, 4 and 24 hours after treatment.*

The UAuNPs – 3 as shown in figure 2.4B were found to be longer time in the blood circulation, this could cause the elimination of the NPs by renal clearance avoiding the hepatic clearance. UAuNPs coated with PEG with a terminal α-ManC$_2$ present a different behaviour. The levels of gold concentration progressively increased arriving to 4000 ng/g at 4 hours after injection in the mice treated with NPs coated with a shorter PEG (UAuNPs – 4, orange). However, the mice treated with the PEG$_{5000}$ UAuNPs – 6 (dark green) showed a gold concentration of 1000 ng/g with nearly no variation overtime. This data proves that the presence of a terminal glycan in the PEG chains reduces the hepatic uptake.
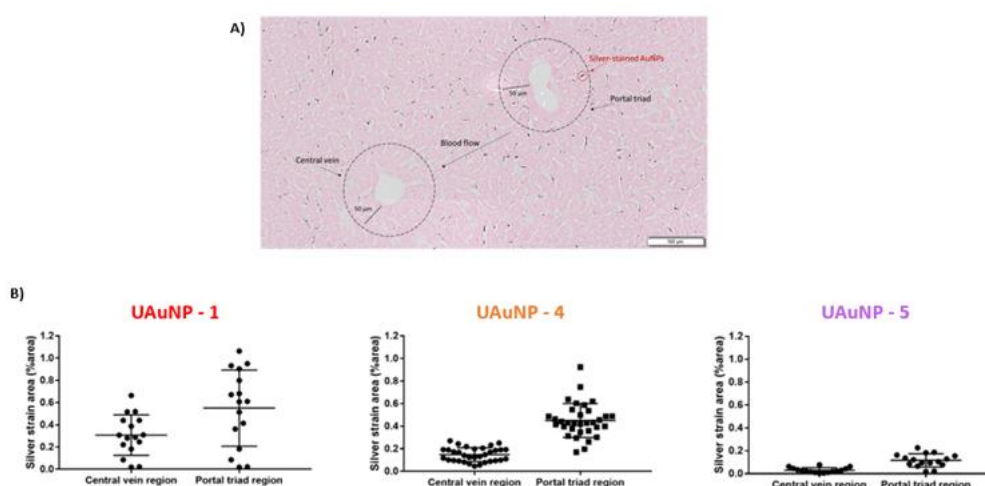
Figure 2.7. *A) AMG of silver stained UAuNPs in liver. B) Scatter plot comparing area of each region of silver staining UAuNPs coated with PEG-α-ManC$_2$ in the zones surrounding portal triad vs. zone surrounding central vein.*

34

Silver staining with AMG was performed in the liver, as it was in the kidneys, to better understand the biodistribution in the liver parenchyma at 1 and 24 hours after injection. Only UAuNPs – 1, UAuNPs – 4 and UAuNPs – 5 were detected by AMG, they are all coated with a shorter PEG chain, most of the signals were detected in the area surrounding the portal triad as shown in figure 2.7A. This could be because the blood flows from the portal triad to the central vein and it can lead most of the NPs to accumulate in the portal triad and a lower amount in the central vein. In figure 2.7B the silver staining amount in central vein and portal triad is compared, a clear effect of the glycan functionalization in the hepatic biodistribution is observed. The presence of α-GalC$_2$ in the coating of the NPs reduced the gold accumulation in the liver, this could be because these NPs avoid the macrophage uptake. Overall, the NPs showed the same tendency of accumulating in the portal triad over the central vein.
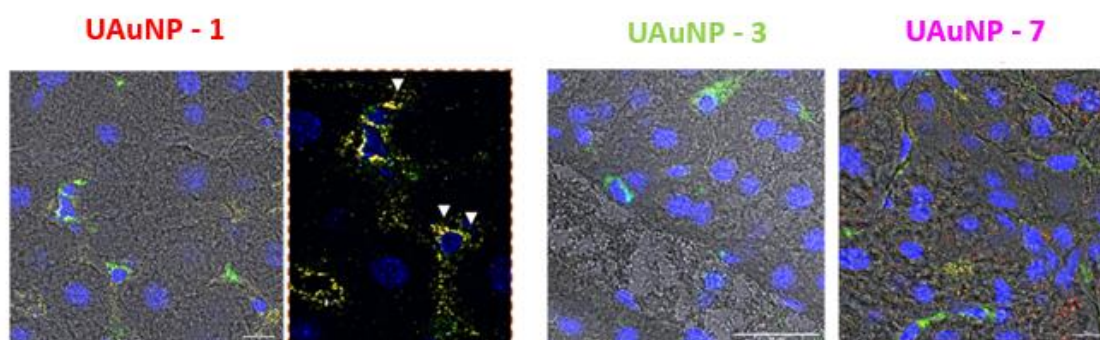
Figure 2.8. Co-localization of UAuNPs in liver tissue. Reflective SIM in liver sections of healthy mice treated with UAuNPs at two different time points (1 and 24 hours). In blue, it is shown the nuclei (Hoescht), in green the macrophages (CD68), in yellow the lymphatic endothelial cells (Lyve-1) and in red UAuNPs (gold-reflective signal).

The fate of the NPs inside the liver was observed by confocal microscopy 1 hour after treatment as they present the higher levels of gold as shown in figure 2.8. UAuNPs – 1 were in the membrane of perinuclear structures and co-localized with Kupffer cells (CD68+ cells). In the other hand NPs coated with long PEG chain (UAuNPs – 3) and post-functionalized with α-ManC$_2$ (UAuNPs – 4, UAuNPs – 5 and UAuNPs – 6) were not identified in the liver parenchyma, this could be due to the low levels found by ICP-OES. The NPs coated solely by α-GalC$_2$ were found in most of the hepatic tissue without co-localization with Kupferr cells and Lyve-1+ cells. These NPs are probably interacting with hepatocytes as they present a galactose-binding receptor in their surface.

2.3.3.3 Spleen clearance of nanoparticles

As mentioned before one of the major obstacles when the NPs are injected in the body is the opsonization. Subsequently the NPs are recognised by macrophages of the mononuclear phagocyte system (MPS), these NPs will then accumulate in the liver and spleen. Therefore, during this biodistribution study we decided to analyse the spleen.

The spleen was studied though silver staining by AMG at 24 hours after treatment but only NPs coated with PEG$_{500}$ were detected (figure 2.9). The NPs were found in the surrounding of the red pulp, the number of NPs found 1 hour after treatment was similar in all cases. The mice spleen

analysed 24 hours after treatment showed that UAuNPs – 4 had a decrease in the gold content, on the contrary UAuNP-5 which are coated with PEG-α-ManC$_2$ and α-GalC$_2$ show an increase of gold levels. The levels of UAuNPs coated only with α-GalC$_2$(data not shown) were high, this could mean that α-GalC$_2$ interacts with splenic macrophages and therefore the levels of UAuNPs – 5 are higher than UAuNPs – 4.
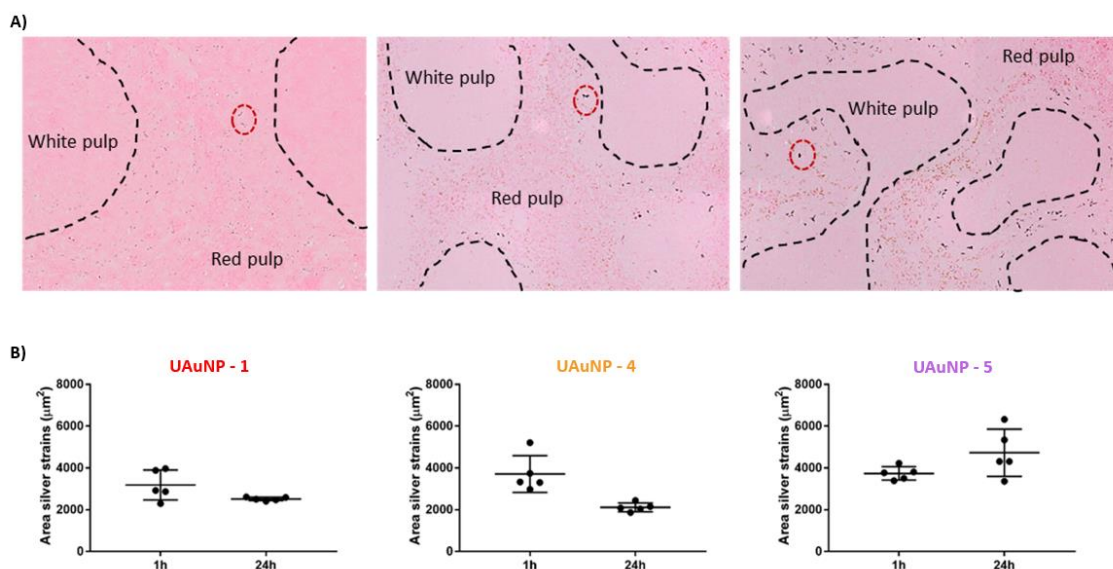
Figure 2.9. *Distribution of GNPs in spleen after treatment A) AMG of silver stained UAuNP-1, UAuNP- 4 and UAuNP – 5 (from left to right) in spleen, mostly found in the red pulp. Red circles indicate the presence of silver stained UAuNPs. Scale bars = 100 µm. D) Scatter plot of area with silver staining in the zones surrounding red pulp vs. areas surrounding the white pulp*

2.4 Conclusions

In this chapter the synthesis of 4 nm UAuNPs was described as well as the synthesis of 2-aminoethyl-α-mannopyranoside and the subsequent post-functionalization of UAuNPs. The UAuNPs were then injected to healthy mice and the organs (kidneys, liver, and spleen) were extracted at 1, 4 and 24 hours. The gold content in organs was analysed by ICP-OES. Selected organs were silver stained by auto metallography and further analysed with bright-field microscopy. Moreover, organs were immune stained to detect the UAuNPs by confocal microscopy.

Overall, the data obtained demonstrated that UAuNPs functionalized with longer PEG chains have a longer half-life compared to the shorter PEG, even though the combination of a shorter PEG with and short aliphatic ligand with a terminal α-galactose can increase the circulation time in the blood stream. UAuNPs functionalized with a terminal α-mannose showed a lower accumulation in the liver and kidneys than the NPs with only PEG, it was also observed a different biodistribution inside the liver. The spleen data showed a higher accumulation of NPs with α-galactose, this could be due to interaction with the splenic macrophages. The data shown in liver and kidneys predict that the NPs were eliminated of the body by renal clearance.

2.5 Experimental

2.5.1 Material and methods

All chemicals were purchased from commercial sources and used without further purification unless otherwise stated. Dry solvents were purchased from Acros Organics and Sigma-Aldrich. All reactions containing moisture or air-sensitive reagents were carried out under argon atmosphere. Thin-layer chromatography (TLC) was used to monitor reactions (Silica Gel 60 F254, Merck) using p-Anisaldehyde/Sulfuric acid/Acetic acid in methanol or ethanol as visualization reagents. Chromatographic purification was performed using a pre-column (Silica Gel 60 F254, Merck) and a commercial 40 µm silica cartridge adapted on a flash chromatography system (Reveleris, Grace Davison Discovery Science). The evaporative light scattering detector (ELSD, monitors non-UV-absorbent molecules) of the device was used to spot, fraction and recover the reaction products. Compounds were purified by flash chromatography using silica gel (SiO2, high-purity grade, pore size 60 Å, mesh particle size 230-400) from Sigma-Aldrich. Characterization of the final product and, when possible, intermediates, was performed by 1H NMR spectroscopy (500 MHz, CDCl3 or D2O). Final products were also analyzed by 13C NMR (126 MHz, D2O). Experiments were performed at 298 K on a Bruker AVANCE III 500 spectrometer at CIC BiomaGUNE (San Sebastian, Spain).

Six-week-old female CD1 mice were purchased from Charles River (Italy) and were maintained under specific pathogen-free conditions (SPF) in the Institute's Animal Care Facilities. Animals were bred in rooms at constant temperature of 21 ± 1°C, humidity of 55 ± 10% with a 12 h light/dark cycle and ad libitum access to food and water. All mice were regularly checked by a veterinarian who is responsible for animal welfare supervision and experimental protocol review. None of the animals died during the study. Briefly, all animals received, by intravenous injection, the same dose of NPs preparation (300 µg/kg). At the selected time points (pre injection, 1, 4 and 24 h) after NPs injection, 5 mice for each group were sacrificed and organs collected for histological analysis.

2.5.2 Synthesis of ultra-small gold nanoparticles

The synthesis and characterization of UAuNPs was performed at Midatech Pharma PLC. PEGylated and galactose functionalized NPs were synthesized at a 200 mg Au scale using a modified Brust-Schiffrin method[16] in a using Syrris Atlas Potassium reactor with a 2000 mL jacketed torispherical vessel and a 500-50 mm blade propeller stirrer without baffles. The temperature was equilibrated before the reagents addition and maintained during the synthesis using Julabo CF40 Cryo-Compact Circulator. The reactions were carried out at 18 °C, with fast stirring (750 rpm). 400 mg of $HAuCl_4$ were dissolved in approximately 1600 mL of H_2O. The pH was adjusted to 11.3 by adding 2 M NaOH solution. An aqueous solution of $NaBH_4$ (25 mL, 1 M) was added to the reaction, shortly after a water solution of PEG_{5000}-COOH-SS, PEG_{500}-COOH-SS, α-Gal-C_2-SS (0.158 mM) or a mixture of two was added. The pH was then adjusted to 12 – 12.3 by adding NaOH 0.01M. A dark red solution was obtained and was left stirring for 30 min before purification by tangential flow filtration (TFF).

2.5.3 Characterization of ultra-small gold nanoparticles

UV-vis absorption spectra were measured using a Perkin-Elmer Lambda 35 UV-Vis Spectrophotometer. Dynamic light scattering (DLS) was measured in triplicate using a Zetasizer Nano ZS (Malvern Instruments Ltd., UK) at 25°C in PBS. Mean volume-weighted hydrodynamic diameter of the particles was used as a measure of UAuNPs size. UAuNPs bound ligands were analysed by ^{1}H NMR (Bruker AVANCE III 500 spectrometer, 500 MHz, D_2O) after dissolution of gold cores by treatment with KCN/KOH (0.3 M/ 0.1 M, respectively in D_2O). The data is shown in figures 2.10,2.11,2.12 and 2.13.
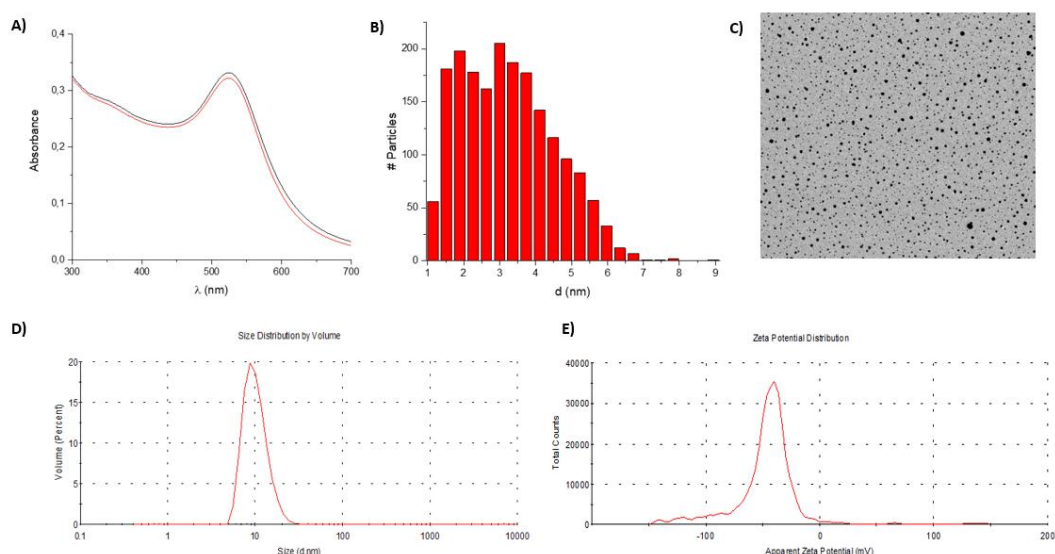
Figure 2.10. Characterization UAuNPs – 1 A) UV-vis B) Size distribution of TEM analysis, mean 3.422 nm SD 1.293nm C) TEM micrograph scale 20 nm D) Hydrodynamic size obtained by DLS E) ζ-Potential
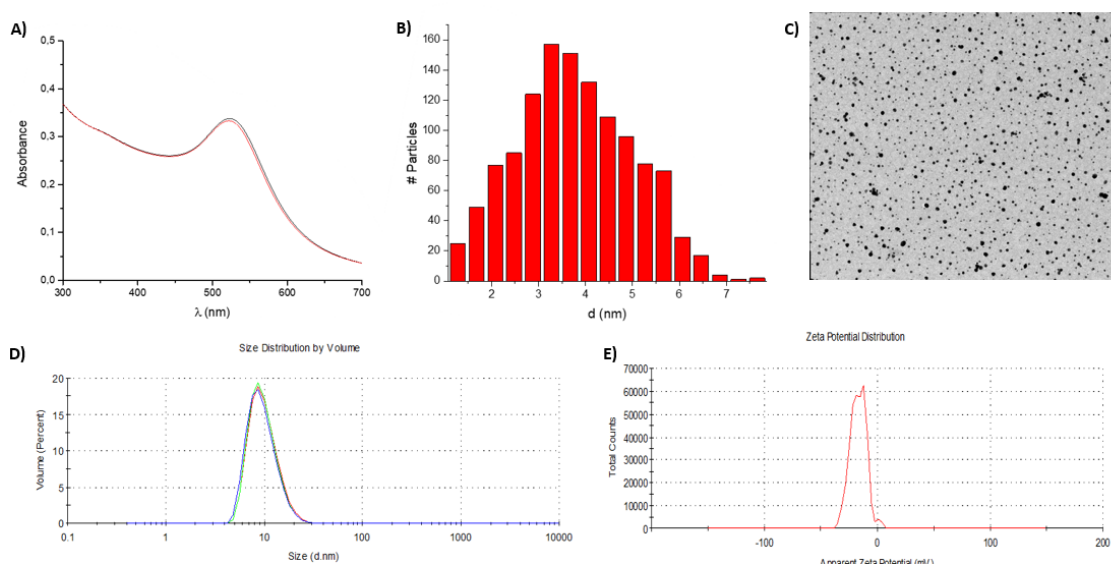
Figure 2.11. Characterization UAuNPs – 2 A) UV-vis B) Size distribution of TEM analysis, Mean 3.976 nm SD 1.233nm C) TEM micrograph scale 20 nm D) Hydrodynamic size obtained by DLS E) ζ-Potential
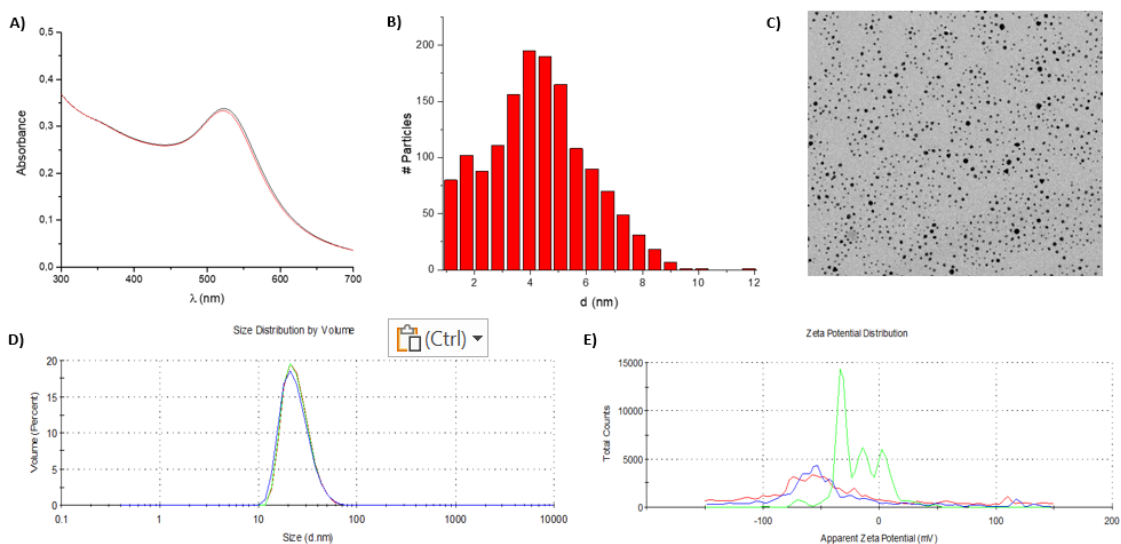
Figure 2.12*. Characterization UAuNPs – 3 A) UV-vis B) Size distribution of TEM analysis, mean 4.561 nm SD 1.786 nm C) TEM micrograph scale 20 nm D) Hydrodynamic size obtained by DLS E) ζ-Potential*
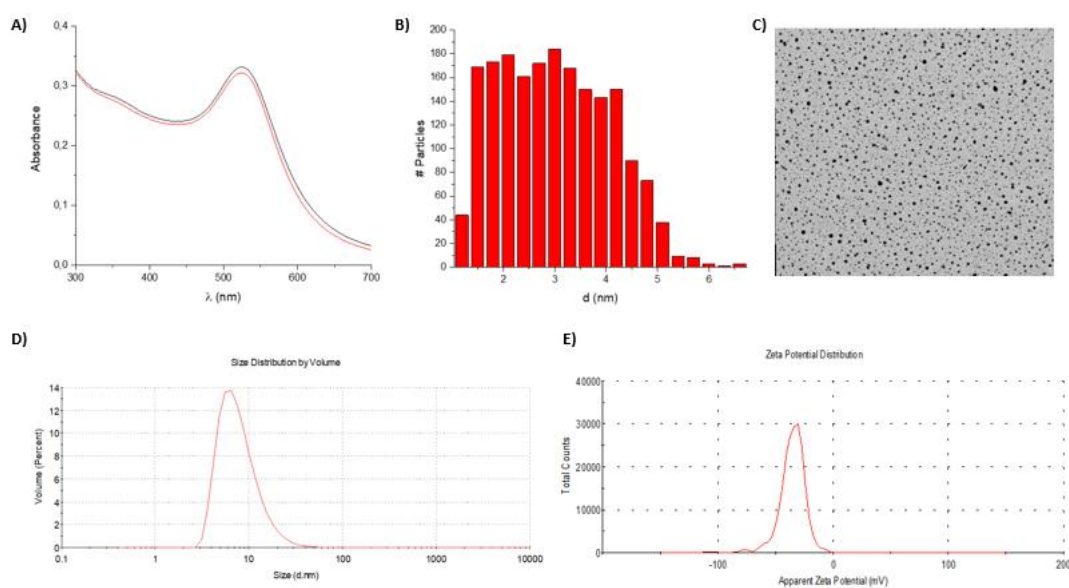
Figure 2.13*. Characterization UAuNPs – 7 A) UV-vis B) Size distribution of TEM analysis, mean 3.149 nm SD 1.065 nm C) TEM micrograph scale 20 nm D) Hydrodynamic size obtained by DLS E) ζ-Potential*

2.5.4 Induced Coupled Plasma optical emission spectroscopy

Kidneys, livers, and blood were stored at -20ºC until the digestion was carried out. All organs were digested following the same procedure, first they were dissolved in 2 mL of a solution of nitric acid: hydrogen peroxide (3:1) this solution was evaporated in a hot plate in a Teflon becker, this process was repeated twice, the next step was to repeat the same process with 1 mL of aqua regia (chlorohydric acid: nitric acid, 3:1): this step was performed twice. After evaporating nearly completely the acid solution, 1 mL of a solution 0.5 M of chlorohydric acid was added and the sample was diluted with water. Elemental analyses were performed by inductively coupled plasma optical emission spectroscopy (ICP-OES iCAP 6200 Duo upgrade, Thermofisher) with external calibration.

2.5.5 Synthesis of 2-aminoethyl-α-D-mannopyranoside

Compounds 1,2,3 and 4 are well known and have already been fully characterized.[26]

- **Synthesis of 2-Bromoethyl 2,3,4,6-tetra-O-acetyl-α-D-mannopyranoside (2)**
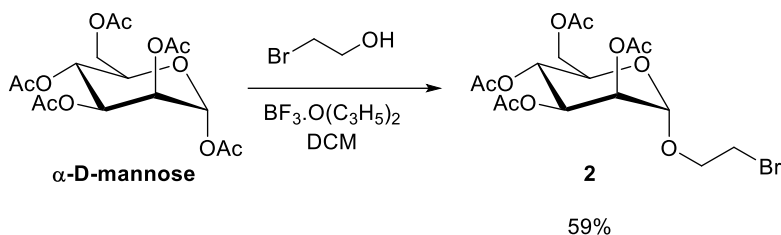
α-D-mannose pentaacetate was put under vacuum during 30min to remove the residual humidity *at Room Temperature (RT) in a stirred flask.* **α-D-mannose** (6 g, 15.37 mmol) was dissolved in DCM (30 mL), $BF_3O(C_3H_5)_2$ (5 mL, 40.5 mmol). The reaction was stirred overnight and monitored by TLC (Hep: EtOAc – 1:1, *eluted twice stained with anisaldehyde*), the reaction was quenched with triethylamine until neutral pH, the solvent was then evaporated. The crude product was purified by column chromatography (Hep: EtOAc 8:2 -> 7:3) to obtain compound **2** (4.135 g, 59,07%).

1H NMR (500 MHz,CDCl3) δ 5.35 (dd, *J* = 10.0, 3.4 Hz, 1H, H-3), 5.32 – 5.25 (m, 2H, H-4, H-2), 4.87 (d, *J* = 1.7 Hz, 1H, H-1), 4.27 (dd, *J* = 12.6, 5.9 Hz, 1H, H-6), 4.17 – 4.09 (m, 2H, H-5,H-6'), 3.98 (dt, *J* = 11.1, 6.3 Hz, 1H,C$\underline{H}_2$O), 3.89 (dt, *J* = 11.3, 5.7 Hz, 1H,C$\underline{H}_2$O,), 3.52 (t, *J* = 6.0 Hz, 2H,CH$_2$Br), 2.16 (s, 3H, CH$_3$-CO), 2.11 (s, 3H, CH$_3$-CO), 2.05 (s, 3H, CH$_3$-CO), 2.00 (s, 3H, CH$_3$-CO). **13C NMR** (126 MHz, CDCl3) δ 170.63 - 169.77(CH$_3$-CO), 97.77 (C-1), 69.44(C-2), 69.04(C-3 or C-4), 68.95(C-5), 68.50(C-3 or C-4), 66.02(C-7), 62.43(C-6), 29.61(C-8), 20.88(CH$_3$-CO), 20.76(CH$_3$-CO), 20.72(CH$_3$-CO), 20.68(CH$_3$-CO).

- **Synthesis of 2-Azidoethyl 2,3,4,6-tetra-O-acetyl-α-D-mannopyranoside (3)**
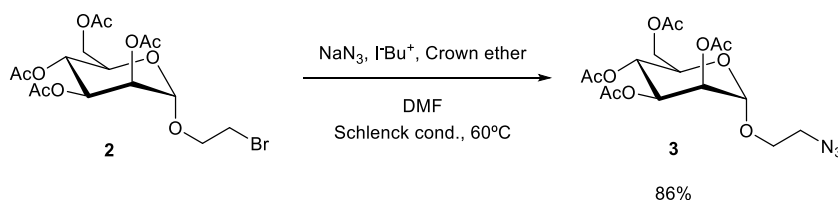
2 (3.66 g, 8.03 mmol) was dissolved in dry DMF (50 mL) and heated at 60°C in a silicon bath in a stirred flask. NaN$_3$ (4.176 g, 64,24 mmol) and catalytic amounts of tetra-n-butylammonium iodide and dibenzo-8-crown-6 were added to the solution and the reaction mixture was stirred for 5 hours and was followed by TLC *(*Hep: EtOAc 1:1, eluted twice stained with anisaldehyde). Once the reaction was considered terminated it was quenched by dilution in 100 mL of EtOAc as was washed three times with NH$_4$CL 0.1 M, H$_2$O and Brine (100 mL each time). The organic phase was recovered and dried over anhydrous Na$_2$SO$_4$ and filtered. The crude was purified by column flash chromatography (Hep: EtOAc 8:2 -> 7:3) to obtain compound **3** (2.87 g, 86%) as a white powder.

¹H NMR (500 MHz, CDCl₃) δ 5.36 (dd, *J* = 10.0, 3.4 Hz, 1H, H-3), 5.33 – 5.26 (m, 2H, H-4, H-2), 4.87 (d, *J* = 1.8 Hz, 1H,H-1), 4.29 (dd, *J* = 12.3, 5.4 Hz, 1H, H-6), 4.13 (dd, *J* = 12.3, 2.4 Hz, 1H, H-5,), 4.05 (ddd, *J* = 9.9, 5.4, 2.4 Hz, 1H, H-6'), 3.87 (ddd, *J* = 10.6, 6.9, 3.7 Hz, 1H, C$\underline{H}_2$O), 3.67 (ddd, *J* = 10.6, 6.0, 3.6 Hz, 1H C$\underline{H}_2$O), 3.47 (qdd, *J* = 13.3, 6.4, 3.6 Hz, 2H, CH₂N₃), 2.16 (s, 3H, CH₃-CO), 2.11 (s, 3H, CH₃-CO), 2.05 (s, 3H, CH₃-CO), 2.00 (s, 3H, CH₃-CO).
¹³C NMR (126 MHz, CDCl₃) δ 170.64 - 169.78 (CH₃-CO), 97.76(C-1), 69.40(C-2), 68.86(C-3 or C-4), 67.06(C-5), 66.01(C-3 or C-4), 62.47(C-7), 50.37(C-6), 20.88(C-8), 20.75(CH₃-CO), 20.72(CH₃-CO), 20.67(CH₃-CO).

- Synthesis of 2-Azidoethyl-α-D-mannopyranoside (4)
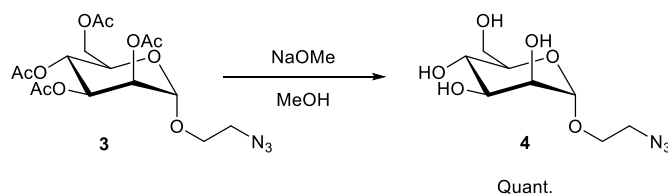
3 (2.85 g, 6.8 mmol) was dissolved in Methanol (50 mL) and NaOMe (0.37 g, 6.8 mmol*) was* added to the solution and the reaction mixture was stirred for 1 hour and was followed by TLC (Hep:EtOAc 1:1, stained with anisaldehyde). Once the reaction was terminated *t*he reaction mixture was quenched using Amberlite IR120 (H+ form), filtered and concentrated in vacuo to afford compound **4** (1.8 g, quant.) as a colourless syrup.

¹H NMR (500 MHz, D₂O) δ 4.83 (d, *J* = 1.8 Hz, 1H, , H-1), 3.89 (dd, *J* = 3.5, 1.8 Hz, 1H, H-2), 3.87 – 3.78 (m, 2H, C$\underline{H}_2$-O, H-6), 3.75 (dd, *J* = 9.1, 3.3 Hz, 1H, H-3), 3.71 – 3.53 (m, 4H, C$\underline{H}_2$-O, H-6´, H-5, H-4), 3.43 (qdd, *J* = 13.6, 6.6, 3.1 Hz, 2H, CH₂-N₃).
¹³C NMR (126 MHz, D₂O) δ 170.41, 99.80(C-1), 72.89(C-5), 70.39(C-3), 69.93(C-2), 66.68(C-4), 66.30(C-7), 60.91(C-6), 50.20(C-8).

- Synthesis of 2-Aminoethyl-α-D-mannopyranoside (1)
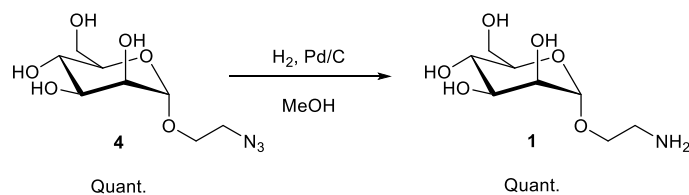
To a solution of compound **4** (0.244 g, 0.98 mmol) in MeOH (20 mL), a catalytic amount of Pd/C was added. The reaction atmosphere was purged with H₂/vacuum cycles and then, stirred under H₂ atmosphere. After 3 h, the Pd/C was filtered and concentrated in vacuo to give compound **1** as a colourless syrup (0.22 g, quant.).

¹H NMR (500 MHz, Deuterium Oxide) δ 4.89 – 4.85 (m, 1H, H-1), 3.96 (td, *J* = 3.5, 1.8 Hz, 1H, H-2), 3.89 (dd, *J* = 12.1, 1.7 Hz, 1H, C$\underline{H}_2$-O, H-6), 3.86 – 3.72 (m, 2H, C$\underline{H}_2$-O, H-6',H-3), 3.73 – 3.48 (m, 3H,H-7,H-4, H-5), 2.83 (dtt, *J* = 18.6, 13.1, 6.0 Hz, 2H, CH₂-NH₂).

¹³C NMR (126 MHz, Deuterium Oxide) δ 99.87 (d, *J* = 7.7 Hz, C-1), 72.74 (d, *J* = 11.1 Hz, C-5), 70.53 (d, *J* = 5.8 Hz,C-3), 69.98(C-2), 68.76(C-4), 66.76(C-7), 60.92(C-6), 39.89(C-8).

2.5.6 Post-functionalization ultra-small gold nanoparticles

2-Aminoethyl-α-mannopyranoside was attached on the NPs by amide condensation post-functionalization. N-ethylcarbodiimide (EDC) (3 equiv.) was dissolved in Milli-Q water (13 mg/mL) and mixed with a solution of 3-sulfo-N-hydroxysuccinimide (Sulfo-NHS) (6 equiv.) in Milli-Q water (30 mg/mL) this solution was added to 2 mL of the nanoparticles(UAuNPs- 1 – 1.978 mg/mL, UAuNPs - 2 – 1.88 mg/mL, UAuNPs - 3 – 3.136 mg/mL) the reaction was stirred for 2 hours, the solution was transferred to an Amicon filter 30 kDa and it was centrifuged for 10 min in order to remove the excess of EDC/Sulfo-NHS, the NPs were then resuspended in 2 mL of PBS 10 mM. 2-aminoethyl-mannopyranoside (5 equiv.) was dissolved in PBS 10 mM (4 mg/mL) and added to the reaction and left overnight. The NPs were then purified with Amicon 30 kDa by centrifugation (6 min, 6000 rpm).

The sections 2.5.7 and 2.5.8 were developed by our collaborators at Istituto Mario Negri.

2.5.7 Histology

2.5.7.1 Immunohistochemistry

At time of autopsy for each mouse, kidneys, liver and spleen were sampled, fixed in 10 % neutral buffered formalin (Bio-Optica, Italy) for at least 24h at RT and then were processed for paraffin embedding. Tissue micrometric sections (4 μm in thickness) were cut with Leica RM55 microtome (Leica Microsystem, Italy) and dried in the oven at 37°C overnight. Samples were dewaxed and rehydrated. To visualize the presence of gold agglomerates in the organ parenchyma, autometallography (AMG) staining was carried out, as previously described. Haematoxylin and eosin staining (H&E) was performed in liver sections treated with GNPs and vehicle-treated mice, to provide a general overview of the tissue structure. Haematoxylin stains cell nuclei blue, and eosin stains the extracellular matrix and cytoplasm pink. Nuclei were stained with Mayer's haematoxylin solution (Bio-Optica, Italy), and counterstain in eosin Y solution (Bio-Optica, Italy) to stain the cytoplasm. Samples were dehydrated and glasses were dried under the hood and mount with xylene-based mounting medium (DPX, Sigma). All images were acquired using Olympus BX61VS.

2.5.7.2 Immunofluorescence

Immunohistochemical analysis in liver and kidneys was performed in tissue slides of 10 μm cut by cryostat. Tissue sections were fixed in 10% neutral buffered formalin (Bio-Optica, Italy), washed with phosphate-buffered saline (PBS) and incubated with a blocking solution (PBS-NGS 10%-Triton X-100 0.1%). For subcellular localization, the following antibodies were used: anti-CD68 (1:200, Serotec, Kidlington, UK) was used to label lysosomes and endosome membranes of macrophages, Lyve-1 (1:300, Biotechne) was used to label lymphatic endothelial cells and Hoescht-33258 (1 μg/mL in PBS, Thermo Fisher Scientific) to label nuclei.

2.5.8 Reflective Confocal Microscopy

In order to visualize ex vivo the GNPs in mice liver and kidneys cryo-sections, reflection confocal microscopy was chosen. An inverted SP5 true filter-less confocal with 8 laser lines and 4 PMTs was used (Leica microsystems). The 514 nm laser line was chosen as optimal gold reflecting excitation light, with reflected emission through opening of AOTF-driven spectral detector in the range of 512-517 nm wavelengths. A 1.40 NA, 63x oil objective was used (Leica microsystems),

coupled with system optical zooming in of 3x-9x range, when needed. For gold reflection scanning modality, the confocal pinhole was set at 0.5 AU. In the sequence of laser-scanning acquisition, besides reflection scan, also transmission signal and fluorescence biological signals were acquired, according to labelled immune-fluorescence reactions. For biological signals scans, the confocal pinhole was set to 1 AU. Either 1 z-plan at best focal plan for each field of view, or 10-micron Z-volume with 0.25-micron Z-step images were acquired, according to need. 16-bit depth of signal resolution was acquired over 1024x1024 pixel dwell/image with 400 Hz lasers acquisition frequency; laser powers were set on negative control samples as following: 405 nm (10%) for Hoechst signal excitation (nuclear detection) and for transmission, 488 nm (25%) for CD68-(af488) signal, 514 nm (50%) for reflection modality, 633 nm (35%) for Lyve-1-(af647) signal. All PMTs were set on 580-690V gain range with a -1/-2.5 % offset range. In order to increase confocal resolution of the reflecting signal, Richardson-Lucy deconvolution algorithm was used, applying the specific module in NIS-Elements software v5.30 (Nikon Instruments/ Lim Instruments). Signal thresholding, binarization, object classification and segmentation, to detect tissue and cell primary and secondary objects, were performed using an ad-hoc computed pipeline of analysis within the General Analysis module in NIS-Elements v5.30.

2.5.9   Statistics

All the tests carried out for the physico-chemical characterization of NPs were performed at least in triplicates. For *in vivo* experiments, the number of animals sacrificed at each data point was minimized (n = 5) according to the 3Rs principle. P values <0.05 were considered statistically significant and reported on graphs. Data are presented as mean values ± SEM and analyzed using Prism 5 (GraphPad Software).

2.6   References

(1)   Li, B.; Lane, L. A. Probing the Biological Obstacles of Nanomedicine with Gold Nanoparticles. *WIREs Nanomed Nanobiotechnol* **2019**, *11* (3). https://doi.org/10.1002/wnan.1542.

(2)   De Jong, W. H.; Hagens, W. I.; Krystek, P.; Burger, M. C.; Sips, A. J. A. M.; Geertsma, R. E. Particle Size-Dependent Organ Distribution of Gold Nanoparticles after Intravenous Administration. *Biomaterials* **2008**, *29* (12), 1912–1919. https://doi.org/10.1016/j.biomaterials.2007.12.037.

(3)   Liu, J.; Yu, M.; Zhou, C.; Yang, S.; Ning, X.; Zheng, J. Passive Tumor Targeting of Renal-Clearable Luminescent Gold Nanoparticles: Long Tumor Retention and Fast Normal Tissue Clearance. *J. Am. Chem. Soc.* **2013**, *135* (13), 4978–4981. https://doi.org/10.1021/ja401612x.

(4)   Zhou, C.; Long, M.; Qin, Y.; Sun, X.; Zheng, J. Luminescent Gold Nanoparticles with Efficient Renal Clearance. *Angew. Chem. Int. Ed.* **2011**, *50* (14), 3168–3172. https://doi.org/10.1002/anie.201007321.

(5)   Poon, W.; Heinmiller, A.; Zhang, X.; Nadeau, J. L. Determination of Biodistribution of Ultrasmall, near-Infrared Emitting Gold Nanoparticles by Photoacoustic and Fluorescence Imaging. *J. Biomed. Opt* **2015**, *20* (6), 066007. https://doi.org/10.1117/1.JBO.20.6.066007.

(6)   Boselli, L.; Polo, E.; Castagnola, V.; Dawson, K. A. Regimes of Biomolecular Ultrasmall Nanoparticle Interactions. *Angew. Chem. Int. Ed.* **2017**, *56* (15), 4215–4218. https://doi.org/10.1002/anie.201700343.

(7)   Chen, T.-Y.; Chen, M.-R.; Liu, S.-W.; Lin, J.-Y.; Yang, Y.-T.; Huang, H.-Y.; Chen, J.-K.; Yang, C.-S.; Lin, K. M.-C. Assessment of Polyethylene Glycol-Coated Gold Nanoparticle Toxicity and Inflammation In Vivo Using NF-ΚB Reporter Mice. *IJMS* **2020**, *21* (21), 8158. https://doi.org/10.3390/ijms21218158.

(8)   Walkey, C. D.; Olsen, J. B.; Guo, H.; Emili, A.; Chan, W. C. W. Nanoparticle Size and Surface Chemistry Determine Serum Protein Adsorption and Macrophage Uptake. *J. Am. Chem. Soc.* **2012**, *134* (4), 2139–2147. https://doi.org/10.1021/ja2084338.

(9)   Sangabathuni, S.; Murthy, R. V.; Chaudhary, P. M.; Subramani, B.; Toraskar, S.; Kikkeri, R. Mapping the Glyco-Gold Nanoparticles of Different Shapes Toxicity, Biodistribution and Sequestration in Adult Zebrafish. *Sci Rep* **2017**, *7* (1), 4239. https://doi.org/10.1038/s41598-017-03350-3.

(10)   Bogdan, N.; Roy, R.; Morin, M. Glycodendrimer Coated Gold Nanoparticles for Proteins Detection Based on Surface Energy Transfer Process. *RSC Adv.* **2012**, *2* (3), 985–991. https://doi.org/10.1039/C1RA00904D.

(11)   Farr, T. D.; Lai, C.-H.; Grünstein, D.; Orts-Gil, G.; Wang, C.-C.; Boehm-Sturm, P.; Seeberger, P. H.; Harms, C. Imaging Early Endothelial Inflammation Following Stroke by Core Shell Silica Superparamagnetic Glyconanoparticles That Target Selectin. *Nano Lett.* **2014**, *14* (4), 2130–2134. https://doi.org/10.1021/nl500388h.

(12)   Meldal, M.; Tornøe, C. W. Cu-Catalyzed Azide–Alkyne Cycloaddition. *Chem. Rev.* **2008**, *108* (8), 2952–3015. https://doi.org/10.1021/cr0783479.

(13)   Poonthiyil, V.; Lindhorst, T. K.; Golovko, V. B.; Fairbanks, A. J. Recent Applications of Click Chemistry for the Functionalization of Gold Nanoparticles and Their Conversion to Glyco-Gold Nanoparticles. *Beilstein J. Org. Chem.* **2018**, *14*, 11–24. https://doi.org/10.3762/bjoc.14.2.

(14)   Roskamp, M.; Coulter, T.; Ding, Y.; Perrins, R.; Espinosa Garcia, C.; Pace, A.; Hale, S.; Robinson, A.; Williams, P.; Aguilera Peral, U.; Patel, K.; Palmer, D. SIKVAV Peptide Functionalized Ultra-Small Gold Nanoparticles for Selective Targeting of Α6β1 Integrin in Hepatocellular Carcinoma. *J. Phys.: Conf. Ser.* **2017**, *829*, 012017. https://doi.org/10.1088/1742-6596/829/1/012017.

(15)   de la Fuente, J. M.; Barrientos, A. G.; Rojas, T. C.; Rojo, J.; Cañada, J.; Fernández, A.; Penadés, S. Gold Glyconanoparticles as Water-Soluble Polyvalent Models To Study Carbohydrate Interactions. *Angew. Chem. Int. Ed.* **2001**, *40* (12), 2257–2261. https://doi.org/10.1002/1521-3773(20010618)40:12<2257::AID-ANIE2257>3.0.CO;2-S.

(16)   Hale, S. J. M.; Perrins, R. D.; García, C. E.; Pace, A.; Peral, U.; Patel, K. R.; Robinson, A.; Williams, P.; Ding, Y.; Saito, G.; Rodriguez, M. Á.; Perera, I.; Barrientos, A.; Conlon, K.; Damment, S.; Porter, J.; Coulter, T. DM1 Loaded Ultrasmall Gold Nanoparticles Display Significant Efficacy and Improved Tolerability in Murine Models of Hepatocellular Carcinoma. *Bioconjugate Chem.* **2019**, *30* (3), 703–713. https://doi.org/10.1021/acs.bioconjchem.8b00873.

(17)   Ghosh, C.; Priegue, P.; Leelayuwapan, H.; Fuchsberger, F. F.; Rademacher, C.; Seeberger, P. H. Synthetic Glyconanoparticles Modulate Innate Immunity but Not the Complement System. *ACS Appl. Bio Mater.* **2022**, *5* (5), 2185–2192. https://doi.org/10.1021/acsabm.2c00026.

(18)   Sweeney, S. F.; Woehrle, G. H.; Hutchison, J. E. Rapid Purification and Size Separation of Gold Nanoparticles via Diafiltration. *J. Am. Chem. Soc.* **2006**, *128* (10), 3190–3197. https://doi.org/10.1021/ja0558241.

(19)   Halwani, A. A. Development of Pharmaceutical Nanomedicines: From the Bench to the Market. *Pharmaceutics* **2022**, *14* (1), 106. https://doi.org/10.3390/pharmaceutics14010106.

(20) Chiodo, F.; Marradi, M.; Tefsen, B.; Snippe, H.; van Die, I.; Penadés, S. High Sensitive Detection of Carbohydrate Binding Proteins in an ELISA-Solid Phase Assay Based on Multivalent Glyconanoparticles. *PLoS ONE* **2013**, *8* (8), e73027. https://doi.org/10.1371/journal.pone.0073027.

(21) Martínez-Ávila, O.; Hijazi, K.; Marradi, M.; Clavel, C.; Campion, C.; Kelly, C.; Penadés, S. Gold *Manno* -Glyconanoparticles: Multivalent Systems to Block HIV-1 Gp120 Binding to the Lectin DC-SIGN. *Chem. Eur. J.* **2009**, *15* (38), 9874–9888. https://doi.org/10.1002/chem.200900923.

(22) Loke, I.; Kolarich, D.; Packer, N. H.; Thaysen-Andersen, M. Emerging Roles of Protein Mannosylation in Inflammation and Infection. *Molecular Aspects of Medicine* **2016**, *51*, 31–55. https://doi.org/10.1016/j.mam.2016.04.004.

(23) Huang, J.; Chen, X.; Jiang, Y.; Zhang, C.; He, S.; Wang, H.; Pu, K. Renal Clearable Polyfluorophore Nanosensors for Early Diagnosis of Cancer and Allograft Rejection. *Nat. Mater.* **2022**, *21* (5), 598–607. https://doi.org/10.1038/s41563-022-01224-2.

(24) Choi, C. H. J.; Alabi, C. A.; Webster, P.; Davis, M. E. Mechanism of Active Targeting in Solid Tumors with Transferrin-Containing Gold Nanoparticles. *Proc. Natl. Acad. Sci. U.S.A.* **2010**, *107* (3), 1235–1240. https://doi.org/10.1073/pnas.0914140107.

(25) Salmaso, S.; Caliceti, P. Stealth Properties to Improve Therapeutic Efficacy of Drug Nanocarriers. *Journal of Drug Delivery* **2013**, *2013*, 1–19. https://doi.org/10.1155/2013/374252.

(26) Lindhorst, T. K.; Kötter, S.; Krallmann-Wenzel, U.; Ehlers, S. Trivalent α-D-Mannoside Clusters as Inhibitors of Type-1 Fimbriae-Mediated Adhesion of Escherichia Coli: Structural Variation and Biotinylation. *J. Chem. Soc., Perkin Trans. 1* **2001**, No. 8, 823–831. https://doi.org/10.1039/b009786l.

Chapter 3

Novel microfluidic synthetic procedure of ultra-small gold nanoparticles

3.1 Introduction

The transition of production of nanomaterials from research to clinical trials present several drawbacks that can be overcome by the production of nanoparticles (NPs) using microfluidic systems. These systems offer the opportunity to produce nanomaterials in big scale without changing the reaction conditions. Moreover, the fine control over the reaction conditions is then translated into a higher reproducibility of the NPs. Microfluidic systems allow a fine control over the morphology, particles size and reproducibility of AuNPs; moreover the scale-up of the production is accessible and therefore microfluidic processes have emerged as outstanding tools for new synthetic procedures of a wide range of AuNPs.[1–3]

The photo reduction of Au implies the use of a photo initiator or the presence of an alcohol solvent as for example ethanol or glycerol, the UV-light can decompose this solvent into hydroxyl groups which can then act as reducing species. The mechanism of the reduction the gold salt in the presence of ethanol proposed by Harada and co-workers is shown in the following equations.[4]

$$AuCl_4^- + CH_3CHOH \xrightarrow{h\nu} AuCl_4^{-2} + CH_3\dot{C}HOH + H^+ \qquad (1)$$

$$AuCl_4^- + CH_3\dot{C}HOH \longrightarrow AuCl_4^{-2} + CH_3\underset{\underset{O}{\|}}{C}\text{-}H + H^+ \qquad (2)$$

$$AuCl_4^{-2} + CH_3CHOH \longrightarrow AuCl_2^- + CH_3CHOH + H^+ + 2Cl^- \qquad (3)$$

$$AuCl_4^- + 2\,CH_3CHOH \xrightarrow{h\nu} AuCl_2^- + 2\,CH_3CHOH + 2H^+ + 2Cl^- \quad (4)$$

$$AuCl_2^- + CH_3\dot{C}HOH \longrightarrow Au^0 + CH_3\underset{\underset{O}{\|}}{C}\text{-}H + H^+ + 2Cl^- \qquad (5)$$

$$(Au)_n^0 + AuCl_2^-\ CH_3CH_2OH \longrightarrow (Au)_{n+1}^0 + CH_3\underset{\underset{O}{\|}}{C}\text{-}H + H^+ + 2Cl^- \qquad (6)$$

$$(Au)_n^0 + (Au)_m^0 \longrightarrow (Au)_{n+m}^0 \qquad (7)$$
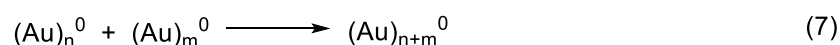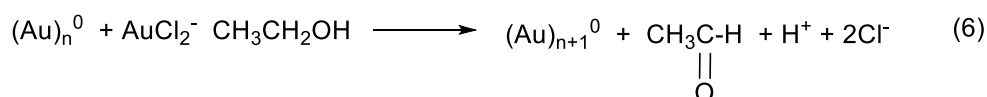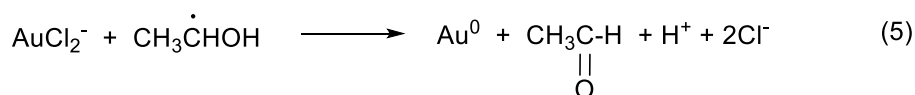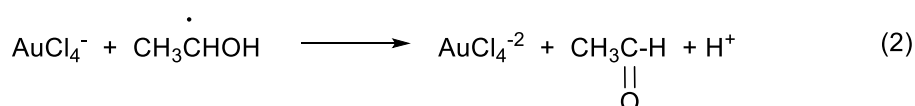
The mechanism proposed consists in a two-step reduction process of Au from Au^{+3} to Au^+ and from Au^+ to Au^0.

In this chapter we propose a new synthetic microfluidic system exploiting the photo reduction of Au to produce functionalized AuNPs. After reducing the Au^{+3} the Au^0 reacts with the thiol ligands present in the solution and a one-pot synthesis of glyco-UAuNPs is achieved.

Regarding the glyco-gold NPs (GAuNPs) one of the major challenges of the design and synthesis is the evaluation (or measure) of the loading of the NPs. The assessment of the amount of glycans on the NPs surface has previously been reported. For example Martinez Avila et al using elemental analysis techniques as thermal gravimetric analysis (TGA) and calculating the amount of atoms of gold.[5,6] Even though this technique facilitates the characterization of the NPs surface, it implies the use and the destruction of high quantities of nanomaterials.

Therefore, during this chapter, a quantitative ^{1}H-NMR analysis system has been developed to analyse the ultra-small glyco gold NPs (GUAuNPs) in an effective way, with the possibility of recovering the samples for future experiments.

3.2   Aim of the work

The goal of this work is the developing of a new synthetic procedure to produce AuNPs with the main focus on a microfluidic process. In order to accomplish the aim of the project the photo induced reduction of Au^{3+} have been exploited. ..[4,12–15]

Microfluidic systems present several advantages such as: reproducibility between batches, easy scale-up, better control in reaction parameters and in the reagents mixing.[16] A microfluidic system for the synthesis of isotropic and anisotropic NPs was developed in our group the past years[17,18], this system was further modified in order to obtain hybrid nanomaterials[19].

Therefore, we intended to combine the advantages of microfluidics systems with the photo induced reduction of gold to obtain ultra-small gold NPs (UAuNPs) functionalized with a set of glycans attached to amphiphilic and aliphatic linkers. In this chapter is reported a novel straightforward photo-induced synthetic procedure of GUAuNPs by employing a microfluidic reactor.

The chapter describes the study of the reduction of gold with a photo-induced system and the optimization protocol applied to obtain functionalized UAuNPs. Moreover, a full characterization section is enclosed and includes UV-vis, Transmission electron microscopy (TEM), Induced couple plasma optical emission spectroscopy (ICP-OES), Nuclear magnetic resonance (NMR).

The microfluidic reactor developed during this thesis is versatile and showed a broad applicability. The microfluidic reactor showed highly promising results for a new protocol to synthesize GUAuNPs through a highly reproducible approach that can be further automatized and customized.

3.3 Results and discussion

3.3.1 Design of novel photo-induced microfluidic system

The key factor in order to develop a synthetic procedure of AuNPs is the reduction of the gold salts; the traditional methods use reducing agents as sodium citrate in the case of Turkevich [20]or a stronger reducing agent such as NaBH$_4$ in the Brust-Schiffrin method. These methods are explained in Chapter 1 section 2.2. Another reducing agent commonly used for the reduction of Au salts is ascorbic acid, which works at room temperature.[18]

During this work the attention was focused on the synthesis of GUAuNPs by exploiting microfluidic approaches. In the in-flow synthesis of AuNPs the challenge is the equilibrium between the nucleation and growing step: the flow production of UAuNPs is more difficult as the fast nucleation must be stopped by a strong passivating agent able to avoid the increment of the nanoclusters size. In literature, it was reported the ability of a UV lamp to reduce the Au^{+3} to Au^0,[4,14] but this procedure has never been coupled with a microfluidic reactor working at room temperature. In order to obtain functionalized UAuNPs in one-pot, thiol ligands have been selected due to the strong bond between gold and sulphur.

A microfluidic reactor was designed using commercially available components. The reaction area was formed by a FEP tube coiled around a UV lamp and a peristaltic pump as shown in figure 3.1.
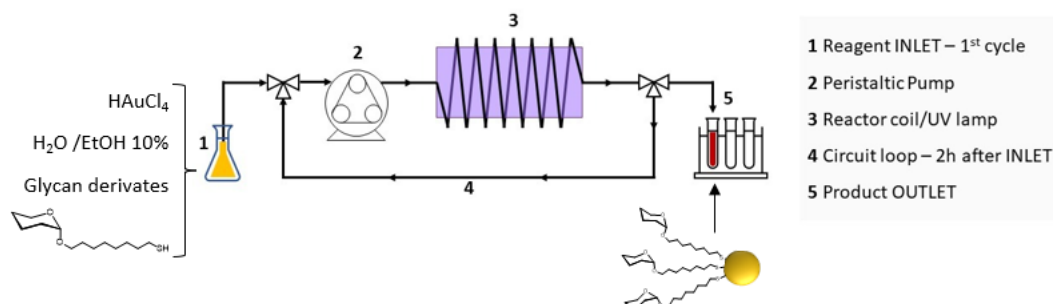
Figure 3.1. *Scheme of the microfluidic reactor developed to produce GUAuNPs*

The reaction consists in the reduction of HAuCl$_4$ by UV-lamp irradiation of 125 W in the presence of glyco-derivatives containing a thiol moiety in a water-ethanol solution degassed with N$_2$ before the irradiation. The reaction was followed by UV-Vis measured at the starting point previous to being exposed to the UV-lamp irradiation and at different time points, in this way the reduction of Au was followed, and it enabled a better understanding of the reaction state.

Microfluidic systems are defined by the internal diameter (ID). In order to define the system as microfluidic the Reynolds number (*Re*) is employed. The Reynolds number is a dimensionless number which is a critical parameter to define fluid behaviour it describes the ratio between viscous inertial forces within fluid. It can be calculated with the following equation:

$$Re=(\rho*v*D)/\mu \qquad\qquad (Eq.1)$$

D = internal pipe diameter (m); v = velocity (m/sec); ρ = density (Kg/m^3); µ = dynamic viscosity (Pas.sec)

Microfluidic systems are characterized by a laminar flow regime and have a *Re* below 250. In the system designed during this thesis the ID was 0,76 mm and the flow rate 0,23 ml/min. The system developed in this project presented a *Re* of 1,90 shown in table 3.1, therefore the system can be defined as a microfluidic reactor.

V (m/sec)	D (m)	ρ (kg/m^3)	µ (Pas.sec)	*Re*
2,44x10^{-3}	0,000762	997	0,0009764	**1,90**

Table 3.1. Reynolds calculation

In order to develop the system several parameters had to be defined as the ratio between Au/glyco-derivatives, the percentage of alcohol present in the reaction solution, the flow rate of the pump and the reaction time.

The percentage and type of alcohol employed in the reaction was the first parameter of the reaction to be established. Previous experience of the group (data not reported) had demonstrated that glycerol could be employed as an initiator for the reduction of Au. Revising the literature[4,13,14] and the previous experiments performed in our group the alcohol selected was ethanol and the amount was fixed at 10% as it showed the best results. After defining this parameter, the other parameters were modulated. The modification of the percentage of ethanol will be performed in future experiments not included in this thesis.

The initial tests were performed with the glycan derivative 2-Glc shown in figure 3.2. This glycan derivative was used to optimize the other parameters of the system as flux rate of the pump, the reaction time and glycan/Au ratio.
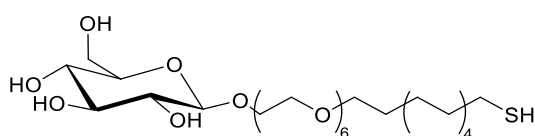
*Figure 3.2. Structure of ligand **2-Glc**. Glucose attached to an amphiphilic linker (EG$_6$C$_{11}$)*

The initial tests performed with the microfluidic system are shown in table 3.2. In the first approach the flux rate was maintained while we modulated the amount of glycan added and the reaction time. The reaction volume in all cases was fixed at 5 mL solution.

The Au/glyco derivatives ratio was extensively studied as the amount of free thiol ligands in solution determined the size distribution of the GUAuNPs.

Three main data were used to determine the efficiency of the system and the most convenient conditions: the UV-vis spectra, the colour of the sample and the TEM analysis. GUAuNPs 1 – 11 were all analysed by UV-vis after the reaction was completed as shown in figure 3.3. GUAuNPs −1 − 8 all presented a localized surface plasmon resonance (LSPR) at around 520 nm. This proved

that the NPs (NPs) or a low percentage of the sample obtained had a diameter bigger than 5 nm. In the case of GUAuNPs – 10 the UV-vis spectra signal at the wavelength between 450 nm and 600 nm is slightly higher than for GUAuNPs – 9 and 11, this sample was then analysed by TEM, and it was proven there was only one population of 2 nm NPs (data not shown).

Sample	EtOH %	Au (10 mM) (mL)	[2-Glc] (mM)	Flux rate (mL/min)	Reaction time (hours)	Evaluation
GUAuNPs – 1	10	0.5	1.1[a]	0.23	0.67	2 size populations
GUAuNPs – 2	10	0.5	1.1[a]	0.23	1	Red/purple colour
GUAuNPs – 3	10	0.5	1.1[a]	0.23	2	2 size populations
GUAuNPs – 4	10	0.5	1.1[a]	0.23	3	Precipitate
GUAuNPs – 5	10	0.5	1.5[a]	0.23	0.67	NPs did not form
GUAuNPs – 6	10	0.5	1.5[a]	0.23	1	Brown colour
GUAuNPs – 7	10	0.5	1.5[a]	0.23	2	2 size populations
GUAuNPs – 8	10	0.5	1.5[a]	0.23	4	Dark purple, brown colour
GUAuNPs – 9	10	0.5	1.9[a]	0.23	2	Light yellow colour
GUAuNPs – 10	10	0.5	1.9[a]	0.23	3	Light yellow colour
GUAuNPs – 11	10	0.5	1.9[a]	0.23	4	Light yellow colour

Table 3.2. GUAuNPs 1 – 11 reaction conditions, a= ligand **2-Glc** 49% glucose 51% OH.
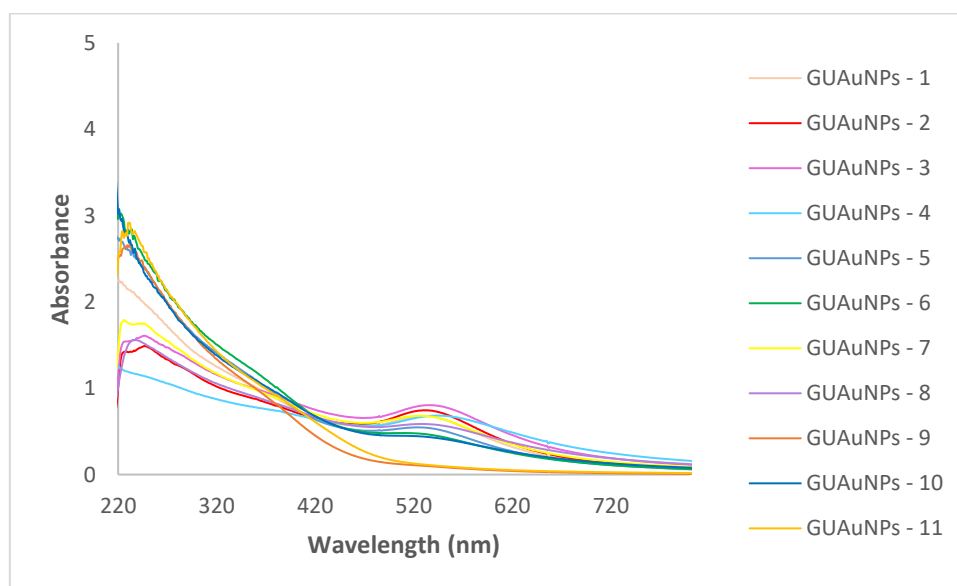
Figure 3.3. GUAuNPs 1 – 11 UV-vis spectra

In the last column at the right of table 3.2, we can see the evaluation made of the NPs depending on the colour of the sample and the results obtained by TEM. In some cases, as GUAuNPs – 1, 3 and 7 the NPs obtained were 2 different sizes this means 2 populations of NPs were formed as it was observed by TEM as shown in figure 3.4. Colour and UV-vis can be an indicator of the size of the NPs[21], therefore in some cases TEM measurements were not performed.

| GUAuNPs - 1 | GUAuNPs - 3 | GUAuNPs - 7 |
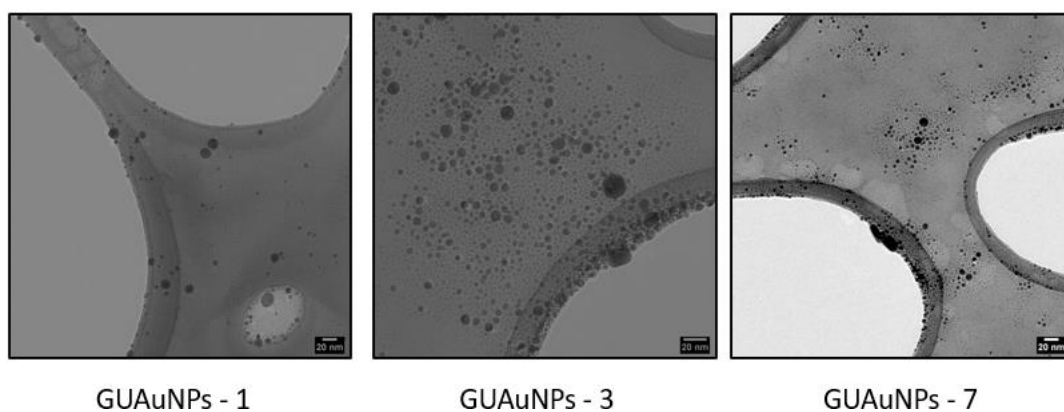
Figure 3.4. GUAuNPs – 1, 3 and 7 TEM micrographs scale 20 nm

In UAuNPs 1 - 8 the concentration of 2-Glc in the solution was either 1.1 mM or 1.5 mM for all cases the NPs either didn't form, precipitate appeared, or 2 size populations were found. On the other hand, UAuNPs 9 – 11 in which the concentration of 2-Glc was 1.9 mM 2 nm UAuNPs were formed in all cases and one population was confirmed by TEM, these NPs all presented a light-yellow colour.

To evaluate the complete reduction of gold precursor, GUAuNPs 9 - 11 were analysed by UV-vis before circulating in the microfluidic system and being irrigated by UV light (starting point) and when the reaction was completed. The reduction of Au was observed as shown in figure 3.5, the peak observed in the starting point represent the unreduced Au^3, when this peak is decreased, the Au is fully reduced to Au^0. Moreover GUAuNPs – 9 – 11 did not exhibit SPR and were assumed to be around 2 nm, as further confirmed by TEM.
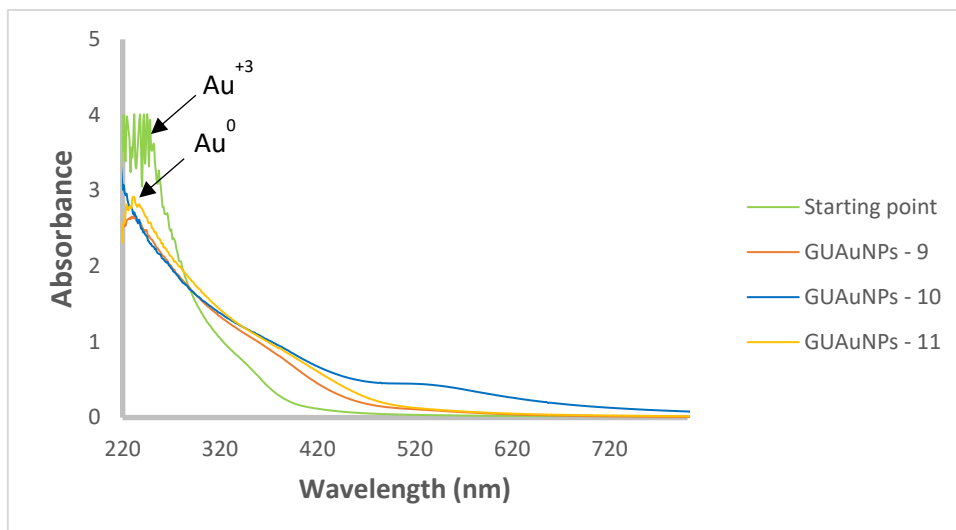
Figure 3.5. GUAuNPs 9 – 11 synthesis followed by UV-vis spectra measured at the starting point and at different time points. The starting point refers to the solution before circulating in the microfluidic system

The next step was to settle the best flow rate and reaction time. Au^{+3} needs long exposure times under the lamp irradiation to be completely reduced (figure 3.5) and therefore the flow rate was established at the minimum of 0,23 mL/min and the system was closed so the solution could circulate in the system during at least 2 hours. In samples GUAuNPs – 9 – 11 the reduction of gold was complete after 2 hours in the cases the reaction time was > 2 hours no changes were observed as shown in figure 3.5.

Taking in account all the data recovered, the best reaction conditions of the system were stablished to be 1 mM of $HAuCl_4$, 1.9 mM of glyco-derivatives, 10 % ethanol in a 5 mL water solution and 2 hours reaction in order to obtain one population 2 nm GUAuNPs. TEM micrograph of GUAuNPs – 9 is shown in figure 3.6.
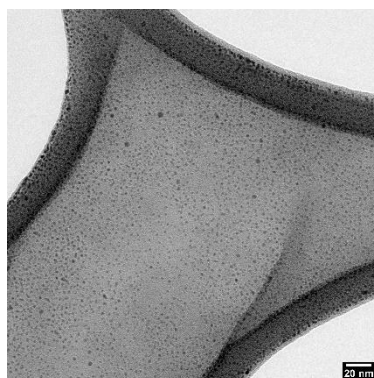
Figure 3.6. GUAuNPs – 9 TEM micrograph scale 20 nm, one population 2nm NPs

After defining all the parameters of the reactor and the reaction conditions the microfluidic system was successfully tested with three different glyco-derivatives containing an amphiphilic thiol ligand shown in table 3, as well as the combination of two different glycan derivatives.

The glycan derivatives shown in table 3.3 were generously donated by Midatech Pharma PLC (Bilbao, Spain).

52
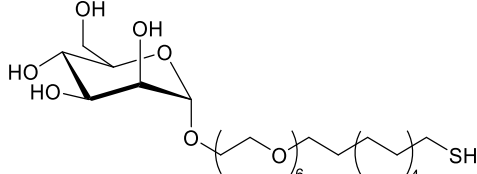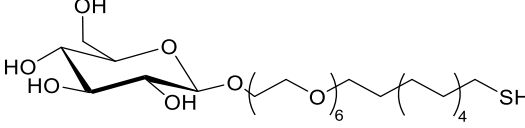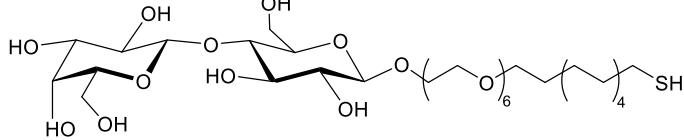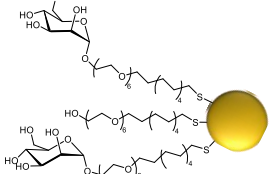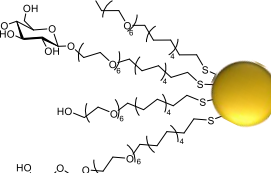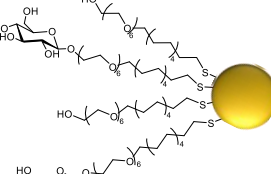
1-Man 61% mannose 39% OH	Mannose derivative	 *29-Thio[3,6,9,12,15,18-hexaoxaundecanyl-α-D-mannopyranoside]*
2-Glc 49% glucose 51% OH	Glucose derivative	 *29-Thio [3,6,9,12,15,18-hexaoxaundecanyl-β-D-glucopyranoside]*
3-Lac 91% lactose 9% OH	Lactose derivative	 29-Thio-[3,6,9,12,15,18-hexaoxaundecanyl-β-D-galactopyranosyl)(1→4)-β-D-glucopyranoside]

Table 3.3.** Glycan derivatives **1 – 3

The system was tested with different amounts of glyco-derivatives as shown in table 3.4 to obtain GUAuNPs with different glycan loadings (see section 3.3.2). The NPs were then analysed by TEM and in all cases the NPs were formed with a diameter of about 2 nm as shown in table 3.5. Moreover GUAuNPs 12 – 18 were analysed by Induce Plasma Optical emission spectroscopy to determine the yield of the synthesis of the NPs.

The formation of GUAuNPs of 2 nm was obtained independently of the glycan nature, proving the broad applicability of the system.

Glyco-UAuNPs	Glycan derivative	[Ligand] in solution (mM)[§]	Yield %[$]
 GUAuNPs – 12	1-Man	[1-Man] 4.5[a]	71
 GUAuNPs – 13	2-Glc	[2-GLc] 1.9[b]	73
	2-Glc	[2-GLc] 2.3[b]	72
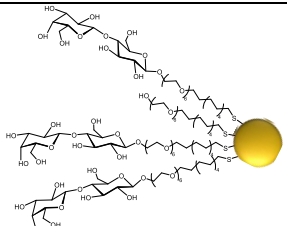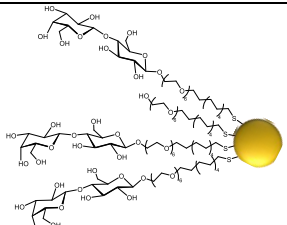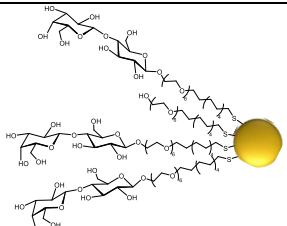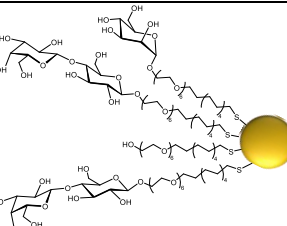
GUAuNPs – 14*			
GUAuNPs - 15	3-Lac	[3-Lac] 1.8[c]	74
GUAuNPs – 16*	3-Lac	[3-Lac] 2.3[c]	74
GUAuNPs – 17	3-Lac	[3-Lac] 2.7[c]	74
GUAuNPs – 18	2-Glc/3-Lac	[2-Glc/3-Lac] 2,3[d]	74

Table 3.4. GUAuNPs 12 – 18 reaction conditions and yield. a= ligand 1-Man 61% mannose 39% OH; b= ligand 2-Glc 49% glucose 51% OH; c=ligand 3-Lac 91% lactose 9% OH; d= ligand 2-Glc; ligand 3-Lac 1:1; ligand 2-Glc: 49% glucose 51% OH; ligand 3-Lac: 91% lactose 9% OH; §= ligand concentration in the 5 mL volume of the starting mixed solution; $= Yield determined by ICP-OES

	Size (nm)		
GUAuNPs - 12	2.3		
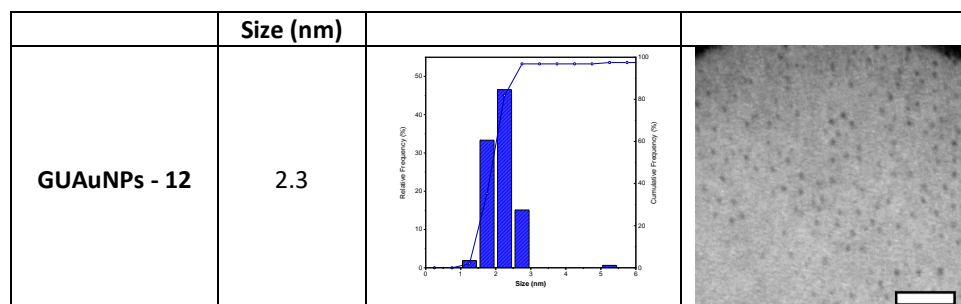
GUAuNPs – 13	2.18		
GUAuNPs – 14*	2.16		
GUAuNPs – 15	2.30		
GUAuNPs – 16*	2.30		
GUAuNPs – 17	2.01		
GUAuNPs – 18	2,67		

***Table 3.5.** Summarized characterization of **GUAuNPs 12 – 18**, NPs size distribution and selected TEM micrographs, scale bar 20 nm*

The NPs were further analysed by X-ray photoelectron spectroscopy (XPS) which was used to analyse the reduction of gold, a complete reduction from Au^{3+} to Au^0 was proven and there was no evidence of Au^+ species. The XPS analysis also showed the presence of S-Au bonds as shown

in figure 3.7 by the S 2p (162.5 eV),[22] the spectra also demonstrated the presence of C-C and C-O species which correspond to the ligand attached to the glycan.
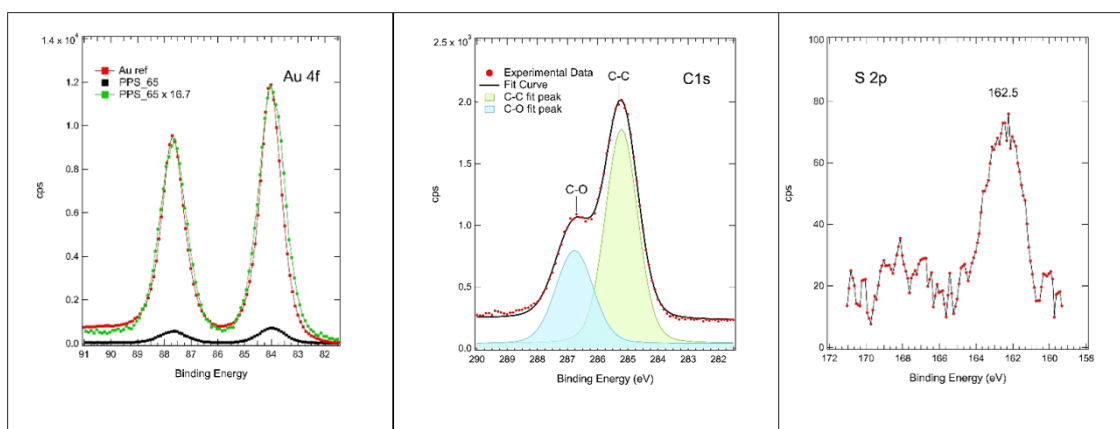
Figure 3.7. *X-ray Photoelectron Spectroscopy (XPS) spectra at Au 4f, C 1s and S 2p edges. The Au 4f spectrum of the **GUAuNPs - 12** is multiplied by a factor 16.7 in order to be comparable to a reference spectrum of polycrystalline gold acquired with same apparatus and working parameters. The slight enlargement of the peak with respect to the reference spectrum can be attributed to the nanosizing of the particles. The C 1s peak shows large intensity as well as a large amount of C-O bonds, not attributable to the usual contamination of sample surface, attesting the functionalization of the UAuNPs. The centroid of the S 2p is placed at 162.5 eV, advising the interaction of sulphur with gold.*

3.3.2 Evaluation of ligand density of glyco-ultra-small gold nanoparticles

The synthetic microfluidic system was proven to work forming NPs displaying different glycan derivatives. Therefore, there was a significant interest in understanding the glycan loading of the NPs and how and if it varied depending on the initial concentration of glycans.

For this purpose we decided to collaborate with Laura Ragona's group at SCITEC-CNR whom calculated the loading of the GUAuNPs by performing ^{1}H-NMR experiments implementing the ERETIC 2 methodology[23]. This methodology consists in an experimental quantitative NMR technique, based on an internal standard method which correlates absolute intensities of two spectras[24].
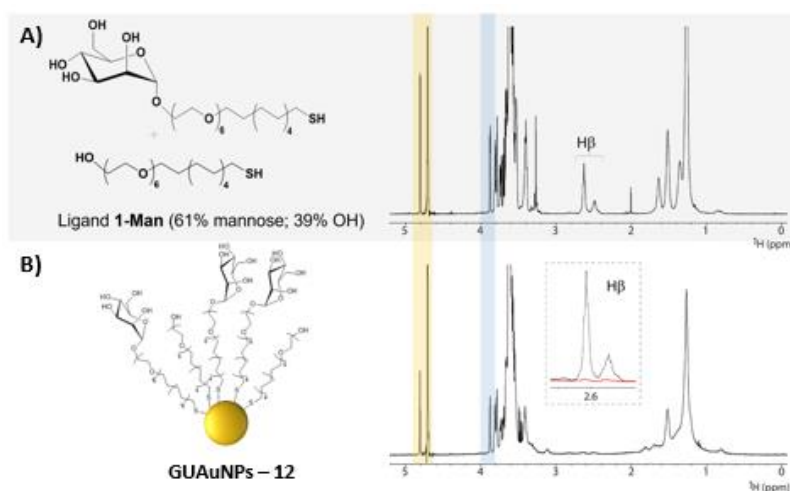
*Figure 3.8. A) ^{1}H-NMR of Glycan derivative **1-Man** B) ^{1}H-NMR of **GUAuNPs – 12***

In order to quantify the loading of GUAuNPs – 12 the ^{1}H-NMR was registered for the ligand 1-Man and the UAuNPs as shown in figure 3.8A. The expand of the signals corresponding to the surrounding of the thiol groups of the glyco derivative at 2,626 ppm for H_β of mannose- EG_6C_{11} and 2,484 ppm for H_β of OH-EG_6C_{11} demonstrates the bound of the ligand to the NPs shown in figure 3.8B. The quantification of the amount of 1 – Man on the GUAuNPs was performed with the ERETIC 2 methodology, signals H1 (4.806 ppm) and H2 (3,876 ppm) were integrated and the amount of mannose on GUAuNPs – 12 was of 7,85 ± 0,36 mM. To test the efficiency of the quantification by ^{1}H-NMR the supernatant obtained after the purification of the GUAuNPs and the UAuNPs not purified were also analysed by ^{1}H-NMR, the results are shown in table 6.

1 – Man	19.74 ± 0.36 mM
GUAuNPs – 12 purified	7.85 ± 0.35 mM
GUAuNPs – 12 supernatant	9.63 ± 0.14 mM
GUAuNPs – 12 not purified	19.16 ± 0.51 mM

Table 3.6. Concentrations obtained by quantitative ^{1}H-NMR in 0.6 ml of D_2O

The sum up of the concentration of 1-Man in the supernatant and the purified GUAuNPs is almost equal than the GUAuNPs not purified, this demonstrated that almost all the unreacted glycan is recovered in the purification step. As this synthetic procedure avoids the use of templating agents or other reducing agents, the supernatant of the GUAuNPs is formed solely by the unreacted glycan derivative: this represents a great advantage compared to other synthetic procedures as the precious glycans can be re used for further experiments.

To further study the loading of the GUAuNPs, GUAuNPs 13 – 18 were also analysed by quantitative ^{1}H-NMR.

In order to compare the initial concentration of the glycan derivatives in solution added to the system with the concentration of glycan derivatives on the purified UAuNPs the concentrations were calculated in a final volume of GUAuNPs of 5ml as shown in table 3.7.

	Glycan derivative	[Ligand] in solution (mM)§	[Ligand] in UAuNPs solution (mM)$^£$
GUAuNPs – 12	1-Man	4.5	2.2
GUAuNPs – 13	2-Glc	1.9	0.3
GUAuNPs – 14*	2-Glc*	**2.3**	0.9
GUAuNPs – 15	3-Lac	1.8	0.2
GUAuNPs – 16*	3-Lac*	**2.3**	0.8
GUAuNPs – 17	3-Lac	2.7	1.3
GUAuNPs – 18*	2-Glc/3-Lac (1:1)*	**2.3**	0.4

Table 3.7. *Concentrations of ligand in solution and in GUAuNPs solution in 5 ml. §= starting mixed solution (as determined by NMR); £= purified final solution (as determined by NMR). * Same [ligand] in solution.*

Furthermore GUAuNPs – 14*,16* and 17 were synthetized with a higher amount of glycan derivative in order to assess the efficiency of the synthetic protocol at higher concentrations. The GUAuNPs indicated with * were synthesized with the same initial ligand concentration.

The correlation between the amount of ligand added to the initial solution and the final amount on the NPs was calculated considering the μmol of each ligand. The first step was to calculate the μmol of ligand in the initial solution and the μmol of ligand on the GUAuNPs. The data obtained is shown in table 3.8. In order to perform this calculation the purity of the ligands was assessed by quantitative NMR (ERETIC 2).These are the results obtained Ligand **1-Man** is a mixture of 61% mannose glycosylated to the amphiphilic linker (EG$_6$C$_{11}$-SH) and 39% of the free HO-EG$_6$C$_{11}$-SH, ligand **2-Glc** is a mixture of 49% glucose glycosylated to the amphiphilic linker (EG$_6$C$_{11}$-SH) and 51% of the free HO-EG$_6$C$_{11}$-SH and ligand **3-Lac** is a mixture of 91% lactose glycosylated to the amphiphilic linker (EG$_6$C$_{11}$-SH) and 9% of the free HO-EG$_6$C$_{11}$-SH.

Glyco UAuNPs	HS-Ligand	μmol HS-Ligand	μmol HS-Ligand on UAuNPs
GUAuNPs – 12	1-Man	22.4	11.1
GUAuNPs – 13	2-Glc	9.4	1.5
GUAuNPs – 14*	2-Glc*	**11.6**	4.2
GUAuNPs – 15	3-Lac	8.9	1.1
GUAuNPs – 16*	3-Lac*	**11.6**	4.1
GUAuNPs – 17	3-Lac°	13.7	6.4
GUAuNPs – 18*	2-Glc + 3-Lac (1:1) *	**11.6**	3.3

Table 3.8. *μmol of glycan derivatives in the initial solution and on the GUAuNPs. Data calculated from NMR.*

The data shown in table 3.8 suggested a linear correlation between the amount of ligand added to the reaction solution and the amount of glycans on the NPs surface independently of the nature of the glycan. These results are plotted in figure 3.9 confirming a linear correlation with the following equation (Eq.1).

$$y = 0.7322x - 4.8019 \qquad\qquad (Eq.\ 1)$$
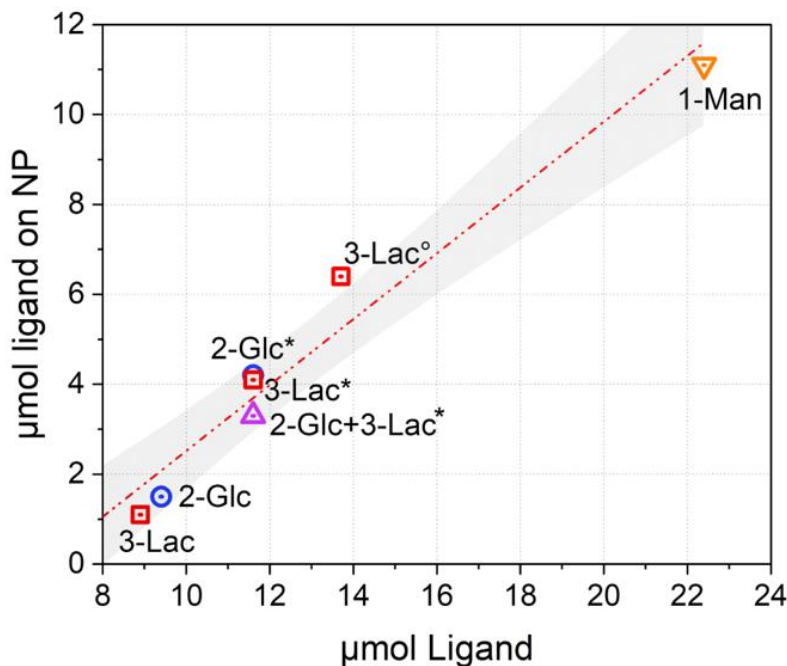
Figure 3.9. *Correlation between μmol of ligand in initial solution and on the GUAuNPs. R^2= 0.958*

The amphiphilic linker (EG_6C_{11}-SH) bond to the anomeric position of the glycans was proved to be an adequate linker for the glycans as it provided a stable colloidal solution and introduced in the new synthetic system it afforded stable GUAuNPs with good yields and a high reproducibility between samples.

Moreover, the quantitative NMR analysis of GUAuNPs – 12 – 18 was shown to be a good protocol to determine the loading of homofunctionalized and heterofunctionalized GUAuNPs. The final quantity of glycans on the NPs was proportional to the amount added in the initial solution, with the data obtained in figure 3.9 it was shown that this correlation was the same in all cases being independent of the nature of the glycan.

This linearity provides a good protocol to predict the final concentration of glycan on the NPs and enables the design of complex GUAuNPs. The data obtained also demonstrated that the final loading of the NPs can be modulated using the novel photo-induced microfluidic system, obtaining in this way GUAuNPs with different amount of glycans exposed on the surface. This is a very interesting point as depending on the final application of the GUAuNPs different surface coverage can be required.

3.3.3 Estimation of glycan molecules per ultra-small gold nanoparticle
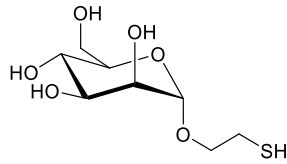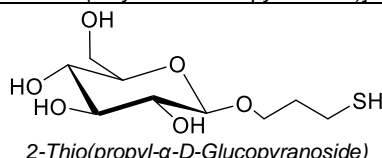
GUAuNPs – 12 – 18 were measured by Induced coupled plasma optical emission spectroscopy (ICP-OES) to obtain the total amount of Au in each sample. This data enables the calculation of the yield of the NPs and in combination with the mmol of GUAuNPs obtained from the quantitative ^{1}H NMR analysis the number of glycans per nanoparticle was calculated. The data shown in table 3.9 was obtained considering a mean radius of 1.15 nm (GUAuNPs core), the density of gold 19.32 g/cm^3 and the mass of a single GUAuNP $1.2*10^{-19}$ g.

GUAuNPs	Gold amount (g) (determined by ICP)	Number of UAuNPs	mmol of Glycan	Total Number of molecules of glycan	Glycan per GUAuNP
GUAuNPs – 12	$6.9*10^{-4}$	$5.6*10^{15}$	$4.4*10^{-3}$	$2.6*10^{18}$	469
GUAuNPs – 13	$7.1*10^{-4}$	$5.8*10^{15}$	$5.0*10^{-4}$	$3.0*10^{17}$	52
GUAuNPs – 14*	$7.0*10^{-4}$	$5.7*10^{15}$	$1.7*10^{-3}$	$1.0*10^{18}$	179
GUAuNPs – 15	$7.2*10^{-4}$	$5.8*10^{15}$	$9.2*10^{-4}$	$5.5*10^{17}$	94
GUAuNPs – 16*	$7.1*10^{-4}$	$5.8*10^{15}$	$3.5*10^{-3}$	$2.1*10^{18}$	360
GUAuNPs – 17	$7.2*10^{-4}$	$5.8*10^{15}$	$5.3*10^{-3}$	$3.2*10^{18}$	543
GUAuNPs – 18*	$7.2*10^{-4}$	$5.8*10^{15}$	$6.4*10^{-4}$ (Glc) $1.1*10^{-3}$(Lac)	$3.8*10^{17}$(Glc) $7.0*10^{17}$(Lac)	65(Glc) 120 (Lac)

Table 3.9. *Estimation of Glycan molecules per GUAuNP*

3.3.4 Generalization of novel photo-induced microfluidic system

The data shown until now proves that the new synthetic procedure is a highly reproducible, reliable synthetic protocol suitable for glycan derivatives containing an amphiphilic linker. Therefore, the system was then tested with the same carbohydrates employed in the previous step but bond to an aliphatic ligand as shown in table 3.10. The concentrations of ligands 5-7 employed for the synthesis of GUAuNPs 19 - 21 are shown in table 3.11.

5-Man	Mannose derivative	*2-Thio(ethyl-α-D-mannopyranoside)]*
6-Glc	Glucose derivative	*2-Thio(propyl-α-D-Glucopyranoside)*

7-Lac	Lactose derivative	 *2-Thio(ethyl- β-D-galactopyranosyl)(1→4)-β-D-glucopyranoside)*
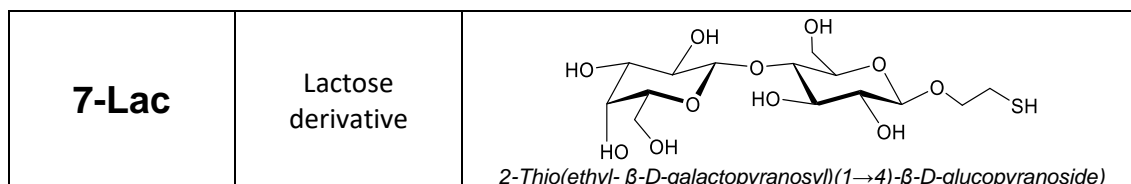
Table 3.10. *Glycan derivatives 5 – 7 – Short aliphatic linker*

	Glycan derivative	[Ligand] in solution (mM)
GUAuNPs – 19	5-Man	3.91
GUAuNPs – 20	6-Glc	2
GUAuNPs – 21	7-Lac	2

Table 3.11. *Concentration of ligand in initial solution of glycan derivatives 5 – 7*

GUAuNPs 19 – 21 were formed successfully following the same protocol as GUAuNPs – 12 – 18 and UAuNPs of 2 nm were obtained as shown in the size distribution in figure 3.10. These results prove that the system can be employed even with short aliphatic linkers even though the water dispersibility of the formed NPs was decreased and therefore the UAuNPs are less stable.
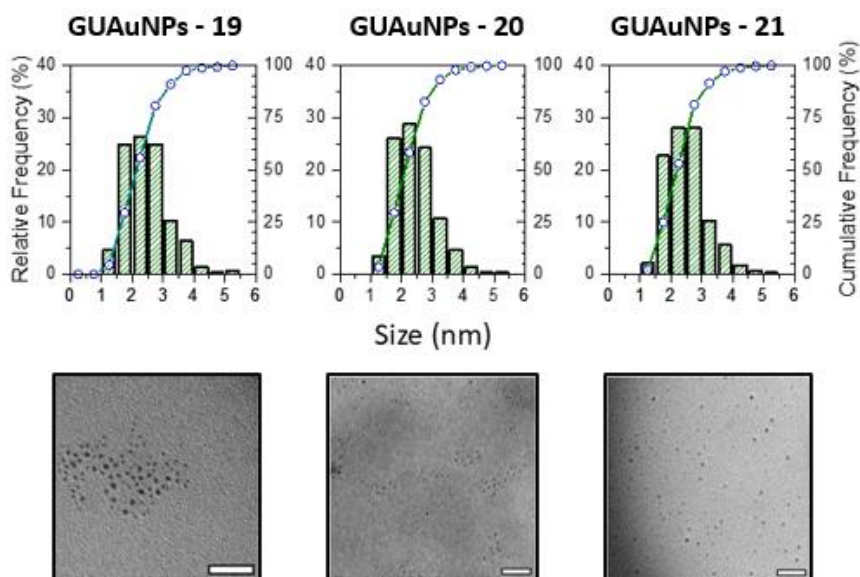
Figure 3.10. *Size distribution and TEM micrographs of **GUAuNPs 19 – 21**. Scale bar 20 nm*

The previous results demonstrate that the synthetic procedure is suitable to form GUAuNPs with linkers bearing a thiol moiety independently of their nature. To further support this theory the system was tested with a PEG$_{5000}$ linker (table 3.12) as it is one of the most common ligand stabilizers used for bio applications[25]. It has been demonstrated that the functionalization of AuNPs with PEG linkers minimizes the unspecific binding to proteins and consequently the NPs are not recognized by the macrophages.

8-PEG	PEG₅₀₀₀-SH	H_2N —(O—ethylene)$_{112}$— SH
9-GalPEG	Galactose-PEG₅₀₀₀	Galactose—O—propyl—NH—C(=O)—(O—ethylene)$_{112}$—SH

*Table 3.12. Glycan derivatives **8 – 9** – Hydrophilic PEG₅₀₀₀ linker*

2 nm GUAuNPs were obtained successfully in both cases using the initial concentration of ligand in table 3.13 and the same reaction conditions as described earlier. The size distribution obtained from the TEM analysis are shown in figure 3.11.

	Glycan derivative	**[Ligand] in solution (mM)**
PEG-UAuNPs	8-PEG	0.8
GUAuNPs – 22	9-GalPEG	0.9

*Table 3.13. Concentration of ligand in initial solution of glycan derivatives **8 – 9***
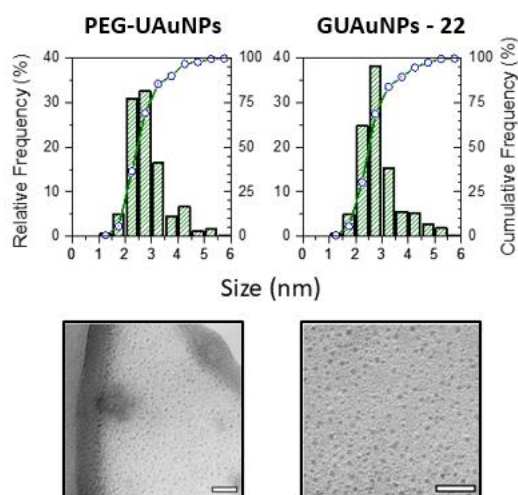
*Figure 3.11. Size distribution and TEM micrographs of **PEG-UAuNPs** and **GUAuNPs – 22**. Scale bar 20 nm*

PEG-UAuNPs were synthesized with a PEG linker without a terminal glycan, this enables the future post-functionalization with any glycan bearing a carboxylic group through carbodiimide chemistry as described in Chapter 2.

Moreover, the loading of GUAuNPs – 22 was calculated by the analysis of the NPs by quantitative ^{1}H-NMR, through this data it was able to obtain the final number of galactose per GUAuNP shown in table 3.14.

Glyco-UAuNPs	Gold amount (g) (determined by ICP)	Number of UAuNPs	mmol of Glycan	Total Number of molecules of glycan	Glycan per UAuNP
GUAuNPs – 22	$3.5*10^{-4}$	$2.8*10^{15}$	$4.0*10^{-4}$	$2.4*10^{17}$	86

Table 3.14. Estimation of Glycan molecules per GUAuNP

Overall, these results demonstrate the broad applicability of the system using from very short aliphatic ligands to long hydrophilic PEG linkers depending on the future application of the UAuNPs.

3.3.5 Hydrodynamic radius of ultra-small gold nanoparticles

UAuNPs – 12 were further characterized by DOSY (diffusion ordered NMR spectroscopy) to obtain the hydrodynamic radius of the GUAuNPs. The translational diffusion coefficient obtained was of $(5.5 \pm 0.1) \times 10^{-11}$ m^2/s as shown in figure 3.12, the Stokes – Einstein equation enables the calculation of the hydrodynamic radius.

$$r_H = \frac{k_B T}{6\pi\eta D} \tag{1}$$

r_H = hydrodynamic radius; k_B = Boltzmann constant; T = temperature; n = viscosity and D = diffusion coefficient.

The hydrodynamic radius obtained was of 3.3 ± 0.1 nm, this means the diameter is approximately 6.6 nm, this value is consistent with the core diameter obtained by TEM analysis.
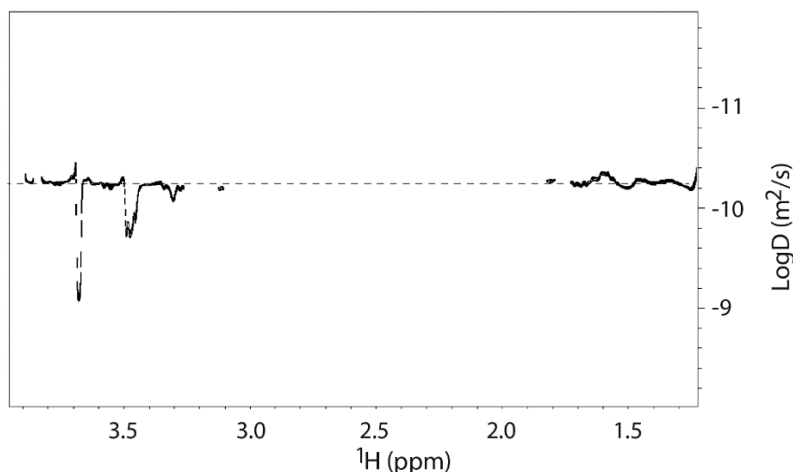
Figure 3.12. *^1H DOSY NMR spectrum of UAuNPs - 12 dissolved in D2O at 25°C. Dashed line corresponds to the D value of (5.5 ± 0.1) x 10^{-11} m^2/s.*

3.3.6 Photoluminescence of ultra-small gold nanoparticles

UAuNPs have previously been reported to have relevance in bioimaging as they are luminescent in the near infrared region (NIR)[26,27] , therefore the fluorescence behaviour of UAuNPs - 12 was studied as shown in figure 3.13. GUAuNPs – 12 dissolved in water showed an excitation peak at 310 nm and an emission peak at 820 nm this data demonstrates the GUAuNPs obtained with the novel photo induced microfluidic system are photoluminescent.
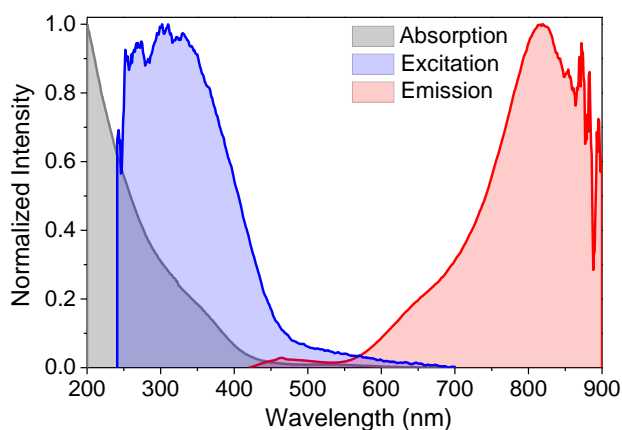
Figure 3.13. *Normalized absorption, excitation (λem = 810 nm) and emission spectra (λexc = 400 nm) of GUAuNPs – 12 in water.*

3.4 Conclusions

In this chapter it has been reported the synthesis of GUAuNPs with a novel photo-induced microfluidic system. The proposed synthetic procedure has a broad applicability. It has been

demonstrated that GUAuNPs can be synthesized with amphiphilic, aliphatic, and hydrophilic linkers bearing a glycan independently of their length. The best reaction parameters were identified by following the reduction of Au by UV-visible spectroscopy, the size of the NPs and the homogeneity of the size distribution by TEM microscopy and modulating the ratio of Au and glycan derivatives. With the described manufacturing method, it was possible to obtain one-pot water soluble functionalized GUAuNPs of 2 nm by photo reduction of Au. Moreover, the glycan loading of the NPs was determined by quantitative ^{1}H NMR using the ERETIC 2 methodology. Overall, this are highly promising results for a new synthetic procedure of GUAuNPs.

3.5   Experimental

3.5.1   Material and methods

$HAuCl_4 \cdot 3H_2O$, ethanol 95% and all the other chemicals were purchased from Sigma-Aldrich and used without further purification. $HAuCl_4 \cdot 3H_2O$ was stored at 4°C, shielded from light, as 10 mM solution. $HS\text{-}PEG_{5000}\text{-}NH_2$ and $HS\text{-}PEG_{5000}\text{-}COOH$ were purchased from Rapp Polymer GmbH, was used as received and stored under dry argon atmosphere at -20 °C. HPLC water was used for the preparation of aqueous solutions. When necessary, reactions were monitored by thin-layer chromatography (TLC) on Silica Gel 60 F254 (Sigma Aldrich) or with high performance thin-layer chromatography (HPTLC); compounds were visualized by heating with 10% (v/v) ethanolic H_2SO_4. Column chromatography was performed using Silica Gel 200–400 mesh or Biotage SNAP Ultra. The fluidic reactor was washed after each synthesis with aqua regia (HCl (37%)/HNO$_3$ (65%) 3:1) and milliQ water (3 x 10 mL). Purification of colloidal AuNPs was performed by ultrafiltration using Millipore Amicon Ultra-4 Centrifugal Filter Units with a cut-off of 30 kDa. UV-lamp used for the microfluidic procedure was a UV high pressure Hg 125W lamp (100V) purchased from Helios Italquarz s.r.l., Cambiago (MI), Italy.

The X-ray Photoelectron Spectroscopy (XPS) measurements were carried out with a PHI 5600 UHV apparatus equipped with a hemispherical electron analyzer and a monochromatized X-ray source (Al Kα = 1486.6 eV, ⊠E=0.48 eV). The edge spectra were acquired in constant step energy mode with Epass =23.8 eV. The pressure in the experimental chamber during experiments was less than $1.2 \cdot 10{-}9$ mbar. The binding energy scale was calibrated via the Au 4f7/2 core level line (located at 83.97 eV) of a clean polycrystalline Au sample. Voigt line-shape and Shirley background were used to fit the peaks and the background respectively. Least square curve-fitting was performed using the programs KolXPD and Igor Pro (Wavemetrics).

^{1}H NMR spectra were measured at 400 MHz or 500 MHz and 298 K (unless otherwise specified) with a Bruker AvanceIII spectrometer; δ_H values were reported in ppm, relative to the internal standard Me$_4$Si (δ_H=0.00, CDCl3) or the water signal (δ_H=4.79 ppm, D2O). ^{13}C NMR spectra were measured at 100 MHz or 126 MHz and 298 K with a Bruker Avance^{III} spectrometer; δ_C values are reported in ppm relative to the signal of CDCl$_3$ (δ_C = 77.0, CDCl$_3$). Mass was measured by Electron Spray Ionization (ESI) or Matrix-Assisted Laser Ionization (MALDI) spectroscopy.

UV–vis spectroscopy measurements were performed with an Agilent 8453 instrument. A disposable cuvette with 1 cm optical path length was used for the outline measurements. Photoluminescence experiments (emission and excitation spectra) were obtained on a FLS 980 spectrofluorometer (Edinburg Instrument Ltd.) equipped with a 450 W Xenon arc lamp. Transmission electron microscopy (TEM) measurements were performed by a ZEISS LIBRA200FE microscope equipped with in-column Ω-filter spectrometer/filter, operating at 200 kV. TEM specimens were prepared dropping the nanoparticle aqueous dispersion onto a supported lacey-carbon copper TEM grids and analyzed after drying overnight. Dimensions of UAuNPs have been measured using ITEM-TEM Imaging platform – Olympus Soft Imaging Solutions. Elemental analyses were performed by inductively coupled plasma optical emission spectroscopy (ICP-OES iCAP 6200 Duo upgrade, Thermofisher) with external calibration. Samples were acid digested on a hotplate in a Teflon becker with aqua regia (HCl:HNO$_3$, 3:1) solution and diluted with water.

3.5.2   General synthesis of glyco-ultra-small gold nanoparticles

A solution of water-ethanol (10%) (4.5 mL) was degassed bubbling N$_2$ at room temperature for 10 minutes. Glycan derivatives (see **Table 3.2**, **Table 3.10 and Table 3.12**) were added at different concentrations (see **Table 3.4, Table 3.11 and Table 3.13**) to the stirring solution and, after 10 minutes, a solution of tetrachloroauric acid (0.5 mL, 10 mM, 0,005mmol, 1 eq) was added. After 5 minutes the mixture was injected in the microfluidic system with a flux rate of 0.23 mL/min and exposed to the UV-light for 2 hours. The synthesized Glyco-UAuNPs were then purified by Amicon Ultra - 15 centrifugal devices (30KDa MWCO, 6 min, 6000 rpm) and stored as 5 mL colloidal solutions. Before NMR analysis, the samples were lyophilized and re-dissolved in 0.6mL of D$_2$O.

3.5.3 Description of microfluidic reactor

The flow within the microfluidic reactor was generated by a programmable peristaltic pump (LabCraft). The initial solution containing water/ethanol, glycan derivatives and HAuCl$_4$ was degassed before flowing in the tubes. The reaction zone was constituted by a FEP tube (Idex Health & Science LLC; 0.762 mm ID, 5 m length) coiled around a water-cooled UV lamp (125W, 100V, Helios Italquartz S.r.l). The circuit was closed, and the mixture was let flowing in the tubes for 2 hours (figure 3.14). The obtained glycol ultrasmall gold NPs were collected in a conical tube, purified and stored as 5 mL colloidal solution at 4 °C over 6 months. The microreactor was fluxed with aqua regia (HCl:HNO$_3$ = 3:1) to remove possible residues of gold from the walls of the tubes at the end of each the reaction.
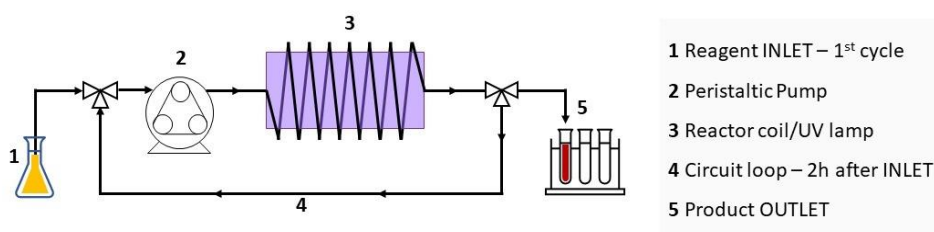
Figure 3.14. *Scheme of the microfluidic reactor developed to produce **GUAuNPs***

3.5.4 Hydrodynamic radius determination

^{1}H-DOSY experiments (diffusion-ordered spectroscopy) were performed on GUAuNPs − 12 functionalized with 1-Man purified sample. Matrices of 16384 (t2) by 80 points (t1) were collected. The z-axis gradient strength was varied linearly from 2 to 98% of its maximum value (53 G cm^{-1}), the gradient pulse duration was 4.4 ms, and the time period between the two gradient pulses was optimized to 200 ms. Self-diffusion coefficients (D) were derived by fitting the NMR data to Stejskal and Tanner equation[28].

3.5.5 UV-vis characterization of glyco-ultra-small gold nanoparticles
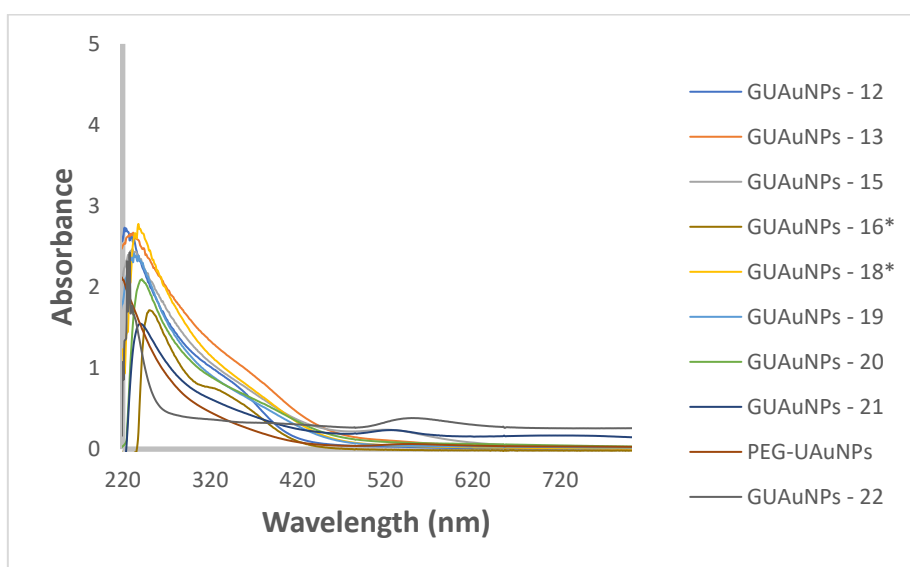
*Figure 3.15. Summary of UV-vis spectra of **GUAuNPs − 12 − 22** and **PEG-UAuNPs***

3.5.6 Size distribution

	Mean Value (nm)	SE of mean	
GUAuNPs – 12	2.29	0.099	
GUAuNPs – 13	2.18	0.031	
GUAuNPs – 14*	2.15	0.021	
GUAuNPs – 15	2.26	0.058	
GUAuNPs – 16*	2.28	0.040	
GUAuNPs – 17	2.01	0.022	
GUAuNPs – 18*	2.66	0.027	
GUAuNPs – 19	2.43	0.040	
GUAuNPs – 20	2.42	0.038	
GUAuNPs – 21	2.51	0.039	
PEG-UAuNPs	2.83	0.041	
GUAuNPs – 22	2.90	0.042	
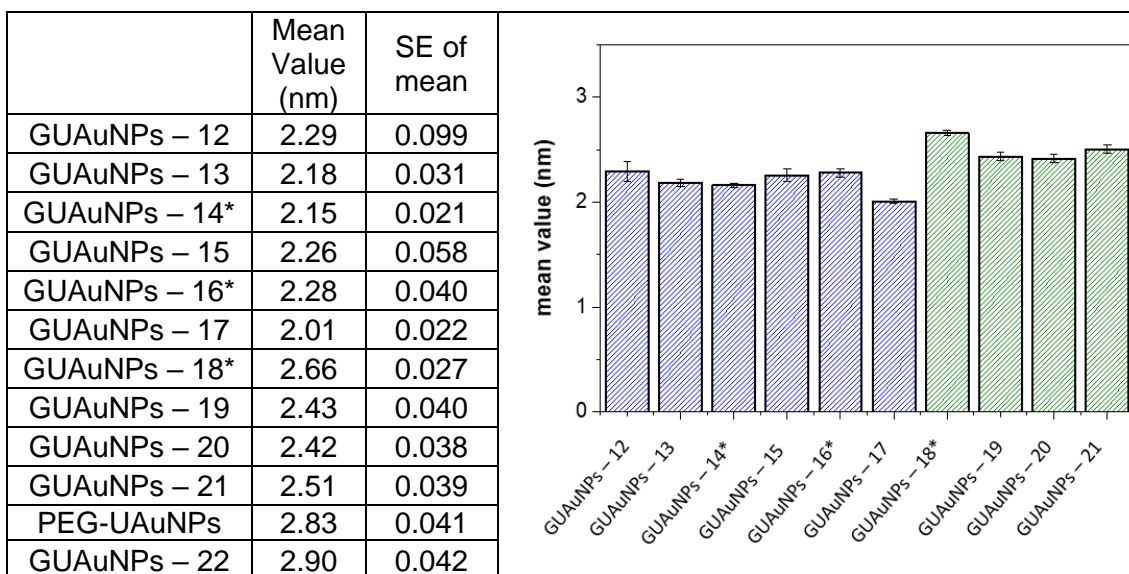
3.5.7 Synthesis of glycan derivatives

Ligand 1 - 3 and 5 -7 bearing the amphiphilic linker EG_6C_{11} and the aliphatic linkers C_2/C_3 were a generous gift from Midatech Pharma PLC (Bilbao, Spain). Their synthesis is detailed described in the literature[5,29]. The NMR spectra are reported in the annex.

29-Thio[3,6,9,12,15,18-hexaoxaundecanyl-α-D-mannopyranoside] (1-Man)
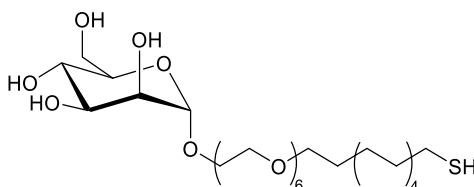
^{1}H NMR (500 MHz, Deuterium Oxide) δ 4.89 (d, J = 1.7 Hz, 1H, H-1), 3.96 (dd, J = 3.5, 1.7 Hz, 1H), 3.88 (ddd, J = 12.1, 4.5, 2.5 Hz, 2H), 3.81 (dd, J = 8.9, 3.3 Hz, 1H), 3.78 (d, J = 5.3 Hz, 1H), 3.76 – 3.63 (m, 33H), 3.61 (tt, J = 6.5, 3.3 Hz, 3H), 3.49 (d, J = 6.8 Hz, 3H), 3.37 – 3.32 (m, 1H), 2.71 (s, 2H), 1.72 (s, 2H), 1.60 (s, 4H), 1.51 – 1.25 (m, 20H).

^{13}C NMR (126 MHz, Deuterium Oxide) δ 99.96, 72.78, 71.92, 71.10, 70.56, 70.01, 69.98, 69.86, 69.80, 69.77, 69.74, 69.61, 66.69, 66.34, 60.92, 60.44, 38.96, 29.98, 29.91, 29.80, 29.59, 29.52, 29.33, 28.90, 28.70, 26.18.

29-Thio [3,6,9,12,15,18-hexaoxaundecanyl-β-D-glucopyranoside] (2-Glc)
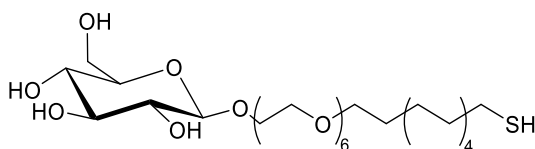
^{1}H NMR (500 MHz, Deuterium Oxide) δ 4.48 (d, J = 7.9 Hz, 1H, H-1), 4.07 (dt, J = 11.4, 4.1 Hz, 1H), 3.92 (dd, J = 12.3, 2.2 Hz, 1H), 3.84 (dt, J = 11.3, 4.7 Hz, 1H), 3.76 (t, J = 4.5 Hz, 2H), 3.75 – 3.59 (m, 46H), 3.53 – 3.43 (m, 6H), 3.40 (d, J = 9.2 Hz, 1H), 3.30 (dd, J = 9.3, 8.0 Hz, 1H), 2.72 (t, J = 7.2 Hz, 3H), 1.72 (d, J = 8.8 Hz, 4H), 1.60 (s, 4H), 1.51 – 1.29 (m, 28H).

^{13}C NMR (126 MHz, Deuterium Oxide) δ 102.33, 75.97, 75.71, 73.15, 71.94, 71.13, 70.04, 69.99, 69.92, 69.89, 69.82, 69.79, 69.70, 69.66, 69.62, 68.63, 60.81, 60.46, 39.02, 30.02, 29.83, 29.60, 29.36, 28.73, 26.21.

29-Thio-[3,6,9,12,15,18-hexaoxaundecanyl-β-D-galactopyranosyl)(1→4)-β-D-glucopyranoside] (3-Lac)
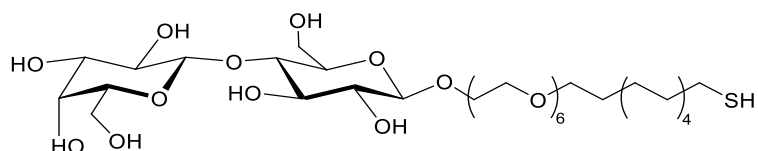
¹H NMR (500 MHz, Deuterium Oxide) δ 4.51 (d, *J* = 8.0 Hz, 1H), 4.46 (d, *J* = 7.8 Hz, 1H), 4.07 (dt, *J* = 11.3, 4.1 Hz, 1H), 4.01 – 3.95 (m, 1H), 3.93 (d, *J* = 3.3 Hz, 1H), 3.88 – 3.63 (m, 29H), 3.56 (dd, *J* = 9.9, 7.8 Hz, 4H), 3.52 – 3.44 (m, 2H), 3.40 – 3.31 (m, 1H), 2.72 (t, *J* = 7.2 Hz, 2H), 1.72 (d, *J* = 9.1 Hz, 2H), 1.60 (s, 2H), 1.50 – 1.25 (m, 14H).

¹³C NMR (126 MHz, Deuterium Oxide) δ 102.98, 102.19, 78.46, 75.36, 74.78, 74.33, 72.81, 72.56, 71.09, 70.94, 69.98, 69.89, 69.86, 69.79, 69.71, 69.68, 68.67, 68.54, 61.02, 60.13, 38.96, 29.92, 29.73, 29.56, 29.48, 29.31, 28.66, 26.14.

2-Thio(ethyl-α-D-mannopyranoside) (5-Man)
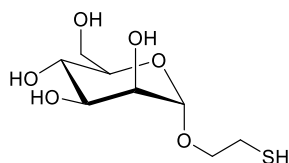
¹H NMR (500 MHz, Deuterium Oxide) δ 4.92 (d, *J* = 1.7 Hz, 1H), 4.01 (dt, *J* = 10.8, 6.2 Hz, 1H), 3.96 (dd, *J* = 3.3, 1.6 Hz, 1H), 3.92 – 3.63 (m, 6H), 3.00 (t, *J* = 5.9 Hz, 2H).

¹³C NMR (126 MHz, Deuterium Oxide) δ 99.74, 72.92, 70.51, 69.96, 66.65, 65.25, 60.85, 37.35.

2-Thio(propyl-α-D-Glucopyranoside) (6-Glc)
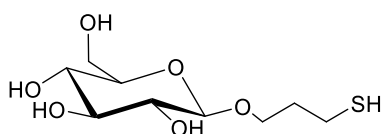
¹H NMR (500 MHz, Deuterium Oxide) δ 4.46 (d, *J* = 8.0 Hz, 1H), 4.01 (dt, *J* = 10.3, 6.3 Hz, 1H), 3.92 (dd, *J* = 12.3, 2.2 Hz, 1H), 3.79 (dt, *J* = 10.4, 6.4 Hz, 1H), 3.72 (dd, *J* = 12.4, 5.9 Hz, 1H), 3.52 – 3.23 (m, 4H), 2.85 (t, *J* = 7.2 Hz, 2H), 2.07 – 2.00 (m, 2H).

¹³C NMR (126 MHz, Deuterium Oxide) δ 102.26, 75.89, 75.74, 73.11, 69.63, 68.59, 60.74, 34.19, 28.37.

2-Thio(ethyl- β-D-galactopyranosyl)(1→4)-β-D-glucopyranoside) (7-Lac)
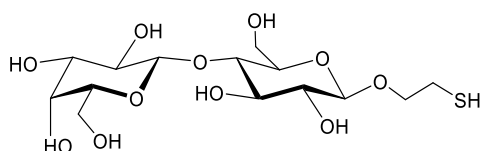
¹H NMR (500 MHz, Deuterium Oxide) δ 4.54 (d, *J* = 8.0 Hz, 1H), 4.45 (d, *J* = 7.8 Hz, 1H), 4.05 – 3.95 (m, 2H), 3.93 (d, *J* = 3.4 Hz, 1H), 3.87 – 3.75 (m, 4H), 3.75 – 3.71 (m, 1H), 3.69 – 3.58 (m, 4H), 3.55 (dd, *J* = 10.0, 7.8 Hz, 1H), 3.37 – 3.32 (m, 1H), 2.78 (t, *J* = 6.3 Hz, 2H).

¹³C NMR (126 MHz, Deuterium Oxide) δ 102.91, 102.05, 78.30, 75.33, 74.78, 74.32, 72.77, 72.50, 71.71, 70.93, 68.52, 61.00, 60.02, 23.34.

Chemical strategy to synthesize 9-GalPEG
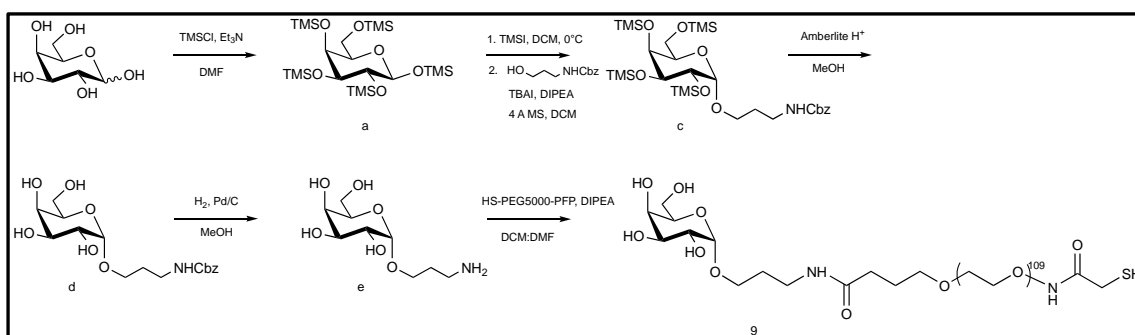
Synthesis of 1,2,3,4,6-penta-O-TMS-β-D-galactopyranose (a)
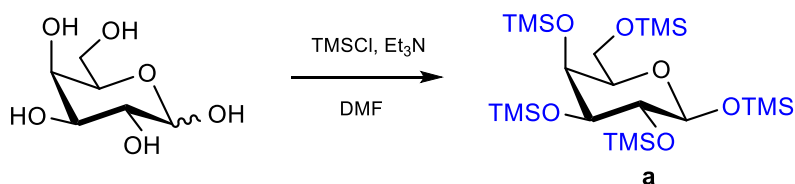
To a suspension of D-galactose (2.04 g, 11.10 mmol, 1 equiv.) in DMF (75 mL, 0,15 M), TEA (8.5 mL, 61.1 mmol, 5.5 eq.) was added. The mixture was cooled down to 0 °C followed by the dropwise addition of TMSCl (7.8 mL, 61.1 mmol, 5.5 eq.). After 17 h, the reaction mixture was diluted in 100 ml of hexane and extracted with cold water (2 x 100 mL). The organic phase was dried over anhydrous Na₂SO₄, filtered and the excess of solvent was removed with a rotary evaporator to give compound **a** (5.02 g, 84 %) as a colourless syrup. TLC: *R_f*: 0.89 (Hex:EtOAc - 7:3).

¹H NMR (400 MHz, CDCl₃, 278 K): δ= 5.07 (d, 1H, *J_{1-2}*= 2.12 Hz, H-1), 3.91 (m, 2H, H-3 and H-5), 3.84 (m, 2H, H-2 and H-4), 3.64 (dd, *J_{6a-6b}*= 9.5 Hz, *J_{6a-5}*=7.9 Hz, 1H, H-6a), 3.55 (dd, *J_{6b-6a}*= 9.5 Hz, *J_{6b-5}*= 5.4 Hz, 1H, H-6b), 0.16 (s, 18H, 2 x -OSi(CH₃)₃), 0.15 (s, 9H, -OSi(CH₃)₃), 0.13 (s, 9H, -OSi(CH₃)₃), 0.12 (s, 9H, -OSi(CH₃)₃) ppm.

13C NMR (100.6 MHz, CDCl$_3$, 278 K): δ= 94.8 (C-1), 72.44 (C-3 or C-5), 71.31 (C-3 or C-5), 70.67 (C-2 or C-4), 70.14 (C-2 or C-4), 61.2 (C-6), 0.74 (-OSi(CH$_3$)$_3$), 0.56 (-OSi(CH$_3$)$_3$), 0.41 (-OSi(CH$_3$)$_3$), 0.26 (-OSi(CH$_3$)$_3$), -0.39 0.74 (-OSi(CH$_3$)$_3$) ppm.

ESI MS (+) Calculated mass: 541.07 m/z Experimental mass [M+Na$^+$]: 563.61 m/z

Synthesis of 3'-(benzyloxycarbonyl)-aminopropyl-2,3,4,6-tetra-O-TMS-α-D-galactopyranoside (c)
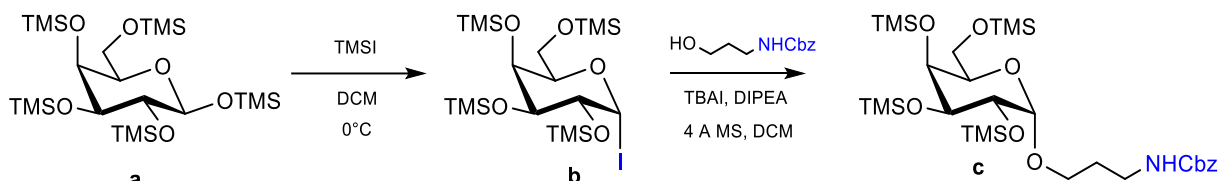
Compound **a** (1.96 g, 3.62 mmol, 1 eq.) was dissolved in dry toluene and the solvent was evaporated, the process was repeated three times to get rid of any water traces. After 12 h, compound **a** was dissolved in dry DCM (20 mL, 0.18 M) under Ar atmosphere and cooled down to 0 °C followed by the dropwise addition of TMSI (0.52 mL, 3.66 mmol, 1 eq.). The reaction mixture was stirred for 90 mins at 0 °C for and monitored by TLC (Hex:EtOAc 8:2). After disappearance of the starting material, the excess of solvent was removed to obtain the galactosyl iodide **b**.

In a separate flask, benzyl N-(3-hydroxypropyl) carbamate (1.14 g, 5.43 mmol, 1.5 eq.) was dissolved in dry toluene and the solvent was evaporated, the process was repeated three times to get rid of any water traces. After 15 h, it was dissolved in 10 mL of dry DCM and 4 Å MS, TBAI (4.01 g, 10.86 mmol, 3 eq.) and DIPEA (1.26 mL, 7.24 mmol, 2 eq.) were added. The mixture was stirred for 15 mins before the addition of a solution of the intermediate **b** in 15 mL of DCM. The reaction mixture was stirred for 15 h and monitored by TLC (Hex:EtOAc 8:2). Once the reaction was complete, it was filtered over celite, the excess of solvent was removed and the crude was purified by column chromatography (Hex:EtOAc 95:5 → 9:1 + 0.5% TEA) to obtain compound **c** (2.37 g, 62 %) as a white solid.

TLC: R_f: 0.61 (Hex:EtOAc - 7:3).

1H NMR (400 MHz, CDCl$_3$, 278 K): δ= 7.38 – 7.28 (m, 5H, -OCH$_2$Ph), 5.81 (m, 1H, -NHCbz), 5.10 (s, 2H, -NHCOOCH$_2$Ph), 4.7 (d, 1H, J_{1-2}= 3.72 Hz, H-1), 3.92 (m, 3H, H-2, H-4, H-7a), 3.78 (m, 2H, H-3, H-5), 3.61 (m, 3H, H6a, H-6b, H-9a), 3.40 (m, 1H, H-7b), 3.14 (m, 1H, H-9b), 1.81 (m, 2H, H-8), 0.15 (s, 9H, -OSi(CH$_3$)$_3$), 0.13 (s, 9H, -OSi(CH$_3$)$_3$), 0.11 (s, 9H, -OSi(CH$_3$)$_3$), 0.10 (s, 9H, -OSi(CH$_3$)$_3$) ppm.

13C NMR (100.6 MHz, CDCl$_3$, 278 K): δ= 128.53 and 128.06 (-OCH$_2$Ph), 100.77 (C-1), 72.55 (C-2 or C-4), 71.75 (C-3 or C-5), 71.32 (C-3 or C-5), 69.91 (C-2 or C-4), 68.92 (C-7), 66.52 (-NHCOOCH$_2$Ph), 61.67 (C-6), 40.52 (C-9), 29.39 (C-8), 0.85 (-OSi(CH$_3$)$_3$), 0.69 (-OSi(CH$_3$)$_3$), 0.43 (-OSi(CH$_3$)$_3$), -0.29 (-OSi(CH$_3$)$_3$) ppm.

Synthesis of 3'-(benzyloxycarbonyl)-aminopropyl-α-D-galactopyranoside (d)
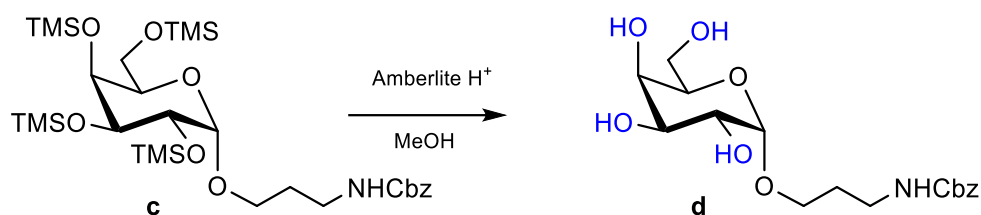
Compound **c** (1.67 g, 2.53 mmol, 1 eq.) was dissolved in MeOH and Amberlite IR120 was added. The reaction mixture was stirred until TLC (DCM:MeOH 8:2) showed disappearance of the starting material. The Amberlite was filtered off using cotton and the excess of solvent was evaporated to obtain compound **d** as a colourless oil (0.92 g, 98 %). TLC: R_f: 0.46 (DCM:MeOH - 8:2)

^{1}H NMR (400 MHz, MeOD, 278 K): δ= 7.40 – 7.28 (m, 5H, -OCH$_2$Ph), 5.09 (s, 2H, -NHCOOC$\underline{H}_2$Ph), 4.81 (d, 1H, J_{1-2}= 3.72 Hz, H-1), 3.89 (dd, J_{3-2}= J_{3-4}< 2 Hz, 1H, H-3), 3.84 – 3.79 (m, 2H, H-5 and H-7a), 3.85 – 3.75 (m, 2H, H-2 and H-4), 3.71 (m, 2H, H-6), 3.49 (m, 1H, H-7b), 3.27 (m, 2H, H-9), 1.82 (m, 2H, H-9) ppm.

^{13}C NMR (100.6 MHz, MeOD, 278 K): δ= 129.56 and 129.05 (-OC$\underline{H}_2$Ph), 100.60 (C-1), 72.59 (C-5), 71.66 (C-2 or C-4), 71.21 (C-3), 70.38 (C-2 or C-4), 67.45 (-NHCOOC$\underline{H}_2$Ph), 66.66 (C-7), 62.94 (C-6), 38.20 (C-9), 30.75 (C-8) ppm.

ESI MS (+) Calculated mass: 371.39 m/z Experimental mass [M+Na$^+$]: 394.33 m/z

Synthesis of 3'-aminopropyl-α-D-galactopyranoside (e)
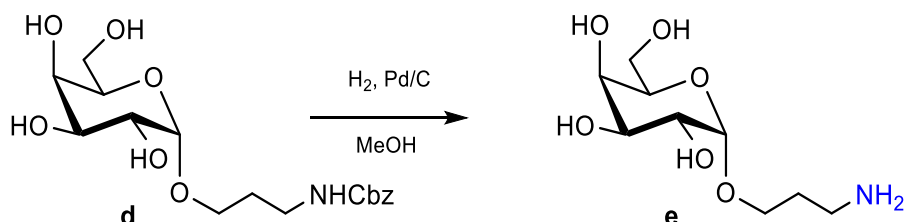
To a solution of compound **d** (0.54 g, 0.15 mmol, 1 eq.) in MeOH (10 mL, 0.01 M), Pd/C was added. The reaction atmosphere was purged with H$_2$/vacuum cycles and then, stirred under H$_2$ atmosphere. After 3 h, the Pd/C was filtered through a whatman syringe filter and concentrated under vacuum to give compound **e** as a colourless foam (0.34 g, quant.).

1H NMR (400 MHz, D_2O, 278 K): δ= 4.95 (d, 1H, J_{1-2}= 3.01 Hz, H-1), 3.98 (bs, 1H, H-3), 3.93 (m, 1H, H-5), 3.88 – 3.80 (m, 3H, H-2, H-4, H-7a), 3.75 (m, 2H, H-6), 3.59 (m, 1H, H-7b), 2.91 (m, 2H, H-9), 1.88 (m, 2H, H-8) ppm.

13C NMR (100.6 MHz, D_2O, 278 K): δ= 98.10 (C-1), 70.67 (C-5), 69.03, 68.84 and 67.63 (C-2, C4 or C-5), 65.46 (C-7), 60.82 (C-6), 37.9 (C-9), 26. 2 (C-8) ppm.

ESI MS (+) Calculated mass: 237.25 m/z Experimental mass [M+H+]: 238.05 m/z

Synthesis of HS-PEG5000-COO-PFP (f)
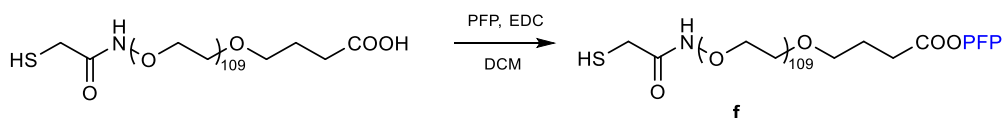
To a solution of HS-PEG5000-COOH (160 mg, 0.032 mmol) in dry DCM (1.5 mL, 0.02 M), pentafluorophenol (PFP) (30 mg, 0.16 mmol) and ethyl-3-(3-dimethylaminopropyl)carbodiimide (EDC) (20 mg, 0.10 mmol) were added. The reaction progress was monitored by TLC (DCM:MeOH 9:1). After 48 h the excess of DCM was removed under reduced pressure, re-dissolved in cold Et_2O (5 mL) and centrifuged for 6 min at 6000 rpm. The supernatant was removed, and the centrifugation process was repeated for 5 times until the formation of a white HS-PEG5000-COO-PFP (162 mg, 98%) precipitate.

Characterized by ^1H and ^{19}F.

Synthesis of HS-PEG5000-Gal (9-GalPEG)
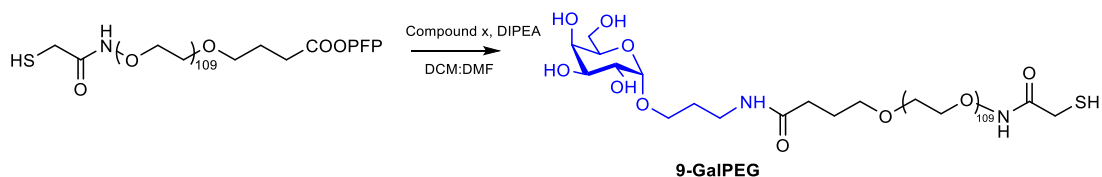
To a solution of HS-PEG5000-COOPFP (47 mg, 0.01 mmol) in dry DCM (0.5 mL, 0.02 M), DIPEA (15 µL, 0.08 mmol) was added. In a separate flask compound **e** (8.5 mg, 0.04 mmol) was dissolved in DMF (0.4 mL) and then added to the reaction mixture. After 48 h, the excess of solvent was removed under reduced pressure and the crude was purified by size exclusion chromatography (Sephadex G-25) using H_2O as a solvent to obtain compound 41 mg as a white foam.

3.6 References

(1)   du Toit, H.; Macdonald, T. J.; Huang, H.; Parkin, I. P.; Gavriilidis, A. Continuous Flow Synthesis of Citrate Capped Gold nanoparticles Using UV Induced Nucleation. *RSC Adv.* **2017**, *7* (16), 9632–9638. https://doi.org/10.1039/C6RA27173A.

(2)   Liu, G.; Yang, X.; Li, Y.; Yang, Z.; Hong, W.; Liu, J. Continuous Flow Controlled Synthesis of Gold Nanoparticles Using Pulsed Mixing Microfluidic System. *Advances in Materials Science and Engineering* 12.

(3)   Sarsfield, M.; Roberts, A.; Streletzky, K. A.; Fodor, P. S.; Kothapalli, C. R. Optimization of Gold Nanoparticle Synthesis in Continuous-Flow Micromixers Using Response Surface Methodology. *Chem. Eng. Technol.* **2021**, *44* (4), 622–630. https://doi.org/10.1002/ceat.202000314.

(4)   Harada, M.; Kizaki, S. Formation Mechanism of Gold Nanoparticles Synthesized by Photoreduction in Aqueous Ethanol Solutions of Polymers Using In Situ Quick Scanning X-Ray Absorption Fine Structure and Small-Angle X-Ray Scattering. *Crystal Growth & Design* **2016**, *16* (3), 1200–1212. https://doi.org/10.1021/acs.cgd.5b01168.

(5)   Martínez-Ávila, O.; Hijazi, K.; Marradi, M.; Clavel, C.; Campion, C.; Kelly, C.; Penadés, S. Gold *Manno* -GlycoNanoparticles: Multivalent Systems to Block HIV-1 Gp120 Binding to the Lectin DC-SIGN. *Chem. Eur. J.* **2009**, *15* (38), 9874–9888. https://doi.org/10.1002/chem.200900923.

(6)   Hostetler, M. J.; Wingate, J. E.; Zhong, C.-J.; Harris, J. E.; Vachet, R. W.; Clark, M. R.; Londono, J. D.; Green, S. J.; Stokes, J. J.; Wignall, G. D.; Glish, G. L.; Porter, M. D.; Evans, N. D.; Murray, R. W. Alkanethiolate Gold Cluster Molecules with Core Diameters from 1.5 to 5.2 Nm: Core and Monolayer Properties as a Function of Core Size. *Langmuir* **1998**, *14* (1), 17–30. https://doi.org/10.1021/la970588w.

(7)   Boselli, L.; Polo, E.; Castagnola, V.; Dawson, K. A. Regimes of Biomolecular Ultrasmall Nanoparticle Interactions. *Angew. Chem. Int. Ed.* **2017**, *56* (15), 4215–4218. https://doi.org/10.1002/anie.201700343.

(8)   Mellor, R. D.; Uchegbu, I. F. Ultrasmall-in-Nano: Why Size Matters. *Nanomaterials* **2022**, *12* (14), 2476. https://doi.org/10.3390/nano12142476.

(9)   Huang, K.; Ma, H.; Liu, J.; Huo, S.; Kumar, A.; Wei, T.; Zhang, X.; Jin, S.; Gan, Y.; Wang, P. C.; He, S.; Zhang, X.; Liang, X.-J. Size-Dependent Localization and Penetration of Ultrasmall Gold Nanoparticles in Cancer Cells, Multicellular Spheroids, and Tumors *in Vivo*. *ACS Nano* **2012**, *6* (5), 4483–4493. https://doi.org/10.1021/nn301282m.

(10)   Lundquist, J. J.; Toone, E. J. The Cluster Glycoside Effect. *Chem. Rev.* **2002**, *102* (2), 555–578. https://doi.org/10.1021/cr000418f.

(11)   de la Fuente, J. M.; Barrientos, A. G.; Rojas, T. C.; Rojo, J.; Cañada, J.; Fernández, A.; Penadés, S. Gold GlycoNanoparticles as Water-Soluble Polyvalent Models To Study Carbohydrate Interactions. *Angew. Chem. Int. Ed.* **2001**, *40* (12), 2257–2261. https://doi.org/10.1002/1521-3773(20010618)40:12<2257::AID-ANIE2257>3.0.CO;2-S.

(12)   Harada, M.; Saijo, K.; Sakamoto, N. Characterization of Metal Nanoparticles Prepared by Photoreduction in Aqueous Solutions of Various Surfactants Using UV–Vis, EXAFS and SAXS. *Colloids and Surfaces A: Physicochemical and Engineering Aspects* **2009**, *349* (1–3), 176–188. https://doi.org/10.1016/j.colsurfa.2009.08.015.

(13)   Harada, M.; Einaga, H. In Situ XAFS Studies of Au Particle Formation by Photoreduction in Polymer Solutions. *Langmuir* **2007**, *23* (12), 6536–6543. https://doi.org/10.1021/la0701071.

(14)   Harada, M.; Okamoto, K.; Terazima, M. Diffusion of Gold Ions and Gold Particles during Photoreduction Processes Probed by the Transient Grating Method. *Journal of Colloid and Interface Science* **2009**, *332* (2), 373–381. https://doi.org/10.1016/j.jcis.2008.12.041.

(15) Harada, M.; Einaga, H. Formation Mechanism of Pt Particles by Photoreduction of Pt Ions in Polymer Solutions. *Langmuir* **2006**, *22* (5), 2371–2377. https://doi.org/10.1021/la052378m.

(16) Yaghmur, A.; Hamad, I. Microfluidic Nanomaterial Synthesis and In Situ SAXS, WAXS, or SANS Characterization: Manipulation of Size Characteristics and Online Elucidation of Dynamic Structural Transitions. *Molecules* **2022**, *27* (14), 4602. https://doi.org/10.3390/molecules27144602.

(17) Silvestri, A.; Zambelli, V.; Ferretti, A. M.; Salerno, D.; Bellani, G.; Polito, L. Design of Functionalized Gold Nanoparticle Probes for Computed Tomography Imaging: Design of Tailored Engineered AuNanoparticles as CT Contrast Agents. *Contrast Media Mol. Imaging* **2016**, *11* (5), 405–414. https://doi.org/10.1002/cmmi.1704.

(18) Silvestri, A.; Lay, L.; Psaro, R.; Polito, L.; Evangelisti, C. Fluidic Manufacture of Star-Shaped Gold Nanoparticles. *Chem. Eur. J.* **2017**, *23* (41), 9732–9735. https://doi.org/10.1002/chem.201701617.

(19) Marelli, M.; Bossola, F.; Spinetti, G.; Sangalli, E.; Santo, V. D.; Psaro, R.; Polito, L. Microfluidic Synthesis of Hybrid TiO $_2$ -Anisotropic Gold Nanoparticles with Visible and Near-Infrared Activity. *ACS Appl. Mater. Interfaces* **2020**, *12* (34), 38522–38529. https://doi.org/10.1021/acsami.0c08241.

(20) Turkevich, J.; Stevenson, P. C.; Hillier, J. A Study of the Nucleation and Growth Processes in the Synthesis of Colloidal Gold. *Discuss. Faraday Soc.* **1951**, *11*, 55. https://doi.org/10.1039/df9511100055.

(21) Elahi, N.; Kamali, M.; Baghersad, M. H. Recent Biomedical Applications of Gold Nanoparticles: A Review. *Talanta* **2018**, *184*, 537–556. https://doi.org/10.1016/j.talanta.2018.02.088.

(22) Mikhlin, Yu.; Likhatski, M.; Tomashevich, Ye.; Romanchenko, A.; Erenburg, S.; Trubina, S. XAS and XPS Examination of the Au–S Nanostructures Produced via the Reduction of Aqueous Gold(III) by Sulfide Ions. *Journal of Electron Spectroscopy and Related Phenomena* **2010**, *177* (1), 24–29. https://doi.org/10.1016/j.elspec.2009.12.007.

(23) Nishizaki, Y.; Lankin, D. C.; Chen, S.-N.; Pauli, G. F. Accurate and Precise External Calibration Enhances the Versatility of Quantitative NMR (QNMR). **2022**, 22.

(24) Wider, G.; Dreier, L. Measuring Protein Concentrations by NMR Spectroscopy. *J. Am. Chem. Soc.* **2006**, *128* (8), 2571–2576. https://doi.org/10.1021/ja055336t.

(25) Floris, P.; Garbujo, S.; Rolla, G.; Giustra, M.; Salvioni, L.; Catelani, T.; Colombo, M.; Mantecca, P.; Fiandra, L. The Role of Polymeric Coatings for a Safe-by-Design Development of Biomedical Gold Nanoparticles Assessed in Zebrafish Embryo. *Nanomaterials* **2021**, *11* (4), 1004. https://doi.org/10.3390/nano11041004.

(26) Tan, Y.; Chen, M.; Chen, H.; Wu, J.; Liu, J. Enhanced Ultrasound Contrast of Renal-Clearable Luminescent Gold Nanoparticles. *Angew. Chem. Int. Ed.* **2021**, *60* (21), 11713–11717. https://doi.org/10.1002/anie.202017273.

(27) Gong, L.; He, K.; Liu, J. Concentration-Dependent Subcellular Distribution of Ultrasmall Near-Infrared-Emitting Gold Nanoparticles. *Angew. Chem. Int. Ed.* **2021**, *60* (11), 5739–5743. https://doi.org/10.1002/anie.202014833.

(28) Stejskal, E. O.; Tanner, J. E. Spin Diffusion Measurements: Spin Echoes in the Presence of a Time-Dependent Field Gradient. *The Journal of Chemical Physics* **1965**, *42* (1), 288–292. https://doi.org/10.1063/1.1695690.

(29) Barrientos, Á. G.; de la Fuente, J. M.; Rojas, T. C.; Fernández, A.; Penadés, S. Gold GlycoNanoparticles: Synthetic Polyvalent Ligands Mimicking Glycocalyx-Like Surfaces as Tools for Glycobiological Studies. *Chem. Eur. J.* **2003**, *9* (9), 1909–1921. https://doi.org/10.1002/chem.200204544.

Chapter 4

Protein corona studies of spherical and anisotropic AuNPs

4.1 Introduction

4.1.1 Anisotropic gold nanoparticles

Anisotropic gold nanoparticles (AuNPs) with a star shape present unique optical and electronic properties due to their geometry. They present a localized surface plasmon resonance (LSPR) which can be tuned to the near infrared region (NIR).[1] Therefore, these nanoparticles (NPs) can be superior to isotropic NPs regarding the tissue penetration. Moreover the surface-enhanced Raman spectroscopy SERS activity has been demonstrated to be higher compared to spherical NPs therefore they are ideal for bioimaging and sensing devices.[2]

Overall star shaped gold NPs present numerous applications due to their particular properties. Some of the applications are photonics[3], catalysis[4], contrast agents in bioimaging techniques and photothermal therapy for cancer treatments[5].

Even though these NPs have shown great advantages for bio applications, one of the major challenges for the translation of clinical uses was the synthetic procedure to obtain reproducible gold nanostars. Therefore, our group developed in the past years a new microfluidic approach to obtain anisotropic AuNPs. This system enables the production of reproducible gold star shaped NPs by using a continuous flow procedure.[1,6]

During this chapter this one-pot protocol was used to obtain star shaped AuNPs which were then further modified to obtain Glyco-star-AuNPs.

4.1.2 Protein corona

The protein corona (PC) formed when the NPs are in contact with biological fluids is of great importance as it can modify the biodistribution of the NPs.[7] The protein corona formation presents drawbacks and advantages. It can induce the recognition of the NPs by the reticuloendothelial system and as a consequence the circulation time of the NPs can be extended.[8] On the other hand, the PC formation can also reduce the specific targeting of the NPs.[9]

The size and shape of the AuNPs has a great impact on the PC formation. Garcia-Alvarez et al. investigated the PC formation *in-vivo* of AuNPs with two different morphologies, nanostars and nano rods and with two sizes 40 nm and 70 nm. The Au nanostars of 70 nm showed a higher adsorption of proteins, this could be due to higher surface are present in these NPs. Even though the number of proteins adsorbed was higher it was concluded that the smaller star shaped AuNPs showed a more complex protein corona. The nanorods showed a higher complexity of

PC than the nanostars of the same size. Overall, this study demonstrated how the PC formed in vivo can be affected by the different size and shape of the AuNPs.

Other factors as the surface coating, the surface charge and the environmental conditions[10] can also affect the protein corona formation of AuNPs some of them are explained in Chapter 1 section 3.

4.2 Aim of the work

The aim of this chapter was to study the colloidal stability of Glyco-AuNPs using 3 carbohydrates attached to two different linkers and using AuNPs of different morphologies.

A set of 6 glyco-star-AuNPs have been synthesized and will be described in this chapter. The star shaped AuNPs were synthesized using a one-pot microfluidic procedure developed in our group (figure 4.1). Exploiting the same apparatus, a further set of 5 glyco-spherical-AuNPs were synthesized.
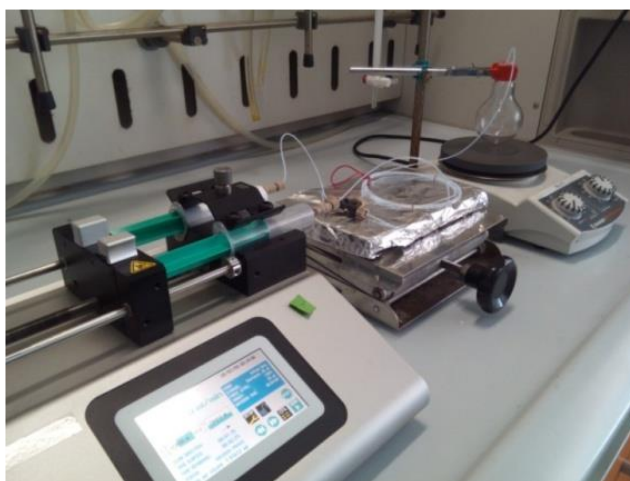
Figure 2.1. Picture of bench-top microfluidic reactor

With this small glyco-AuNPs library ready, the goal was to study the colloidal stability of the AuNPs in different media. The colloidal stability was evaluated by measuring Dynamic light scattering and ζ-potential measurements by means of a DLS instrument.

The media analysed are:

- Phosphate Buffered Saline (PBS) : buffer solution used commonly in biological research as it has a stable pH and the ion concentration simulates the biological fluid in the body.[11]
- Fetal Bovine Serum (FBS): serum obtained from bovine fetus, it is used typically in cell culture as it contains growth factors and low levels of antibodies. It is composed by a mix of proteins, lipids, enzymes and undefined constituents.
- Rosswell Park Memorial Institute (RPMI): a cell growth medium. It contains amino acids, vitamins, salts and sodium bicarbonate.

4.3 Results and discussion

4.3.1 Glyco-star-gold nanoparticles

4.3.1.1 Synthesis of glyco-star-gold nanoparticles

The synthesis of the star shaped AuNPs was performed following a microfluidic procedure developed in our group. The system consists in a syringe pump, a mixing zone with a PEEK T-mixer all connected by PTFE tubes with an internal diameter of 1 mm and the reaction zone which is a PTFE tube of 160 cm length. As shown in figure 4.2 Syringe A contains a solution of $HAuCl_4$ and silver nitrate ($AgNO_3$) and syringe B a solution of ascorbic acid. In this case ascorbic acid is used as the reducing agent of Au and a temporary stabilizer. The $AgNO_3$ is used as a templating agent to control the shape of the NPs. A fine control of the pH and the amount of $AgNO_3$ is needed to obtain the star AuNPs.
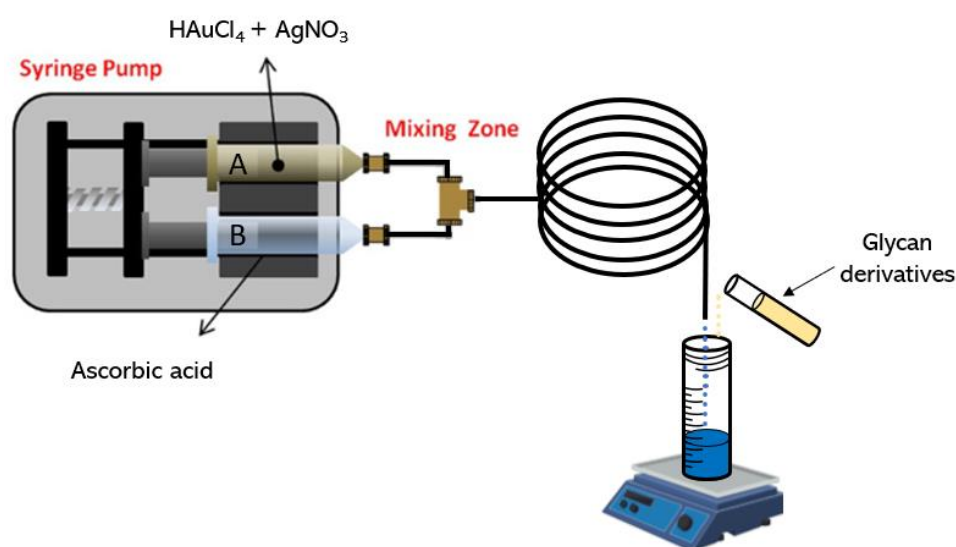
Figure 4.2. Schematic representation of bench-top microfluidic reactor

In order to obtain the glyco-star AuNPs 3 glycans were used. α-Mannose, β-glucose and lactose with a short aliphatic ligand and a longer amphiphilic linker as shown in table 3.3 and 3.10.

The glyco-star-AuNPs 1 – 6 shown in table 4.1 were obtained by adding the amount of glycan derivative indicated in table 2 to the star shaped AuNPs solution obtained with the microfluidic system (figure 4.2). The reaction was left stirring overnight. The star-AuNPs were then isolated by centrifugation, in all cases the NPs were obtained successfully.
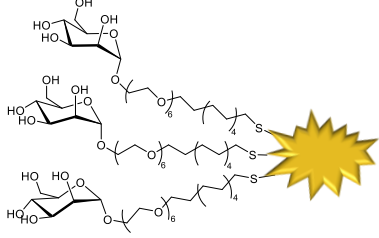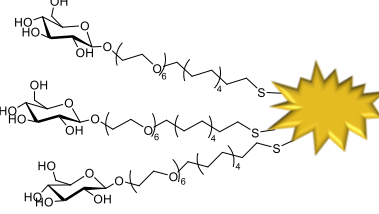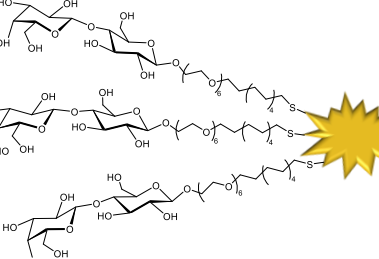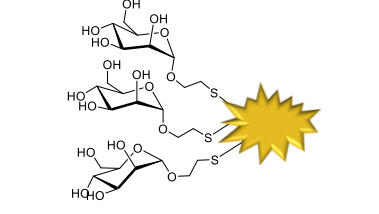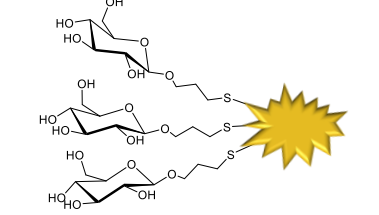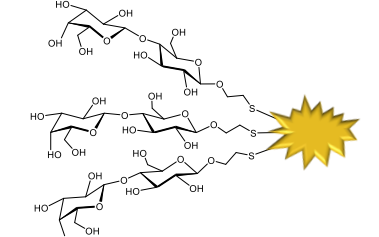
Glyco-star-AuNPs	Glycan derivative	Amount of glycan added (µmol)
AuNPs – 1	**1-Man** $\text{Man-EG}_6\text{C}_{11}$	2.5
AuNPs – 2	**2-Glc** $\text{Glc-EG}_6\text{C}_{11}$	2.5
AuNPs – 3	**3-Lac** $\text{Lac-EG}_6\text{C}_{11}$	1.9
AuNPs – 4	**5-Man** Man-C_2	6.6
AuNPs – 5	**6-Glc** Glc-C_3	6.3
AuNPs – 6	**7-Lac** Lac-C_2	3.7

Table 4.1. Glyco-star-AuNPs 1- 7

4.3.1.2 Characterization of glyco-star-gold nanoparticles

The glyco-star-AuNPs were characterized by UV-visible and Transmission Electron Microscopy (TEM). The UV-vis spectra and TEM micrographs are shown in figure 4.3 and 4.4. Star shaped gold NPs are characterized by having a wide plasmonic band around 600 – 700. In all cases for the star shaped NPs synthesized in this chapter the surface plasmon was around 600 nm as observed by UV-vis.
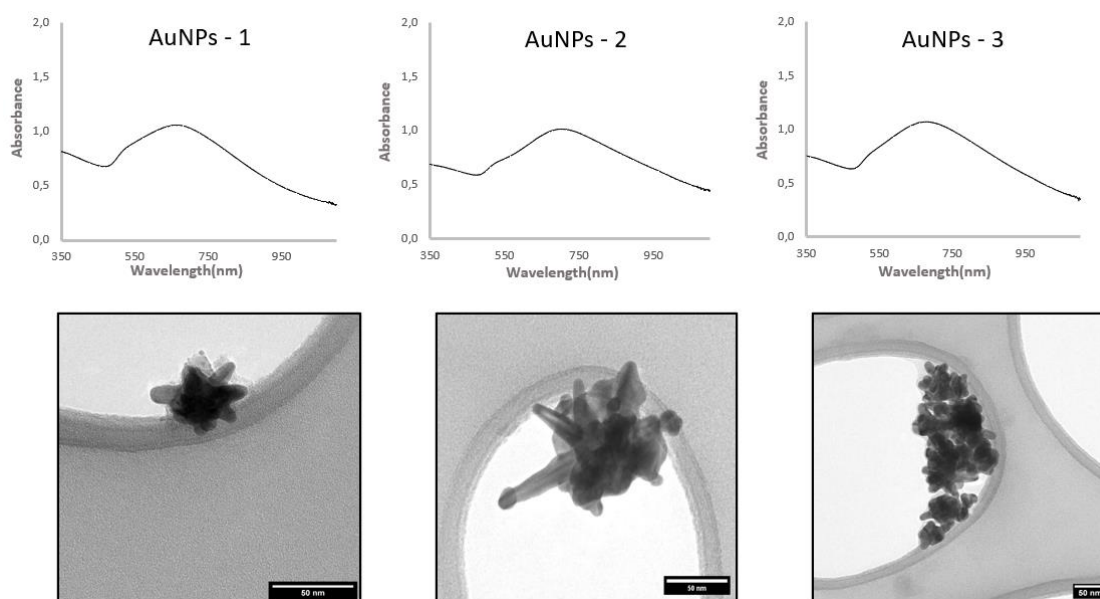
Figure 4.3. *UV-vis spectra and TEM micrographs of **AuNPs 1-3** (amphiphilic linker). Scale bar 50 nm*
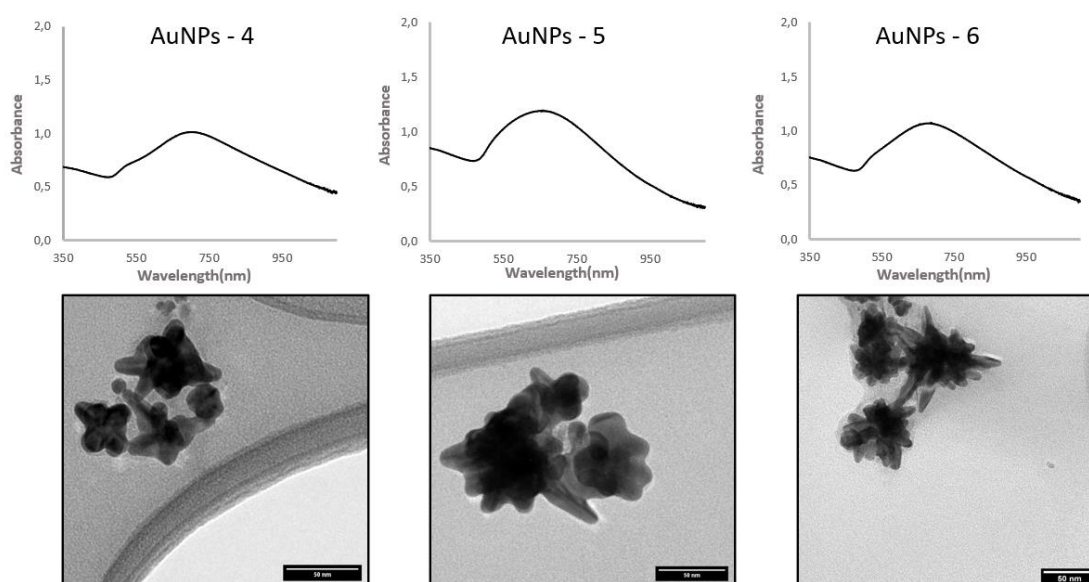
Figure 4.4. *UV-vis spectra and TEM micrographs of **AuNPs 4 – 6** (aliphatic linker). Scale bar 50 nm*

4.3.2 Long-term colloidal stability glyco-star-gold nanoparticles

The long-term colloidal stability of the star shaped gold NPs was studied by dynamic light scattering (DLS) and ζ-potential. The stability was studied by adding to the NPs different mediums and measuring their hydrodynamic diameter and surface charge over time.

The AuNPs were tested in PBS, it's a buffer with a pH 7.4 which is normally used in biological experiments as it simulates the conditions of the body. Moreover, the protein corona formation was investigated by using FBS and RPMI + 10 % FBS. The AuNPs diluted in water were also measured over time as a control and a stability test.

The AuNPs were kept at 4 °C between measurements. The same concentration of the AuNPs was obtained in all cases and it was checked by UV-vis. Preparation of solutions:

- Deionized water

50 μL AuNPs were diluted with 200 μL Milli-Q water

- Phosphate buffered saline (PBS)

20 μL AuNPs were diluted with 30 μL Milli-Q water and 200 μL PBS 10 mM

- Fetal bovine serum (FBS)

20 μL AuNPs were diluted with 30 μL Milli-Q water and 200 μL FBS

- RPMI + 10% FBS

20 μL AuNPs were diluted with 200 μL RPMI enriched with 10% FBS

After preparation the samples were sonicated for 2 minutes and then were left other 2 mins to stabilize.

4.3.2.1 Dynamic Light Scattering

All AuNPs were measured by DLS at different time points after the addition of the different medium solutions as shown in figure 4.5. The hydrodynamic diameter of AuNPs 1 - 5 was stable after the addition of PBS, except for AuNPs – 5. In all cases the diameter was increased after addition of RPMI + 10% FBS as expected, the increase varied for each nanoparticle as the interactions with RPMI + 10% FBS can vary depending on the glycans coating the AuNPs and the linker bond to them. The major increase was observed in the AuNPs with FBS, this could be due to the amount of glycans, lipids and other biological factors present in the solution.
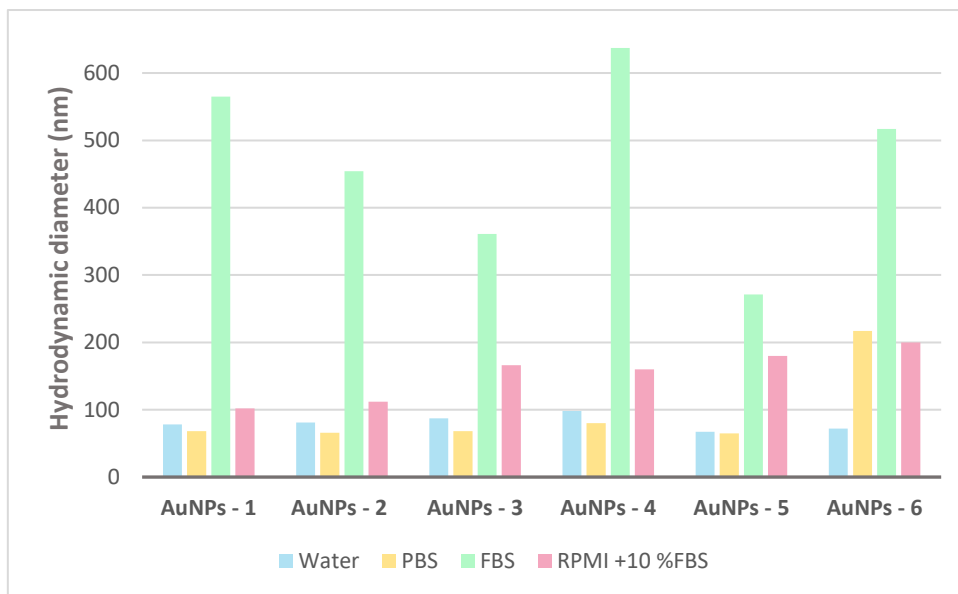
Figure 4.5. Hydrodynamic diameter after addition of water, PBS, FBS and RPMI +10% FBS

In order to study the stability of the Glyco-star-AuNPs in water, DLS measurements were registered over 6 months as shown in figure 4.6. In general, all the samples didn't suffer any major modification over time proving Glyco-star-AuNPs kept at 4°C are stable and reliable for at least 6 months.
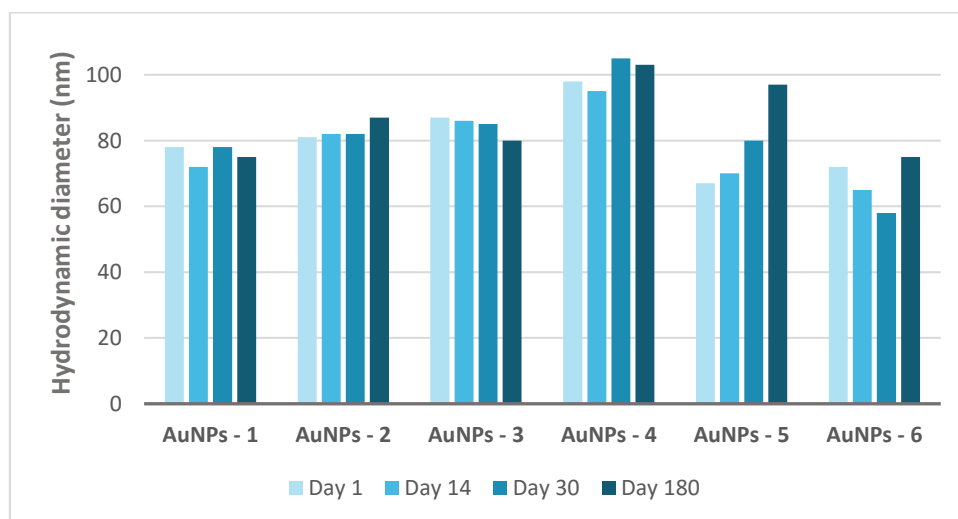
*Figure 4.6. Hydrodynamic diameter of **AuNPs 1 – 6** in water over 180 days*

The stability in PBS was also studied over 6 months as shown in figure 4.7. The AuNPs 4 - 6 coated with glycan derivatives bond to an aliphatic linker underwent only minor variations over 180 days. On the other hand, AuNPs 1 – 3 did suffer some diameter variations, increasing progressively with the pass of time. AuNPs – 3 varied were strongly affected by the addition of PBS as the diameter increased from 68 to 380 nm in 6 months.
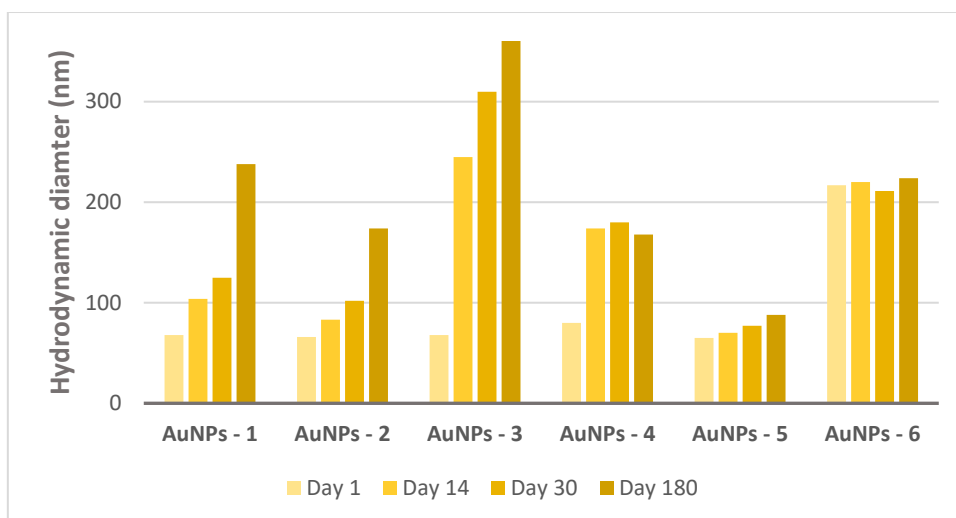
*Figure 4.7. Hydrodynamic diameter of **AuNPs 1 – 6** in PBS over 180 days*

The colloidal stability of AuNPs – 1 – 6 after the addition of FBS was observed by measuring the hydrodynamic diameter over 30 days shown in figure 4.8. The diameter in all cases increased dramatically from around 60 – 80 nm in water to 280 nm in the case of AuNPs – 5 and up to 650 nm for AuNPs – 2 after the addition of FBS. This could be explained by the number of proteins present in the FBS solution which have consequently attached to the AuNPs surface.
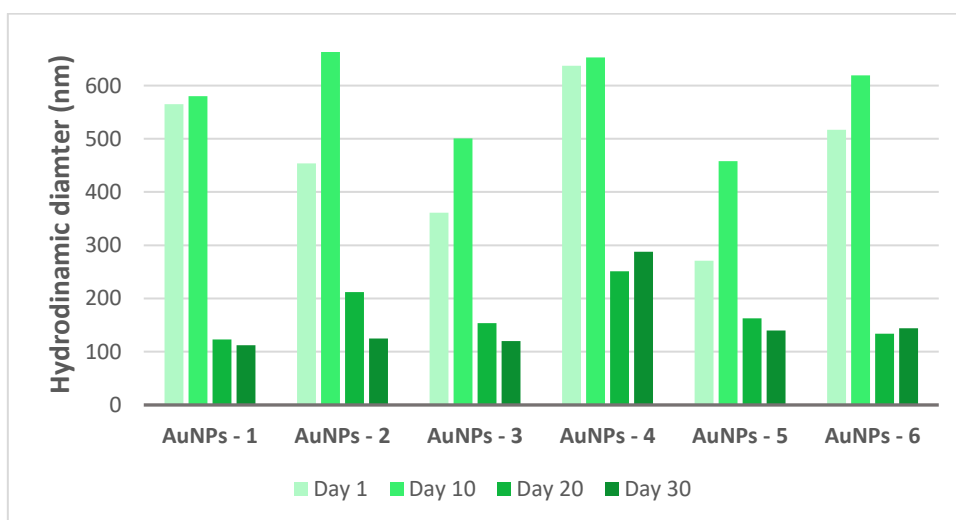
*Figure 4.8. Hydrodynamic diameter of **AuNPs 1 – 6** in FBS over 30 days*

As explained previously all samples are sonicated before the measurement for 2 minutes, but in the case of the samples measured after 20 and 30 days were sonicated for 10 minutes. The sonication had an evident effect on the diameter of the NPs for example for AuNPs – 1 the diameter measured after 10 days was 580 nm and in day 20 123 nm. This could be due to the removal of the soft corona which is dynamic and can be modified and the permanence of the

hard corona. The sonication of the samples was further increased to 15 minutes, but the size didn't decrease, meaning the hard corona could not be removed.

The hydrodynamic diameter of the AuNPs exposed to RPMI + 10% FBS were mostly stable overtime as shown in figure 4.9, except for the case of AuNPs – 1 and AuNPs – 2. The size of AuNPs – 2 was increased after 10 days but after 30 days it returned to around 110 nm as in day 1. In the case of AuNPs – 1 the NPs are stable after 10 days and then after 20 days the size increases.
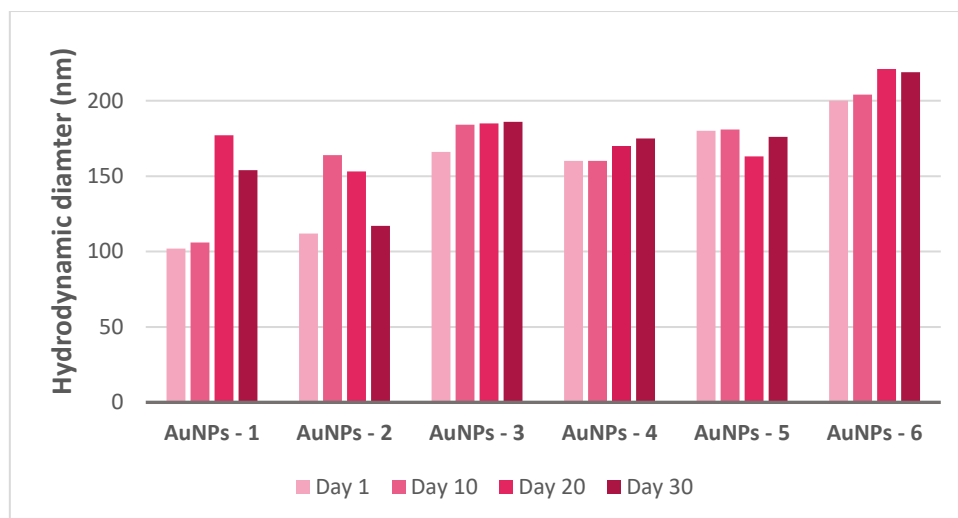
Figure 4.9. Hydrodynamic diameter of **AuNPs 1 – 6** in RPMI + 10% FBS over 30 days

AuNPs 1 – 6 in FBS and RPMI enriched with 10% FBS were centrifuged after 30 days and washed in water. This experiment was done to test if the AuNPs could be resuspend in water. The AuNPs were then measured by DLS, the data obtained is shown in figure 4.10 and 4.11.
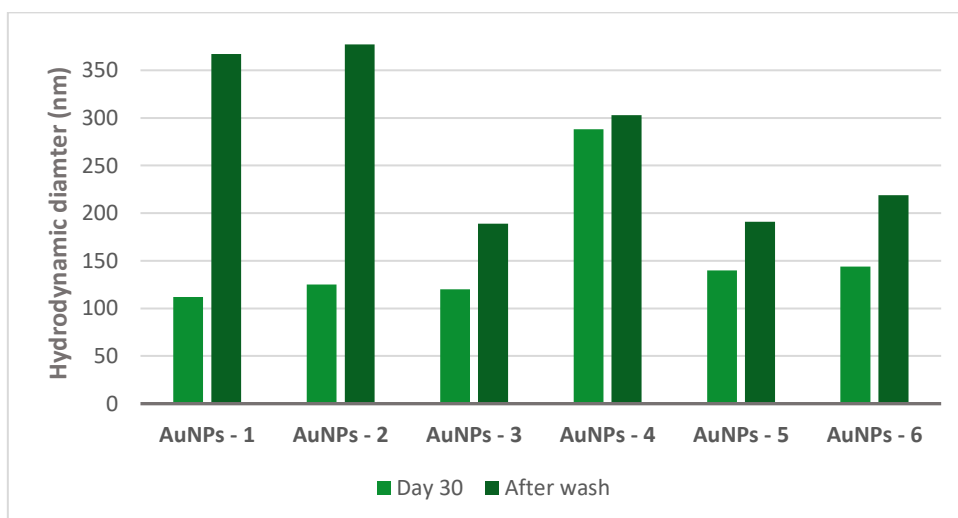
Figure 4.10. Hydrodynamic diameter of **AuNPs 1 – 6** in FBS after washing
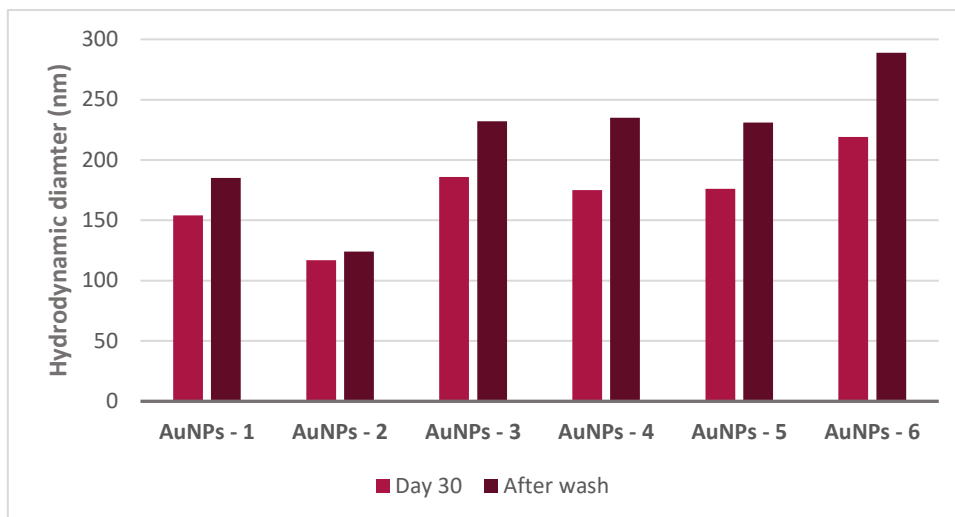
Figure 4.11. *Hydrodynamic diameter of **AuNPs 1 – 6** in RPMI + 10% FBS after washing*

The results obtained in both cases show that the NPs can be resuspend in water after forming the protein corona. The hydrodynamic diameter after washing and removing the biological medium had in all cases increased. This could be because in the previous cases when the NPs are in the biological medium the protein corona was a dynamic bond. After the centrifugation and resuspension in water the hard corona is not any more in a dynamic equilibrium instead in water the bond between the NPs is stronger as there is a higher affinity between the AuNPs and the hard corona.

4.3.2.2 ζ potential

The colloidal stability of AuNPs 1 – 6 in water and PBS was analysed over 180 days by controlling the change in the surface charge as shown in figure 4.12 and 4.13. In all cases the variation observed over time are of a maximum of 10 mV, these are considered very low variations and therefore it was determined that the surface charge of the star shaped AuNPs 1 – 6 were stable in water and PBS.
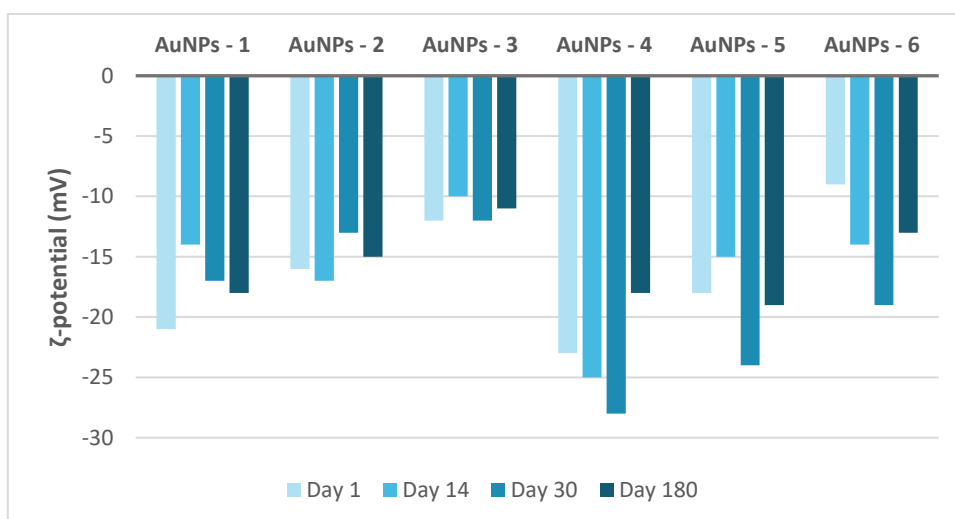
Figure 4.12. *ζ- potential of **AuNPs 1 – 6** in water*

85
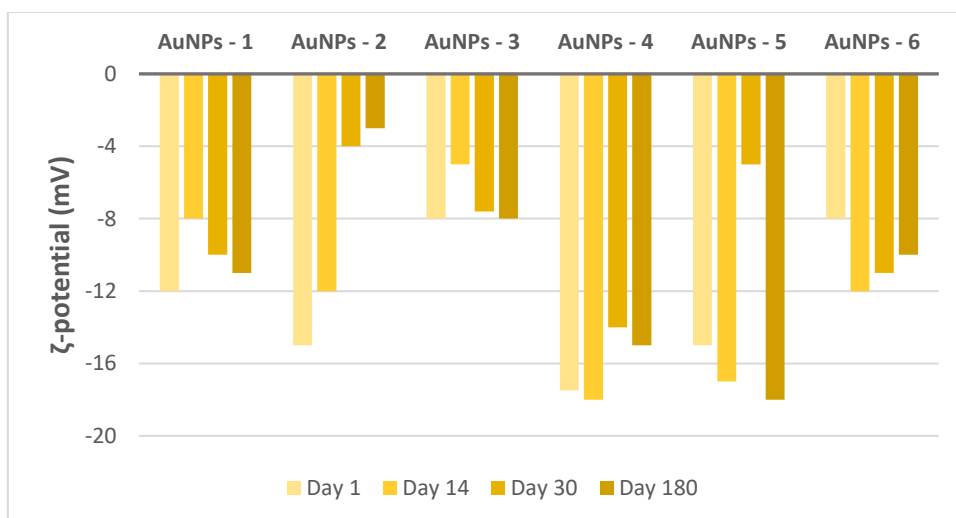
Figure 4.13. ζ- potential of **AuNPs 1 – 6** in PBS

The ζ- potential of the AuNPs 1 – 6 after the addition of RPMI + 10 % FBS was measured over 30 days as shown in figure 4.14. The surface charge of the NPs was decreased in all cases, this could be caused by the protein corona formation. As the AuNPs are covered in proteins their charge is modified, this is consistent with the data obtained by DLS. The increase of size for AuNPs 1 – 6 after the addition of RPMI + 10% FBS and the decrease of the ζ potential can confirm there has been a protein corona formation around the NPs. Moreover, the ζ- potential was registered after the centrifuge and resuspension in water, a decrease of the charge was observed this could be due to a higher stability of the NPs in water instead of RPMI +10% FBS.
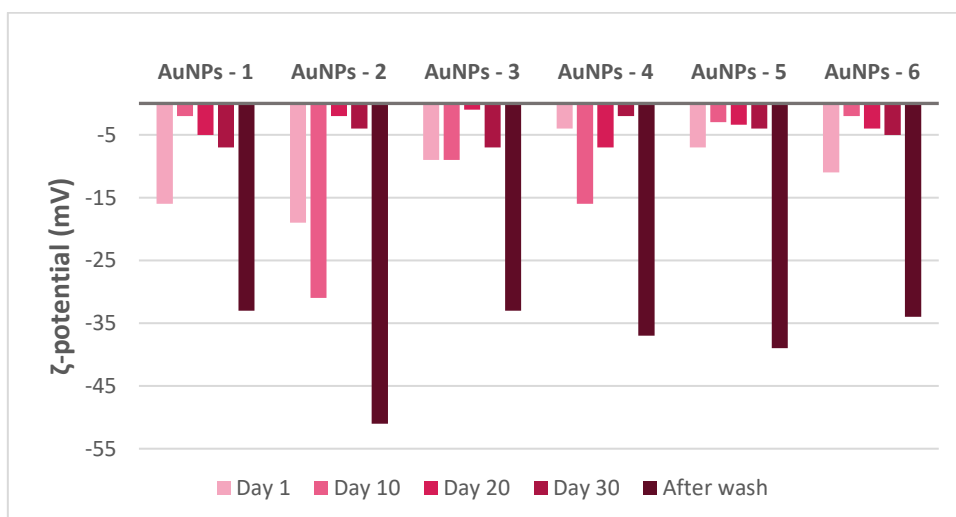
Figure 4.14. ζ- potential of **AuNPs 1 – 6** in RPMI + 10% FBS

The results obtained of the ζ- potential of AuNPs 1 – 6 with FBS were not reliable and therefore are not shown.

4.3.3 Glyco-spherical-gold nanoparticles

4.3.3.1 Synthesis of glyco-spherical-gold nanoparticles

Spherical Glyco AuNPs were synthesized following the same microfluidic shown previously in figure 4.15, removing $AgNO_3$. Solution A contained the gold salt $HAuCl_4$ dissolved in water and solution B the reducing agent and stabilizer ascorbic acid dissolved in water.
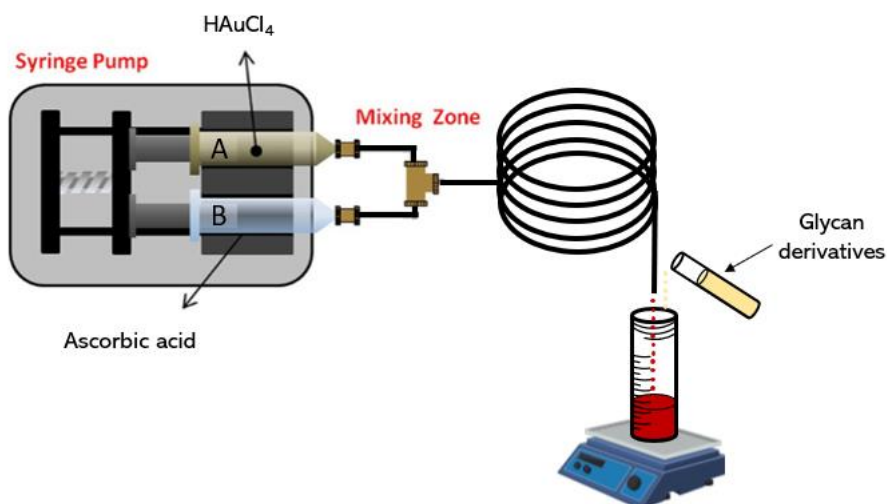
Figure 4.15. *Schematic representation of bench-top microfluidic reactor*

The glyco spherical AuNPs shown in table 4.2 were acquired by adding the glycan derivatives 2-Glc,3-Lac, 5-Man, 6-Glc and 7-Lac (table 3.3 and 3.10) to the AuNPs and leaving the solution stirring overnight (figure 4.15). The quantity of glycans added are indicated in table 4.2. AuNPs 7 – 11 were obtained successfully after purification.

Glyco-AuNPs	Glycan derivative	Amount of glycan added (μmol)
AuNPs – 7	**2-Glc** Glc-EG$_6$C$_{11}$	2.8
	3-Lac Lac-EG$_6$C$_{11}$	2.4
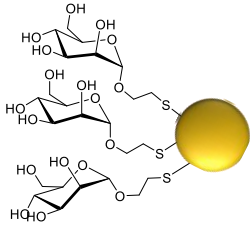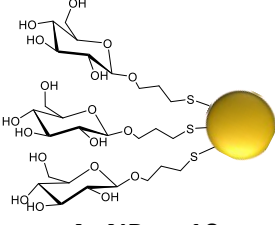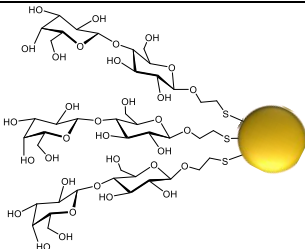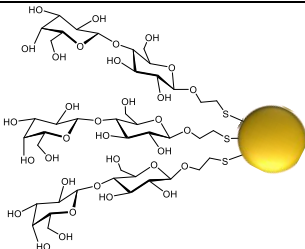
AuNPs – 8		
AuNPs – 9	**5-Man** Man-C$_2$	6.2
AuNPs – 10	**6-Glc** Glc-C$_3$	6.3
AuNPs – 11	**7-Lac** Lac-C$_2$	3.6

*Table 4.2. Glyco spherical **AuNPs 7 - 11***

4.3.3.2 Characterization of glyco-spherical-gold nanoparticles

AuNPs 7 – 11 were al characterized by UV-vis and TEM as shown in figure 4.16 and 4.17. AuNPs of around 30 nm were obtained, and surface plasmon resonance was observed by UV-vis around 520 nm.
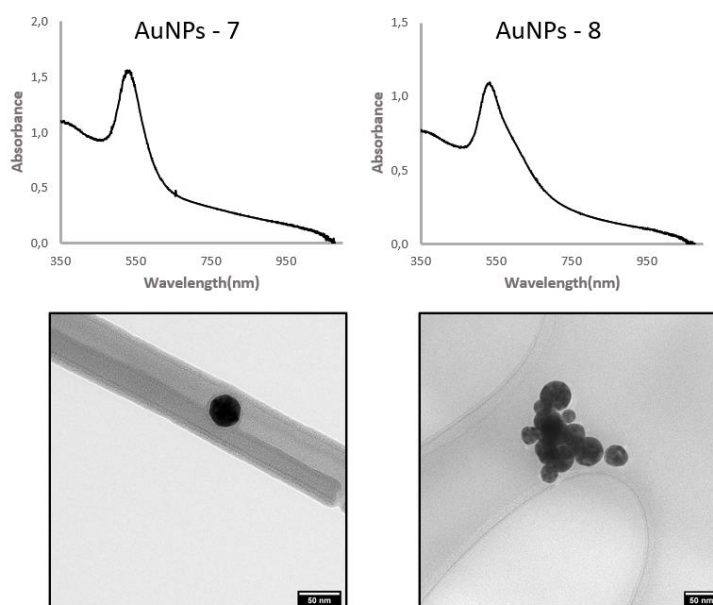
Figure 4.16. *UV-vis spectra and TEM micrographs of **AuNPs 7 – 8** (amphiphilic linker). Scale bar 50 nm*
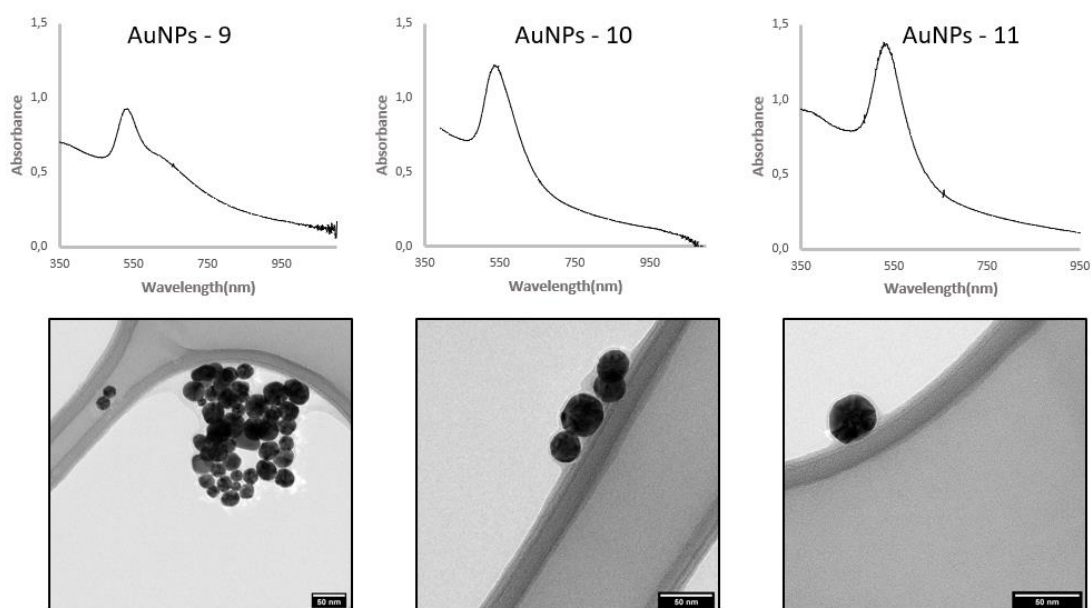
Figure 4.17. *UV-vis spectra and TEM micrographs of* **AuNPs 9 – 11** *(aliphatic linker). Scale bar 50 nm*

4.3.4 Long-term colloidal stability glyco-spherical-gold nanoparticles

The long-term colloidal stability of spherical Glyco-AuNPs was analysed by DLS and ζ - potential over 30 days in water and PBS.

The AuNPs were kept at 4 °C between measurements. The same concentration of the AuNPs was obtained in all cases and it was checked by UV-vis. Preparation of solutions:

-   Deionized water

50 µL AuNPs were diluted with 200 µL Milli-Q water

-   Phosphate buffered saline (PBS)

20 µL AuNPs were diluted with 30 µL Milli-Q water and 200 µL PBS 10 mM

After preparation the samples were sonicated for 2 minutes and then were left other 2 mins to stabilize.

4.3.4.1 Dynamic light scattering

The hydrodynamic diameter of AuNPs 7 – 11 diluted in water was measured at 4-time points; the first day, after two weeks, after 3 weeks and after one month. The DLS data shows minor variations in the diameter over 30 days, therefore it was determined that the spherical glyco AuNPs were stable over time (figure 4.18).
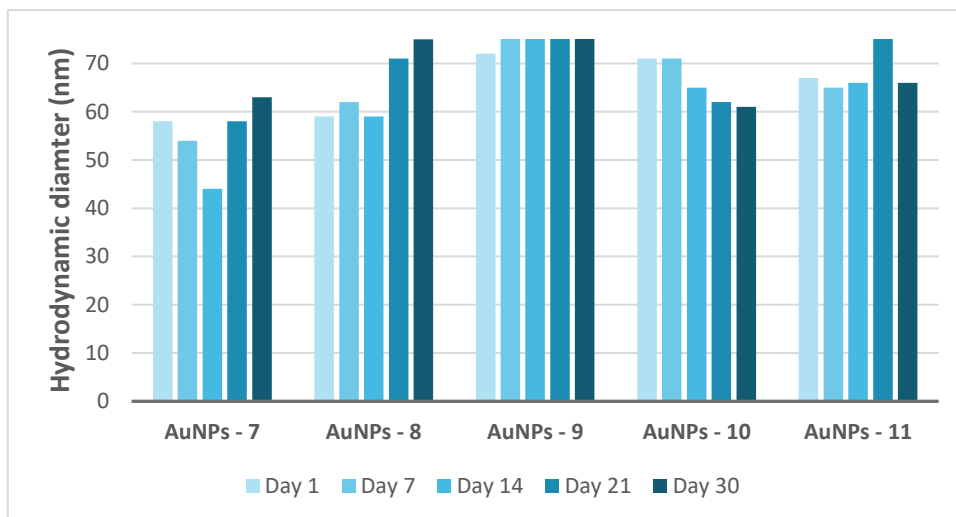
Figure 4.18. *Hydrodynamic diameter of* **AuNPs 7 – 11** *in water*

The stability of the AuNPs in PBS was analysed over 30 days at 3 time points as shown in figure 4.19. In all cases a decrease of the hydrodynamic diameter was observed over time, except for AuNPs – 9 where the opposite phenomenon was observed. AuNPs 7, 8, 10 and 11 seem to have aggregated overtime when exposed to PBS. In the case AuNPs – 9 the NPs seemed to have suffered a reversible aggregation meaning at the start a higher aggregation was observed and over time the NPs are more disperse.
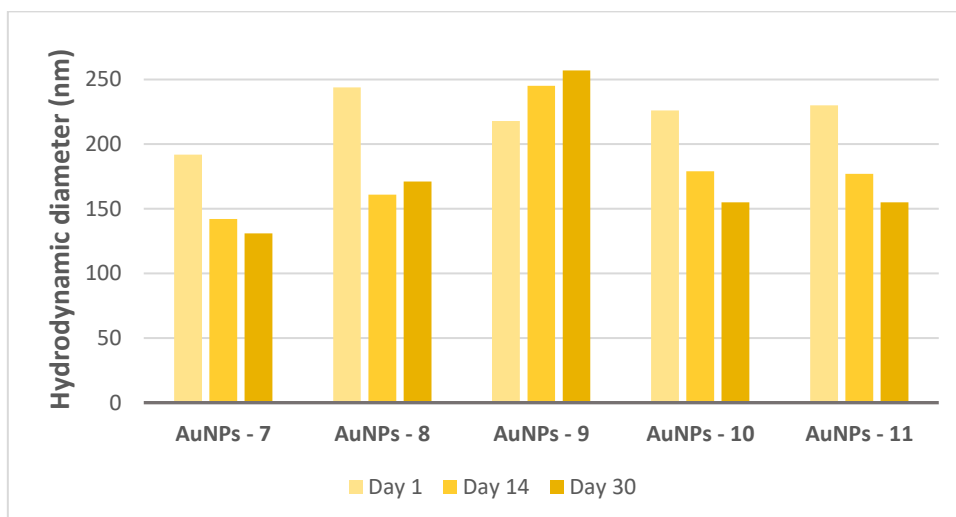
Figure 4.19. *Hydrodynamic diameter of* **AuNPs 7 – 11** *in PBS*

The long-term colloidal stability studies of spherical AuNPs in FBS and RPMI enriched with 10% FBS have not been performed yet.

4.3.4.2 ζ potential

The surface charge of spherical AuNPs 7 -11 was measured by ζ potential over 30 days in PBS and water as shown in figure 4.20 and 4.21. Very small variations are observed over 30 days in

the AuNPs diluted in water. Except for AuNPs – 11 where the surface charge increases after 7 days but then it is maintained mostly stable until the last measurement.
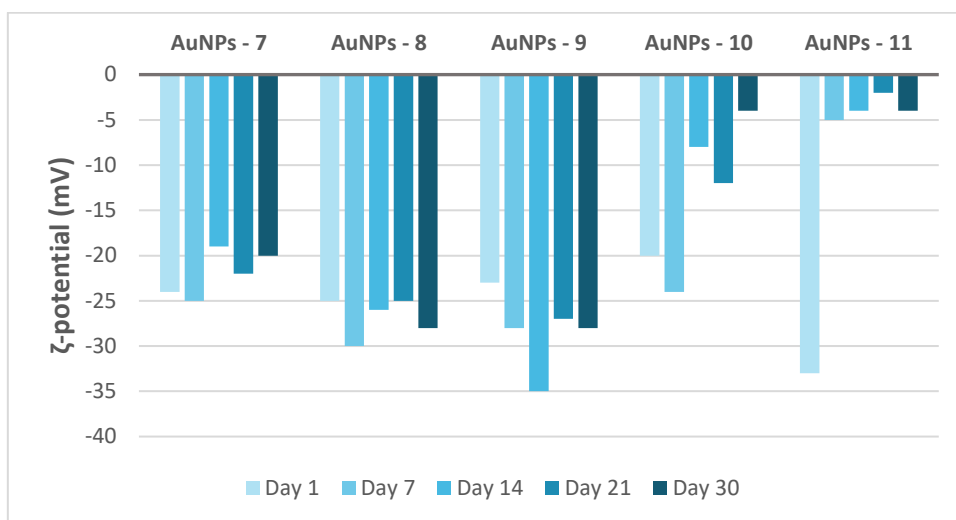
Figure 4.20. ζ-potential of **AuNPs 7 – 11** in water

The AuNPs in PBS do not suffer major changes in their surface charge over 30 days. Comparing to the results in water the charge of the NPs is less negative in PBS. As observed by DLS the hydrodynamic diameter of these AuNPs in PBS had increased this could be due to aggregation, this aggregation could also be affecting the ζ potential of the AuNPs.

On the other hand, AuNPs – 7 showed less aggregation by DLS as well as a more negative charge, it seems like the spherical NPs functionalized with mannose-EG_6C_{11} are the more stable AuNPs in PBS. The future experiments in RPMI + 10% FBS and FBS will show if the same stability is observed when the NPs are exposed to biological mediums.
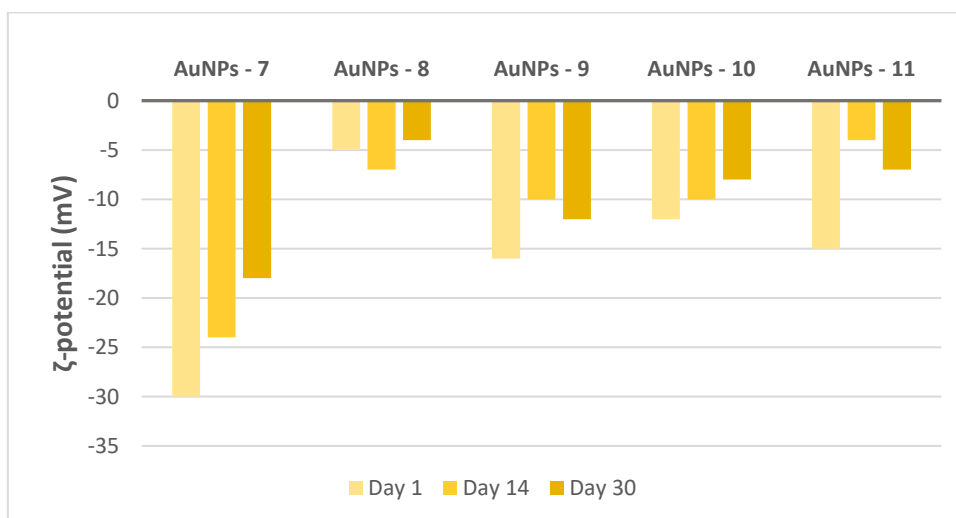
Figure 4.21. ζ-potential of **AuNPs 7 – 11** in PBS

4.4 Conclusions

In this chapter six glyco-star-AuNPs and five spherical glyco-AuNPs were synthesized using microfluidic system developed in our group.

The long-term colloidal stability of the glyco-star-AuNPs in water and PBS was analysed by DLS and ζ-potential. Overall, the AuNPs were stable over 6 months. The colloidal stability was also analysed after the addition of FBS and RPMI enriched with a 10% of FBS over 30 days, in all cases a protein corona was observed. The star shapes AuNPs with FBS after 20 days were sonicated for 10 minutes and a decrease in the size was observed this could be due to the removal of the soft corona layer. After 30 days the AuNPs in FBS and RPMI +10% FBS were centrifuged and washed with water to obtain a final solution of the AuNPs suspended in water, this experiment proved the NPs still presented a hard corona. The HC presented a stronger bond towards the NPs instead of the dynamic equilibrium present when the AuNPs were in biological medium.

The colloidal stability of the spherical glyco-AuNPs in water and PBS was analysed over 30 days and overall, they were stable. The data of spherical AuNPs over 180 days hasn't been obtained yet as the experiments are undergoing at the moment. Therefore, this data cannot be compared to the star shaped NPs. The long—term colloidal stability of the spherical glyco-AuNPs in FBS and RPMI + 10% FBS will also be performed in the near future.

4.5 Experimental

4.5.1 Material and methods

$HAuCl_4 \cdot 3H_2O$, $AgNO_3$ and ascorbic acid were purchased from Sigma-Aldrich and used without further purification. $HAuCl_4 \cdot 3H_2O$ was stored at 4°C, shielded from light. $AgNO_3$ 10 mM and ascorbic acid 100 mM solutions were freshly prepared before each synthesis (avoiding the exposition to the light). The fluidic reactor, between the different synthesis, was washed in the order with aqua regia (HCl (37%):HNO3 (65%) 3:1) and copious deionized water. Ultrapure deionized water, MilliQ water, was used for the preparation of aqueous solutions. Purification of water dispersible colloidal Au NPs was performed by ultrafiltration using Millipore Amicon Ultra-4 Centrifugal Filter Units with a cut-off of 30 kDa.

UV–vis spectroscopy measurements were performed with an Agilent 8453 instrument. A disposable cuvette with 1 cm optical path length was used for the outline measurements. Transmission electron microscopy (TEM) measurements were performed by a ZEISS LIBRA200FE microscope equipped with in-column Ω-filter spectrometer/filter, operating at 200 kV. TEM specimens were prepared dropping the nanoparticle aqueous dispersion onto a supported lacey-carbon copper TEM grids and analysed after drying overnight. Dynamic Light Scattering (DLS) measurements were performed employing a 90 Plus Particle Size Analyzer (Brookhaven

Instrument Corporation; Holtsville, NY). The experiment was performed by registering each NP at room temperature, each one composed of 10 runs of 10 seconds.

4.5.2   Synthesis of gold nanoparticles

All the presented Au NPs were synthesized using the apparatus described in the section 3.1 Prior to proceed with the synthesis, the fluidic reactor was washed with deionized water and dried with air. Syringe B was loaded of a solution of $HAuCl_4$ and $AgNO_3$ of 20 mL, prepared just before the beginning of the reaction. In the syringe B were loaded 20 mL of a solution of ascorbic acid. The reaction conditions and amounts of reagents were modulated in order to obtain the desired products as shown in table 4.

AuNPs morphology	[HAuCl$_4$] (mM)	[AgNO$_3$] (mM)	[AA] (mM)	Final volume * (mL)	Flow (mL/min)
Star	0.2	0.02	0.2	20	5
Spherical	0.2	0	0.4	20	5

***Table 4.4.** Reaction conditions and amounts of reagents employed for the synthesis of star and spherical Glyco-AuNPs. * The volume is referred to the solution charged in the syringe*

The glycan derivatives were added to the AuNPs solutions as indicated in section 3.1 and 3.3. The star AuNPs were purified by centrifugation, the AuNPs were then washed 3 times with water. The spherical AuNPs were purified by ultra-filtration, using Millipore Amicon Ultra-4 Centrifugal Filter Units with a cut-off of 30 kDa. The aqueous supernatant was removed, and NPs were recovered, dispersed, and stored in 5 mL water. At the end of the reaction the PTFE tubes and the flasks were washed, in the order, with aqua regia and copious distilled water. The PEEK mixer was sonicated in distilled water.

4.5.3   Synthesis of glycan derivatives

Glycan derivatives bearing the amphiphilic linker EG_6C_{11} and the aliphatic linkers C_2/C_3 were a generous gift from Midatech Pharma PLC (Bilbao, Spain). Their synthesis is detailed described in the literature[12,13]. The characterization of the glycan derivatives is described in Chapter 3 section 3.5.7. The NMR spectra are reported in the Annex.

4.6   References

(1)   Silvestri, A.; Lay, L.; Psaro, R.; Polito, L.; Evangelisti, C. Fluidic Manufacture of Star-Shaped Gold Nanoparticles. *Chem. Eur. J.* **2017**, *23* (41), 9732–9735. https://doi.org/10.1002/chem.201701617.

(2)   Minati, L.; Benetti, F.; Chiappini, A.; Speranza, G. One-Step Synthesis of Star-Shaped Gold Nanoparticles. *Colloids and Surfaces A: Physicochemical and Engineering Aspects* **2014**, *441*, 623–628. https://doi.org/10.1016/j.colsurfa.2013.10.025.

(3)   Ziegler, J.; Wörister, C.; Vidal, C.; Hrelescu, C.; Klar, T. A. Plasmonic Nanostars as Efficient Broadband Scatterers for Random Lasing. *ACS Photonics* **2016**, *3* (6), 919–923. https://doi.org/10.1021/acsphotonics.6b00111.

(4)   Martinsson, E.; Shahjamali, M. M.; Large, N.; Zaraee, N.; Zhou, Y.; Schatz, G. C.; Mirkin, C. A.; Aili, D. Influence of Surfactant Bilayers on the Refractive Index Sensitivity and Catalytic Properties of Anisotropic Gold Nanoparticles. *Small* **2016**, *12* (3), 330–342. https://doi.org/10.1002/smll.201502449.

(5)   Sasidharan, S.; Bahadur, D.; Srivastava, R. Protein-Poly(Amino Acid) Nanocore–Shell Mediated Synthesis of Branched Gold Nanostructures for Computed Tomographic Imaging and Photothermal Therapy of Cancer. *ACS Appl. Mater. Interfaces* **2016**, *8* (25), 15889–15903. https://doi.org/10.1021/acsami.6b03428.

(6)   Marelli, M.; Bossola, F.; Spinetti, G.; Sangalli, E.; Santo, V. D.; Psaro, R.; Polito, L. Microfluidic Synthesis of Hybrid TiO $_2$ -Anisotropic Gold Nanoparticles with Visible and Near-Infrared Activity. *ACS Appl. Mater. Interfaces* **2020**, *12* (34), 38522–38529. https://doi.org/10.1021/acsami.0c08241.

(7)   García-Álvarez, R.; Hadjidemetriou, M.; Sánchez-Iglesias, A.; Liz-Marzán, L. M.; Kostarelos, K. *In Vivo* Formation of Protein Corona on Gold Nanoparticles. The Effect of Their Size and Shape. *Nanoscale* **2018**, *10* (3), 1256–1264. https://doi.org/10.1039/C7NR08322J.

(8)   Owensiii, D.; Peppas, N. Opsonization, Biodistribution, and Pharmacokinetics of Polymeric Nanoparticles. *International Journal of Pharmaceutics* **2006**, *307* (1), 93–102. https://doi.org/10.1016/j.ijpharm.2005.10.010.

(9)   Salvati, A.; Pitek, A. S.; Monopoli, M. P.; Prapainop, K.; Bombelli, F. B.; Hristov, D. R.; Kelly, P. M.; Åberg, C.; Mahon, E.; Dawson, K. A. Transferrin-Functionalized Nanoparticles Lose Their Targeting Capabilities When a Biomolecule Corona Adsorbs on the Surface. *Nature Nanotech* **2013**, *8* (2), 137–143. https://doi.org/10.1038/nnano.2012.237.

(10)   Nguyen, V. H.; Lee, B.-J. Protein Corona: A New Approach for Nanomedicine Design. *IJN* **2017**, *Volume 12*, 3137–3151. https://doi.org/10.2147/IJN.S129300.

(11)   Du, S.; Kendall, K.; Toloueinia, P.; Mehrabadi, Y.; Gupta, G.; Newton, J. Aggregation and Adhesion of Gold Nanoparticles in Phosphate Buffered Saline. *J Nanopart Res* **2012**, *14* (3), 758. https://doi.org/10.1007/s11051-012-0758-z.

(12)   Barrientos, Á. G.; de la Fuente, J. M.; Rojas, T. C.; Fernández, A.; Penadés, S. Gold GlycoNanoparticles: Synthetic Polyvalent Ligands Mimicking Glycocalyx-Like Surfaces as Tools for Glycobiological Studies. *Chem. Eur. J.* **2003**, *9* (9), 1909–1921. https://doi.org/10.1002/chem.200204544.

(13)   Martínez-Ávila, O.; Hijazi, K.; Marradi, M.; Clavel, C.; Campion, C.; Kelly, C.; Penadés, S. Gold *Manno* -GlycoNanoparticles: Multivalent Systems to Block HIV-1 Gp120 Binding to the Lectin DC-SIGN. *Chem. Eur. J.* **2009**, *15* (38), 9874–9888. https://doi.org/10.1002/chem.200900923.

Chapter 5

PEGylated Glyco-Polyamine phosphate NPs

5.1 Introduction

5.1.1 Polyamine phosphate nanoparticles

Polyamine phosphate NPs (PANs) are colloidal complexes formed by poly (allylamine hydrochloride) and phosphate ions by self-assembly. PANs are stable at physiological pH but they are unstable at endosomal pH, therefore they are interesting candidates for drug delivery.[1–4]

As mentioned in Chapter 1 Section 1.5, PEGylation of PANs was recently reported by Andreozzi et al. The PEGylation was demonstrated able to change the size and surface charge of the NPs. Under the protocol developed, small NPs of around 10 nm were obtained, characterized by a core of PANs and a shell formed by the PEG chains. The so obtained NPs resulted neutral and the absence of charge was justified by the core shell morphology, as the unreacted amines remain in the inside.[5]

PANs were synthesized with different amounts of polyethylene glycol (PEG) and it was demonstrated that the higher the number of PEG chains the smaller the size of the NPs obtained. Moreover, during this study it was demonstrated by means of Fluorescence correlation spectroscopy (FCS) that the PEGylation was able to prevent the binding of PANs to unspecific proteins.

During this chapter the synthesis of Glyco-PEG PANs will be described in order to achieve specific targeting of glycans towards proteins (i.e. lectins).[6]

5.1.2 Fluorescence correlation spectroscopy

Fluorescent correlation spectroscopy (FCS) is a spectroscopic technique used to study the molecular dynamics. This technique has numerous applications in the biomedical field, as for example studying in detail the encapsulation of a drug in self-assembly NPs. This technique can also be used to study the binding affinities between biomolecules.[1,7]

The technique consists in the measurement of the diffusion coefficient of fluorescently labelled molecules overtime in a small volume. The diffusion coefficient can then be translated to the hydrodynamic radius.
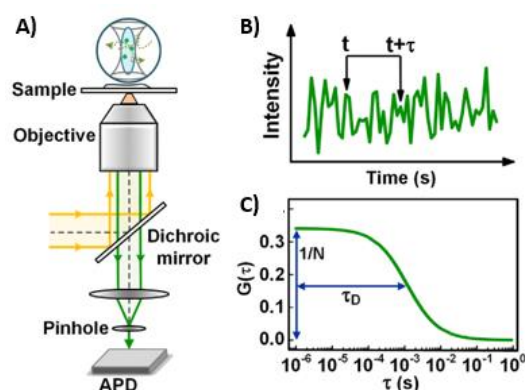
Figure 5.1. *Instrumentation and data analysis of FCS. A) Schematic view of confocal based FCS setup B) The intensity trace collected from the observation volume C) The autocorrelation curve calculated with the intensity trace.*[7]

FCS is commonly used in a confocal microscope as shown in figure 5.1A. In figure 5.1B the results obtained during the measurement are shown: the results are the time-dependant intensity fluctuations of the labelled molecules. The intensity fluctuations are then fitted into an autocorrelation function shown in figure 5.1C.[6]

Moreover, a variation of FCS denominated Fluorescence Cross-Correlation Spectroscopy (FCCS) allows the study of the interaction between two biomolecules. In order to perform the study both molecules must be labelled with spectrally differing fluorophores as the particles are observed with two laser channels. This analysis has been performed in a competitive assay of Glyco AuNPs by Sergio Moya's group. The NPs were previously incubated with Bovine Serum Albumin (BSA) to form a protein corona complex to which the binding lectin was added to prove the higher affinity of the lectin towards the particles.[8] A similar analysis will be discussed in this chapter using Glyco-PEG-PANs.

5.2   Aim of the work

The aim of this chapter was to synthesize PEGylated PANs with three different terminal glycans and study the formation of the NPs. The further step consisted in studying the interaction with glycan binding lectins by Fluorescence Correlation Spectroscopy (FCS) and Fluorescence Cross-Correlation Spectroscopy (FCCS).

The first part of the chapter describes the design and synthesis of Glyco-PEG-PANs. The synthesis was performed through carbodiimide chemistry, the poly(allylamine hydrochloride) (PAH) was reacted with two heterobifunctional PEG molecules with different PEG lengths. The heterobifunctional PEG was formed by N-hydroxysuccinimide (NHS) which is reactive to amines and a maleimide that reacts with thiols. The initial reaction scheme is shown in scheme 5.1.
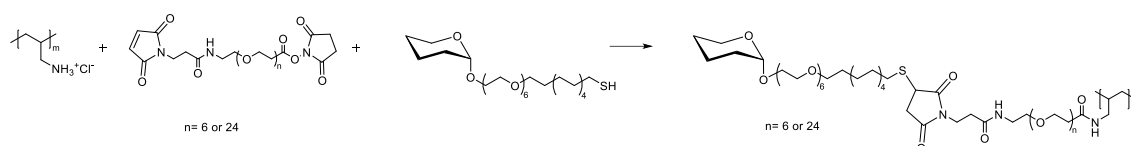
Scheme 5.1. Synthesis of Glyco-PEG-PANs

The PANs were spontaneously formed using a phosphate buffer solution (PBS) as shown in figure 5.2. The formation and stability of the PANs was studied at different PBS concentrations by Dynamic Light Scattering (DLS).
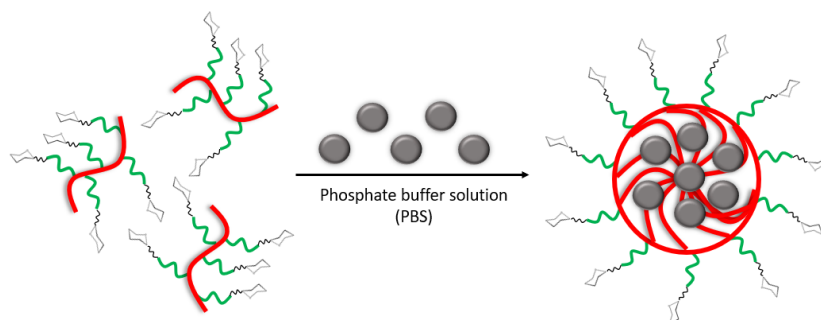
Figure 5.2. PANs formation

The second part of the chapter describes the formation of the PANs and the interaction of PANs functionalized with α-mannose and lactose with Concanavalin-A (Con-A) and Jacalin. In order to perform FCS and FCCS studies the polymers were labelled with ATTO 633.

All the work described in this chapter was performed during the secondment at CIC-BiomaGUNE. The FCS and FCCS studies were performed by Sergio Moya's group at CIC BiomaGUNE.

5.3   Results and discussion

5.3.1   Synthesis of glyco-PEG-poly allylamine polymers

PEGylation of poly (allylamine hydrochloride) (PAH) was performed through carbodiimide chemistry, exploiting the reactivity of N-hydroxysuccinimide (NHS) towards the amine groups of PAH. In addition to the PEGylation step, the goal was to attach three different glycan derivatives bearing an amphiphilic thiol linker (1-Man, 2-Glc and 3-Lac shown in table 3.3) to the PEG-PAH. Therefore, a heterobifunctional PEG molecule (Mal-PEG-NHS) was selected as suitable PEGylation linker, containing an NHS moiety able to react with amino groups and a maleimide group reactive towards the thiol groups. Two heterobifunctional PEG molecules with 6 and 24 PEG units were used during this chapter to test the effect of the chain length on the affinity of the glycans towards the lectins.

The first reaction was performed between PAH (**1**) and the NHS moiety of the heterobifunctional PEG (**2**), as shown in scheme 5.2. The reaction conditions were designed considering the reactivity and stability of both functional groups present in the PEG linker. The first reaction was conducted at a pH 7 – 7.5 to maintain the maleimide reactivity.[9]
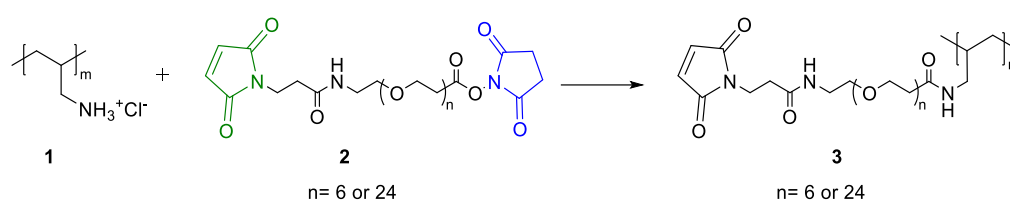
Scheme 5.2. *Reaction between PAH and NHS. In green maleimide, in blue NHS*

The second reaction was performed immediately after without further purification. Glyco-thio derivatives (**4**) reacted in the presence of maleimide fragments (**3**) at pH 6 – 6.5, which are the best conditions for the maleimide reaction (scheme 5.3). A set of 6 polymers (table 5.1) were obtained after purification by ultracentrifugation.
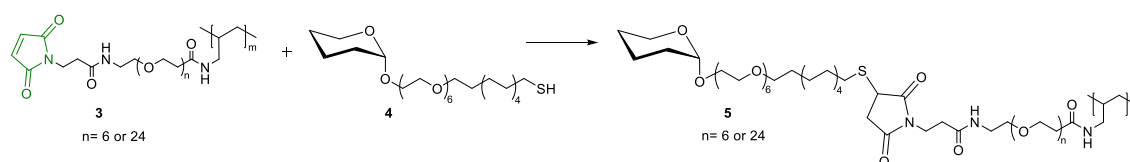
Scheme 5.3. *Reaction between Mal-PEG-PAH and the glycan derivates*

1a	α-Mannose (1-Man)	PEG$_6$
1b	α-Mannose (1-Man)	PEG$_{24}$
2a	β-Glucose (2-Glc)	PEG$_6$
2b	β-Glucose (2-Glc)	PEG$_{24}$
3a	Lactose (3-Lac)	PEG$_6$
3b	Lactose (3-Lac)	PEG$_{24}$

Table 5.1. *Glyco-PEG-PANs*

5.3.2 Characterization of glyco-PEG-poly allylamine polymers by ^{1}H-NMR

All polymers were analysed by ^{1}H-NMR to confirm the bond of the Glyco-PEG-PAHs. The PEGylation degree was calculated comparing the ^{1}H-NMR spectra of PAH and the final polymer. The integral of the anomeric position of the glycan was compared to the integral corresponding to the PAH. This comparison was done considering the presence of one glycan per PEG chain.

The ^{1}H-NMR of PAH shown in figure 5.4, has three broad signals **a** (1.40 ppm), **b** (1.93 ppm) and **c** (2.94 ppm), the ratio of the integrals of these peaks is 2-1-2. Peak **c** corresponds to the two methylene groups in α to the amino group shown in figure 5.3.
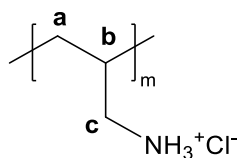
Figure 5.3. Structure PAH
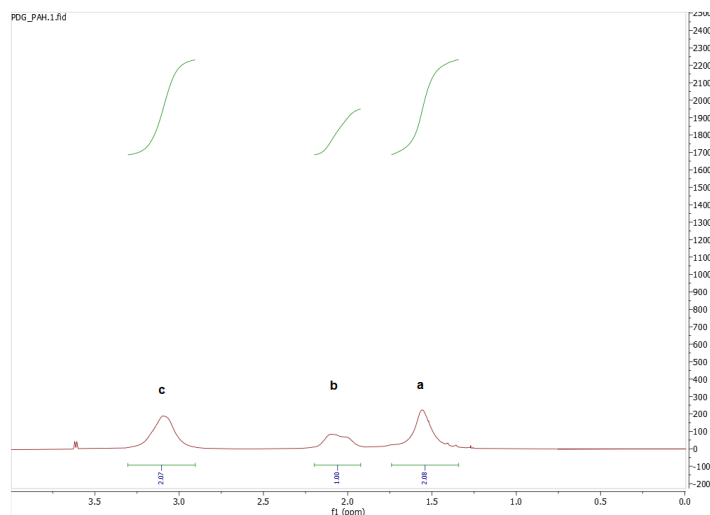
Figure 5.4. ^{1}H-NMR of PAH
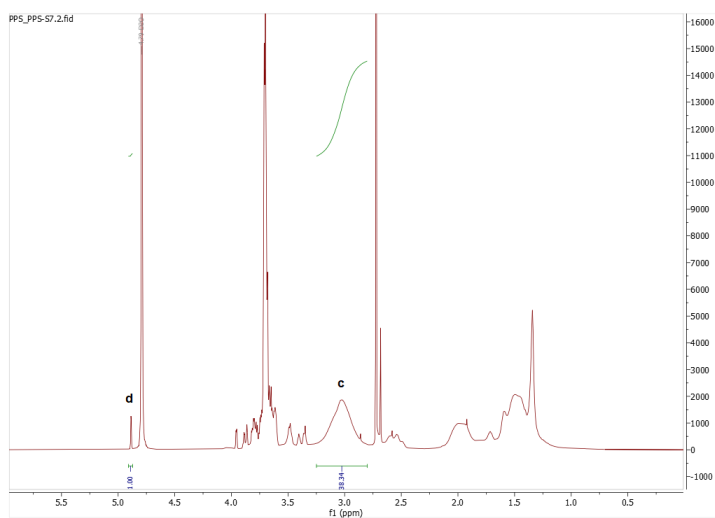
Figure 5.5. ^{1}H-NMR of **1a**

In order to calculate the number of PEG chains per PAH chain the integral of **c** was compared to **d**, the integral of the anomeric position of the glycan. ^{1}H-NMR of **1a** is shown in figure 5.5. PAH has an average of 175 monomeric units, **c** integral corresponds to two therefore **c** represents (175 x 2 = 350 protons) 350 protons. Peak **d** corresponds to one proton. In order to obtain the number of PEG chains per PAH 350 is divided by **c**. The number of PEG chains was calculated for all the samples as shown in table 5.2. The number of PEG chains per PAH was around 15.

	Sample		Integral c	PEG chains**	Final PEG chains***
1a	Mannose	PEG$_6$	38,34	9,12	**15**
1b	Mannose	PEG$_{24}$	46,48	7,53	**12**
2a	Glucose	PEG$_6$	51,09	6,85	**14**
2b	Glucose	PEG$_{24}$	47,48	7,37	**15**
3a	Lactose	PEG$_6$	25,56	13,69	**15**
3b	Lactose	PEG$_{24}$	28,31	12,36	**14**

Table 5.2. *Number of PEG chains per PAH chain. **** Calculation 350/c; *** PEG chains considering the purity of glyco-derivatives 1-Man (61% mannose 39% OH) 3-Lac (91% lactose 9% OH)*

The purity of 1-Man,2-Glc and 3-Lac glycan derivatives was obtained by ^{1}H-NMR (ERETIC 2), as mentioned in Chapter 3 Section 3.3.2.

The number of PEG chains obtained in this study is higher than the one obtained in the previous study[5] where 10 PEG chains were detected by NMR. This could be due to the fact that the PEG molecules used have a lower molecular weight. Moreover, the pH conditions were finely controlled to achieve a higher yield of the reaction and consequently a higher number of PEG chains per PAH.

5.3.3 Synthesis and characterization of polyamine phosphate nanoparticles

Once the library of Glyco-PEG-PAHs was obtained, the PANs were formed by self-assembly after the addition of PBS. The presence of phosphate ions leads to electrostatic interactions with the amine groups present in the PAH and consequently the NPs are formed.

The formation of the NPs was confirmed by Dynamic Light Scattering (DLS) and Transmission Electron Microscopy (TEM) as shown in figure 5.6 and 5.7.
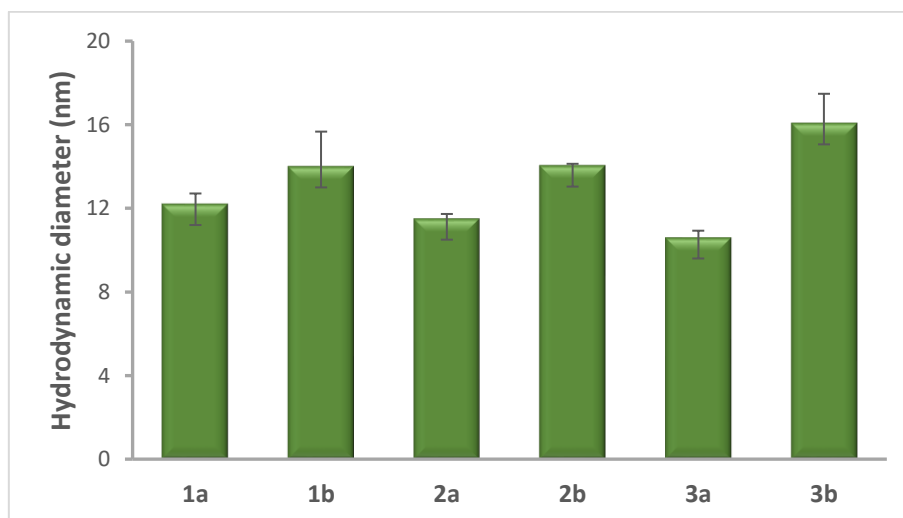
Figure 5.6. *Hydrodynamic diameter of PANs assembled with PBS 5 mM*
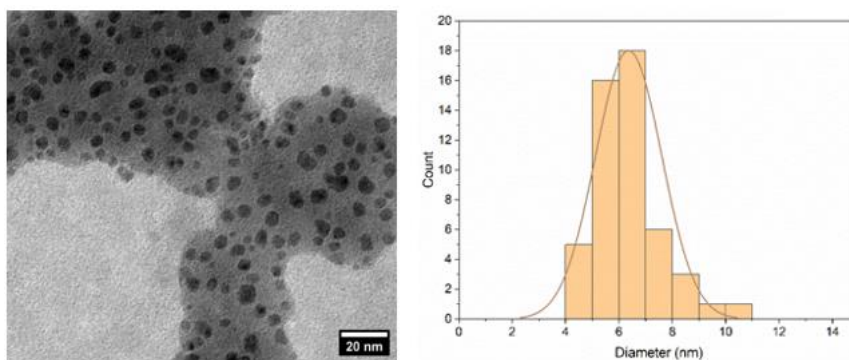
*Figure 5.7. TEM micrograph and size distribution obtained by TEM analysis of **1b***

The formation of the PANs with different concentrations of PBS (5 mM and 10 mM) was evaluated by DLS as show in figure 5.8.
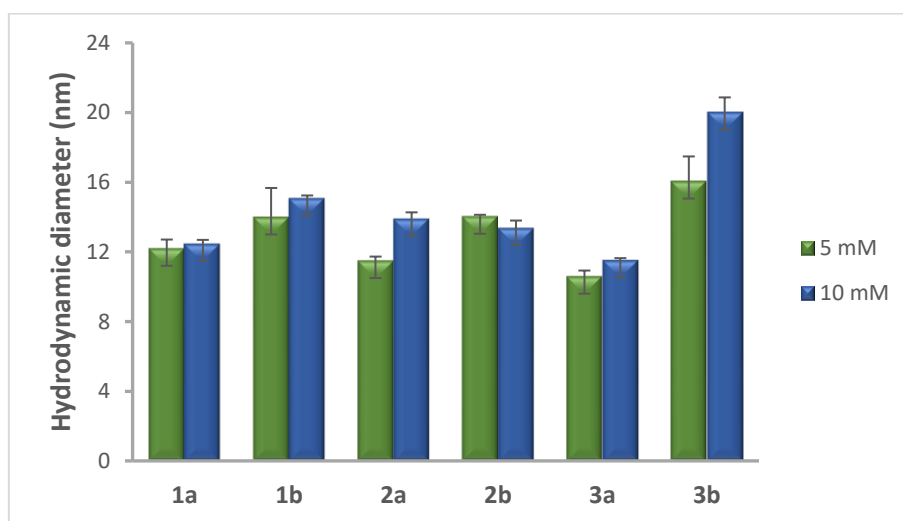
Figure 5.8. Hydrodynamic diameter of PANs assembled with PBS 5 mM and 10 mM

The NPs formed with PBS 10 mM have a slightly bigger diameter. In order to study deeply the effect of using PBS of different concentrations the diameter was measured after 2 weeks, shown in figure 5.9 and 5.10. The PANs formed with PBS 5 mM have small variations in their diameter after two weeks, on the other hand the PANs formed using PBS 10 mM show in most cases a bigger change in their diameter and some of them had completely disassembled. Therefore PBS 5 mM was the crosslinking ion solution selected and used to form the PANs in the subsequent experiments
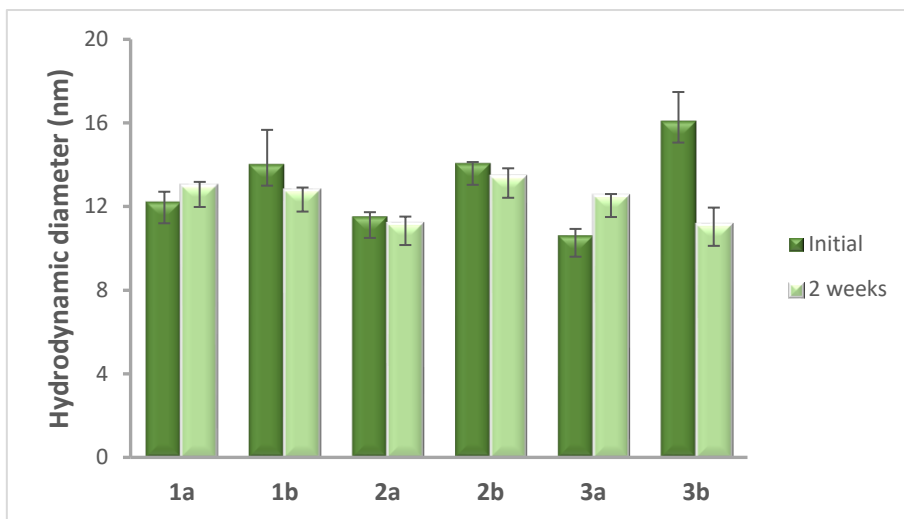
Figure 5.9. Hydrodynamic diameter of PANs assembled with PBS 5 mM
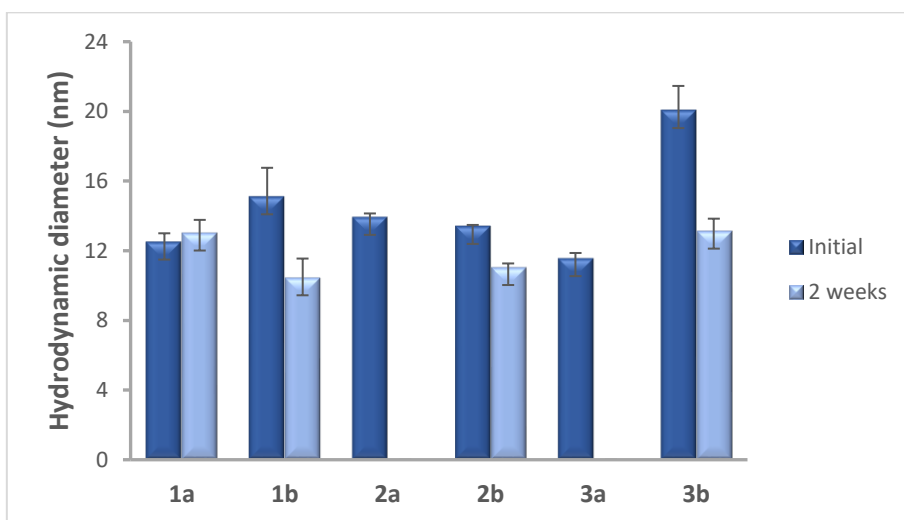
Figure 5.10. Hydrodynamic diameter of PANs assembled with PBS 10 mM

Furthermore, the scattering of the Glyco-PEGylated PANs was studied at different pHs as shown in figure 5.11. PANs and PEGylated PANs are responsive to pH and at lower pH they disassemble, this is prevented with the glycosylated NPs. Even though the NPs are not completely disassembled when the pH is decreased, and effect can be observed as a lower number of Glyco-PEGylated-PANs are scattered.
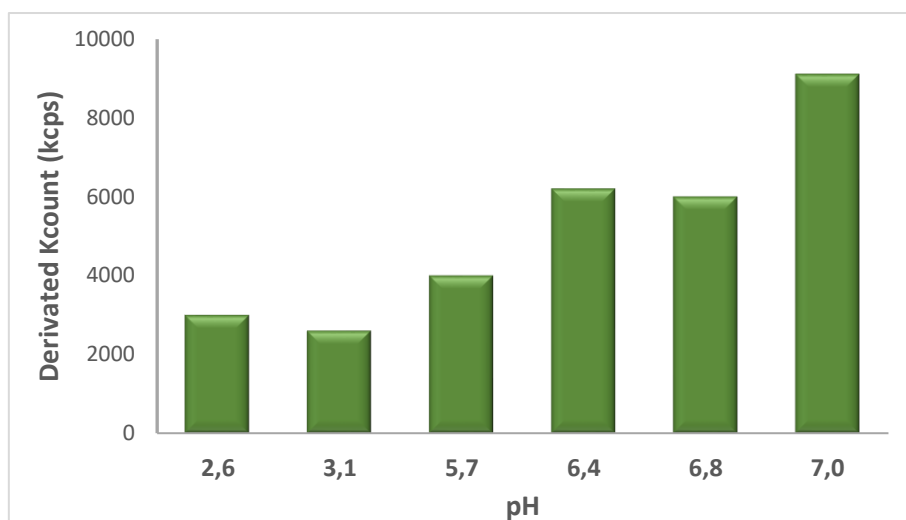
Figure 5.11. *Derivated kilocounts per second of Glyco-PEG-PANs in PBS 5 mM **(2a)***

In order to fully characterize Glycosylated PEG PANs, we measured ζ-potential: all the NPs showed a ζ-potential of around +5 mV as observed in figure 5.12. A similar effect had been observed in the previous study due to the formation of the PEG core shell.[5]
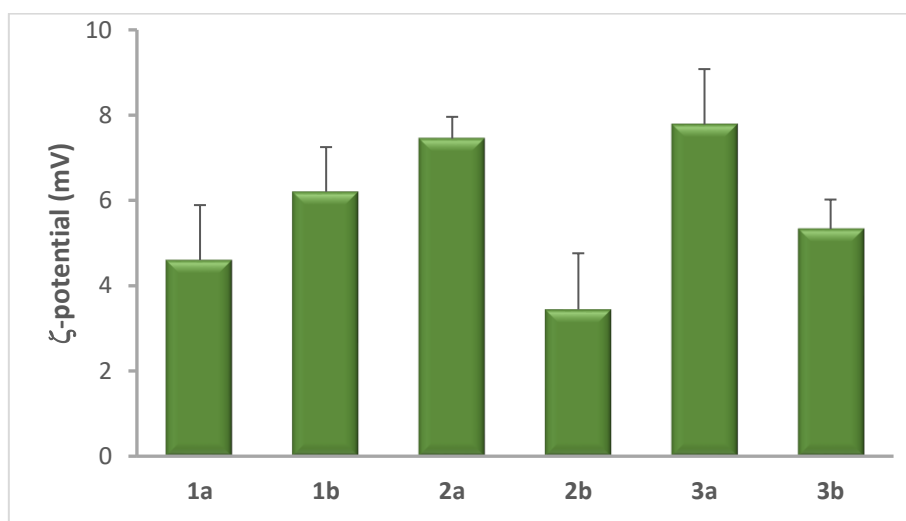
Figure 5.12. *ζ.-potential of Glyco-PEG-PANs in PBS 5 mM*

5.3.4 Study of formation of glyco-PEG-polyamine nanoparticles by FCS

The Fluorescent Correlation Spectroscopy (FCS) studies were performed at CIC BiomaGUNE by Sergio Moya's research group.

FCS is a technique that can be used to characterize fluorescently labelled species dynamic events as for example the intermolecular interactions. Therefore, in order to study the formation of the Glyco-PEG-PANs, the PAH had to be fluorescently labelled and in this case ATTO 633 was selected as the fluorescent label.

5.3.4.1 Labelling of poly allylamine hydrochloride

The labelling of PAH was analysed by FCS. First the diffusion time of the free ATTO633 was obtained and then the PAH-ATTO633, the diffusion time decreased from 340 μm^2/s to 36.13 μm^2/s after labelling the PAH this proves a successful binding between the fluorescent label and the PAH.

After labelling PAH it was further modified with two heterobifunctional PEG molecules and two selected glycan derivates as shown in scheme 5.4. The same procedure described previously was performed to obtain the final Glyco-PEG-PAHs.
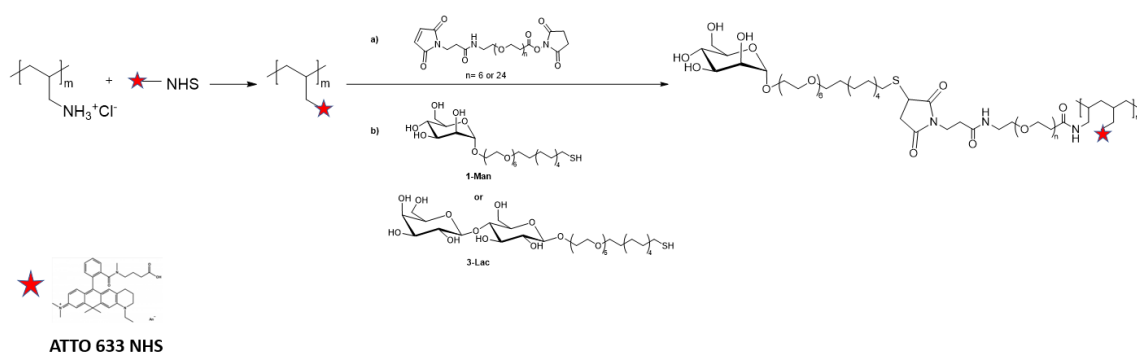
Scheme 5.4. *Synthesis of ATTO633 labelled Glyco-PEG-PANs*

The number of PEG chains per PAH-ATTO633 was obtained as shown in table 5.3, following the previously described procedure. In this case around 20 PEG chains are present per PAH.

Sample			Integral c	PEG chains**	Final PEG chains***
1a*	1-Man	PEG$_6$	27,22	12,85	**21**
1b*	1-Man	PEG$_{24}$	24,52	14,27	**23**
3a*	3-Lac	PEG$_6$	19,20	18,23	**20**
3b*	3-Lac	PEG$_{24}$	19,28	18,15	**20**

Table 5.3. *Number of PEG chains per PAH chain. * PAH labelled with ATTO633 ** Calculation 350/c ; *** PEG chains considering the purity of glyco-derivatives 1-Man (61% mannose 39% OH) 3-Lac (91% lactose 9% OH)*

5.3.4.2 Assessment of poly allylamine hydrochloride labelling by UV-vis

The amount of ATTO633 label on PAH was calculated with a linear regression (y = a + b*c) of UV-vis measurements performed of standard solutions of free ATTO633. Through the comparison of this measurements with the absorption of labelled PAH with a certain mass concentration, the exact amount of ATTP633 on PAH was obtained as shown in figure 5.13.

Sample	A_{max} [a.u.]	Estimated mass of fluorophore [μg]	Weight percentage [wt %]
1a*	0.35691	2.96233	2.63319
1b*	0.27839	2.31967	2.06193
3a*	0.25723	2.14667	1.90815
3b*	0.25388	2.119	1.88356
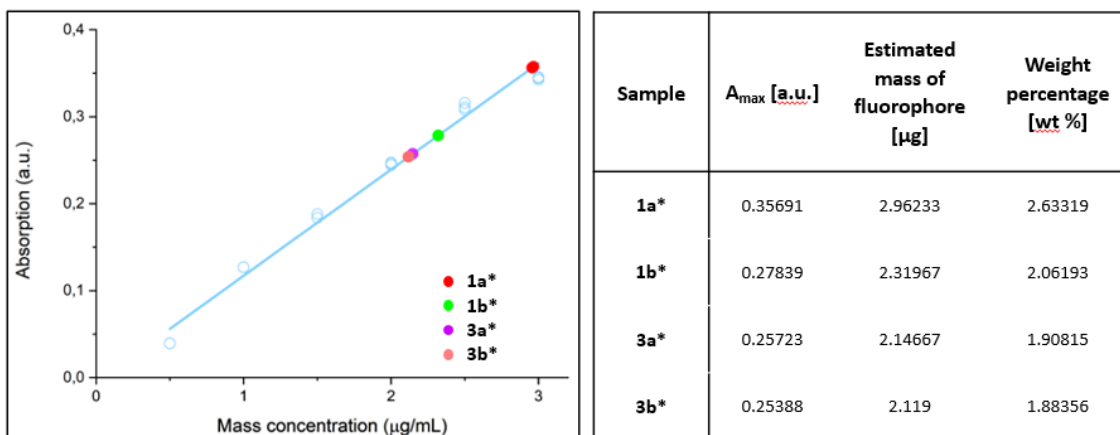
Figure 5.13. *Linear regression obtained by Uv-vis and weight percentage of ATTO633 in **1a*,1b*,3a*** and **3b***

5.3.4.3 Fluorescent correlation spectroscopy experiments

Through the analysis by FCS the self-assembly of PANs can be studied as big and small molecules present different diffusion times. The autocorrelation functions, obtained by FCS, of the initial polymers and the formed Glyco-PEG-PANs were compared to study the formation of the NPs. The formation of the PANs clearly changes the autocorrelation function of the polymers. The amplitude of the PANs is higher than the polymers as shown in figure 5.14.

The amplitude of the autocorrelation function offers information of the concentration of the molecules diffusing as they are inversely proportional. If the value G(t) increases it means the polymers are forming the NPs, the biggest change observed for all the samples was two times bigger than the value of the polymer this means the NPs are formed by two polymer chains.

In the case of **1a*** the polymer chain has a G of 0.032 which increases to 0.054 for the PANs, likewise for **1b*** the polymer chains G is 0.089 and arrives to 0.198 for the NPs. Both cases show an increase of the amplitude by two, this means the number of diffusing molecules is decreased to half therefore the PANs are formed by a maximum of two polymer chains.
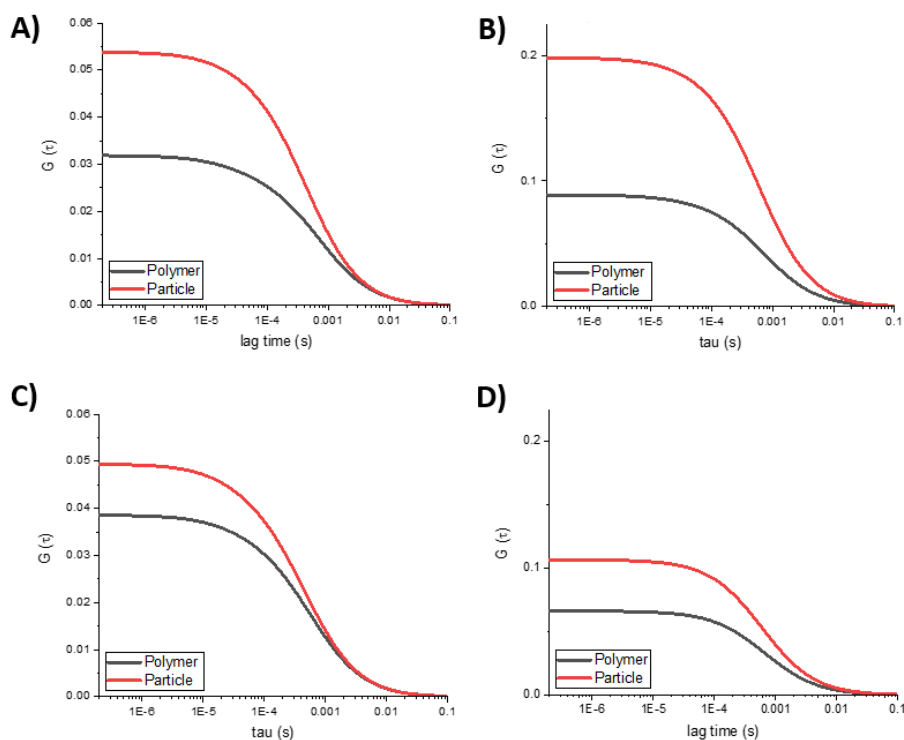
Figure 5.14. Autocorrelation functions of the Glyco-PEGylated PAH before and after exposure to phosphate buffer, leading to particle formation. A) **1a*** B) **1b*** C) **2a***D) **2b***

In the four cases it's observed an increase in the amplitude of the PANs compared to the polymers. For **3a*** and **3b*** the increase is less than double thus the particles are formed by one single polymer chain.

The values shown in table 5.4 show the effect of the formation of the PANs by addition of phosphate ions to the solution. For mannose-PEG$_6$ (**1a***) the diffusion coefficient for the polymer is 16.75 μm^2/s and for the particles 27.51 μm^2/s this means the particles are more rapid diffusing species. The same effect is observed for mannose-PEG$_{24}$ (**1b***) lactose-PEG$_6$ (**3a***) and lactose-PEG$_{24}$ (**3b***), even though in the cases with a longer PEG length this effect is lower.

The diffusion of the polymer compared to the particle can be understood by observing the hydrodynamic radius(r_H) obtained with the Stokes-Einstein equation. In all cases a reduction of the radius is detected when the particles are formed. **1a*** shows the higher decrease of r_H which for the polymer is 12.82 nm and for the particles 7.80 nm, whereas for the polymers containing lactose the decrease is lower. **3a*** has a r_H of 9.43 nm for the polymer and 7.75 nm for the particle this can be explained by the autocorrelation functions as the amplitude increase in this case is only one-fold meaning the particles are formed solely by one polymer chain. The particles formed with a shorter PEG have a bigger hydrodynamic radius of around 10 nm and the polymers with a longer PEG have a radius of around 7.8 nm.

Sample		Diffusion time τ [μs]	Diffusion coefficient D [μm²/s]	r_H [nm]	Amplitude G (2.00e-07)	Fit: 1/N CC	X^2
1a*	Polymer	760.52 ± 7.22	16.75 ± 7.22	12.82	0.031833	0.0318657	1.95e-05
	Particle	462.95 ± 3.67	27.51 ± 0.22	7.80	0.053777	0.0538265	1.41e-05
1b*	Polymer	740.724 ± 7.34	17.74 ± 0.57	12.10	0.08902	0.089071	2.44e-05
	Particle	617.09 ± 7.81	21.30 ± 0.70	10.08	0.198177	0.198287	2.64e-04
3a*	Polymer	597.50 ± 4.58	22.77 ± 0.18	9.43	0.038531	0.0385669	9.66e-06
	Particle	490.99 ± 3.81	27.72 ± 0.22	7.75	0.049348	0.0494	2.01e-05
3b*	Polymer	638.55 ± 5.61	21.31 ± 5.61	10.08	0.08168	0.08293	4.44e-05
	Particle	644.51 ± 9.66	21.39 ± 0.32	9.84	0.108172	0.108237	5.24e-05

*Table 5.4. Representative values of **1a***,**1b***,**3a*** and **3b*** before and after forming the PANs*

5.3.5   Interaction of glyco-PEG-polyamine phosphate nanoparticles

Fluorescent cross-correlation spectroscopy measurements were performed to study the affinity of Glyco-PEG-PANs towards specific lectins. In order to perform these experiments two spectrally different fluorophores must be employed, as the intensity fluctuations are registered with two different detectors, consequently the signals are cross correlated.[10]

In the case that the PANs bind with the proteins both fluorophores will be attached to the PAN and the sample will diffuse at the same speed through the observation volume, this will lead to a rise of the cross correlation between the diffusing species. The concentration of the formed complex between the PANs and the proteins is proportional to the amplitude of the cross-correlation.

The design of the experiment consists in the study of the affinity of the samples with bovine serum albumin (BSA) followed by the replacement of BSA by a lectin with higher affinity towards the glycan. As mentioned before two spectrally different fluorophores are used, the PANs are labelled with ATTO633 which has an emission maximum at 657 nm and the BSA with Alexa fluor 488 with an emission maximum at 510 nm.

The first step consists in the incubation of the Glyco-PEG-PANs with BSA for 1 hour at 37°C to display a corona on the NPs surface. After that the unlabelled lectin was added and the cross-correlation measurements were performed at 30, 70 and 120 minutes. The affinity of PANs **1a*** and **1b*** with a mannose moiety was studied with Concanavalin-A (Con-A), a mannose binding lectin, in the case of PANs **3a*** and 3**b*** Jacalin was used.
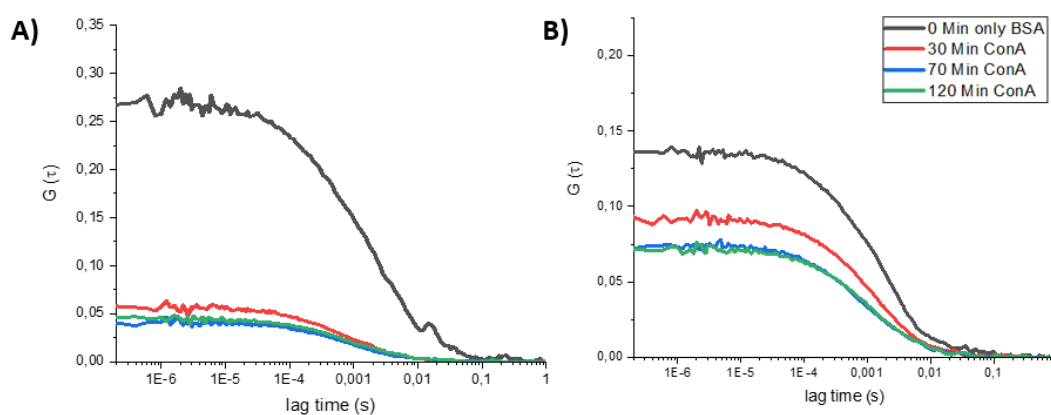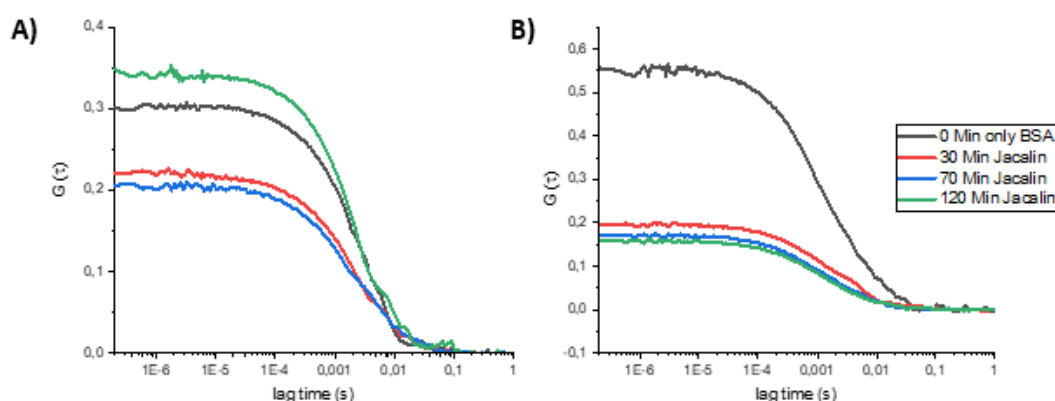
Figure 5.15. *Development of the cross-correlation functions of the labelled nanoparticle-labelled BSA complex after addition of unlabelled Concanavalin A.*

The data obtained after the addition of unlabelled Con-A are shown in figure 5.15 and table 5.5. The cross-correlation amplitude (1/N) in the case of **1a*** decreases from 0.245 at 0 minutes to 0.04046 at 120 minutes. The highest change of amplitude is observed in the first 30 minutes. **1b*** shows a stepwise decrease from 0.13291 to 0.08946 after 30 min of addition of Con-A, this value decreases further to 0.069 at 120 min. The decrease in the cross-correlation amplitude represents the replacement of BSA by Con-A and the decrease of concentration of double labelled species.

The diffusion coefficients in both cases increase after the addition of Con-A in the solution. **1a*** presents a diffusion coefficient of 4.09 $\mu m^2/s$ at the starting point and 5.96 $\mu m^2/s$ 120 min after the addition of Con-A, whereas for **1b*** the diffusion coefficients increases from 8.12 $\mu m^2/s$ to 9.16 $\mu m^2/s$. The PANs at this time point bond only to Con-A upon removal of BSA, the PAN-Con-A complexes consequently diffuse faster. Regarding the binding affinity, a stronger binding is observed between the shorter PEG and Con-A.

Sample		Diffusion time τ [μs]	Diffusion coefficient D [μm²/s]	r_H [nm]	Amplitude G (2.00e-07)	Fit: 1/N CC	$θ_{particle}$ CC/AC$_{BSA}$	$θ_{particle}$ CC/AC$_{particle}$
1a*	0 min	2861.88 ± 56	4.09 ± 0.08	52.49	0.267564	0.245	0.04145	1.93523
	30 min	1767.26 ± 91	7.44 ± 0.21	28.86	0.05775	0.05072	0.02596	1.01485
	70 min	1827.36 ± 140	6.40 ± 0.65	33.55	0.040556	0.03715	0.02538	1.02083
	120 min	1962.86 ± 100	5.96 ± 4.2	36.02	0.046178	0.04046	0.02578	1.58789
1b*	0 min	1498.17 ± 47	8.12 ± 0.26	26.44	0.135728	0.13291	0.07251	2.01817
	30 min	1256.99 ± 38	9.67 ± 0.29	22.20	0.093044	0.08946	0.05905	1.85861
	70 min	1279.45 ± 54	9.50 ± 0.4	22.60	0.072248	0.07081	0.05926	1.51953
	120 min	1327.04 ± 28	9.16 ± 0.19	23.44	0.072005	0.069	0.06525	1.45618

Table 5.5. *Results of the cross-correlation of polymeric glyco-NPs with BSA and after addition of Concanavalin A*

The binding of **3a*** and **3b*** towards Jacalin was also analysed by FCCS as shown in figure 5.16 and table 5.6. The cross-correlation amplitude for **3a*** decreases after 30 min from 0.3084 to 0.2171, meaning there is a replacement of BSA by Jacalin, but after 120 min the amplitude increases again. In the case of **3b*** which is formed with the longer PEG length, the cross-correlation amplitude values continue decreasing with time after the addition of Jacalin. The results obtained demonstrate that the affinity of Jacalin towards lactose is weaker than the affinity between α-mannose and Con-A.

Figure 5.16. *Development of the cross-correlation functions of the labelled nanoparticle-labelled BSA complex after addition of unlabelled Jacalin. A) 3a* B) 3b***

Sample		Diffusion time τ [μs]	Diffusion coefficient D [μm²/s]	r_H [nm]	Amplitude G (2.00e-07)	Fit: 1/N CC	$θ_{particle}$ CC/AC$_{BSA}$	$θ_{particle}$ CC/AC$_{particle}$
3a*	0 min	1525.39 ± 29	7.26 ± 0.14	29.57	0.300741	0.3084	0.07762	4.16194
	30 min	1820.14 ± 33	6.08 ± 0.11	35.31	0.221436	0.2171	0.07772	3.07507
	70 min	2109.43 ± 30	5.25 ± 0.07	40.90	0.206088	0.2006	0.06766	3.05374
	120 min	1298.77 ± 25	8.53 ± 0.16	25.17	0.348126	0.3504	0.08201	4.09825
3b*	0 min	1517.43 ± 14	7.30 ± 0.07	29.41	0.556455	0.523855	0.12007	1.64181
	30 min	1981.77 ± 55	5.59 ± 0.15	38.41	0.196923	0.18933	0.196923	1.55469
	70 min	1631.81 ± 44	6.79 ± 0.18	31.62	0.172812	0.16448	0.10818	1.65382
	120 min	1502.32 ± 39	7.37 ± 0.19	29.13	0.16127	0.15332	0.10969	1.77636

Table 5.6. *Results of the cross-correlation of polymeric glyco-NPs with BSA and after addition of Jacalin*

5.4   Conclusions

In this chapter the synthesis of novel Glyco-PEG-PANs with two different PEG lengths has been described. The formation of PANs with different phosphate buffer concentrations was studied as well as the pH stability of the NPs, concluding that the Glyco-PEG-PANS are stable at lower pHs than PEGylated PANs and the PANs formed with PBS 5 mM are more stable overtime. The interaction of the Glyco-PEG-PANs with specific lectins was studied by FCCS, even though not the same trend could be observed for Con-A and Jacalin. The affinity observed between α-mannose present in **1a*** and **1b*** towards Con-A was stronger than the affinity observed between lactose PANs and Jacalin. The FCCS studies also demonstrated that the PANs with shorter PEG chains showed a higher affinity towards the lectins.

The data described in this chapter will be part of a manuscript that will be soon submitted to a scientific journal.

5.5   Experimental

5.5.1   Materials and methods

Poly (allylamine hydrochloride) salt (PAH) (MW: 15 × 104 g mol−1), phosphate buffer salt tablets (PBS), HPLC water, bovine serum albumin, Concanavalin A, Jacalin and ATTO 633-NHS ester were

purchased from Sigma Aldrich. Unconjugated RCA I, RCA 120 was supplied from Vector Laboratories. Mal-dPEG®$_6$-NHS ester and Mal-dPEG®$_{24}$-NHS ester were purchased from Quanto Biodesign.

All Nuclear Magnetic Resonance (NMR) experiments were measured at room temperature using a Bruker AVANCE III 500 MHz for proton equipped with a 5mm BBI NMR probe. Proton experiments were acquired using a pulse-acquire sequence using the following parameters, 32K complex points, flip angle 30 degrees, repetition time 4.5 sec, SW 20 ppm, Dummy scans 8 and 64 averages. Data were zero filled to 64K and apodised using an exponential multiplication routine with 0.3 Hz of line broadening. Carbon spectra were measured using Bruker's zgpg30 sequence using the following parameters, 32K complex points, repetition time 3 sec, SW 230 ppm, Dummy scans 8 and 256 averages. Data were zero filled to 64K and apodised using an exponential multiplication routine with 1 Hz of line broadening.

UV-Visible measurements were performed by using the Bio UV-Vis V630 Spectrophotometer from Jasco and disposable cuvettes with 10 mm path length.

The performance of FCS and FCCS measurements was carried out with a Zeiss LSM 880 confocal microscope with Zen black software. The samples were excited with a HeNe laser with a wavelength of 633 nm and an Ar laser with an excitation wavelength of 488 nm with a 40X C Apo/1.2 W DICIII with water immersion objective. For detection at an excitation wavelength of 488 nm (green laser) a GaAsP and for 633 nm a Pmt detector was used. The detector ranges were chosen 500 – 560 nm and 650 – 710 nm to keep cross talk as low as possible.

5.5.2 Synthetic procedure of glyco-PEG-poly allylamine polymers

Poly(allylamine) hydrochloride (PAH) (20 mg, 1.14 µmol) is dissolved in Milli-Q water in a concentration of 500 mg/ml, it is added to a falcon tube of 50 mL with 17 mL of water, the pH is then adjusted to 7-7.5 and Mal-PEG$_n$-NHS (11.,4 µmol) is added dissolved in 300 µL of DMSO. Add water until we have a final volume of 20 mL. The reaction is left 1h RT, then the pH is adjusted to 6.5-7 and the Glycan-EG$_6$C$_{11}$ (17,1 µmol) is added dissolved in 1 ml of Milli-Q water. The reaction is then left stirring for 2 hours, the polymer is then purified by Amicon 10kDa, and the sample is lyophilized 48 hours. The sample are then analyzed by NMR. The same process was followed with the ATTO633-PAH.

5.5.3   Fluorescent labelling of poly allylamine polymers

Poly(allylamine) hydrochloride (PAH) (28 mg,1.6 µmol) is dissolved in Milli-Q water and ATTO633-NHS (1.2 mg, 1.6 µmol) was added to the reaction, it was left stirring overnight. The reaction mixture was then purified using Sephadex G-25 and lyophilized to obtain the final product.

5.5.4   Glyco-PEG-Polyamine phosphate nanoparticles assembly

Form the PANs by self-assembly, for this purpose the polymer was dissolved in Milli-Q water at a concentration of 10 g/mL and then PBS 5 mM was added to obtain a final concentration of 1 mg/mL. The PANs are formed immediately by self-assembly.

5.5.5   Transmission emission microscopy

3 µL of a 1 mg/mL dispersion of NPs was placed on an ultra-thin grid that was pre-treated with a glow discharge system and incubated for 5 Min, followed by 3 µL of an ammonium molybdate solution for 5 Min and one washing step with water. Excess sample was removed with a filter paper after the incubation time finished.

Sample	Average diameter (nm)	Standard deviation (nm)
1a	5.90	1.35
1b	6.36	1.25
2a	3.69	0.88
2b	5.40	1.13
3a	5.93	1.32
3b	6.04	1.26

Table 5.7. *Average size of PANs by means of TEM*

5.5.6   Quantification of fluorophore by means of UV-Vis measurements

For the calibration standard solutions with 0.5, 1.0, 1.5, 2.0, 2.5 and 3.5 µg·mL^{-1} were prepared and measured. The polymers were diluted to a concentration of 112.5 µg·mL^{-1} and the resulting absorbance was compared with the linear regression based on the standard solutions. All measurements were done in triplicates.

5.5.7   Measurements of polymers and formed PANs by means of FCS

The FCS and FCCS measurements were performed by Sergio Moya's group at CIC BiomaGUNE.

The ATTO633 conjugated polymers were dissolved in water to reach a concentration of 10 mg·mL^{-1} and diluted with 5 mM PBS to receive a concentration of 1 mg·mL^{-1} leading to particle formation. The formed particles were further diluted with water to reach a concentration of 7 µg·mL^{-1} for the FCS measurements. A similar concentration of the ATTO633 conjugated polymer was measured as a control without any source of phosphate, in order to avoid particle formation. The experiment was performed in triplicates.

The resulting autocorrelation functions of the polymers and particles were fitted with a 2-component fitting, whereas the first component was the free fluorophore.

5.5.8   Interaction of nanoparticles with BSA and lectins

The NPs were formed as described in previous with subsequent exposure to 15 nM bovine serum albumin labelled with Alexa488 and incubation at 37 °C for 1 h under agitation (200 rpm). The binding of the nanoparticle-BSA complex at 0 Min is measured by Fluorescence Cross-

Correlation Spectroscopy followed by the addition of unlabelled Concanavalin A/Jacalin to the sample to reach a concentration 40 nM.

5.5.9 ^{1}H-NMR

1a- PAH-PEG$_6$- Mannose-EG$_6$C$_{11}$
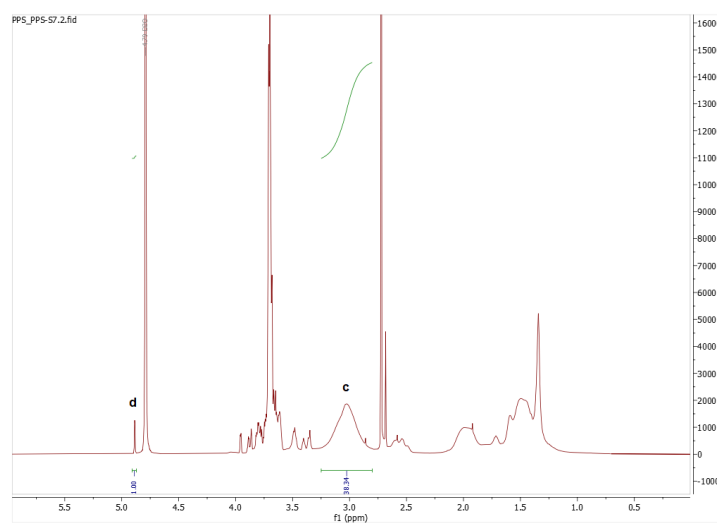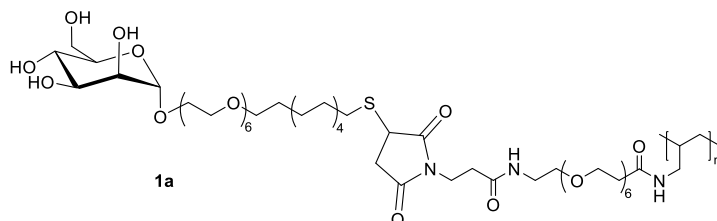
1b- PAH-PEG$_{24}$- Mannose-EG$_6$C$_{11}$
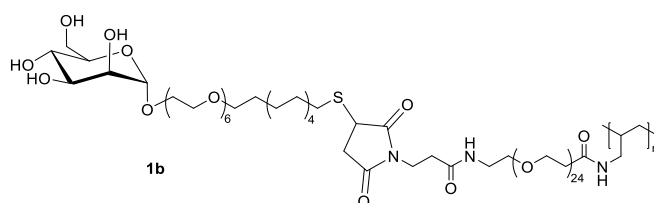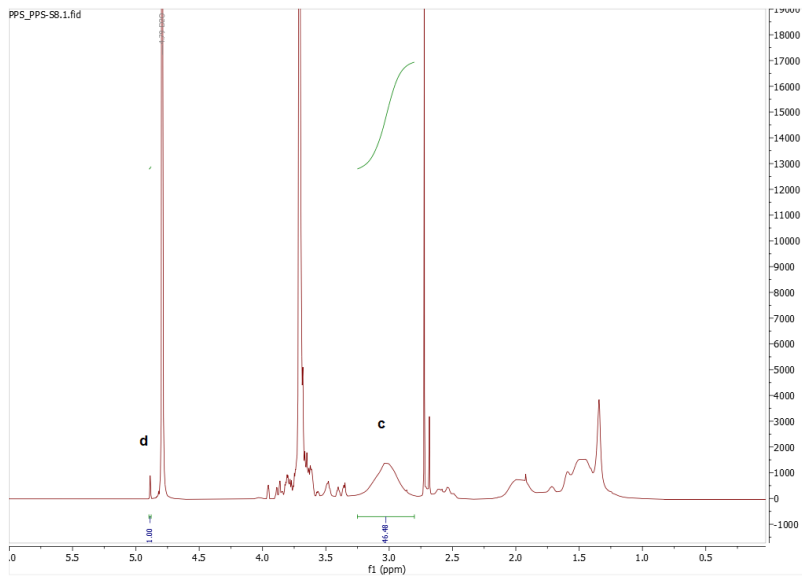
2a- PAH-PEG₆- Glucose-EG₆C₁₁
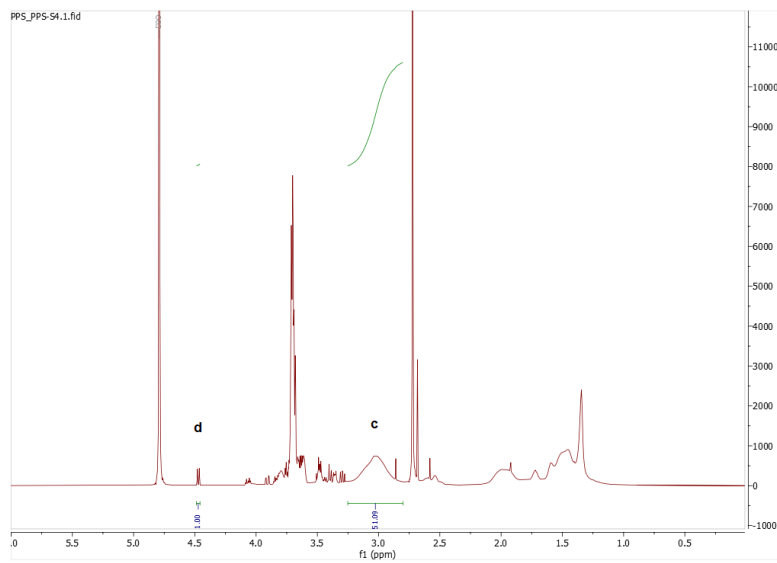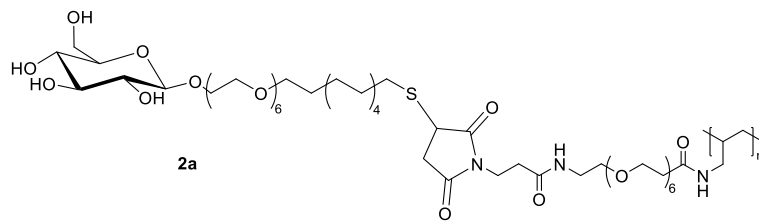
2b- PAH-PEG₂₄- Glucose-EG₆C₁₁
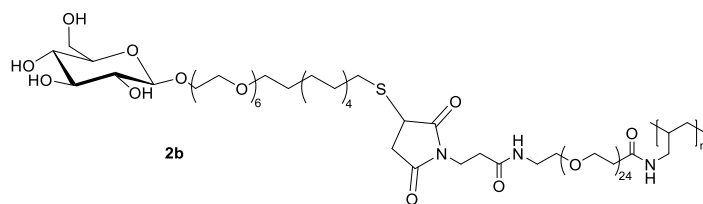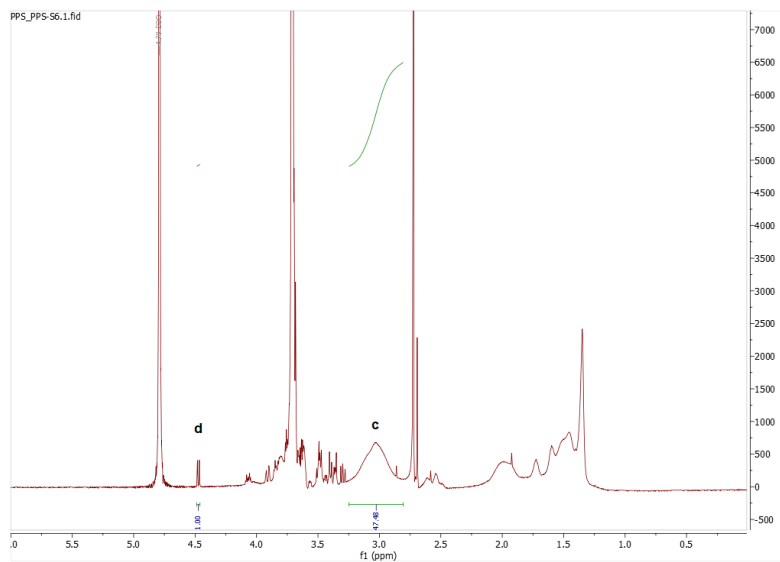
3a - PAH-PEG₆- Lactose-EG₆C₁₁

3a
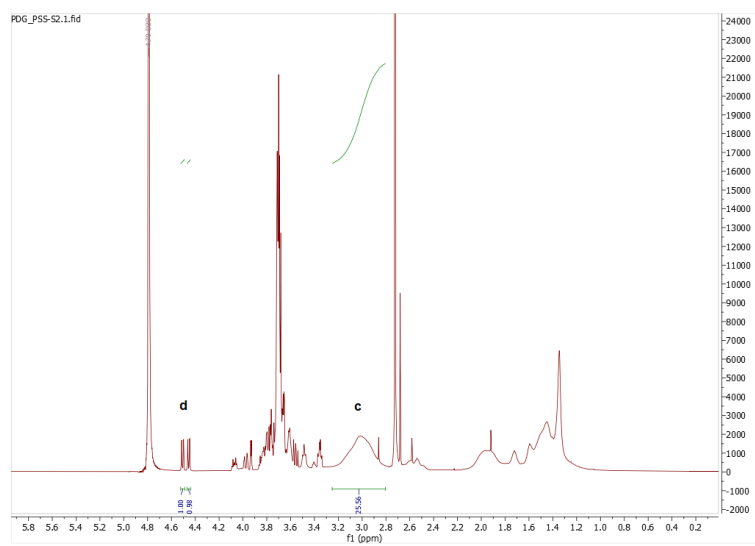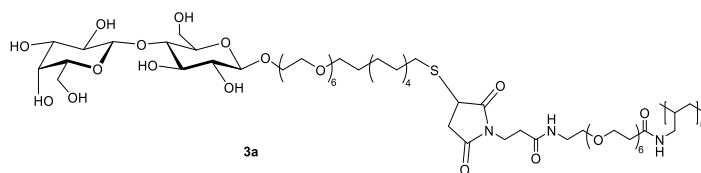
3b PAH-PEG₂₄- Lactose-EG₆C₁₁

3b
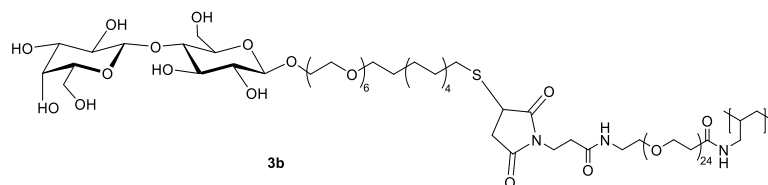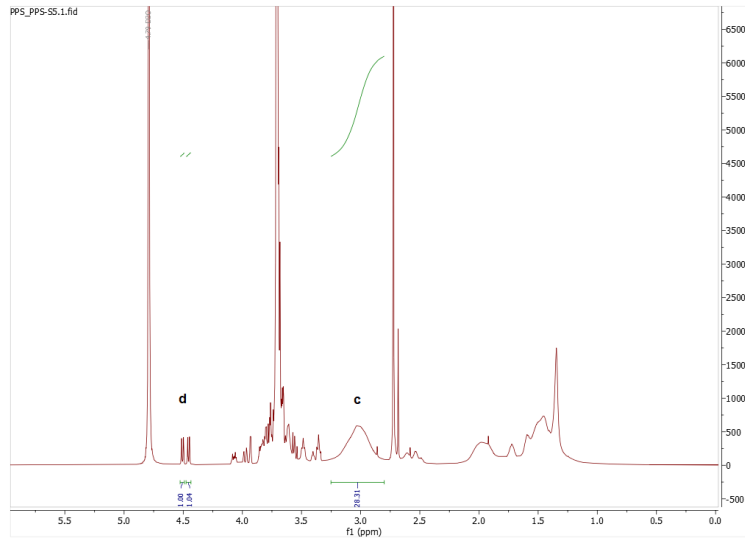
- Labelled Glyco-PEG-PAHs

1a** - ATTO633-PAH-PEG$_6$- Mannose-EG$_6$C$_{11}$
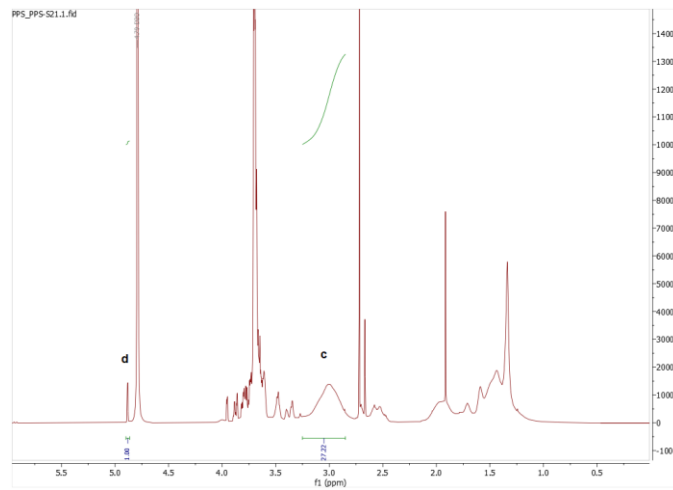
1b** - ATTO633-PAH-PEG$_{24}$- Mannose-EG$_6$C$_{11}$
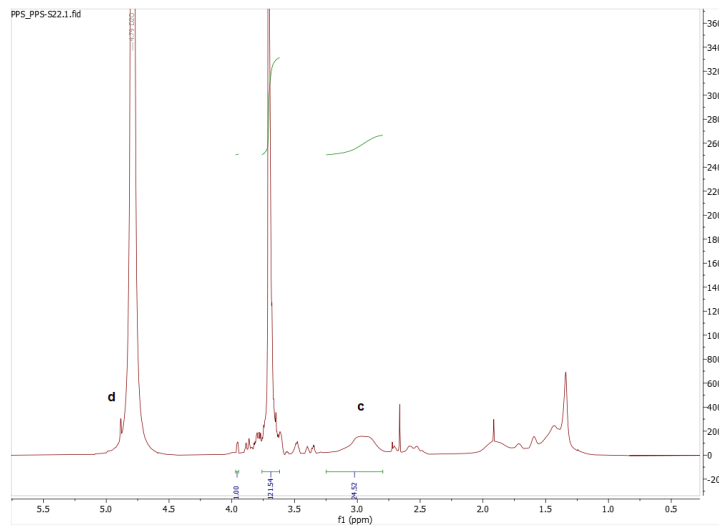
3a* - ATTO633-PAH-PEG$_6$- Lactose-EG$_6$C$_{11}$
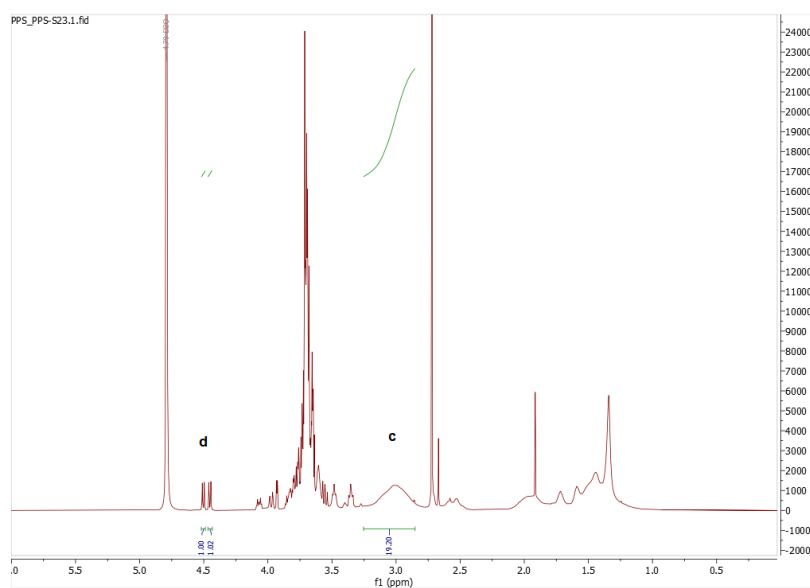
3b* - ATTO633 PAH-PEG$_{24}$- Lactose-EG$_6$C$_{11}$
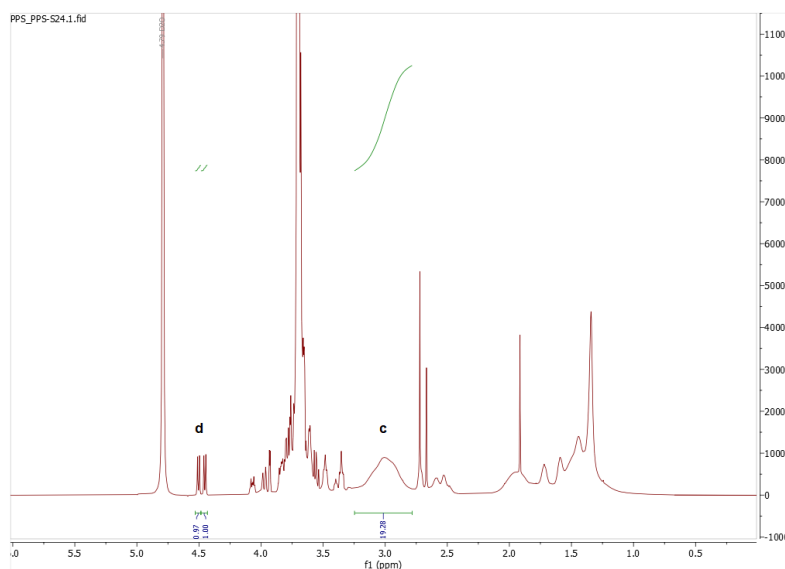
Characterization of glycan derivatives is described in Chapter 3 section 3.5.7 and the NMR spectra are reported are in the annex.

SCHEMES
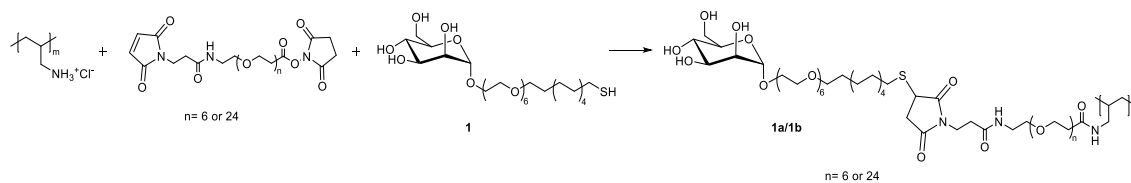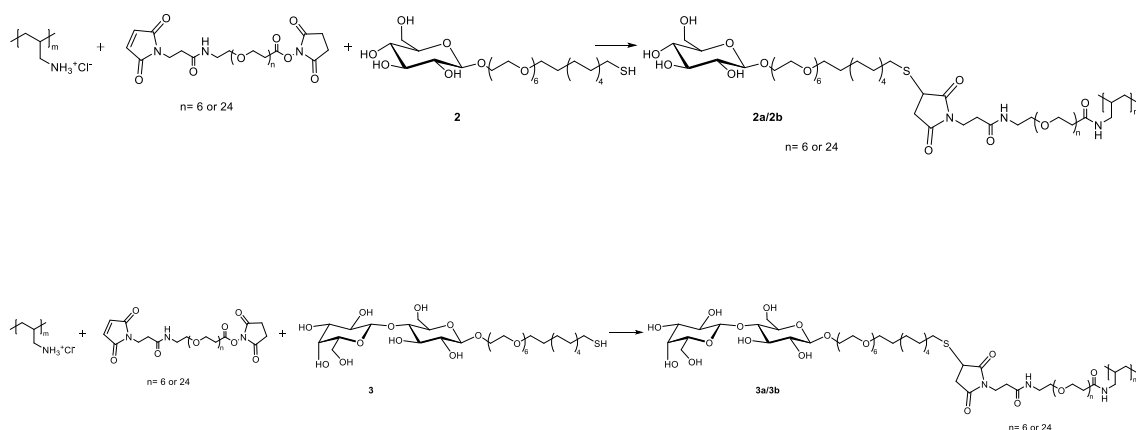
5.6   References

(1)   Di Silvio, D.; Martínez-Moro, M.; Salvador, C.; de los Angeles Ramirez, M.; Caceres-Velez, P. R.; Ortore, M. G.; Dupin, D.; Andreozzi, P.; Moya, S. E. Self-Assembly of Poly(Allylamine)/SiRNA Nanoparticles, Their Intracellular Fate and SiRNA Delivery. *Journal of Colloid and Interface Science* **2019**, *557*, 757–766. https://doi.org/10.1016/j.jcis.2019.09.082.

(2)   Andreozzi, P.; Ricci, C.; Porcel, J. E. M.; Moretti, P.; Di Silvio, D.; Amenitsch, H.; Ortore, M. G.; Moya, S. E. Mechanistic Study of the Nucleation and Conformational Changes of Polyamines in Presence of Phosphate Ions. *Journal of Colloid and Interface Science* **2019**, *543*, 335–342. https://doi.org/10.1016/j.jcis.2019.02.040.

(3)   Andreozzi, P.; Diamanti, E.; Py-Daniel, K. R.; Cáceres-Vélez, P. R.; Martinelli, C.; Politakos, N.; Escobar, A.; Muzi-Falconi, M.; Azevedo, R.; Moya, S. E. Exploring the PH Sensitivity of Poly(Allylamine) Phosphate Supramolecular Nanocarriers for Intracellular SiRNA Delivery. *ACS Appl. Mater. Interfaces* **2017**, *9* (44), 38242–38254. https://doi.org/10.1021/acsami.7b11132.

(4)   Cuenca, V. E.; Martinelli, H.; Ramirez, M. de los A.; Ritacco, H. A.; Andreozzi, P.; Moya, S. E. Polyphosphate Poly(Amine) Nanoparticles: Self-Assembly, Thermodynamics, and Stability Studies. *Langmuir* **2019**, *35* (44), 14300–14309. https://doi.org/10.1021/acs.langmuir.9b02636.

(5)   Andreozzi, P.; Simó, C.; Moretti, P.; Porcel, J. M.; Lüdtke, T. U.; Ramirez, M. de los A.; Tamberi, L.; Marradi, M.; Amenitsch, H.; Llop, J.; Ortore, M. G.; Moya, S. E. Novel Core–Shell Polyamine Phosphate Nanoparticles Self-Assembled from PEGylated Poly(Allylamine Hydrochloride) with Low Toxicity and Increased In Vivo Circulation Time. *Small* **2021**, *17* (35), 2102211. https://doi.org/10.1002/smll.202102211.

(6)   Mattox, D. E.; Bailey-Kellogg, C. Comprehensive Analysis of Lectin-Glycan Interactions Reveals Determinants of Lectin Specificity. *PLoS Comput Biol* **2021**, *17* (10), e1009470. https://doi.org/10.1371/journal.pcbi.1009470.

(7)   Yu, L.; Lei, Y.; Ma, Y.; Liu, M.; Zheng, J.; Dan, D.; Gao, P. A Comprehensive Review of Fluorescence Correlation Spectroscopy. *Front. Phys.* **2021**, *9*, 644450. https://doi.org/10.3389/fphy.2021.644450.

(8)   Di Silvio, D.; Silvestri, A.; Lay, L.; Polito, L.; Moya, S. E. Impact of ConcanavalinA Affinity in the Intracellular Fate of Protein Corona on Glucosamine Au Nanoparticles. *Sci Rep* **2018**, *8* (1), 9046. https://doi.org/10.1038/s41598-018-27418-w.

(9)   Hermanson, G. T. Heterobifunctional Crosslinkers. In *Bioconjugate Techniques*; Elsevier, 2013; pp 299–339. https://doi.org/10.1016/B978-0-12-382239-0.00006-6.

(10) Jeyaraj, M.; Gurunathan, S.; Qasim, M.; Kang, M.-H.; Kim, J.-H. A Comprehensive Review on the Synthesis, Characterization, and Biomedical Application of Platinum Nanoparticles. *Nanomaterials* **2019**, *9* (12), 1719. https://doi.org/10.3390/nano9121719.

Chapter 6

Conclusions

6.1 Overall conclusion and next steps

Even though great efforts have been made in the last 20 years on gold nanoparticles, at the moment there are no AuNPs based nanomedicines approved by Food and Drugs Administration(FDA) and European Medicines Agency (EMA). These NPs present several challenges in order to enter clinical trials and exist a general lack of universal regulatory guidelines regarding the evaluation and characterization of the NPs. This is due to the complexity of the nano systems as the properties and the final fate of the nanoparticles don't only depend on the size and shape of the nanoparticles but also on the surface coating. Therefore, continuous, and detailed studies and characterization on nano systems are highly needed to boost their spread into the market.

The present thesis based on the rationale that glycans play a crucial role in physiological processes and therefore glyco nanoparticles have a high potential to be used for biological applications. Throughout this thesis the experiments have focused on understanding the effect regarding the circulation time of using different linkers in the coating of the nanoparticles as well as coating the nanoparticles with a library glycan derivatives.

It has been demonstrated that the coating of the ultrasmall NPs with polyethylene glycol (PEG) of two lengths (MW 500 and 5000) can highly affect the half-life of the nanoparticles in healthy mice. Moreover, it was also demonstrated that the combination of PEG_{500} with α-Gal-C_2 could also increase the circulation time of the NPs without the need of using costly PEG_{5000}. The biodistribution of the NPs was further modified by the addition of a terminal α-Man-C_2 on the PEG linkers, showing in this case a lower accumulation of the nanoparticles in the liver and kidneys. This could be explained by the different receptors present on the surface of the organs as well as by the protein corona formed when the NPs are in contact with biological fluids as plasma. The protein corona, as explained in Chapter 1 section 1.3, can highly affect the final fate of the NPs, therefore on the future experiments there should be an extensive study of the protein corona formation to better understand the results obtained with these functionalized 4 nm AuNPs, even recovering the NPs from the urine and studying the protein corona formed on the NPs.

Size and shape can strongly affect the formation of protein corona for this reason a long-term colloidal stability of glyco-star shaped AuNPs (70 nm) and 30 nm glyco-spherical AuNPs was studied by observing the changes in the hydrodynamic diameter by dynamic light scattering (DLS). This study demonstrated the formation of the soft corona and the hard corona on star shaped AuNPs when in contact with RPMI + 10% FBS and FBS. The stability of the nanoparticles in water and PBS for 180 days was also proven. The stability of the spherical AuNPs in water and PBS was also studied for 30 days. Further experiments must be performed to study the stability of the AuNPs over a longer period of time, as well as the protein corona formation in RPMI + 10% FBS and FBS in order to compare with the results obtained for the star shaped NPs and in

this way determine the effect of the shape of the NPs. A similar study could be performed in the 4 nm NPs previously mentioned as well as for example SDS page studies to determine the specific proteins that form the protein corona and, in this way, better understand the behaviour of the NPs in the biodistribution study.

In order to overcome some of the current challenges regarding surface coating of the AuNPs it is necessary to have a fine control over the ligand density on the surface of the NPs. The novel photo-induced microfluidic synthetic procedure of glyco-UAuNPs (GUAuNPs) developed during this thesis addresses this challenge by obtaining a linear correlation between the ligands added to the initial solution and the ligands on the NPs surface. This data was obtained by performing quantitative ^{1}H-NMR with ERETIC 2 program. The microfluidic system employs photo-reduction of gold being in this way a green synthetic procedure avoiding the use of reducing agents and surfactants. Additionally, the absence of reducing agents in the reaction allows the recovery of the precious glyco-derivatives. Hypothesizing about a big scale production of AuNPs the recovery of the linkers could be a great economical advantage.

Moreover, novel Glyco-PEGylated polyamine phosphate nanoparticles (Glyco-PEGylated PANs) were synthesized successfully exploiting carbodiimide chemistry. The next steps could be to encapsulate for example siRNA, as it has previously been performed in PEGylated PANs, to then study by Fluorescence Correlation Spectroscopy (FCS) the encapsulation. Additionally, a biodistribution study could be performed in order to compare the Glyco-PEGylated PANs to PEGylated PANs study reported in literature and determine if the glycans present in the NPs can modify the final fate of the NPs.

These nanoparticles were synthesized in order to compare the effect of using the same glycan derivatives in different type of nanomaterials. The affinity of the Glyco-PEGylated PANs towards specific lectins was studied by Fluorescence Cross-Correlation Spectroscopy (FCCS). Therefore, the same studies could be carried out for the 2 nm Glyco-UAuNPs as the same glycan derivatives were employed and determine in this way the effect of using different types of nanomaterials.

Overall, the results obtained for the different types of nanoparticles are promising but more experiments must be conducted in order to obtain the optimal glyco nanomaterial to use for biological applications.

6.2   Impact of the thesis and future perspectives

The major impact of this thesis in the current research of AuNPs is the new photo-induced microfluidic system developed for the synthesis of GUAuNPs. This system presents several advantages for the industrial production of GUAuNPs as mentioned before due to the absence of toxic agents as reducing agent and surfactants, the possibility of recovering the unreacted glycans, and the simple scale-up of microfluidic systems. Moreover, this system can be automated and therefore it provides an optimum advantage towards transferring the system to Good Manufacture Practice (GMP) conditions. Additionally, the system also enables a fine control of the surface coating of the nanoparticles which is a very important feature regarding the future biological applications of the nanoparticles.

The future perspective of this new synthetic procedure could be the modification of the synthetic procedure in order to obtain different AuNPs of bigger sizes. The protein corona has

been demonstrated to play a crucial role in the final fate of the nanoparticles therefore a thorough study of the protein corona formation of these nanoparticles should be performed.

Furthermore, the system could be expanded to be used to obtain UAuNPs with different coating as it has been demonstrated that the only factor modulating the formation of the 2 nm NPs is the characteristics of the thiol linker but not the nature of the terminal molecules. Therefore, the AuNPs could be coated for example by peptides, RNA or commercial drugs as well as the combination of 2 or more biomolecules in one nanoparticle.

Additionally in order to transfer this system towards industrial production of AuNPs the sterility of the NPs should be investigated as the synthesis is performed under a UV lamp which has been widely used to sterilize. In that case the microfluidic system could be directly connected to purification system denominate Tangential Flow Filtration (TFF) which is a GMP compatible system used in the industry to purify NPs.

The biodistribution studies performed throughout the thesis demonstrated that the combination of a PEG_{500} linker with a short aliphatic linker with a terminal α-Gal had a similar effect over the circulation time of the nanoparticles than PEG_{5000}. This has a substantial impact on the research of AuNPs as the coating of the nanoparticles can be modulated by adding shorter linkers which are cheaper and easier to modify from a chemical point of view respect to PEG_{5000}.

Moreover, the modification of polyamine nanoparticles with PEG and a final glycan derivative has a significant repercussion over the current research of PANs, as it could enhance the active targeting of the nanoparticles towards specific lectins and pave the way of new biological applications.

ANNEX

29-Thio[3,6,9,12,15,18-hexaoxaundecanyl-α-D-mannopyranoside] (1-Man)
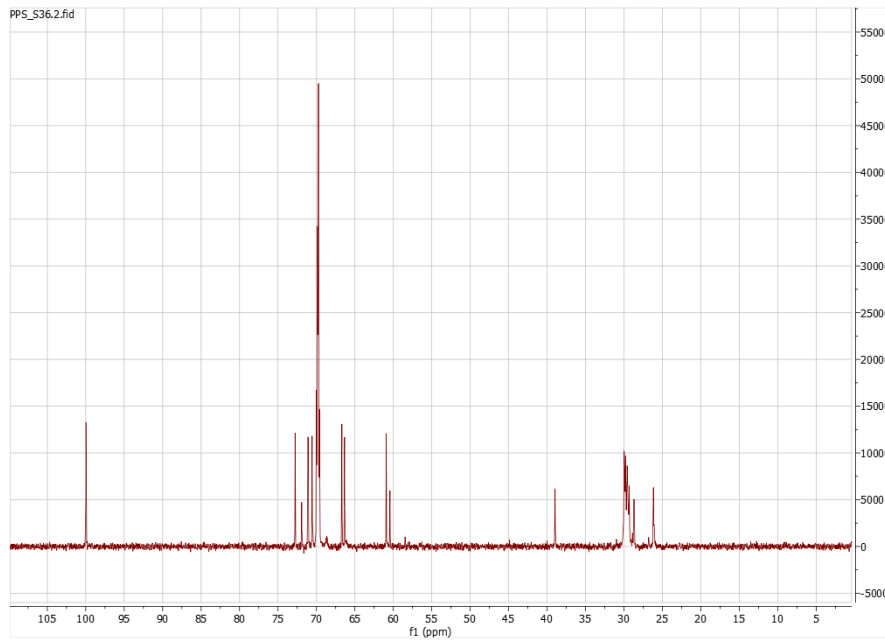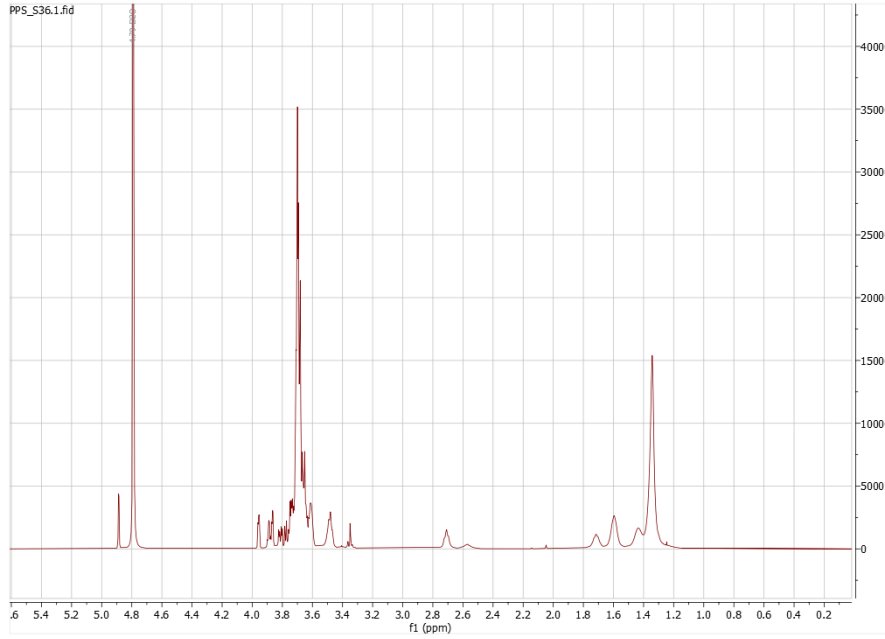
29-Thio [3,6,9,12,15,18-hexaoxaundecanyl-β-D-glucopyranoside] (2-Glc)
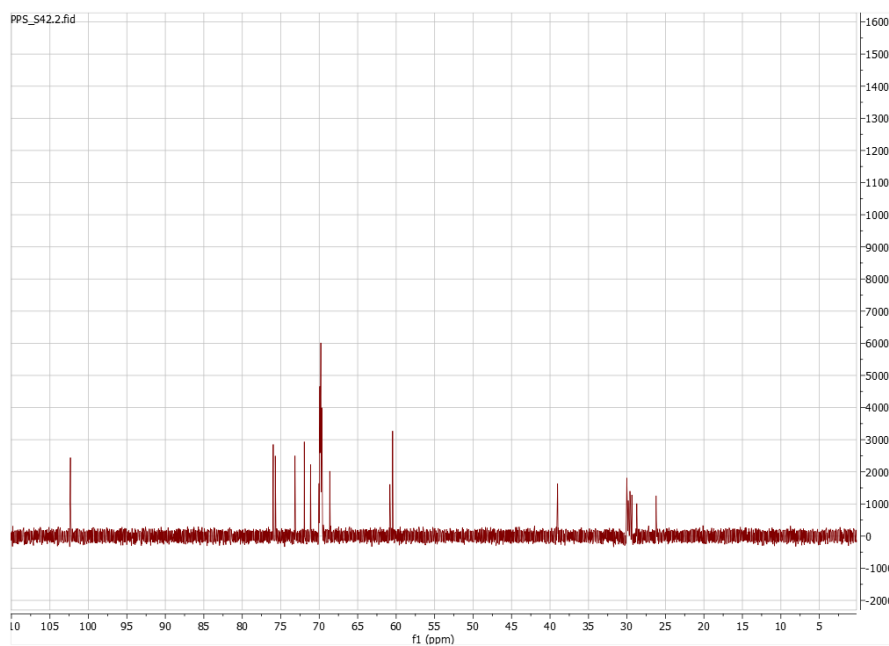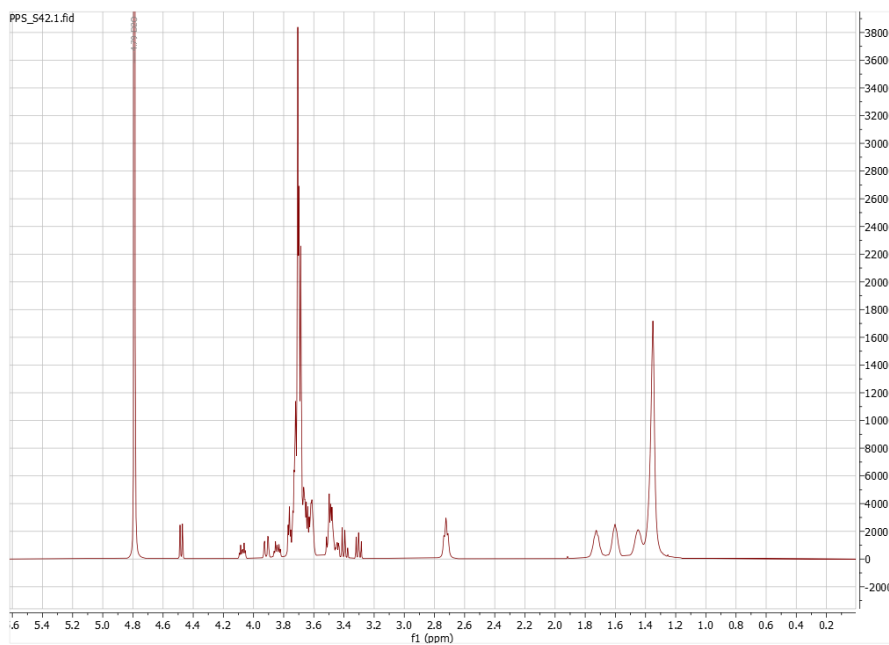
29-Thio-[3,6,9,12,15,18-hexaoxaundecanyl-β-D-galactopyranosyl)(1→4)-β-D-glucopyranoside] (3-Lac)
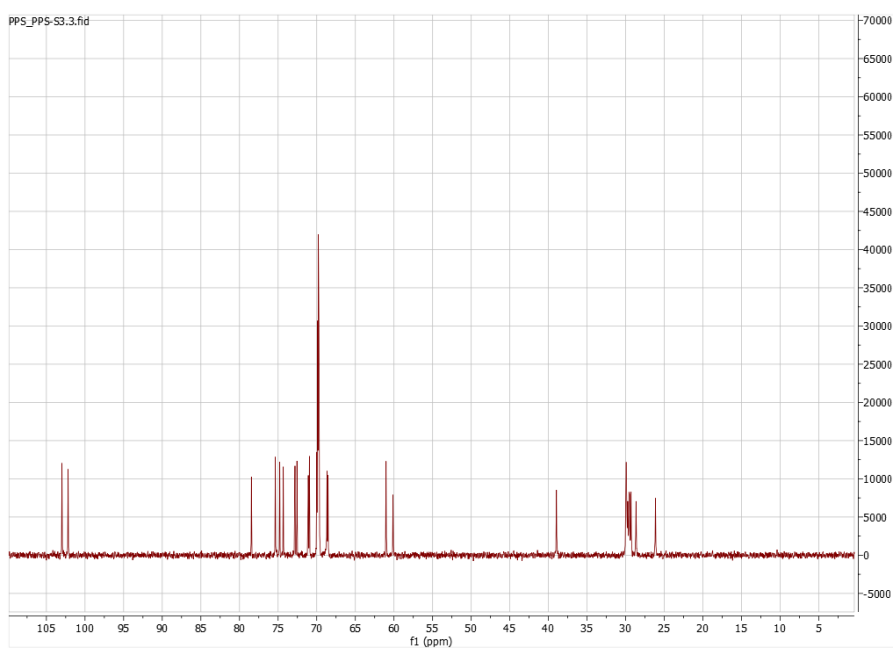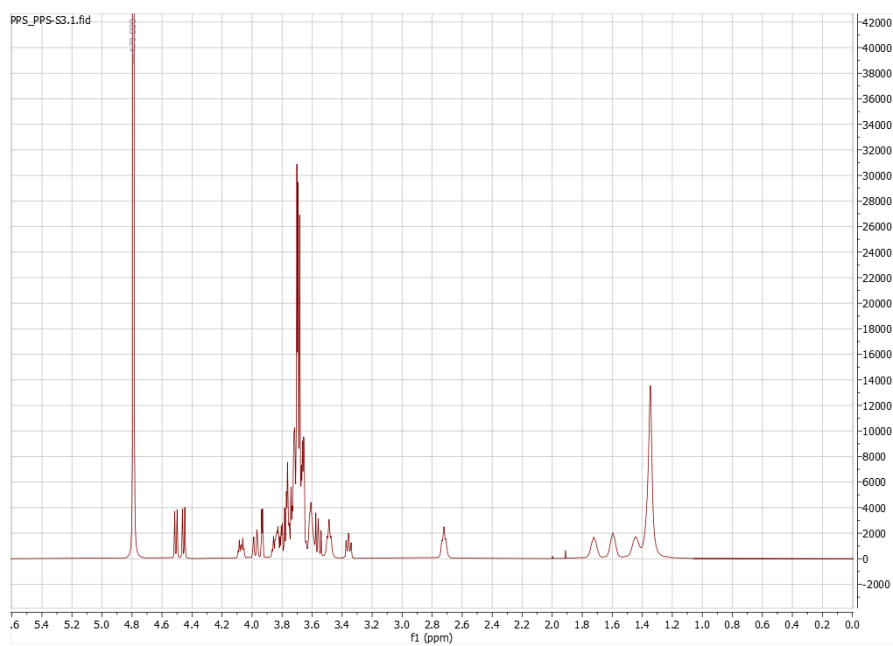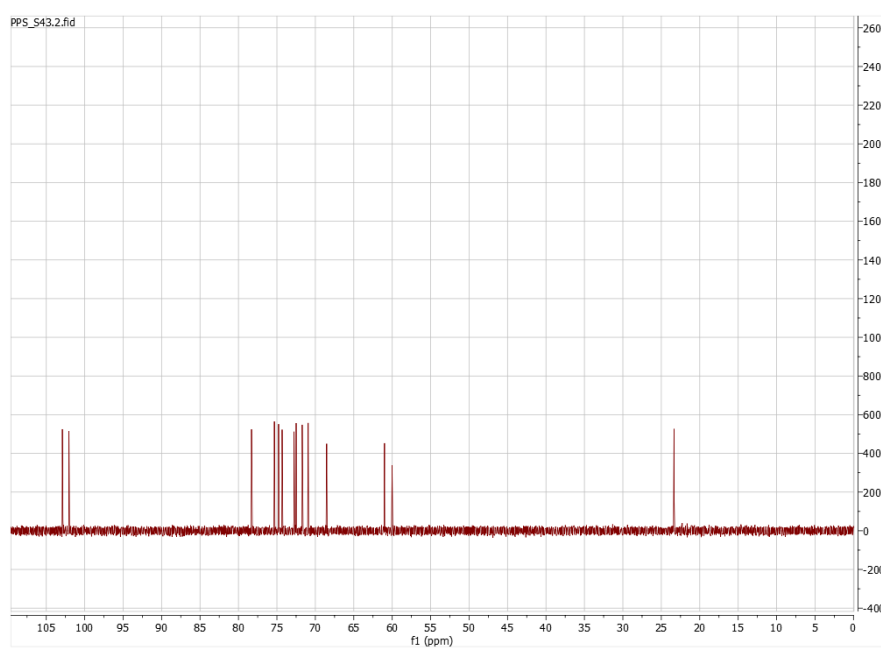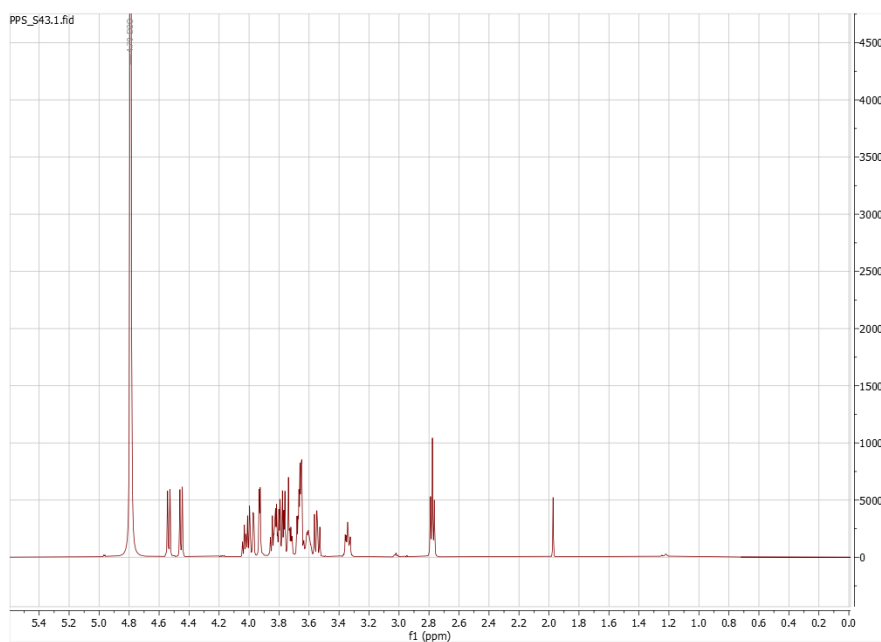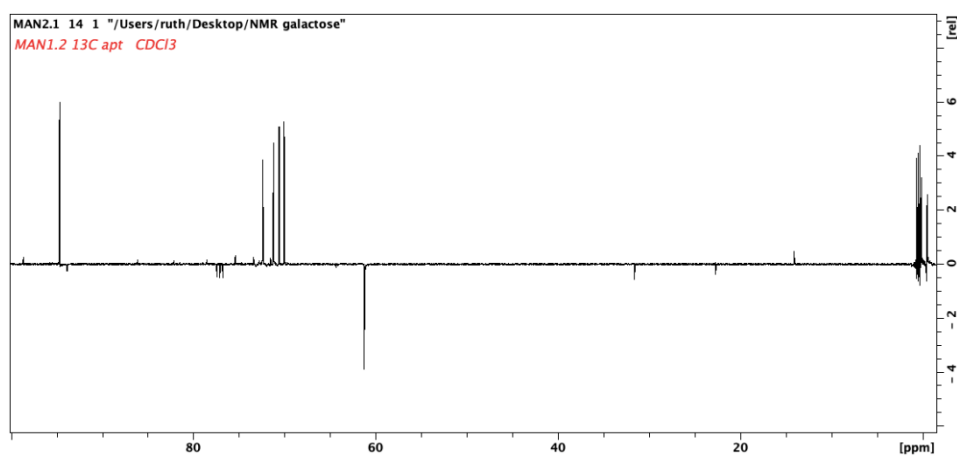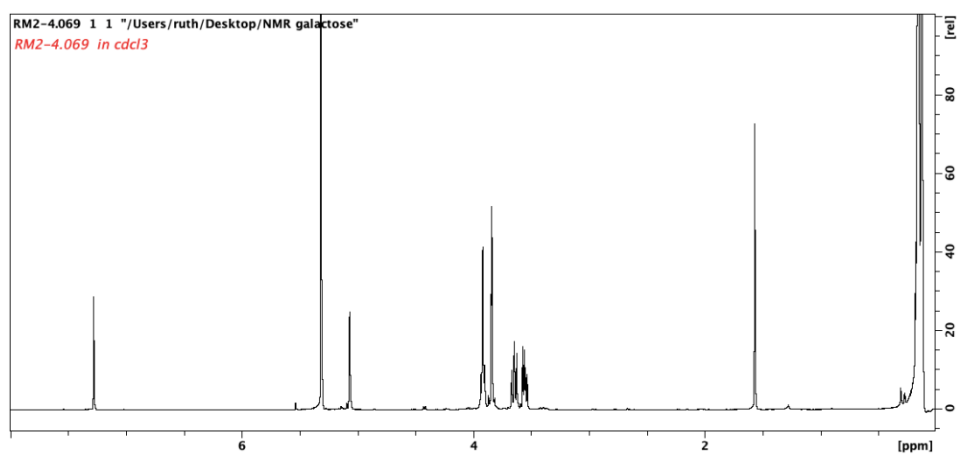
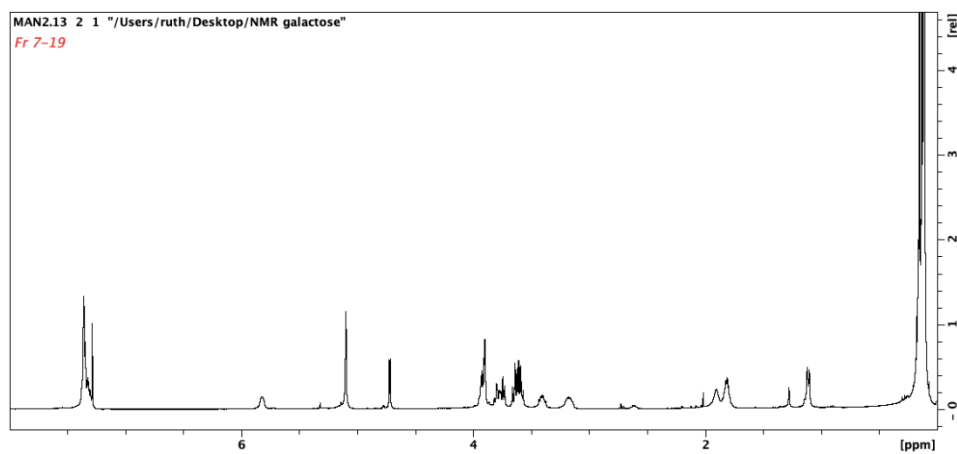**2-Thio(ethyl-α-D-mannopyranoside) (5-Man)**
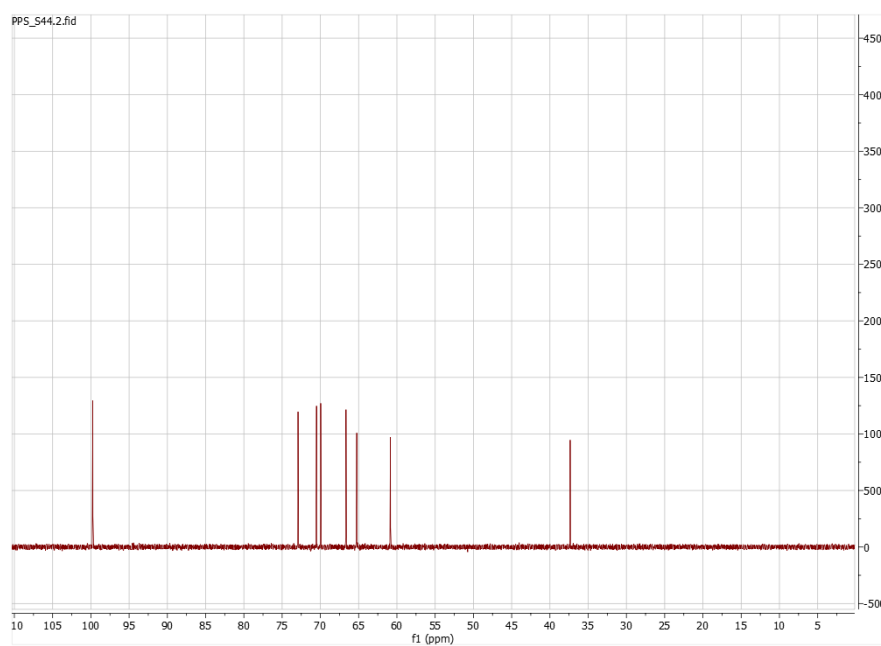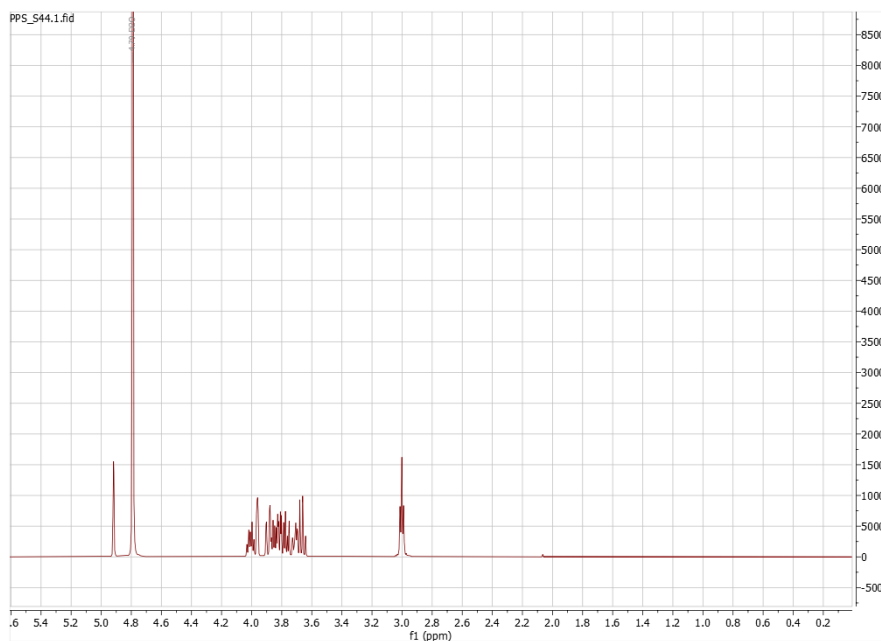
2-Thio(propyl-α-D-Glucopyranoside) (6-Glc)
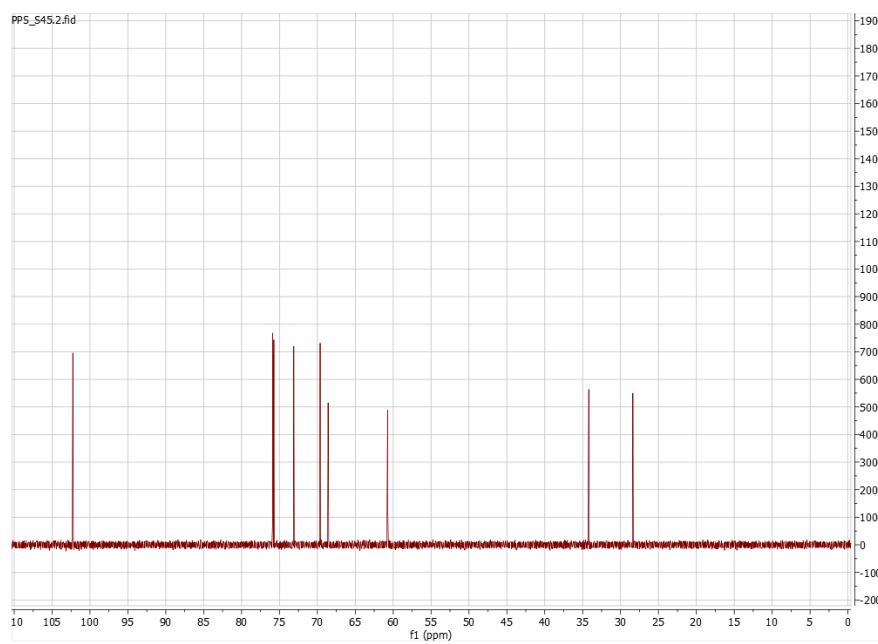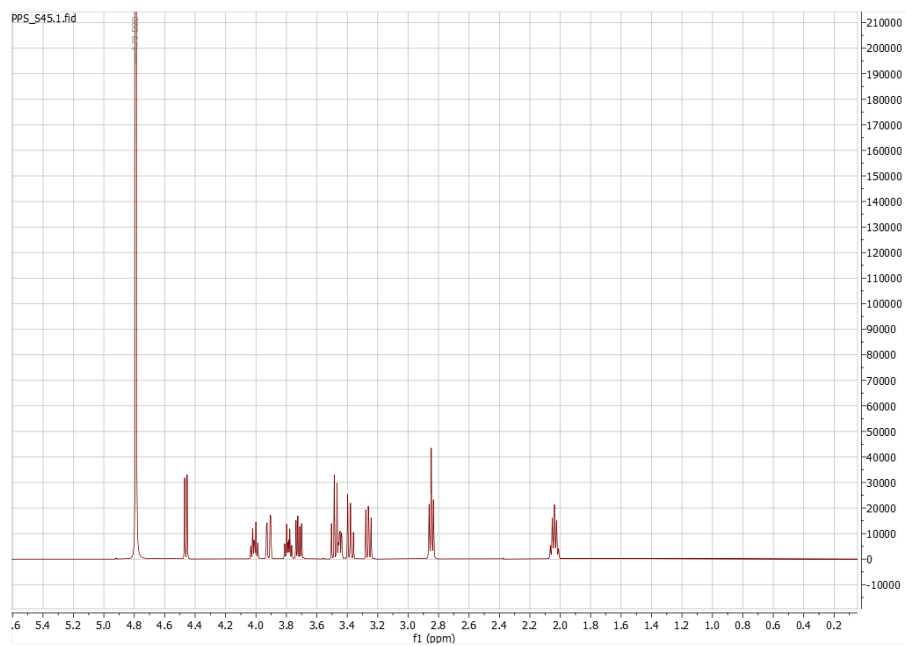
2-Thio(ethyl- β-D-galactopyranosyl)(1→4)-β-D-glucopyranoside) (7-Lac)
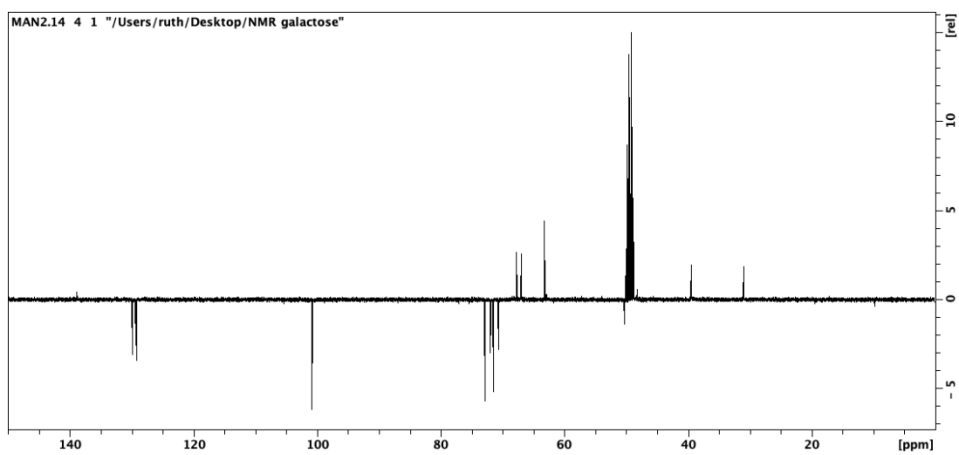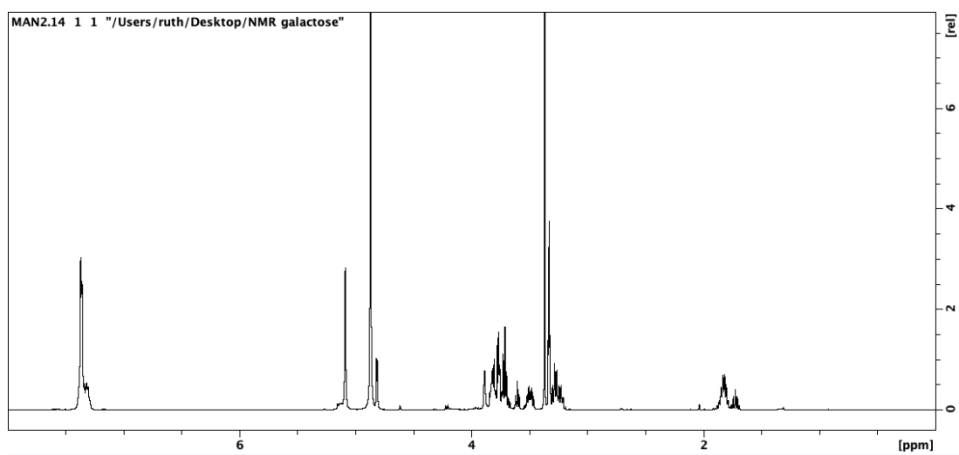
1,2,3,4,6-penta-O-TMS-β-D-galactopyranose (a)

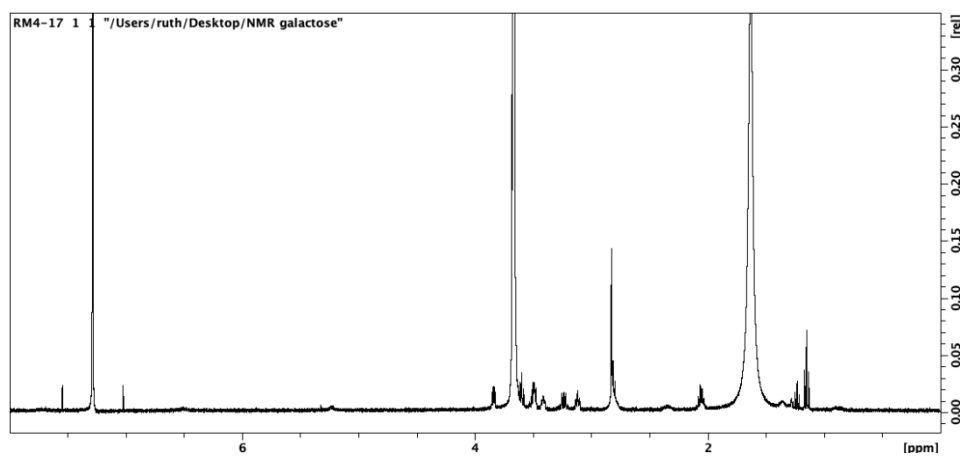**3'-(benzyloxycarbonyl)-aminopropyl-2,3,4,6-tetra-O-TMS-α-D-galactopyranoside (c)**
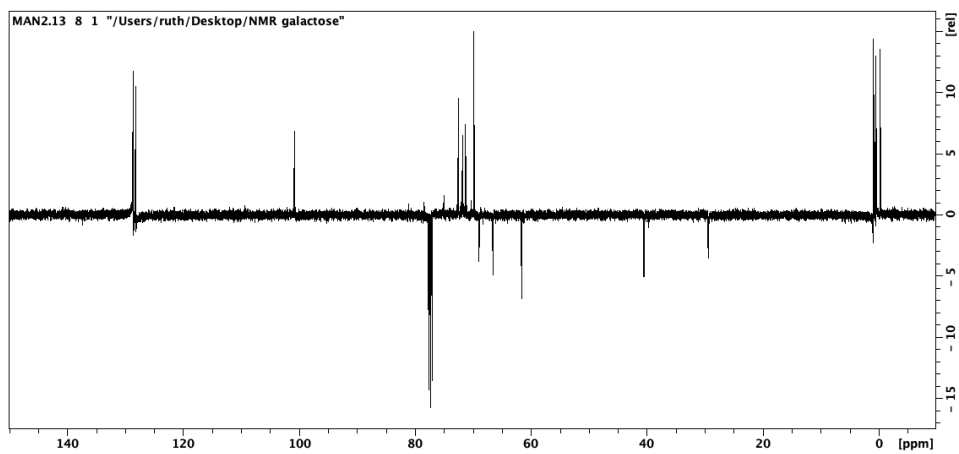
3'-(Benzyloxycarbonyl)-aminopropyl-α-D-galactopyranoside (d)

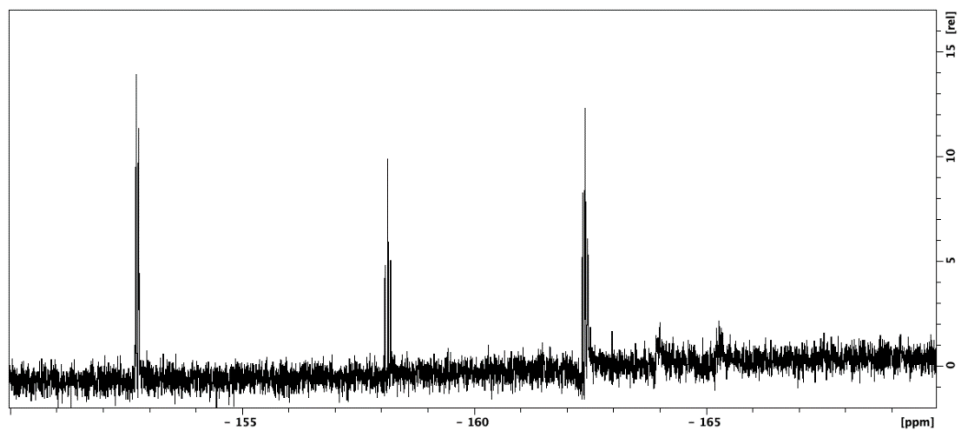## 3'-Aminopropyl-α-D-galactopyranoside (e)
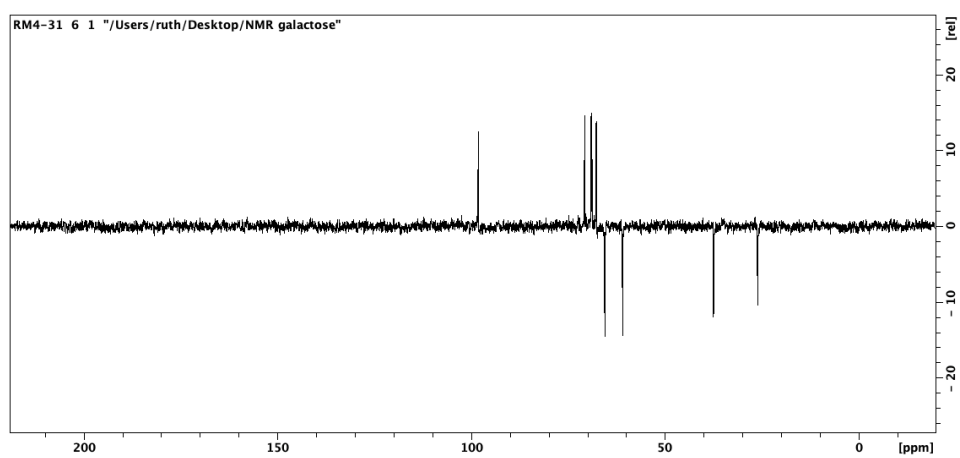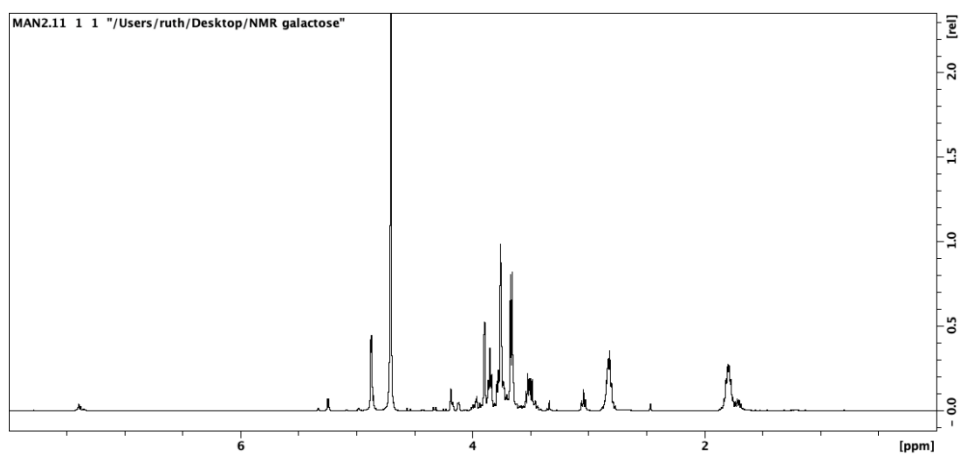
HS-PEG5000-COO-PFP (f)

HS-PEG5000-Gal (9-GalPEG)